TARGETED MODULATION OF CARDIAC ENERGETICS VIA THE CREATINE KINASE SYSTEM:

NOVEL TARGETS FOR CARDIOPROTECTIVE THERAPY



Dr. Filip Ostrowski
Christ Church

A thesis submitted in partial fulfillment of the requirements for the degree of
Doctor of Philosophy in Cardiovascular Medicine

Supervisors:
Prof. Stefan Neubauer
Dr. Sevasti Zervou

Division of Cardiovascular Medicine
Radcliffe Department of Medicine
University of Oxford

Michaelmas Term, 2013

TABLE OF CONTENTS

List of Figures **5**

List of Tables **7**

List of Abbreviations **8**

Abstract **9**

Declaration of own work **10**

Publications **10**

Acknowledgements **11**

1. Introduction **13**
1.1. Ischemic heart disease and heart failure **13**
1.2. Myocardial energetics and the CK system **15**
1.2.1. Myocardial energetics – overview 15
1.2.2. The creatine kinase reaction 16
1.2.3. Synthesis and metabolism of creatine 18
1.2.4. Creatine kinase isoenzymes 21
1.2.4.1. Genetics 21
1.2.4.2. Tissue specificity of creatine kinase isoenzyme expression 22
1.2.4.3. Creatine kinase isoenzyme expression during development 24
1.2.4.4. Protein structure and localization 24
1.2.4.5. Regulation of creatine kinase expression and activity 27
1.3. The creatine kinase system in heart failure – results of observational studies **29**
1.4. Experimental loss-of-function in the creatine kinase system **30**
1.4.1. Models targeting creatine synthesis or availability 30
1.4.1.1. Pharmacological inhibition of creatine uptake 30
1.4.1.2. Genetic ablation of creatine synthesis 31
1.4.2. Models targeting the creatine kinase isoenzymes 33
1.4.2.1. Pharmacological inhibition of creatine kinase activity 33
1.4.2.2. Transgenic loss-of-function models 34
1.5. Experimental gain-of-function in the creatine kinase system **38**
1.5.1. Overexpression of the creatine transporter 38
1.5.2. Inducible overexpression of M-type creatine kinase 40
1.5.3. Transgenic expression of creatine kinase isoenzymes in liver 41
1.6. Summary and experimental aims **41**

2. General materials and methods **43**
2.1. Materials **43**
2.1.1. Chemicals and laboratory equipment 43
2.1.2. Software 43
2.2. General methods **44**
2.2.1. Tissue culture 44
2.2.1.1. Mammalian cell lines 44
2.2.1.2. Tissue culture conditions 45
2.2.1.3. Transfection of cultured mammalian cells 45
2.2.2. Mouse husbandry and use of tissues 46
2.2.2.1. Mouse husbandry 46
2.2.2.2. DNA extraction from mouse ear biopsy 47
2.2.2.3. Harvesting of tissues 48
2.2.3. Polymerase chain reaction (PCR) 48
2.2.3.1. Reaction conditions 48
2.2.3.2. Primers 48
2.2.3.3. Agarose gel electrophoresis 49
2.2.4. Molecular cloning of DNA constructs 49
2.2.4.1. Cloning vectors 49
2.2.4.2. Polymerase chain reaction (PCR) 50

2.2.4.3. Extraction and precipitation of PCR products ... 50
2.2.4.4. Restriction digest ... 51
2.2.4.5. DNA electrophoresis and extraction ... 51
2.2.4.6. Ligation of vectors and inserts ... 52
2.2.4.7. Bacterial transformation and culture ... 52
2.2.4.8. Amplification of generated plasmids ... 53
2.2.4.9. DNA sequencing ... 54
2.2.5. RNA extraction and quantitative RT-PCR ... 54
2.2.5.1. RNA extraction from cultured cells ... 54
2.2.5.2. RNA extraction from mammalian tissues ... 54
2.2.5.3. Quantitative RT-PCR ... 55
2.2.6. Protein extraction and western blotting ... 56
2.2.6.1. Protein extraction from cultured cells ... 56
2.2.6.2. Protein extraction from mouse tissues ... 56
2.2.6.3. Sample preparation ... 57
2.2.6.4. Polyacrylamide gel electrophoresis ... 57
2.2.6.5. Immunoblotting and detection ... 57
2.2.7. Immunocytochemistry ... 58
2.2.8. Microscopy ... 58
2.2.9. Enzyme activity assays ... 59
2.2.9.1. Total creatine kinase activity ... 59
2.2.9.2. Relative activities of creatine kinase isoenzymes ... 60
2.2.9.3. Citrate synthase activity ... 60
2.2.9.4. Lowry protein assay ... 61
2.2.10. Statistical analysis ... 61

3. *In vitro* models of augmented creatine kinase expression– experiments in cultured cells ... 62
3.1. Introduction ... 62
3.2. Aims and hypotheses ... 63
3.3. Methods and results I: Overexpression of creatine kinase isoenzymes ... 64
3.3.1. *In vitro* overexpression of HA-tagged creatine kinase isoenzymes ... 64
3.3.1.1. pcDNA3.1+/- expression vectors ... 64
3.3.1.2. PCR amplification of CKmt, CK-M, and CK-B coding sequences ... 65
3.3.1.3. Cloning of expression constructs ... 66
3.3.1.4. Transient transfection of HEK293 and HL-1 cells ... 68
3.3.1.5. Protein expression by western blot ... 69
3.3.1.6. Enzymatic activity assays ... 70
3.3.1.7. Immunocytochemical localization of CKmt-HA ... 71
3.3.1.8. Generation of stably transfected cell lines ... 74
3.3.2. EGFP-tagged mitochondrial creatine kinase ... 75
3.3.2.1. Design and cloning of pCKmt-EGFP ... 75
3.3.2.2. Expression of pCKmt-EGFP ... 76
3.4. Methods and results II: Response to simulated ischemia/reperfusion injury ... 80
3.4.1. Protocol optimization ... 80
3.4.1.1. Hypoxic tissue culture ... 80
3.4.1.2. Quantification of cell viability ... 80
3.4.1.3. Optimization of incubation conditions ... 82
3.4.1.4. The caspase inhibitor zVAD-FMK as a positive control for prevention of cell death ... 87
3.4.1.5. Identification of transfected cells with pBFP2-nuc ... 88
3.4.2. Final protocol and results ... 90
3.5. Discussion ... 91
3.5.1. Generation of stably transfected cell lines ... 92
3.5.2. Expression of GFP-tagged mitochondrial creatine kinase ... 93
3.5.3. CKmt overexpression reduces cell death in an *in vitro* model of ischemia/reperfusion injury ... 94
3.6. Conclusions and future work ... 96

4. *In vivo* models of augmented cardiac energetics – overexpression of mitochondrial creatine kinase by targeted integration at the ROSA26 locus ... 97
4.1. Introduction ... 97
4.1.1. Targeted transgenesis at the ROSA26 locus ... 97
4.1.2. PhiC31 integrase–mediated cassette exchange ... 98
4.1.3. Constitutive transgene expression ... 99

4.1.4. The alpha–myosin heavy chain promoter 100
4.1.5. The hemagglutinin tag 101
4.1.6. Choice of background strain 101
4.2. Aims and hypotheses 102
4.3. Methods and Results 102
4.3.1. Generation of transgenic mice 102
4.3.1.1. Cloning of vectors for transgenesis 103
4.3.1.2. Generation of chimeric founder mice by blastocyst injection of embryonic stem cells 105
4.3.1.3. *In vitro* differentiation to confirm promoter activity in embryoid bodies 106
4.3.1.4. Mouse husbandry and genotyping 110
4.3.2. Validation of the transgenic model 117
4.3.2.1. Detection of transgenic mRNA by qRT–PCR 117
4.3.2.2. Detection of transgenic protein by western blot 119
4.3.2.3. Creatine kinase activity 121
4.3.2.4. Quantification of transgenic, endogenous, and total mRNA transcripts 122
4.3.3. Generation of homozygous transgenic mice 124
4.3.3.1. Genotyping of transgene zygosity 124
4.3.3.2. Breeding statistics 128
4.3.3.3. Confirmation of increased transgene activity in homozygous mice 129
4.3.3.4. Subcellular localization of transgenic protein by transmission electron microscopy 133
4.3.4. Phenotyping studies 136
4.3.4.1. Growth curves 136
4.3.4.2. Organ weights 137
4.3.4.3. Cardiac cine–MR imaging 138
4.3.4.4. *In vivo* left ventricular hemodynamics 140
4.3.4.5. Citrate synthase activity 142
4.4. Discussion 142
4.4.1. Generation of transgenic mice 143
4.4.1.1. Chimeric founder mice 143
4.4.1.2. Breeding of transgenic mice 144
4.4.2. Validation of transgene expression 146
4.4.2.1. Initial validation by *in vitro* differentiation in embryoid bodies 146
4.4.2.2. Transgene expression and activity 147
4.4.2.3. Total CKmt mRNA, protein and enzymatic activity 147
4.4.2.4. Possible causes for the relatively modest increase in total CKmt activity 148
4.4.2.5. Subcellular localization of CKmt–HA 151
4.4.3. Baseline phenotyping 152
4.4.3.1. Cardiovascular phenotype 152
4.4.3.2. Citrate synthase activity is decreased in CKmt–OE mice 153
4.5. Conclusions and future work 154

5. *In vivo* models of augmented cardiac energetics – overexpression of CK-M and CK-B by random-integration transgenesis 157
5.1. Introduction 157
5.1.1. Choice of transgenesis strategy 157
5.1.2. Random integration of transgenic DNA 158
5.2. Hypotheses and aims 158
5.3. Methods and results 160
5.3.1. Design and cloning of expression vectors 160
5.3.1.1. Design of expression vectors 160
5.3.1.2. PCR amplification of *Ckb* and *Ckm* cDNA 161
5.3.1.3. Cloning of expression vectors 163
5.3.2. Generation of founder mice by pronuclear microinjection 170
5.3.3. Mouse husbandry and genotyping 170
5.3.3.1. Founder mice 170
5.3.3.2. Genotyping protocols 170
5.3.3.3. Breeding transgenic mice 171
5.3.3.4. Determination of transgene copy number by qPCR 173
5.3.3.5. Visualization of transgene integration sites in CK-M mice by FISH 180
5.3.3.6. Breeding strategy 182
5.3.4. Validation of the models 183
5.3.4.1. mRNA expression by qRT-PCR 183

5.3.4.2. Protein expression by western blot ... 187
5.3.4.3. Enzymatic activity ... 189
5.3.4.4. Citrate synthase activity as a marker of mitochondrial volume ... 193
5.4. Discussion ... 194
5.4.1. Generation of transgenic mice by pronuclear microinjection and random integration ... 195
5.4.2. Transgene copy number ... 196
5.4.3. Multiple integration sites in individual founder mice ... 196
5.4.4. Transgene expression and activity ... 197
5.4.4.1. CK-M ... 197
5.4.4.2. CK-B ... 198
5.5. Conclusions and future work ... 199

6. Creatine and the mitochondrial permeability transition pore ... 201
6.1. Introduction ... 201
6.1.1. The mitochondrial permeability pore (mPTP) ... 201
6.1.1.1. Calcium-induced mitochondrial permeabilization ... 201
6.1.1.2. Function and structure of the mPTP ... 202
6.1.1.3. Inhibition by cyclosporin A ... 204
6.1.2. The mPTP in cardiac ischemia/reperfusion injury, and evidence for a protective effect of mPTP inhibition ... 205
6.1.3. The mPTP and the creatine kinase system ... 206
6.1.4. The cardioprotective effect of creatine and creatine kinase ... 207
6.2. Aims and hypotheses ... 208
6.3. Methods and results ... 208
6.3.1. Experimental design ... 208
6.3.2. Optimization of creatine incubation conditions ... 209
6.3.3. Measurement of mPTP opening ... 211
6.3.3.1. Calcein release as an indicator of mPTP opening ... 211
6.3.3.2. Photoactivation of tetramethylrhodamine methyl ester (TMRM) and mPTP opening ... 222
6.3.3.3. Results ... 229
6.4. Discussion ... 231
6.5. Conclusions and future work ... 234

7. Summary and future work ... 235

Appendices ... 240

A. Supplementary materials and methods ... 241
A.1. PCR protocols ... 241
A.2. PCR primers ... 242
A.3. Quantitative real-time PCR protocols ... 245
A.4. Antibodies ... 246
A.5. Solutions and media ... 247
A.5.1. Media and antibiotics for bacterial culture ... 247
A.5.2. Solutions for nucleic acid work ... 248
A.5.3. Solutions for protein work ... 249

B. Generation of transgenic models ... 250
B.1. Transgenics report: CKmt-OE ... 250
B.2. Transgenics report: CKm-OE and CKb-OE ... 261

C. References ... 266

LIST OF FIGURES

Figure 1-1: The creatine kinase system. 18
Figure 1-2: Summary of creatine metabolism. 20
Figure 1-3: Genetic homology of mammalian and avian CK isoenzymes. 22
Figure 1-4: Crystal structures of the human creatine kinase isoenzymes. 26
Figure 2-1: Creatine kinase assay. 60
Figure 2-2: Citrate synthase assay. 60
Figure 3-1: pcDNA3.1(+/-) vector. 64
Figure 3-2: Cloning PCR. 66
Figure 3-3: CK-M and CK-B restriction digest. 66
Figure 3-4: Maps of *in vitro* expression vectors. 67
Figure 3-5: pEGFP-N1 vector map. 68
Figure 3-6: GFP expression in transiently transfected cells. 69
Figure 3-7: Representative *in vitro* construct western blots. 70
Figure 3-8: CK isoenzyme electrophoresis in transfected HEK293 cells. 71
Figure 3-9: Immunocytochemical staining in HL-1 cells expressing CKmtHA. 73
Figure 3-10: G-418 kill curves. 74
Figure 3-11: Selection of stably transfected cells. 75
Figure 3-12: pCKmt-EGFP vector. 76
Figure 3-13: HL-1 cells transfected with GFP constructs. 77
Figure 3-14: Selection of HL–1 and HEK293 cells stably transformed with pCKmt-EGFP. 78
Figure 3-15: Bacterial growth curves. 79
Figure 3-16: Cell viability stain. 81
Figure 3-17: Quantification of cell death by flow cytometry with propidium iodide staining. 82
Figure 3-18: Effect of duration of hypoxia on cell viability. 84
Figure 3-19: Effect of duration of reoxygenation on cell viability. 84
Figure 3-20: Optimization of O_2 concentration and incubation media in HL-1 cells. 85
Figure 3-21: Optimization of hypoxic incubation time, O_2 concentration, and incubation media. 86
Figure 3-22: Effect of seeding density on cell viability. 86
Figure 3-23: Pilot experiment to determine the effectiveness of zVAD-FMK as a positive control in HL-1 simulated ischemia/reperfusion. 88
Figure 3-24: Expression of EBFP2-Nuc in HL-1 cells. 89
Figure 3-25: Results of simulated ischemia/reperfusion experiments in transiently transfected HL-1 cells. 90
Figure 4-1: Developmental expression of CKmt and αMHC. 100
Figure 4-2: Restriction digest of *Ckmt2* PCR product and αMHC vector. 103
Figure 4-3: Restriction digest of αMHC–CkmtHA MiniPrep products. 104
Figure 4-4: αMHC–CKmt–HA cloning for generation of the transgenic model. 105
Figure 4-5: *ROSA26* recombination using PhiC31 integrase. 106
Figure 4-6: Generation of embryoid bodies. 108
Figure 4-7: Optimization of αMHC/HA immunocytochemistry. 109
Figure 4-8: Immunocytochemistry in differentiated embryoid bodies. 110
Figure 4-9: Chimeric founder. 111
Figure 4-10: Genotyping primer binding sites in exons 4/5 of *Ckmt2*. 112
Figure 4-11: Test CKmt–OE genotyping PCR. 113
Figure 4-12: CKmt–HA genotyping – troubleshooting. 114
Figure 4-13: Results of F_1 genotyping. 114
Figure 4-14: CKmt-OE F_1 pups. 115

Figure 4-15: Genotyping of transgenic CKmt–OE F_1 pups. 116
Figure 4-16: Expression of transgenic mRNA in left ventricles from CKmt–OE mice. 118
Figure 4-17: Tissue specificity of CKmt–HA transgenic mRNA expression. 118
Figure 4-18: Western blot for transgene expression in CKmt-OE mice (anti-HA). 119
Figure 4-19: Western blot for total CKmt expression in CKmt-OE mice (anti-CKmt). 120
Figure 4-20: Creatine kinase activity in CKmt–OE mice. 121
Figure 4-21: CKmt activity in CKmt–OE mice (relative). 122
Figure 4-22: Summary of qRT–PCR results in CKmt–OE mice. 123
Figure 4-23: Transgene zygosity qPCR. 125
Figure 4-24: CKmt-OE transgene zygosity PCR. 127
Figure 4-25: Results of $Tg^{+/-}$ x $Tg^{+/-}$ breeding. 129
Figure 4-26: Allele–specific qRT–PCR in hemi– and homozygous CKmt–OE mice. 130
Figure 4-27: Total CKmt protein expression. 131
Figure 4-28: Creatine kinase activity in $Tg^{+/-}$ and $Tg^{+/+}$ CKmt–OE mice. 132
Figure 4-29: CKmt activity in $Tg^{+/-}$ and $Tg^{+/+}$ CKmt–OE mice (relative). 132
Figure 4-30: Transmission electron microscopy with immunogold staining of CKmt–HA in left ventricular tissue. 135
Figure 4-31: Growth curves in CKmt-OE mice. 136
Figure 4-32: Adult body weights in CKmt-OE mice. 137
Figure 4-33: Organ weights in CKmt-OE mice. 137
Figure 4-34: Cardiac cine-MR in CKmt-OE mice. 138
Figure 4-35: Left ventricular volumes and cardiac index in CKmt-OE mice. 139
Figure 4-36: Left ventricular mass in CKmt-OE mice, measured by cine-MR. 140
Figure 4-37: Left ventricular hemodynamics in CKmt-OE mice. 141
Figure 4-38: Citrate synthase activity in CKmt–OE mice. 142
Figure 4-39: Transmission electron microscopy with immunogold labeling of CKmt. 152
Figure 4-40: Backcrossing CKmt-OE mice onto a pure C57BL/6 background. 156
Figure 5-1: PCR amplification of *Ckb* and *Ckm* for expression vectors. 162
Figure 5-2: Restriction digests for CK-B cloning. 163
Figure 5-3: Restriction digest of alphaMHC-CKbHA MiniPrep products and *Ckm* PCR product. 164
Figure 5-4: αMHC-CKbHA vector for generation of transgenic mice. 164
Figure 5-5: Diagnostic restriction digest of alphaMHC-CKbHA. 165
Figure 5-6: Diagnostic restriction digest of the alphaMHC-CKbHA vector. 166
Figure 5-7: Gel electrophoresis of *Ckm* PCR product. 167
Figure 5-8: Cloning/diagnostic restriction digest of alphaMHC-Linker vector and *Ckm* PCR product. 168
Figure 5-9: Restriction digest of alphaMHC_L-CKmHA MiniPrep products. 169
Figure 5-10: Final alphaMHC_L-CKmHA vector. 169
Figure 5-11: PCR genotyping of potential CK-M founders. 172
Figure 5-12: PCR genotyping of potential CK-B founders. 173
Figure 5-13: Results of total copy number qPCR in CK-M mice. 175
Figure 5-14: Results of transgene copy number qPCR in CK-M mice. 176
Figure 5-15: Results of total copy number qPCR in CK-B mice. 178
Figure 5-16: Results of transgene copy number qPCR in CK-B mice. 178
Figure 5-17: Results of total copy number qPCR in CK-B mice derived from mouse #4541. 179
Figure 5-18: FISH assay in CKm-OE mice. 181
Figure 5-19: Transgenic mRNA expression in CKm-OE mice. 184
Figure 5-20: Total mRNA expression in CKm-OE mice. 184
Figure 5-21: Endogenous mRNA expression in CKm-OE mice. 185
Figure 5-22: Transgenic mRNA expression in CKb-OE mice. 185
Figure 5-23: Total mRNA expression in CKb-OE mice. 186
Figure 5-24: Endogenous mRNA expression in CKb-OE mice. 186
Figure 5-25: Tissue-specificity of transgenic mRNA expression in CK-M mice. 187
Figure 5-26: Representative western blot in CK-M mice. 188
Figure 5-27: Total CK-M protein expression in CKm-OE mice. 188

Figure 5-28: Representative western blot in CK-B mice. 189
Figure 5-29: Creatine kinase activity in CKm-OE mice. 190
Figure 5-30: Relative activity of creatine kinase MM in CKm-OE mice. 191
Figure 5-31: Creatine kinase activity in CKb-OE mice. 192
Figure 5-32: Creatine kinase MB and BB activity in CKb-OE mice, expressed as a percentage of total CK activity. 193
Figure 5-33: Citrate synthase activity in CKm-OE and CKb-OE mice. 194
Figure 6-1: Putative structure of the mitochondrial permeability transition pore. 203
Figure 6-2: Optimization of creatine pre-incubation conditions for mPTP assays. 210
Figure 6-3: Calcein-AM mPTP protocol. 212
Figure 6-4: Calcein pilot experiment. 212
Figure 6-5: Calcein photostability. 213
Figure 6-6: Dose-response experiment for H_2O_2 induction of mPTP opening in HL-1 cells. 214
Figure 6-7: mPTP induction by H_2O_2. 215
Figure 6-8: Quantification of calcein release in response to H_2O_2. 216
Figure 6-9: Time-lapse imaging of calcein release in response to H_2O_2. 217
Figure 6-10: Mitochondrial and lysosomal staining in HL-1 cells. 218
Figure 6-11: General incubation protocol for calcein subcellular localization experiments. 219
Figure 6-12: MitoTracker Red and calcein. 220
Figure 6-13: LysoTracker Red and calcein. 221
Figure 6-14: TMRM mPTP protocol. 223
Figure 6-15: TMRM and calcein. 224
Figure 6-16: MitoTracker Red and Green. 225
Figure 6-17: TMRM and MitoTracker Green. 226
Figure 6-18: TMRM pilot assay. 227
Figure 6-19: Quantification of TMRM fluorescence. 228
Figure 6-20: mPTP inhibition by cyclosporin A (CsA). 229
Figure 6-21: Elevation of intracellular creatine inhibits mPTP opening. 230

LIST OF TABLES

Table 1-1: Subcellular localization and tissue-specific expression of CK isoenzymes. 23
Table 3-1: Primers for *in vitro* expression constructs. 65
Table 3-2: Composition of buffers for simulated ischemia/reperfusion experiments. 83
Table 4-1: Primers used for generation of the CKmt overexpression construct. 103
Table 4-2: Antibodies used for immunocytochemical staining of embryoid bodies. 109
Table 4-3: Breeding statistics for CKmt–OE founder mice derived from the first two rounds of blastocyst injections. 115
Table 4-4: Breeding statistics for CKmt–OE founder mice derived from the third round of blastocyst injections. 116
Table 4-5: Comparison of PCR and qPCR for genotyping transgene zygosity. 128
Table 4-6: Breeding statistics for CKmt-OE $Tg^{+/-}$ x $Tg^{+/-}$ breeding pairs. 129
Table 4-7: Success rates of transgenesis by blastocyst injection. 144
Table 5-1: Optimized PCR protocol for *Ckb* and *Ckm* cloning. 162
Table 5-2: Summary of CK-M copy number qPCR results. 176
Table 5-3: Summary of CK-B copy number qPCR results. 179
Table 5-4: Breeding statistics for CKm-OE mice. 182
Table 5-5: Breeding statistics for CKb-OE mice. 182
Table 7-1: Summary of molecular validation of all CK-overexpressing transgenic lines. 237

List of Abbreviations

ADP, adenosine diphosphate
AGAT, arginine:glycine amidinotransferase
aMHC (αMHC), alpha-myosin heavy chain
AMP, adenosine monophosphate
AMPK, AMP-activated protein kinase
ANT, adenine nucleotide translocase
ATP, adenosine triphosphate
BCA, bicinchoninic acid (assay)
BFP, blue fluorescent protein
BLAST, Basic Local Alignment Search Tool
βGPA, beta-guanidinopropionate
bp, base pair
BSA, bovine serum albumin
cDNA, complementary DNA
CHF, chronic heart failure
CK, creatine kinase
CK-B, B-type ("brain") creatine kinase
CK-M, M-type ("muscle") creatine kinase
CKmt, mitochondrial creatine kinase
Cr, creatine
Crn, creatinine
CrT, creatine transporter
CS, citrate synthase
CsA, cyclosporin A
CypD, cyclophilin D
DNA, deoxyribonucleic acid
DMEM, Dulbecco's Modified Eagle's Medium
dNTP, deoxynucleotide triphosphate
DTNB, 5,5'-dithiobis-(2-nitrobenzoic acid) *or* Ellman's reagent
DTT, dithiothreitol *or* Cleland's reagent
EB, embryoid body
EC, Enzyme Commission (number)
ECG, electrocardiogram
EDTA, ethylenediamine tetraacetic acid
EF, ejection fraction
EGFP, enhanced green fluorescent protein
ES, embryonic stem (cells)
FBS, fetal bovine serum
FISH, fluorescence *in-situ* hybridization
ΔG_{ATP}, free energy change of ATP hydrolysis
GAA, guanidinoacetate
GAMT, guanidinoacetate-N-methyltransferase
gDNA, genomic DNA
GFP, green fluorescent protein
GTP, guanosine triphosphate
HA, hemagglutinin (tag)
HBSS, Hank's Buffered Salt Solution
HEK293, human embryonic kidney 293 (cells)
HEPES, 4-(2-hydroxyethyl)piperazine-1-ethanesulfonic acid
Het, heterozygous/heterozygote
HF, heart failure
HPLC, high performance liquid chromatography
IHD, ischemic heart disease
IMM, inner mitochondrial membrane
kDa, kilodalton
KO, knockout
LDH, lactate dehydrogenase
LV, left ventricle
LVDP, left ventricular developed pressure
MLC2v, ventricular myosin light chain 2
mPTP, mitochondrial permeability transition pore
MR/MRI, magnetic resonance (imaging)
mRNA, messenger RNA
mtTFA/TFAM, mitochondrial transcription factor A
MuRF1, muscle RING-finger protein 1
NAD, nicotinamide adenine dinucleotide
NADH, reduced form of NAD
NCBI, National Center for Biotechnology Information
NEB, New England Biolabs
NGS, normal goat serum
NYHA, New York Heart Association
OE, overexpression
OMM, outer mitochondrial membrane
ORF, open reading frame
PBS, phosphate buffered saline
PCR, polymerase chain reaction
PCr, phosphocreatine
PGC-1α, PPAR-γ coactivator 1α
PI, propidium iodide
P_i, inorganic phosphate
^{31}P-MRS, phosphorus-31 magnetic resonance spectroscopy
PPAR-γ, peroxisome proliferator-activated receptor γ
qPCR, quantitative polymerase chain reaction
qRT-PCR, quantitative reverse-transcriptase polymerase chain reaction
RCSB, Research Collaboratory for Structural Bioinformatics
RIPA, radioimmunoprecipitation assay (buffer)
ROI, region of interest
ROS, reactive oxygen species
ROSA26, reverse orientation splice acceptor 26
RT, room temperature
RV, right ventricle
SDS, sodium dodecyl sulfate
SfA, sanglifehrin A
sI/R, simulated ischemia/reperfusion
TAC, transverse aortic constriction
TBE, Tris/borate/EDTA
TEM, transmission electron microscopy
Tg, transgenic
$Tg^{+/-}$ & $Tg^{+/+}$, hemi-/homozygous transgenic
TMRM, tetramethylrhodamine methyl ester
TNB, 5-thio-2-nitrobenzoic acid
TX, Triton X-100
UTR, untranslated region
UV, ultraviolet
VDAC, voltage dependent anion channel
WT, wild-type
zVAD-FMK, benzyloxycarbonyl-Val-Ala-Asp-fluoromethylketone

ABSTRACT

There is a large body of clinical and experimental evidence linking heart disease with impairment of myocardial energetics, particularly the creatine kinase (CK) system. The goal of the experiments described in this thesis was to develop and study models of increased CK phosphotransfer, by overexpressing the CK isoenzymes and/or augmenting intracellular creatine stores.

Pilot experiments were performed in cultured cells, which were used to (a) study the effects of CK overexpression *in vitro*, and (b) validate constructs prior to generation of transgenic mice. Expression was verified at the protein level for all constructs in HL-1 and HEK293 cells, and enzymatic activity was confirmed. Mitochondrial CK (CKmt) was expressed in the mitochondria, as expected, and CKmt overexpression was associated with a significant reduction in cell death in a model of ischemia/reperfusion injury (68.1 ± 7.1% of control, $p \leq 0.05$).

Transgenic mice overexpressing CKmt in the heart were generated by a targeted approach, using PhiC31 integration at the ROSA26 locus. Transgene expression was confirmed *in vitro* in embryonic stem cells, and *in vivo* at the mRNA and protein levels. There was only a modest increase in CKmt activity; therefore, homozygous transgenic mice were generated to increase expression levels, and had 27% higher CKmt activity than wild-types ($p \leq 0.01$). Mitochondrial localization of CKmt was confirmed by electron microscopy. Citrate synthase activity, a marker of mitochondrial volume, was ~10% lower in transgenic mice ($p \leq 0.05$). Baseline phenotyping studies found that CKmt-overexpressing mice have normal cardiac structure and function. These mice are currently being backcrossed onto a pure C57BL/6 background for further studies in models of heart disease.

In addition to CKmt, transgenic mice overexpressing the cytosolic CK isoenzymes, CK-M and CK-B, were generated. Due to the modest level of expression observed at ROSA26, random-integration transgenesis was used, and multiple lines were generated for each construct (carrying 2 or 6 transgene copies in the CK-M line; 2, 3, or ~30 in CK-B). Transgene expression was validated at the mRNA, protein, and activity levels. These lines are currently being expanded for further validation and phenotyping studies.

Previous experiments in our group have demonstrated that increasing intracellular creatine (Cr) reduces ischemia/reperfusion injury, and a series of *in vitro* experiments was performed to determine whether this effect may be mediated by inhibition of the mitochondrial permeability transition pore (mPTP). The mPTP plays a significant role in ischemia/reperfusion, and there is evidence linking the CK system to regulation of the mPTP. Therefore, a model was developed to test whether Cr affects mPTP opening in cardiac-derived HL-1 cells, as this mechanism may contribute to the protective effect observed *in vivo*. Cr incubation conditions were determined empirically, and 24-hour incubation with 5mM or 10mM Cr was found to significantly delay mPTP opening, to a similar degree to the established mPTP inhibitor, cyclosporin A. This provides evidence that Cr may exert protective effects in the heart by a variety of mechanisms, in addition to its traditional role in energy metabolism.

In summary, the experiments conducted in this thesis have produced a range of tools for studying augmentation of the creatine kinase system as a therapeutic target in heart disease. The results of *in vitro* assays indicate that mitochondrial CK may be a particularly promising target, and that inhibition of the mitochondrial permeability transition pore may contribute to the cardioprotective effect of creatine. Finally, the transgenic models generated and validated over the course of this project will allow for a wide range of future studies into the potential benefits of CK overexpression in the mammalian heart.

DECLARATION OF OWN WORK

This thesis is entirely my own work unless otherwise indicated. It has not been submitted, either wholly or substantially, for another degree of this University, or for a degree at any other institution. Any assistance from colleagues or collaborators has been appropriately acknowledged in the text.

PUBLICATIONS

The following publications have included data resulting from experiments described in this thesis, as well as other work conducted by the author, not directly related to this thesis:

Lygate, C. A. *et al.* Moderate elevation of intracellular creatine by targeting the creatine transporter protects mice from acute myocardial infarction. Cardiovascular Research 96, 466–475 (2012).

Lygate, C. A. *et al.* Chronic creatine kinase deficiency eventually leads to congestive heart failure, but severity is dependent on genetic background, gender and age. Basic Res Cardiol 107, 276 (2012).

Zervou, S. *et al.* A role for Thioredoxin interacting protein (Txnip) in cellular creatine homeostasis. AJP: Endocrinology and Metabolism 305, E263-E270 (2013).

ACKNOWLEDGEMENTS

I approached the writing of this section with a mixture of excitement and trepidation. On one hand, this is an opportunity to thank all the people – and there have been many – without whom my experience in Oxford would not have been as productive and enjoyable as it was. On the other, there simply isn't enough room to include everyone who has made a difference over the past four years; in the (admittedly unlikely) event that someone decides to read this thesis, but is not acknowledged below, please accept my sincere apologies.

To put it quite simply, I would not be here without the support of Prof. Stefan Neubauer, who was instrumental in bringing me to Oxford in the first place, and has been an exemplary supervisor. Unless the 7T magnet at OCMR is disrupting the space-time continuum, I doubt I'll ever understand how it's possible to work 30-hour days, and still be available at a moment's notice whenever a graduate student needs your help or guidance. Dr. Sevasti Zervou has been a fantastic supervisor in the lab trenches, and always seems to find the right piece of advice, whether we're discussing the minutiae of molecular biology, or my project as a whole. I would especially like to thank Dr. Craig Lygate - a supervisor in everything but name - for his review of this thesis (always critical, but always fair), and for judicious use of carrot, stick, and whisky.

My D.Phil. would have been a far more difficult undertaking if I was not walking a trail blazed by previous students. Dr. Imre Hunyor, who was in the final stages of his project when I arrived in Oxford, showed me how to set up my first PCR (it failed). With my clinical background, a basic-science project of this magnitude was always going to involve a steep learning curve, but Imre's training and guidance provided a massive push to set me on my way. Dr. Liam Sebag-Montefiore spent three years sitting directly across from me, and coincidentally decided to quit science and never set foot in a lab again. I would like to thank Liam for putting up with my sense of humor for so long, joining me as Co-Master of the Punts at Christ Church for one memorable term, and - perhaps most pertinently - sharing his hard-earned practical wisdom over the years. Dr. Kiterie Faller was an inspirational figure in and out of the lab, despite being French. Her work-rate and baking prowess are the stuff of legend, and the fact that she survived the sleep deprivation and toxic amounts of caffeine she was consuming towards the end of her write-up made me feel more confident when the time came for me to do the same.

The experience of working in the Neubauer group has been shaped, first and foremost, by the people. Debra Medway stepped in to support my project in the crucial final stages, and I would like to thank her - as is becoming traditional among outgoing D.Phil. students - for not "decking" me during my time in the lab. Becky Cross, our resident chemist (and DJ), managed to keep things up-beat on the most depressing of days - even in tissue culture, which is no mean feat. Dr. Hannah Whittington has only recently joined our group, and our work interaction has mainly consisted of me prefacing statements with "this isn't the most exciting experiment, but…" Despite this, she's off to a great start, and will be a valuable member of the group for years to come. Tanmoy Ray, who has since moved on to do a PhD in the Netherlands, was an unerring positive presence in the lab, despite the occasional threat of violence. I would particularly like to thank him for his expert advice during our regular curry nights (except for the time when he ordered me a vindaloo and just sat there smirking to himself), and for always knowing people's birthdays (except for the time he memorably got one wrong). Dr. Jürgen Schneider's BMRU group were always a pleasure to work with, and the efforts of Dr. Leonie Diffley and Vicky Thornton deserve special thanks.

In addition to our own lab, several groups and individuals have made significant contributions to my research in Oxford. There are too many to mention, but I would particularly like to thank Dr. Ben Davies and the Transgenics Core, who generated the transgenic mice described in this thesis. Part of me is concerned that the Channon group may have been keeping a record of the reagents and equipment I've "borrowed" from them. I would also like to thank the Casadei group, particularly Dr. Ricardo Carnicer and Dr. Greg Lim, for my first-year rotation in their lab. Dr. James Brown, our lab manager, strikes a rare balance between authority and friendliness - throw in his quiz prowess, and it's a unique combination indeed. I would like to thank James for his patience, particularly for resisting the urge to immediately confiscate my building access card after I poured molten agar down the sink. Dr. Keith Morris taught me everything I know about microscopy, and didn't seem to mind when I established permanent residence at his confocal for most of my second year. The flow cytometry experiments would not have been possible without the support of Drew Worth at the Jenner Institute. Finally, animal work was a key aspect of my project, and I would like to thank the Functional Genomics Facility staff for their efforts in maintaining my colonies over the years.

I would like to thank the British Heart Foundation for generously funding my project, and the University of Oxford and Wellcome Trust for providing the facilities without which my work would have been impossible. Prof. David Greaves fostered a real sense of community among the students in the BHF 4-Year Programme, which allowed us to create links between diverse research groups.

Finding free time during a research D.Phil. is by no means an easy task, but I was fortunate enough to take part in a variety of extra-curricular activities during my time in Oxford. It has been a privilege to study at Christ Church, and I would like to thank the Dean, The Very Reverend Christopher Lewis, and my college adviser, Prof. Graham Ogg, for their ongoing support. The GCR was an always exciting, often chaotic place, and I am honored to have served in a variety of positions on its Committee. The sporting life in Oxford is second to none, and I will always have fond memories of Saturday mornings in the glorious green-and-gold of the GCR football "1st" XI. Racing for Christ Church Boat Club was a formative experience, from an "undefeated" Regatta all the way through a hull-shattering bump on the Saturday of Eights Week, via far too many exhausting erg sessions. The wonderful Magdalen Film Society will always be my destination of choice if I find myself with an evening to spare in Oxford. I would also like to thank my team-mates from the 2013/14 University Challenge squad: Ewan, Andreas, and George - we'll always have Céline.

Finally, I would like to thank my family, particularly my parents and grandparents, who not only provided for my education, but also taught me to strive to improve myself every day. It's no exaggeration to say that, without their constant support and encouragement, none of this would have been possible. My brother Alex has kept me on my toes by embarking on a career trajectory which, if the early signs are anything to go by, will leave me scrambling to keep up (indeed, on the day I am submitting this thesis, he's sitting the GMAT). We've clearly settled on different paths, but – although this is an obvious cliché, that doesn't make it any less true – I know we'll always have a special bond… and if all else fails, there's always Arsenal to fall back on. My aunt and uncle, Ania and Piotr Pruszczyk, provided a much-needed medical connection in the family, and have always been there for me with sound advice and words of encouragement, while also serving as an example that you can indeed juggle clinical work, a research career, a house, three kids, and a dog. Last, but certainly not least, my long-suffering fiancée Lija has had to put up with my increasingly anti-social working hours, but has been an inexhaustible source of strength, comfort, and - recently - editorial supervision. I'm greatly looking forward to having our evenings and weekends back, and making plans for what lies ahead!

1. INTRODUCTION

1.1. Ischemic heart disease and heart failure

Ischemic heart disease (IHD) is a condition resulting from insufficient supply of blood to the myocardium. IHD is classically caused by atherosclerotic lesions in the coronary arteries, but may also be due to other causes, such as vasomotor abnormalities or microvascular dysfunction. According to the most recent statistics published by the World Health Organization, IHD is the leading cause of death worldwide, accounting for 17.3% of all deaths in high-income countries and 11.8% of deaths in middle/low-income countries[1]. Although age-standardized mortality has progressively decreased in developed countries, population aging ensures that IHD will remain a substantial economic and societal burden for the foreseeable future.

Patients with IHD are at increased risk of developing hazardous complications, including acute coronary syndromes and chronic heart failure. Acute coronary syndromes are most commonly the result of atherosclerotic plaque instability, and comprise unstable angina and myocardial infarction. Heart failure (HF) is a complex syndrome with many possible etiologies, defined by the European Society of Cardiology as "an abnormality of cardiac structure or function leading to failure of the heart to deliver oxygen at a rate commensurate with the requirements of the metabolizing tissues, despite normal filling pressures (or only at the expense of increased filling pressures)[2]," and more broadly by the American Heart Association as "a complex clinical syndrome that results from any structural or functional impairment of ventricular filling or ejection of blood[3]." The diagnosis of HF is primarily a clinical one, largely due to the heterogeneous etiology of the condition.

According to recent estimates, there are over 5 million patients with HF in the United States alone, and the condition is thought to be responsible for over 50,000 deaths annually[4]. The individual lifetime risk of

developing HF is greater than 1 in 5 from the age of 40 onwards, in both men and women[5]. The prevalence of HF is on the rise, and is estimated to reach 3.5% by the year 2030[6]. There is evidence that the incidence of HF is gradually increasing in the elderly[7], and is estimated at >80 per 1,000 above the age of 85[8], which is of particular concern given the aging population. It is also worth noting that the financial burden of HF is increasing at an alarming rate, with recent estimates suggesting that the total (direct and indirect) cost of HF to the United States budget may increase almost three-fold by the year 2030, to $95 billion per year[4,6].

There are several treatment options which have been shown to improve clinical outcomes in HF, including angiotensin converting enzyme inhibitors[9,10] and/or angiotensin II receptor antagonists[11-13], β-receptor antagonists[14-16], mineralocorticoid receptor antagonists[17], resynchronization therapy[18,19], heart rate reduction with ivabradine[20] and revascularization in patients with coronary artery disease[21]. Despite this, the overall prognosis remains relatively poor. While advances in management led to a gradual improvement in outcomes over the second half of the 20th century, 5-year mortality remains unacceptably high at >50%[22-24]. Therefore, there is a compelling case for research into new therapeutic targets in heart failure, beyond the traditional scope of neuroendocrine antagonism and heart rate control. Modulation of myocardial energetics is a particularly promising target. Since there is ample evidence that heart disease is associated with impairment of cardiac metabolism at the cellular level[25], it has been suggested that interventions which correct these abnormalities may have protective effects – indeed, some of the most widely used drugs (renin/angiotensin/aldosterone system antagonists and β-blockers) are known to reduce energy demand. If more specific, targeted interventions in myocardial metabolism are found to have beneficial effects in experimental models, they could be harnessed to develop new methods of treatment. The following sections describe the physiology and pathophysiology of myocardial energetics, with particular focus on the creatine kinase system.

1.2. Myocardial energetics and the CK system

1.2.1. Myocardial energetics – overview

The heart relies on chemical energy in the form of adenosine triphosphate (ATP) to perform contractile work. The concept of myocardial energetics comprises multiple integrated processes and systems, including (1) uptake and catabolism of substrates (*e.g.*, glycolysis and β-oxidation of fatty acids), (2) production of ATP, and (3) ATP transfer and utilization (*e.g.*, by the contractile apparatus or ATPase ion pumps)[25]. The experiments described in this thesis are primarily concerned with energy transfer and utilization, particularly the central role of the creatine kinase (CK) system in the transport and homeostasis of high-energy phosphates. Therefore, the physiology of ATP metabolism and role of the CK system are described below.

Myocardial ATP is primarily synthesized by oxidative phosphorylation in the mitochondria (>95%), with a smaller contribution from glycolysis and GTP produced in the Krebs cycle[26]. Hydrolysis of the high-energy γ-phosphate bond of ATP releases chemical energy, which can be used to drive energetically unfavorable processes, primarily myofilament contraction (60-70% of total ATP) and active transport by ion pumps (>30%). ATP hydrolysis yields adenosine diphosphate (ADP) and inorganic phosphate (P_i), and can be simplified as the following reaction:

$$ATP + H_2O \Rightarrow ADP + P_i$$

The amount of energy released by this reaction is termed the Gibbs free energy change of ATP hydrolysis (ΔG_{ATP}), and is determined by the relative concentrations of the reactants, specifically ATP, adenosine diphosphate (ADP), and inorganic phosphate (P_i):

$$\Delta G_{ATP} = \Delta G^0_{ATP} - RT ln [ATP] / [ADP][P_i]$$

where ΔG^0_{ATP} is the free energy change of ATP hydrolysis under standard conditions, R is the universal gas constant, and T is the absolute temperature. Since values of ΔG_{ATP} in the heart are negative, in the interest of clarity the absolute value $|\Delta G_{ATP}|$ will be referred to throughout this thesis. The above equation effectively determines how much energy cellular ATPases can obtain from each molecule of ATP. Indeed, studies have shown that the heart's capacity to perform mechanical work correlates with ΔG_{ATP}, rather than the absolute concentration of ATP; when $|\Delta G_{ATP}|$ drops below a certain threshold, ATPases are no longer able to efficiently extract energy from ATP, and diastolic and systolic dysfunction ensues[27].

The absolute concentration of ATP in cardiomyocytes is relatively low, approximately 5μmol/g wet weight; since ATP turnover is estimated at 0.5μmol/gww/second, the heart would theoretically consume its entire ATP pool within 10 seconds if it was not rapidly replenished[26]. Therefore, additional mechanisms are required to ensure that ATP concentrations remain stable, particularly under conditions of increased workload. The creatine kinase system plays a central role in this process, and is described below.

1.2.2. The creatine kinase reaction

Creatine kinase (CK, EC 2.7.3.2) catalyzes the reversible transfer of a phosphoryl residue between creatine and ATP. The role of creatine in muscular phosphate metabolism was first postulated in the 1920's[28,29], but it was not until Lohmann described the CK reaction in 1934 that the precise mechanism was established[30]:

$$\text{Creatine} + \text{ATP} \Leftrightarrow \text{Phosphocreatine} + \text{ADP} + H^+$$

The CK system performs a variety of functions in cardiomyocytes[31]. The first is to act as an energy buffer by storing high-energy phosphate in the form of phosphocreatine (PCr), which can be used to regenerate ATP in response to demand. The CK reaction can produce ATP at a rate of 30μmol/gww/s, which is far greater than the rate of baseline consumption, or the maximal rate of ATP synthesis by oxidative phosphorylation

and glycolysis combined (<3μmol/gww/s)[31]. Therefore, the cell is able to store energy in the form of PCr, which is used to replenish ATP as it is consumed, maintaining a stable ATP concentration.

The second function of the CK system is as a transport system (Figure 1-1). ATP is primarily synthesized in the mitochondria by oxidative phosphorylation, and utilized by cytosolic ATPases. While ATP itself is capable of diffusing across the cell, PCr is a smaller and less polar molecule, and can therefore diffuse more efficiently[32]. Therefore, the mitochondrial CK isoenzyme catalyzes a phosphotransfer reaction from ATP to PCr, which is exported into the cytosol and transported to the site of utilization, where it is used to regenerate ATP[33].

In addition to acting as a temporal buffer, as described above, the CK system also acts as a spatial buffer by regulating local concentrations of ATP and ADP[34]. At the site of energy production, *i.e.* mitochondria, CK converts newly synthesized ATP to ADP, maintaining a high local ADP concentration, which favors further synthesis of ATP by the mitochondrion (Figure 1-1). Conversely, at the site of energy utilization, *e.g.* the contractile apparatus, production of ATP and consumption of ADP by the CK reaction maintains a high ATP/ADP ratio, and therefore an energetically favorable $|\Delta G_{ATP}|$. Furthermore, cycling of adenine nucleotides by mitochondrial CK has been shown to participate in regulation of oxidative phosphorylation, by controlling the local ADP concentration and direct interaction with mitochondrial proteins[35,36]. Therefore, the CK system plays a significant role in coupling energy production to demand, by stimulating mitochondrial production of ATP in response to increased workloads.

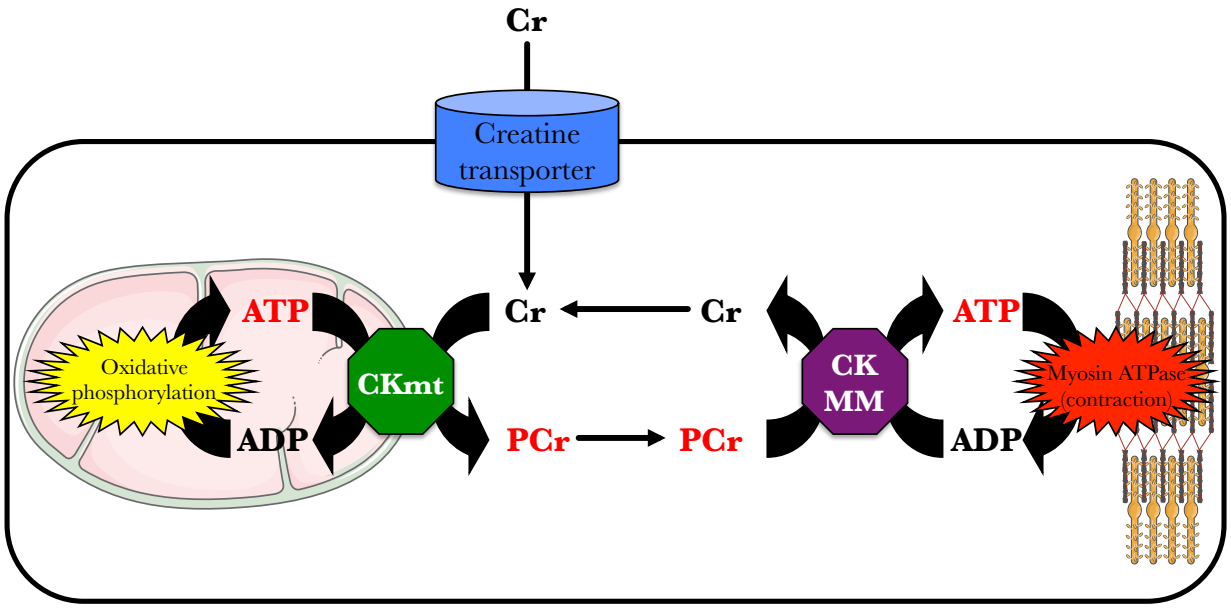


Figure 1-1: The creatine kinase system.

In oxidative tissues, such as the heart, the majority of ATP is produced by mitochondrial oxidative phosphorylation. Mitochondrial creatine kinase (CKmt) catalyzes the transfer of a high-energy phosphoryl residue from ATP to creatine (Cr), forming phosphocreatine (PCr). PCr is exported from the mitochondrion, and can be used by cytosolic creatine kinases (*e.g.,* CK-MM) to replenish ATP at the sites of energy utilization, such as the contractile apparatus. Note that the CK reaction proceeds in opposite directions at the mitochondria and contractile apparatus, maintaining favorable local ATP/ADP ratios. Figure adapted from Wallimann *et al.*[37]

1.2.3. Synthesis and metabolism of creatine

Creatine is an amino acid derivative which can be acquired through the diet, primarily by consuming meat or fish; however, it is estimated that dietary sources supply only 50% of the total creatine requirement in a typical omnivore[38]. To make up for this deficit, additional creatine must be synthesized *de novo*. This endogenous creatine is synthesized in a two-step enzymatic process (Figure 1-2). In the first step, which takes place in the kidney, a reaction between arginine and glycine is catalyzed by arginine:glycine amidinotransferase (AGAT, EC 2.1.4.1), forming the creatine precursor guanidinoacetate (GAA) and ornithine. The second reaction, which occurs primarily in the liver, is methylation of GAA by guanidinoacetate-N-methyltransferase (GAMT, EC 2.1.1.2) to form creatine.

Creatine is transported to the heart and other tissues via the bloodstream, and is actively imported into the cell against a large concentration gradient, by a Na^+/Cl-dependent specific creatine transporter (CrT,

Slc6a8)[39]. Uptake via the CrT is the main factor limiting intracellular accumulation of creatine, as transport is downregulated in response to elevated extracellular Cr[40].

Degradation of creatine is a non-enzymatic process, involving spontaneous and irreversible conversion to creatinine[41]. The rate of degradation is constant, corresponding to ~1.7% of the total Cr pool per day[42]. Creatinine is exported by passive diffusion across the cell membrane, transported to the kidneys in the bloodstream, and excreted in urine.

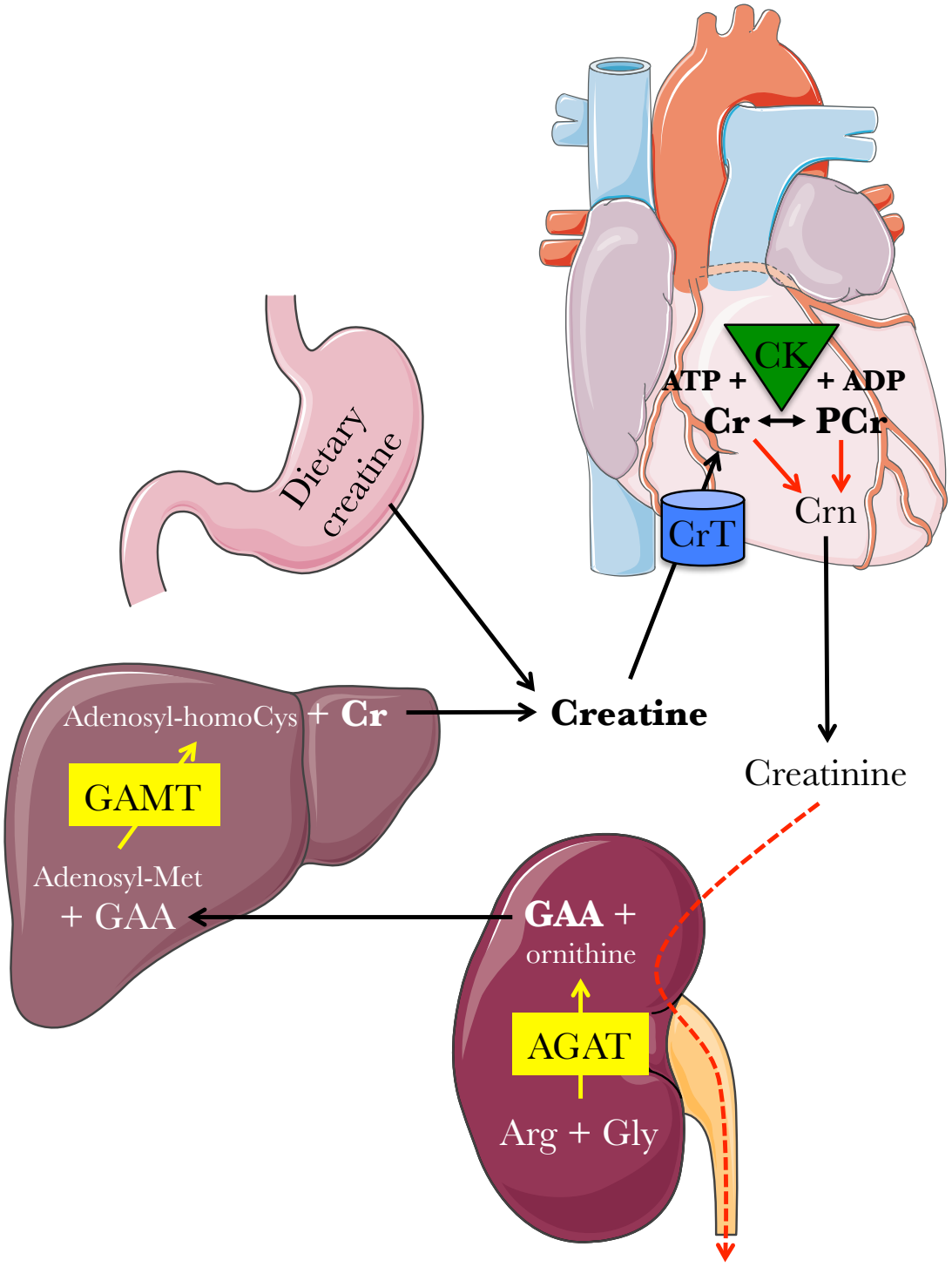


Figure 1-2: Summary of creatine metabolism.

Creatine is absorbed from dietary sources, and synthesized *de novo* in a two-step enzymatic process. The renal enzyme arginine:glycine amidinotransferase (AGAT) catalyzes a reaction between arginine (Arg) and glycine (Gly), to form guanidinoacetate (GAA). GAA is transported to the liver, where it is converted to creatine (Cr) by the enzyme guanidinoacetate-N-methyltransferase (GAMT). Creatine enters the cardiomyocyte via a specific transporter (CrT), where it is reversibly phosphorylated to phosphocreatine (PCr) by creatine kinase (CK). Both creatine and phosphocreatine undergo spontaneous degradation to creatinine (Crn), which is excreted by the kidneys. Figure adapted from Wyss *et al.*[42]

1.2.4. Creatine kinase isoenzymes

The existence of multiple cytosolic isoenzymes within the CK system was first proposed by Burger *et al.* in 1964[43]. Soon afterwards, Jacobs *et al.* provided evidence for the existence of a discrete mitochondrial isoenzyme in muscle and brain[44]. There are currently four known CK isoenzymes: the cytosolic enzymes (M-CK and B-CK) and two mitochondrial enzymes (ubiquitous CKmt and sarcomeric CKmt). Further complexity is added by the fact that the cytosolic enzymes form homo- and heterodimers, and can therefore exist as CK-MM, CK-BB, and CK-MB. This section describes the individual isoenzymes in more detail.

1.2.4.1. Genetics

The four CK isoenzymes are encoded by separate nuclear genes, each located on a different chromosome in both mice and humans. There is a significant degree of sequence homology between isoenzymes, both within and across species, with conserved regions forming a "CK framework" thought to be responsible for enzymatic activity (Figure 1-3)[45]. There is a greater degree of sequence conservation (~80%) within the cytosolic isoenzymes (CK-M and CK-B) and mitochondrial isoenzymes (sCKmt and uCKmt), respectively, than between these groups (~60%). This suggests that, in evolutionary terms, the divergence of cytosolic and mitochondrial CK isoenzymes predates the development of more specific subtypes. The mitochondrial isoenzymes are also notable for the presence of N-terminal transit peptide sequences, which are responsible for targeting of the protein to mitochondria.

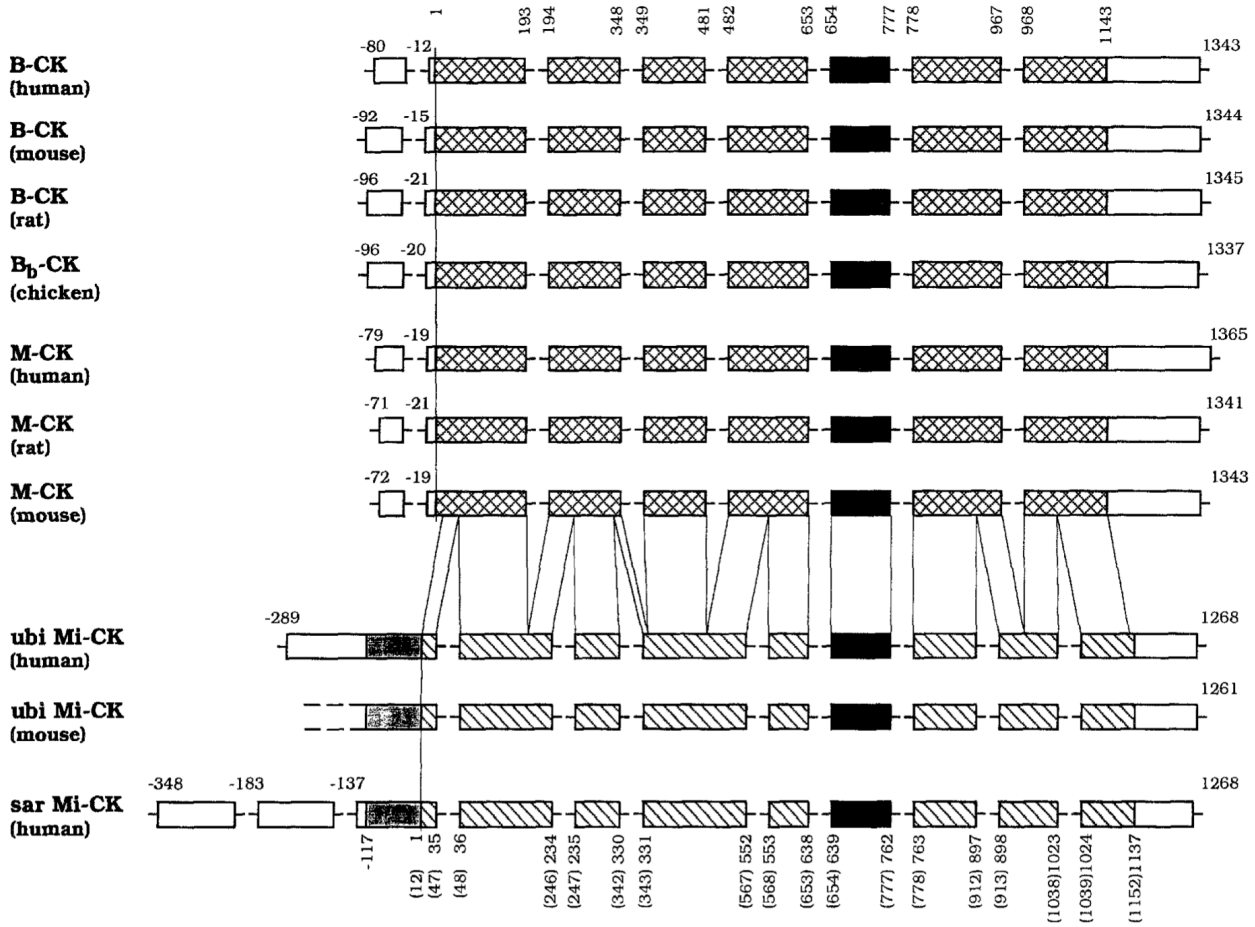


Figure 1-3: Genetic homology of mammalian and avian CK isoenzymes.

Boxes represent exons, which are largely conserved across isoenzymes and species (note that intronic regions are not to scale). There are differences in splice sites between the cytosolic and mitochondrial CK isoenzymes, with the exception of the solid black exon (#8 in sCKmt, #6 in other genes). The N-terminal transit peptide sequences of the mitochondrial isoenzymes are shaded. Figure from Mühlebach *et al.*[45]

1.2.4.2. Tissue specificity of creatine kinase isoenzyme expression

Creatine kinase expression is generally highest in tissues with high energy demands; however, there are significant differences between the individual CK isoenzymes with respect to their tissue distribution[31,46,47], including between the two mitochondrial isoenzymes[48] (Table 1-1). CK-M and sarcomeric CKmt are both exclusively expressed in striated muscle. The ratio between CK-M and sCKmt activity varies between skeletal and cardiac muscle; in rodents, CK-MM is responsible for ≥95% of total CK activity in skeletal muscle, but only 50-70% in ventricular muscle[49,50]. It has been suggested that this difference corresponds to the metabolic profile of these types of muscle. Fast-twitch skeletal muscle produces the majority of its energy

by glycolysis, and cytosolic CK-MM is the predominant isoform. Cardiac and slow-twitch muscle rely to a greater extent on mitochondrial oxidative phosphorylation for generation of ATP, and therefore require higher CKmt activity to export high-energy phosphates from the mitochondria. Further evidence linking the balance between cytosolic/mitochondrial CK isoenzymes and metabolic profile is provided by studies into the effects of endurance training on skeletal muscle – in both animal models[51] and human subjects[52], the shift towards slow-twitch fibers and oxidative metabolism is accompanied by an increase in mitochondrial CK activity, and a decrease in cytosolic CK. This suggests that cytosolic/mitochondrial CK isoenzyme distribution is closely and dynamically linked with cellular energetic phenotype.

Expression of CK-B and ubiquitous CKmt follows a broader pattern. CK-B and uCKmt are expressed concurrently in a wide variety of non-muscle tissues[47]. In addition, CK-B expression is present in the myocardium, but negligible in skeletal muscle – since CK-M is specific to these tissues, the CK-MB heterodimer only occurs in the heart (with the exception of transient developmental expression of CK-MB in skeletal muscle, as described below). The contribution of CK-B to myocardial CK activity is relatively low, with CK-MB and CK-BB combined constituting <5% of total CK activity in the murine heart.

CK Isoenzyme	Functional unit	Subcellular localization	Tissue expression
CK-M	Homodimer (MM)	Cytosolic Sarcomeric	Myocardium (mammalian), skeletal muscle
CK-B	Heterodimer (MB)	Cytosolic	Myocardium (mammalian) Skeletal muscle (during development)
	Homodimer (BB)	Cytosolic	Myocardium (avian), several tissues including brain, intestine, kidney, placenta, spermatozoa Myocardium (mammalian: low-level and developmental expression), skeletal muscle (during development)
Mitochondrial (ubiquitous)	Dimer/ octamer	Mitochondrial (intermembrane space)	Several tissues including brain, intestine, kidney, placenta, spermatozoa
Mitochondrial (sarcomeric)	Dimer/ octamer	Mitochondrial (intermembrane space)	Myocardium, skeletal muscle

Table 1-1: Subcellular localization and tissue-specific expression of CK isoenzymes.

1.2.4.3. Creatine kinase isoenzyme expression during development

While the CK isoenzymes differ with respect to their tissue distribution, there are also significant changes in their expression patterns during embryonic and post-natal development. In the mouse embryo, CK-B mRNA is expressed in the myotomes as early as 8.5 days post-coitum; CK-M is not detectable until day 13[53]. Studies in rats have shown that myocardial CK (and Cr transporter) expression increases significantly after birth, in parallel with a shift towards increased oxidative metabolism[54]. Furthermore, there is a perinatal transition between CK-B and CK-M; while CK-BB is the predominant isoform *in utero*, its expression decreases rapidly in the first weeks of life, as it is progressively replaced by CK-MB and ultimately CK-MM (although a low level of CK-MB and CK-BB expression is maintained)[55]. A similar, but more complete, developmental switch is observed in skeletal muscle, with CK-B expression negligible in adult life. Other tissues, such as brain or intestine, do not undergo this transition, and continue to express CK-B at relatively high levels.

The mitochondrial CK isoenzymes also exhibit distinct temporal expression patterns. In the rat embryo, ubiquitous CKmt is expressed in brain and intestine[56]. Expression of sarcomeric CKmt is not detectable in any tissue *in utero*, but increases rapidly by 28 days post-partum, in both skeletal and cardiac muscle. It is worth noting that uCKmt is not expressed in these tissues at any stage of development; therefore, unlike the cytosolic isoenzymes, there is a clear distinction between tissues which express uCKmt or sCKmt, rather than a developmental switch between expression of the two isoforms.

1.2.4.4. Protein structure and localization

The first detailed crystal structure of a CK enzyme to be published was chicken sarcomeric mitochondrial CK[57]. The sCKmt monomer consists of two domains – a relatively small series of 5 α-helices, and a larger domain comprising an 8-stranded β-sheet flanked by 7 α-helices. Due to the presence of specific contact site regions, sCKmt aggregates to form homodimers, which in turn combine to form symmetrical, cuboidal octamers, approximately 93 Å across, with a 20 Å central channel. The octameric structure of mitochondrial

CK appears to be particularly significant for association of the protein complex with the mitochondrial membranes[58,59]. Conserved residues, corresponding to the "CK framework" described above, form a compact cluster, which constitutes the active site of the enzyme. Finally, the distribution of positively-charged lysine residues on the octamer surface suggests that these domains may mediate interaction with negatively-charged mitochondrial membranes.

Subsequent studies have solved the crystal structures of the remaining CK isoenzymes. The structure of rabbit CK-MM dimer was described by Rao *et al.*, who identified putative active sites and dimerization interfaces in the protein[60]. Eder *et al.* established the most detailed structure of a CK enzyme to date by visualizing chicken CK-BB at a resolution of 1.41 Å, and noted that dimer formation may be mediated by structural differences in the N-terminal domains between CK-B monomers[61]. Finally, the structure of human ubiquitous CKmt was published by Eder *et al.*, and the protein was found to form similar octamers to those described for sCKmt[62].

More recently, crystal structures have been described for the human CK-MM[63] and CK-BB[64] dimers. The structure of human sCKmt has been deposited in the RCSB Protein Data Bank by Raveh *et al.* (ref. 2GL6), but remains unpublished. The crystal structures of all four human CK isoenzymes are presented in Figure 1-4. While this thesis deals specifically with the murine CK enzymes, and their crystal structures have not been published to date, the significant degree of sequence homology between human and murine CK isoforms suggests that their structure is likely to be similar.

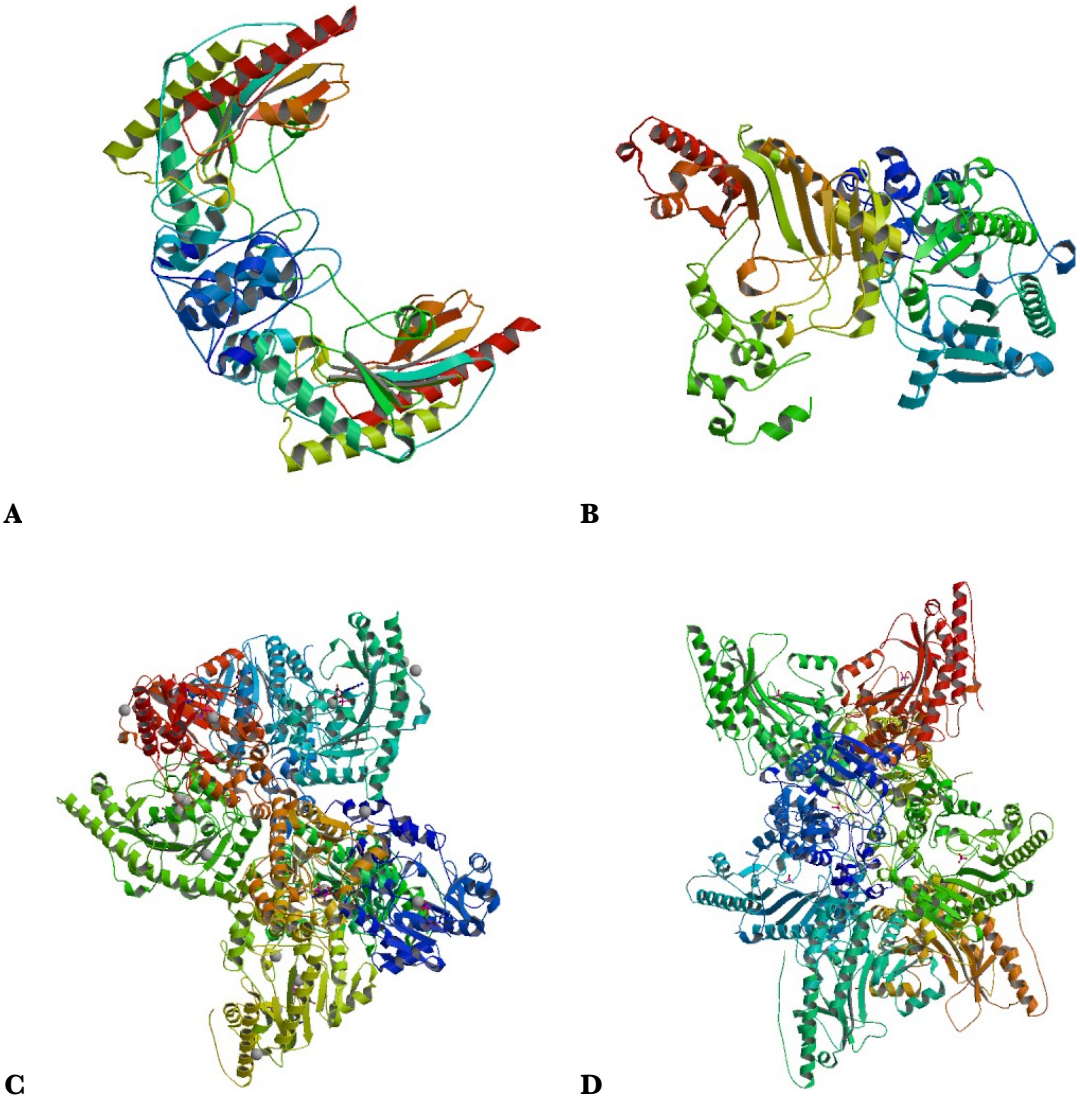


Figure 1-4: Crystal structures of the human creatine kinase isoenzymes.

(A) CK-MM dimer (Protein Data Bank ref. 1I0E). **(B)** CK-BB dimer (3DRE). **(C)** Sarcomeric CKmt octamer (2GL6). **(D)** Ubiquitous CKmt octamer (1QK1). All images were obtained from the RCSB Protein Data Bank website (http://www.rcsb.org/pdb/).

The individual functions of the CK isoenzymes are associated with specific subcellular localizations and structural interactions. CKmt octamers are tightly packed into the mitochondrial intermembrane space, both at the periphery of the mitochondrion and along the cristae[65]. CKmt is particularly associated with contact sites, where the distance between the inner and outer membranes is decreased[66], and is thought to contribute to the stabilization of these sites[67]. Of the cytosolic isoenzymes, CK-MM is known to be closely associated with the sites of energy utilization, particularly the sarcomeric myosin ATPase and sarcoplasmic reticulum[68,69]. Relatively little is known about the subcellular localization or functional associations of CK-

MB or CK-BB; in avian and amphibian cardiac muscle, where CK-B is the predominant cytosolic enzyme, there is no evidence for coupling of CK activity to the contractile apparatus[69].

1.2.4.5. Regulation of creatine kinase expression and activity

There is evidence that expression and activity of the creatine kinase enzymes is regulated at both the transcriptional and post-translation levels.

1.2.4.5.1. *Transcriptional regulation of creatine kinase expression*

The significant variation between CK isoenzymes with respect to tissue and developmental expression patterns is reflected in the diversity of regulatory elements present in their respective genes. Expression of the cytosolic isoform specific to striated muscle, CK-M, is strongly dependent on an upstream 5' flanking sequence[70], containing binding sites for the transcription factors MEF2[71] and MyoD[72]. Expression of sarcomeric mitochondrial CK (sCKmt) follows a similar distribution, and is primarily regulated by an analogous 5' sequence with a MEF2 binding site[46,73].

Unlike the muscle-specific isoenzymes described above, cytosolic CK-B and the ubiquitous isoform of mitochondrial CK (uCKmt) are expressed in a wide range of tissues, often concomitantly. While CK-B shares some common regulatory sequences with CK-M[74], expression also appears to be affected by sequences within the coding sequence itself[75]. In addition, it has been suggested that the high degree of interspecies homology in the 3'UTR of CK-B and uCKmt indicates that this region may contain further regulatory sequences[76]. Finally, there is evidence that expression of both CK-B and uCKmt is regulated by a variety of steroid hormones[77,78].

1.2.4.5.2. *Post-translational regulation of creatine kinase activity*

In addition to changes in gene expression, there is evidence that CK activity can be regulated at the protein level. Two main mechanisms have been identified – phosphorylation and oxidation.

Phosphorylation by intracellular kinases is a common method of modifying protein function, and has been implicated in regulation of CK activity. A study into potential links between regulation of energy metabolism by AMP-activated protein kinase (AMPK) and the CK system found that AMPK phosphorylates the cytosolic CK-MM dimer, inhibiting its activity[79]. This result was, however, called into question by a subsequent study, which found that the effect of AMPK on CK activity may depend on the experimental model[80]. More recently, it was demonstrated that phosphorylation of CK in frog skeletal muscle is associated with an *increase* in enzymatic activity[81]. In addition to AMPK, M-CK is also a substrate for protein kinase C; interestingly, phosphorylation was found to have opposite effects on the forward and reverse CK reactions (favoring synthesis of PCr over ATP)[82]. Finally, it has been demonstrated that mitochondrial CK also undergoes phosphorylation, although the functional consequences have not been studied[83]. Therefore, while there is strong evidence that CK isoenzymes are substrates for phosphorylation by kinases, the precise mechanisms by which phosphorylation affects CK activity remain unclear.

There is evidence that cytosolic CK-M exists in two forms, reduced and oxidized. Oxidation of CK has been shown to inhibit enzymatic activity, and possibly destabilize tertiary structure of the protein[84]. Furthermore, oxidation is thought to promote degradation of CK, possibly via ubiquitination by muscle ring finger protein 1 (MuRF1)[84]. Studies in transgenic mice lacking[85] or overexpressing[86] MuRF1 have found that CK turnover is affected by changes in MuRF1, suggesting a causal role of MuRF1 in CK degradation.

Finally, a study into the effects of aging on skeletal muscle discovered other types of post-translational modification of CK, such as carbonylation and 3-nitrotyrosine modification[87]. It is unclear whether these processes play a role in physiological regulation of CK activity, but they may contribute to the progressive loss of CK activity in aging, as well as under pathological conditions of increased oxidative stress.

1.3. The creatine kinase system in heart failure – results of observational studies

There is a significant body of evidence documenting the existence of metabolic impairment in heart failure, both in experimental models and in human patients. Although the failing heart has been described as "an engine out of fuel[25]," myocardial ATP levels are sustained until relatively late in the progression of heart failure, ultimately decreasing by only ~30%[88,89]. Phosphocreatine levels decline to a greater degree, commonly ~50%[89,90], which is due in part to a decline in total creatine pool as a result of downregulation of creatine uptake[91,92]. In addition to decreased substrate availability, the activity of CKmt and CK-MM is reduced (conversely, there is an *increase* in CK-BB activity, but the absolute level of CK-B expression is too low to compensate for the loss of CKmt and CK-M)[90,93-96]. Significantly, these changes are observed across several mammalian and non-mammalian species, regardless of the etiology of heart failure, suggesting that they are inextricably linked to the disease process[97].

In addition to experimental studies in animals, clinical observational studies have demonstrated that myocardial energetics are progressively impaired in human disease. A recent study found that ATP flux through the CK reaction is reduced in a step-wise manner in left ventricular hypertrophy (by 30%) and heart failure (65%), despite normal metabolite concentrations[98], suggesting that impairment of the global function of the CK system correlates with disease progression. Furthermore, a study in patients with dilated cardiomyopathy found that PCr:ATP ratio was found to be of similar value to NYHA functional class in prediction of mortality, and a better predictor than ejection fraction[99]. Perhaps most strikingly, PCr:ATP ratio was found to increase in response to treatment, in patients with coronary artery disease undergoing revascularization[100] and following pharmacological treatment of dilated cardiomyopathy[101].

While these findings clearly demonstrate a link between heart failure and disturbances in myocardial energetics, it is difficult to assess whether there is a causal relationship on the basis of observational studies alone. The following section describes models which have attempted to address this question by using

pharmacological or genetic tools to modify energy metabolism, particularly in the context of modulation of the CK system.

1.4. Experimental loss-of-function in the creatine kinase system

This section describes pharmacological and genetic models which sought to determine the physiological importance of an intact CK system, by targeting substrate availability (creatine) or enzymatic activity (CK isoenzymes).

1.4.1. Models targeting creatine synthesis or availability

1.4.1.1. Pharmacological inhibition of creatine uptake

Early studies into the effect of reducing creatine content relied on competitive inhibitors of creatine transport, such as β-guanidinopropionate (β-GPA)[102]. Chronic administration of β-GPA leads to a progressive decline in intracellular creatine levels, particularly in skeletal and cardiac muscle[103]. Studies in rats have demonstrated that administration of β-GPA leads to a decrease in myocardial PCr, CK flux, and ATP levels, and is associated with impairment of contractile function comparable to the effect of a myocardial infarction[104]. Most strikingly, induction of myocardial infarction by coronary artery ligation in rats pre-treated with β-GPA led to 93-100% mortality, in two independent studies[104,105]. While this indicates that β-GPA administration is detrimental to the heart, there are several factors which limit the conclusions that can be drawn from these studies. First of all, it is difficult to distinguish between a specific effect of creatine depletion, and non-specific toxic effects of β-GPA itself – particularly since these models were confounded by severe weight loss. Furthermore, creatine depletion in response to β-GPA feeding is a gradual process, taking several weeks, and it is possible that residual creatine may have been present in these models. Finally, β-GPA

itself is a substrate for the CK reaction, which could influence the energetic phenotype. Due to these limitations, these studies have been largely supplanted by targeted genetic models, which provide an alternative approach by specifically targeting creatine synthesis or uptake, without the requirement for pharmacological tools with potential off-target effects.

1.4.1.2. Genetic ablation of creatine synthesis

1.4.1.2.1. *Guanidinoacetate-N-methyltransferase knockout mice (GAMT$^{-/-}$)*

In order to determine the effect of creatine depletion, Isbrandt's group established a line of GAMT$^{-/-}$ mice, which lack the final enzyme in the creatine biosynthesis pathway[106]. They found that GAMT deficiency was associated with increased neonatal mortality, low body mass, muscular abnormalities, and male infertility. Our group studied these mice as a model of creatine depletion in the heart[107]. Provided that GAMT$^{-/-}$ mice are maintained on a diet free of exogenous creatine and housed separately from wild-type littermates (which prevents consumption of excreted creatine by coprophagia), their myocardial creatine levels are undetectable. Despite the lack of creatine, these mice do not exhibit left ventricular hypertrophy or dysfunction up to 1 year of age, suggesting that creatine is not obligatory for myocardial function under normal conditions[108]. This may be explained by a concomitant increase in the creatine precursor, guanidinoacetate (GAA), which can also undergo reversible phosphorylation and act as an energy reservoir, albeit at significantly lower rates than creatine itself (~1% of the reaction velocity for creatine)[109]. *In vivo* hemodynamic experiments demonstrated that contractile reserve in response to dobutamine stimulation was blunted in these mice. In *ex vivo* ischemia/reperfusion, recovery of systolic and diastolic function was also impaired; unlike wild-type hearts, which replenished PCr stores within minutes of reperfusion, GAMT$^{-/-}$ hearts were unable to re-phosphorylate GAA to pre-ischemic levels. These findings indicate that, although creatine may not be absolutely required for normal cardiac function, it plays a significant role in energy metabolism under conditions of increased workload or ischemic injury.

More recently, follow-up studies have examined GAMT$^{-/-}$ mice in more detail. In measurements of running performance, GAMT$^{-/-}$ mice were surprisingly found to have the same voluntary and forced exercise capacity as wild-types[110]. In chronic myocardial infarction experiments, there was no difference between GAMT$^{-/-}$ and wild-type mice with respect to survival, ventricular remodeling, or development of heart failure. No significant adaptations were observed in proteomic studies or alternative phosphotransfer systems[110], and no compensatory changes were detected in mitochondrial organization[110,111]. These findings are in stark contrast to earlier studies of pharmacological creatine depletion by administration of β-GPA in rats, which were associated with near-total mortality within 24 hours of coronary ligation[104,105]. In order to resolve this apparent contradiction, the β-GPA study was replicated in wild-type and GAMT$^{-/-}$ mice, to determine whether β-GPA was exerting a cardiotoxic effect by mechanisms other than creatine depletion[110]. There was no mortality in either group, indicating that the link between β-GPA and post-infarct mortality may be species-specific. This finding, combined with the observation that creatine-deficient GAMT$^{-/-}$ mice have normal cardiac function at baseline, suggests that the more modest reduction in myocardial creatine observed in cardiac disease models (10-50%)[97] may not be as harmful as previously thought.

1.4.1.2.2. *Arginine:glycine amidinotransferase knockout mice (AGAT$^{-/-}$)*

Since interpretation of the results of studies in GAMT$^{-/-}$ mice may be confounded by elevated GAA levels, an additional transgenic model was generated, lacking the first enzyme in the creatine synthesis pathway, AGAT[112,113]. The reaction catalyzed by AGAT is required for formation of GAA; therefore, AGAT$^{-/-}$ mice are deficient in both creatine and GAA, and should not have a functional CK phosphotransfer system. Initial studies assessed the effect on skeletal muscle, and found that AGAT$^{-/-}$ mice had 50% lower ATP levels, with signs of muscular atrophy. Significantly, these abnormalities were rapidly corrected by creatine feeding, suggesting that deficiency of creatine/GAA was the cause of the skeletal muscle phenotype in these mice. Our group is currently conducting studies to determine the effect of AGAT$^{-/-}$ on the myocardium, and initial results indicate that cardiovascular function is impaired, but this phenotype is *not* due to creatine deficiency[114]; further work is ongoing. Finally, it has recently been demonstrated that AGAT is also

responsible for synthesis of homoarginine, indicating that the AGAT$^{-/-}$ mouse is not a model of pure creatine deficiency[115], which can confound interpretation of these results.

1.4.1.2.3. *Creatine transporter knockout mice (CrT$^{-/-}$)*

An alternative strategy to test the effect of creatine depletion is to abolish cellular uptake, rather than synthesis, of creatine. Transgenic mice lacking the creatine transporter (CrT$^{-/-}$) have recently been developed as a model of human CrT deficiency, and were found to have impaired memory and learning capacity[116]. The cardiac phenotype has not been studied in these mice; however, the authors reported that although creatine was not detectable in the brain or skeletal muscle, it was present in several tissues, including heart (albeit at ~20% of wild-type levels). Since the model is a ubiquitous, constitutive CrT knockout, and the heart is thought to depend entirely on the CrT for accumulation of creatine, this calls into question the validity of the model. Therefore, further validation work is required before any conclusions can be drawn.

1.4.2. Models targeting the creatine kinase isoenzymes

1.4.2.1. Pharmacological inhibition of creatine kinase activity

To date, no specific pharmacological inhibitors of CK activity have been described; however, certain compounds, such as gliotoxin[117] or iodoacetamide[118] have been shown to inhibit CK activity, and the latter has been applied to study the effect of CK inhibition in the myocardium[118-120]. Administration of iodoacetamide during *ex vivo* perfusion was not found to affect cardiac function at baseline, which is in agreement with the hypothesis that the CK system is not required under normal conditions; however, the contractile response to increased workloads was impaired. Significantly, this effect was found to be dose-dependent, with reduction of CK activity to 1% of baseline levels associated with a 72% decrease in contractile reserve[120]. However, these results should be interpreted with caution, as the effects of iodoacetamide may be at least partially due to additional, non-CK targets, such as inhibition of the glycolytic

enzyme glyceraldehyde-3-phosphate dehydrogenase[118]. More specific conclusions can be drawn from the results of studies in genetic knockout models, as described below.

1.4.2.2. Transgenic loss-of-function models

1.4.2.2.1. *M-type CK (CK-M$^{-/-}$), sarcomeric mitochondrial CK (CKmt$^{-/-}$), and double (M/Mt-CK$^{-/-}$) knockout mice*

In order to determine the effect of specific ablation of the creatine kinase isoenzymes in striated muscle, transgenic models were developed by knocking out CK-M[121], CKmt[122], and both CK-M and CKmt[123]. Rather than addressing each isoenzyme individually, these models are discussed in conjunction, as they were frequently analyzed in parallel.

In the initial study describing the CK-M$^{-/-}$ model, contractile function and high-energy phosphate metabolism were evaluated in skeletal muscle of CK-M$^{-/-}$ mice[121]. There was no impairment of maximal force of contraction, and PCr and ATP levels were normal; however, rapid burst activity was abolished, and phosphate flux between PCr and ATP was significantly decreased. In a subsequent study, analogous results were observed in cardiac muscle – maximal tension was normal, but the rate of tension development was significantly slower in myocardial samples from CK-M$^{-/-}$ mice[124]. This indicates that, in this model, the amount of energy available to the contractile apparatus is not affected, but the rate at which it can be delivered is limited due to lack of the local ATP-replenishing activity of CK-M.

CKmt$^{-/-}$ mice were developed shortly after the CK-M$^{-/-}$ model[122], and a double-knockout model was derived by the same group[123]. Initial studies into the effect of CK ablation in the myocardium were performed by *ex vivo* perfusion of hearts from CK-M$^{-/-}$ and M/Mt-CK$^{-/-}$ mice[125]. There was no significant difference with respect to cardiac function in either line, at baseline or under increased workload. However, assessment of high-energy phosphate metabolism by ^{31}P-MRS demonstrated a 95% elevation in ADP during increased work in M/Mt-CK$^{-/-}$ mice, which was not observed in M-CK$^{-/-}$ or wild-types. There was a corresponding decrease in $|\Delta G_{ATP}|$, suggesting that while hearts lacking CK-M and CKmt are capable of sustaining

contractile function, an imbalance develops when energetic requirements are increased. These findings were replicated in CKmt$^{-/-}$ mice, which had normal function, but a two-fold increase in ADP and ~30% reduction in PCr under increased workload[126]. In an *ex vivo* ischemia/reperfusion study, ischemic contracture was found to be more severe and develop earlier in M/Mt-CK$^{-/-}$ hearts, compared to wild-types[127]. Diastolic calcium concentrations were significantly higher in M/Mt-CK$^{-/-}$ hearts, suggesting that impaired calcium handling may be responsible for this effect. Functional recovery during reperfusion was also adversely affected, with impaired recovery of diastolic function and delayed recovery of systolic function.

In addition to studies in perfused hearts, the effect of CK-M and CKmt ablation on cardiac phenotype has been studied *in vivo*[128]. Baseline cardiac MRI demonstrated that CK-M$^{-/-}$, CKmt$^{-/-}$, and M/Mt-CK$^{-/-}$ mice had normal ejection fraction at 10 months. There was, however, a significant degree of LV hypertrophy and dilatation in both CKmt$^{-/-}$ and M/Mt-CK$^{-/-}$ mice, neither of which was observed in CK-M$^{-/-}$. The apparent discrepancy between normal function and LV hypertrophy was addressed in a follow-up study, in which multimodal MR imaging again demonstrated normal ejection fraction, but decreased maximal contraction velocity and reduced myocardial perfusion[129]. This suggests that, while global cardiac function was not obviously impaired, there may have been more subtle abnormalities which contributed to the phenotype (although it remains possible that these differences were secondary to LV hypertrophy). Perhaps surprisingly, infarct studies found that there was no difference in survival between M/Mt-CK$^{-/-}$ and wild-type mice, and the degree of LV hypertrophy and dilatation was similar in both groups[128].

The results of previous studies in knockout mice are not entirely consistent, particularly with respect to development of left ventricular hypertrophy. This may be due in part to the fact that these models were originally generated on a mixed genetic background (C57BL/6 / 129sv), which could cause unpredictable variation between various cohorts – particularly when mice were generated by KO x KO breeding, which would not yield wild-type littermate controls. To resolve this issue, our group backcrossed CKmt$^{-/-}$ mice onto a pure C57BL/6 background for ≥10 generations, and determined that these mice did not develop left ventricular hypertrophy or dysfunction[130]. Interestingly, CKmt$^{-/-}$ were found to have increased CK-MM

activity and mitochondrial volume, which may be compensatory changes aimed at preserving energy metabolism in the absence of CKmt.

Our group also conducted a similar study to determine the effect of background strain on development of hypertrophy in M/Mt-CK$^{-/-}$ mice at 1 year of age[131]. Mice on a mixed background were found to develop left ventricular hypertrophy and heart failure, as observed in other studies, although females were less severely affected than males. Mice backcrossed onto a C57BL/6 background had impaired indices of systolic and diastolic function and decreased contractile reserve, but did not develop spontaneous left ventricular hypertrophy or heart failure. This suggests that, while chronic ablation of the myocardial CK system may have a detrimental effect, the phenotype is not as severe as could be expected, and may depend on other factors, such as background strain, gender, or age.

It is worth noting that several adaptations have been observed in CK-knockout mice, which may further complicate interpretation of these results. One of the initial studies on CKmt$^{-/-}$ mice observed that phosphotransfer between creatine and ATP was normal in skeletal muscle[122], and a subsequent study found that regulation of mitochondrial oxidative phosphorylation by cytosolic ADP was preserved, despite the absence of CKmt[132]. These findings could be attributed to cytosolic CK-MM compensating for the lack of CKmt, and possibly relocating to the outer mitochondrial membrane to replace the local ADP-processing function of CKmt. A study by our group found that CK-MM activity was increased in CKmt$^{-/-}$ mice on a pure C57BL/6 background, with a concomitant increase in citrate synthase activity, a marker of mitochondrial volume[130]. It was argued that these could be compensatory mechanisms; however, when mice lacking both CKmt and CK-M were studied on a pure C57BL/6 background, no differences in citrate synthase activity were observed[131]. It is also possible that additional phosphotransfer systems play a compensatory role in CK-deficient hearts. The original paper describing the double-knockout model (on a mixed genetic background) noted lipid accumulation, which was interpreted as a consequence of decreased fatty acid β-oxidation and an increased reliance on glycolysis[123]. It was subsequently shown that the glycolytic pathway can effectively replace the function of the CK system in fueling the sarcoplasmic reticulum Ca^{2+} ATPase, but not the contractile apparatus[133]. Dzeja *et al.* observed increased mitochondrial and glycolytic

capacity in CK-deficient mice, as well as increased flux through the adenylate kinase system and guanine nucleotides, providing further evidence that other networks may be able to compensate for lack of a functional CK system[134]. An alternative mechanism was proposed by Kaasik *et al.*, who found evidence of direct channeling of adenine nucleotides between the mitochondria and sites of energy utilization, suggesting that alternative phosphotransfer systems may not be required to sustain an ATP/ADP shuttle[135].

In summary, the results of studies in transgenic mice lacking CKmt and/or CK-M are difficult to interpret. In addition to significant differences between the studies themselves, *e.g.* with respect to background strain, there are several possible adaptations to CK deficiency which may be confounding the phenotypes observed in these studies.

1.4.2.2.2. *Ubiquitous mitochondrial CK (uCKmt$^{-/-}$), B-type CK (CK-B$^{-/-}$), and double (B/uMt-CK$^{-/-}$) knockout mice*

The remaining CK isoenzymes, ubiquitous mitochondrial CK and B-type CK, do not play a major role in myocardial high-energy phosphate metabolism. Since cardiac phenotype has not been evaluated in the relevant knockout models, they will only be discussed briefly to demonstrate parallels between the consequences of sCKmt/CK-M ablation in muscle, and uCKmt/CK-B ablation in brain.

The first description of uCKmt$^{-/-}$ mice simply noted that these mice were viable, fertile, and demonstrated no overt phenotype[136]. Since uCKmt is expressed in the brain, a follow-up study examined neurological function in these mice in more detail, and found a degree of learning impairment, without changes in sensory or motor function[137]. In parallel, mice lacking CK-B were developed[138], and the energetic effect of CK-B ablation in brain was similar to that observed in CK-M-deficient muscle[121] – namely, PCr and ATP levels were normal, but energy transfer between PCr and ATP was impaired. Neurological findings in CK-B$^{-/-}$ mice were similar to those observed in uCKmt$^{-/-}$, and it was suggested that the relatively mild phenotype in this model may be explained by compensatory effects of uCKmt[138]. To determine whether this was the case, double-knockout (B/uMt-CK$^{-/-}$) mice were generated[139]. These mice had severely impaired learning ability,

as well as morphological changes in cerebral tissue, suggesting total ablation of the CK system in brain cannot be adequately compensated by other adaptations.

1.5. Experimental gain-of-function in the creatine kinase system

While a significant amount of effort has been devoted to the study of loss-of-function models in the creatine kinase system, it is difficult to unequivocally delineate the effects of CK impairment, as described above. An alternative approach is to study gain-of-function models, by specifically augmenting individual elements of the CK system. This has the added benefit of testing the experimental hypothesis that the CK system is a potential therapeutic target, as interventions aimed at improving CK-mediated phosphotransfer would be expected to improve outcomes in models of cardiac disease.

To date, no pharmacological tools have been developed to specifically increase the activity of the CK system; however, two transgenic lines of myocardial gain-of-function mice have been described. The first model, developed by our group, increased substrate availability by overexpressing the creatine transporter. The second, published during the course of the current project by Weiss's group, is a model of inducible overexpression of CK-M. In addition, transgenic mice expressing CK isoenzymes in liver have also been described. These models are discussed in detail below, as they provide important proof-of-principle that targeted augmentation of the CK system can have cardioprotective effects.

1.5.1. Overexpression of the creatine transporter

Myocardial creatine uptake is an active process, limited by the activity of the creatine transporter (CrT). Supplementation of exogenous creatine does not lead to increases in its intracellular concentration[140] due to downregulation of CrT activity and possibly intracellular sequestration of the CrT[141]. In order to overcome this limitation, our group developed two lines of transgenic mice, constitutively overexpressing the CrT in the

heart, under the control of the ventricular myosin light chain 2 (MLC2v) promoter[142]. Transgenic mice were found to accumulate supranormal amounts of creatine in the myocardium, and initial experiments were performed in the line with higher myocardial creatine content (Tg55, intracellular Cr 133±52 nmol/mg protein [range, 65-240] vs 66±6 [58-74] in wild-type controls). Surprisingly, these mice developed left ventricular hypertrophy, dilatation, and contractile dysfunction at 5-9 months; furthermore, indices of structural abnormality and functional impairment correlated with [Cr], suggesting that this was a dose-dependent effect. Phosphorus MR spectroscopy confirmed that Tg55 mice had higher myocardial phosphocreatine content (1.4- to 2.4-fold), although the PCr:Cr ratio was inversely related to [Cr], suggesting that cardiomyocytes with a large creatine pool were unable to keep it phosphorylated (it was also confirmed that there was no change in CK activity). Significantly, there was a correlation between myocardial creatine and free ADP, which were elevated up to 2-fold. This accumulation of ADP to supranormal levels may explain the phenotype, as it was associated with a decrease in $|\Delta G_{ATP}|$, which would reduce the energy yield of ATP hydrolysis, paradoxically mirroring the energetic imbalance observed in heart failure. Subsequent experiments demonstrated that glycolytic capacity, particularly enolase activity, is impaired in these mice, suggesting that additional metabolic adaptations may contribute to the phenotype[143].

While a large elevation in myocardial [Cr] was found to be detrimental, it was hypothesized that a more moderate increase could augment energy reserves, without the toxic effects of ADP accumulation. Mice from the second transgenic line, Tg46, were selected based on a 20-100% increase in myocardial [Cr], and were found to have normal cardiac structure and function up to 18 months[144]. In chronic heart failure experiments, cardiac function and survival were similar in Tg46 mice and controls matched for infarct size, indicating that creatine elevation was neither detrimental nor beneficial (assuming a similar magnitude of the initial injury). However, in acute infarct studies Tg46 mice were found to be protected against ischemia/reperfusion injury, with a 27% reduction in infarct size compared to wild-type controls. Furthermore, in *ex vivo* ischemia/reperfusion experiments, Tg46 hearts demonstrated a slower decrease in rate-pressure product during early ischemia, shorter period of hypercontractility on reperfusion, and improved functional recovery. There was no observable difference in ATP levels during ischemia/reperfusion, although this may have been due to the temporal resolution of ^{31}P-MRS (~5min).

Tg46 hearts had higher PCr levels before and after reperfusion, although PCr was effectively consumed in both groups during ischemia. There was also a trend towards decreased ADP levels, which was in turn associated with a higher $|\Delta G_{ATP}|$, theoretically increasing the energy yield from an equivalent concentration of ATP. This is of particular interest in the context of the shorter period of post-reperfusion hypercontractility observed in Tg46 hearts, as maintaining $|\Delta G_{ATP}|$ could sustain the function of sarcoplasmic reticulum Ca^{2+} ATPase, ensuring more rapid removal of cytosolic Ca^{2+} into the SR, thereby accelerating the correction of calcium overload.

1.5.2. Inducible overexpression of M-type creatine kinase

The first study to examine the effect of overexpressing creatine kinase in the heart was recently reported by Weiss's group[145,146]. In mice overexpressing CK-M in an inducible (tet-off) system, CK activity was increased 2-to-3-fold when transgene expression was activated by withdrawal of doxycycline. In *ex vivo* studies[146], transgenic hearts were characterized by improved recovery of both PCr levels and contractile function after ischemia/reperfusion. In addition, overexpression of CK-M attenuated ischemic acidosis, and was associated with reduced LDH release. There was no difference between groups with respect to creatine or ADP concentrations, or $|\Delta G_{ATP}|$.

In baseline *in vivo* studies[145], no significant differences were observed between mice overexpressing CK-M and controls with respect to cardiac structure, function, or high-energy phosphate metabolism. Pressure overload was induced by transverse aortic constriction (TAC) at 6-10 weeks, and transgenic mice were found to develop a similar degree of left ventricular hypertrophy to controls, but sustained a slightly higher PCr:ATP ratio. Transgenic mice were also characterized by improved myocardial function and contractile reserve post-TAC, and there was a significant reduction in mortality over a follow-up period of 2 months (~10% vs ~40% in controls). In a separate cohort, transgenic mice were randomized at 4 weeks post-TAC to either continue overexpressing CK-M, or switch off expression by administration of doxycycline. After a further 8 weeks, continued overexpression of CK-M was associated with improved contractile function, while mice in which the transgene had been inactivated had similar functional indices to controls. Therefore, while

overexpression of CK-M was found to be beneficial in this model of TAC-induced hypertrophy, it must be continued in order for the effect to be sustained, at least over a 12-week period. This suggests that increasing CK activity is causally responsible for preservation of contractile activity in this setting, and may prove effective as long-term treatment in chronic heart failure.

1.5.3. Transgenic expression of creatine kinase isoenzymes in liver

The first model of CK overexpression was a line of transgenic mice overexpressing CK-B in the liver, an organ which has negligible CK activity[147]. Livers overexpressing CK-B were found to be protected against ischemia/reperfusion injury, with a slower rate of ATP depletion and less pronounced acidosis and LDH release during ischemia, as well as improved recovery of pH and ATP during reperfusion[148]. While it is difficult to draw conclusions based on studies in a tissue which does not normally rely on a functional CK system, this suggests that improving ATP supply via the CK system may protect cells against the effects of ischemia/reperfusion injury. In addition to the CK-B mice, an additional model was generated, expressing human ubiquitous CKmt in the liver[149]. Expression of CKmt was associated with inhibition of the mitochondrial permeability transition pore, which plays a significant role in ischemia/reperfusion injury, including in the myocardium[150]. This provides further evidence that increasing activity of the CK system can protect against acute ischemia/reperfusion injury.

1.6. Summary and experimental aims

There is a significant body of experimental and clinical research linking impaired myocardial energetics with the progression of heart disease, but it has not yet been definitively demonstrated whether these changes are causal in nature – or whether correcting them can have a beneficial effect in a clinical setting. The results of knockout studies are somewhat inconsistent, but support the hypothesis that loss of function in the creatine kinase system is in itself detrimental to cardiac function, particularly under conditions of increased workload

and in disease models. To date, relatively few studies have examined the effects of increasing CK activity in the heart, but individual experiments from our laboratory and others indicate that this could be a therapeutic intervention. In order to address this question in more detail, the experiments described in the following chapters were performed to generate a comprehensive range of *in vitro* and *in vivo* models of CK overexpression, with the ultimate aim of using these models to study whether targeted intervention in the creatine kinase system is a potential candidate for development of novel therapies in human cardiac disease.

2. GENERAL MATERIALS AND METHODS

This chapter introduces the general materials and methods applied throughout this thesis. Methods specific to individual experiments are described in the relevant chapters.

2.1. Materials

2.1.1. Chemicals and laboratory equipment

Sources of reagents and other materials are noted on their first appearance in this thesis. Standard laboratory-grade chemicals were acquired from Sigma-Aldrich. Compositions of solutions and media are detailed in Appendix A.5.

2.1.2. Software

Word processing was performed in Microsoft Word (v. 14.3.9). Figures were plotted in Microsoft PowerPoint (v. 14.3.9), using selected images from the Servier Medical Art bank. Data processing and plotting were performed in Microsoft Excel (v. 14.3.9) and GraphPad Prism (v. 6.0c). Cloning constructs and primers were designed using Serial Cloner (v. 2.6), ApE (v. 2.0.45), EnzymeX (v. 3.1), 4Peaks (v. 1.7.2), PrimerBLAST (www.ncbi.nlm.nih.gov/tools/primer-blast), and OligoAnalyzer (v. 3.1). Quantitative PCR data were analyzed using BioRad CFX Manager (v. 2.0). Microscopy images were acquired and processed using IPLab (v. 3.7), Zeiss LSM 510, and ImageJ (v. 1.46). Spectrophotometric measurements were acquired using SWIFT II (v. 2.2.16). Flow cytometry data were analyzed using Summit (v. 4.3). References were managed using Papers (v. 2.7.1).

2.2. General methods

2.2.1. Tissue culture

2.2.1.1. Mammalian cell lines

Two different types of mammalian cells were used for *in vitro* experiments – HEK293 cells for general expression and validation of constructs, and cardiac-derived HL-1 cells for functional experiments in which it was desirable to use a line more closely related to cardiomyocytes.

2.2.1.1.1. *HEK293 cells*

HEK293 cells are a human-derived cell line, generated by transformation of cultured embryonic kidney cells with adenoviral DNA[151]. They are relatively easy to culture and transfect, and were therefore used for preliminary validation of transgenic constructs.

2.2.1.1.2. *HL-1 cells*

HL-1 cells (a kind gift from Dr. William Claycomb) are an immortalized cell line derived from the murine heart[152]. They were generated by serial passaging of an atrial tumor cell line, AT-1, which was originally developed by *in vivo* expression of the SV40 large T antigen under the control of the atrial natriuretic factor promoter[153]. Unlike AT-1 cells, which must be grown as tumor grafts *in vivo*, HL-1 cells can be cultured indefinitely *in vitro*. They retain several morphological, functional, and molecular characteristics of cardiomyocytes. HL-1 cells were therefore selected as a model for *in vitro* studies of cardiac cellular function.

2.2.1.2. Tissue culture conditions

2.2.1.2.1. *General culture conditions*

Cells were cultured in a humidified incubator at 37°C, 5% CO_2. HEK293 cells were grown in standard tissue culture vessels, in Dulbecco's modified Eagle medium supplemented with fetal bovine serum (FBS, 10%), L–glutamine (2mM), and penicillin/streptomycin (100U/ml, 100µg/ml). HL-1 cells were grown in pre-coated vessels (0.02% gelatin, 5µg/ml fibronectin), in Claycomb medium with FBS (10%, HL-1-specific batch #058K8426), L–glutamine (2mM), penicillin/streptomycin (100U/ml, 100µg/ml), and norepinephrine (0.1mM).

2.2.1.2.2. *Passaging*

Cells were passaged 2-3 times a week as required for experiments, after achieving confluence. HEK293 cells were washed with PBS, trypsinized for 2min (0.05% trypsin / 0.02% EDTA), washed with culture medium, and centrifuged at 500g for 5min. For HL-1 cells, an additional 2-5min trypsinization step was necessary to detach cells.

For long-term storage, confluent T75 flasks of cells were harvested by trypsinization, resuspended in freezing medium (95% FBS, 5% dimethyl sulfoxide), cooled overnight to -80°C in an isopropanol bath, and transferred to liquid nitrogen stocks.

2.2.1.3. Transfection of cultured mammalian cells

2.2.1.3.1. *Transient transfection*

Transfections were performed using the non-liposomal cationic lipid reagent FuGENE HD (Roche), which was found to yield the best results in HL-1 cells after optimization. Cells were seeded at 2.5–5.0 x $10^4/cm^2$, and transfected 24-48 hours after plating, at 60-90% confluence. Prior to transfection, culture media were changed to antibiotic-free media. Transfection mixtures were prepared in the reduced-serum medium Opti-

MEM (Invitrogen), and consisted of 10µl FuGENE HD and 2µg plasmid DNA in 100µl Opti-MEM per well (for a 6-well plate, scaled down for 12/24-well plates). Transfection mixtures were vortexed, incubated at room temperature for 30 minutes, and added directly to the cells. Optimization experiments indicated that 24-hour transfection yielded better results than shorter incubations (3/6h), without evidence of significant toxicity. Cells were therefore exposed to transfection mixture for 24h, washed with PBS, and subsequently incubated in standard culture medium. Further experiments were conducted at ≥48h post-transfection, to allow sufficient time for protein synthesis.

2.2.1.3.2. *Stable transfection*

Prior to selection of stably transfected cells, antibiotic sensitivity was determined empirically using a kill curve. Vectors were linearized by restriction digest before stable transfection, to ensure that vectors could integrate into genomic DNA without breakage in the expression cassette. Cells were transfected as described above, and culture media were supplemented with selective antibiotics from 48 hours post-transfection onwards. Individual antibiotic-resistant colonies were picked and expanded to establish stably transfected lines.

2.2.2. Mouse husbandry and use of tissues

2.2.2.1. Mouse husbandry

Animal experiments were conducted in accordance with Home Office regulations, specifically the Animals (Scientific Procedures) Act 1986, including Amendment Regulations 2012 (SI 2012/3039). Mice were housed in individually ventilated cages, in a specific-pathogen-free environment, on a fixed 12-hour light/dark cycle, and fed standard chow and water *ad libitum*. Generation of transgenic founder mice is described in sections 4.3.1 and 5.3.2; wild-type C57BL/6 breeding partners were obtained from Harlan UK Ltd. Pups were weaned at 3 weeks, and ear-notched for genotyping and identification purposes (see below).

2.2.2.2. DNA extraction from mouse ear biopsy

2.2.2.2.1. *Proteinase K digestion and ethanol precipitation*

DNA was extracted from ear biopsies by digestion in 500µl of lysis buffer (100 mM EDTA, 50mM Tris-HCl, 1% SDS, 200mM NaCl, 60µg/ml proteinase K) at 55°C overnight. DNA lysate was purified by addition of 600µl of isopropanol and centrifugation at 16,000g for 10min at room temperature. The supernatant was discarded and the pellet was precipitated by addition of 500µl of ethanol and centrifugation at 16,000g for 5min at room temperature. The final pellet was resuspended in 200µl of T0.1E buffer, and allowed to resuspend before further use (overnight at room temperature, or ≥48h at 4°C).

2.2.2.2.2. *HotSHOT DNA extraction*

Proteinase K digestion was the previously established method of DNA extraction in our lab; however, it has two significant limitations: (1) PCR failure was a recurring problem, and was found to be due to low DNA yield, and (2) it is a relatively time-consuming method, which became a significant consideration when multiple colonies were being generated and screened in parallel. To overcome these problems, alternative methods were researched, and the HotSHOT DNA extraction protocol was tested, as it is theoretically faster (notch-to-PCR ~1hr vs. ≥2 days), and more reliable (no risk of losing pelleted DNA due to lack of a centrifugation step) than proteinase K digestion[154].

Ear biopsies were harvested into a 96-well PCR plate, and incubated in 75µl of alkaline lysis buffer (25mM NaOH, 0.2mM EDTA, pH 12) at 95°C for 30min, followed by neutralization with 75µl of 40mM Tris-HCl (pH 5). Combining the two buffers yields a final solution similar to T0.1E, which is suitable for long-term storage of DNA. Direct comparison with proteinase K digestion found that HotSHOT produced a higher yield of DNA (>10µg per notch vs. ~5µg), but the DNA was less pure ($A_{260/280}$ ~1.5 vs. ~2.0) – as would be

expected, given the lack of a centrifugation step. The presence of impurities did not adversely affect PCR performance, and HotSHOT was therefore selected as the method of choice for DNA extraction.

2.2.2.3. Harvesting of tissues

Mice were sacrificed by cervical dislocation. Tissues were dissected as quickly as possible, excised, washed in heparinized saline (125 U/ml heparin in 0.9% NaCl), and immediately snap-frozen in liquid nitrogen. Cardiac chambers were harvested by removing and washing the heart as a whole, followed by *ex vivo* dissection of individual chambers. Tissues were powdered on dry ice using a percussion homogenizer, and stored at -80°C.

2.2.3. Polymerase chain reaction (PCR)

2.2.3.1. Reaction conditions

Cloning PCR was performed using Phusion high-fidelity DNA polymerase, in 50µl reactions. All other PCRs were performed using Immolase DNA polymerase, in 20µl reactions. Milli-Q water was used for all PCR buffers, and all pre- and post-PCR reagents and equipment were kept separate to avoid contamination; no-template controls were included in all reactions. $MgCl_2$ concentration was optimized for all reactions. Specific PCR protocols are detailed in the relevant chapters, and summarized in Appendix A.

2.2.3.2. Primers

Primers were designed using NCBI reference sequences as templates. Cloning primers were designed manually to incorporate the required restriction sites and features, and specificity was confirmed using PrimerBLAST. All other primers were designed using PrimerBLAST, and evaluated for specificity against the reference databases for *Mus musculus* mRNA (qPCR primers) or genomic DNA (all others). Finally,

OligoAnalyzer was used to exclude primers with unfavorable characteristics (*e.g.*, formation of hairpins or self-/hetero-dimers). Custom primers were purchased from Sigma-Genosys. Primer design and sequences are detailed in the relevant chapters, and summarized in Appendix A.2.

2.2.3.3. Agarose gel electrophoresis

DNA (*e.g.*, PCR product, restriction digest product) was separated by electrophoresis in 1.0% agarose gels, stained with 0.5μg/ml ethidium bromide. For gel extraction, 0.8% low-melting-temperature agarose was used. Electrophoresis was performed in TBE buffer, supplemented with 0.5μg/ml ethidium bromide. DNA ladders were used in all experiments, and are labelled in individual figures as required.

2.2.4. Molecular cloning of DNA constructs

2.2.4.1. Cloning vectors

The following vectors were used for cloning and protein expression:

pEGFP-N1	(Clontech)
pcDNA3.1+	(Invitrogen)
pcDNA3.1-	(Invitrogen)
pDNR-lib-CKMT2	(Source Bioscience)
αMHC-AMPK	(a gift from Dr. Arash Yavari)
CB92	(a gift from Dr. Ben Davies)
pEBFP2-nuc	(a gift from Dr. Matthew Daniels)

Detailed descriptions and maps of each vector are included in the relevant chapters.

2.2.4.2. Polymerase chain reaction (PCR)

Cloning PCR was performed in 50µl reactions using high-fidelity Phusion polymerase. Specific vectors containing the amplified sequence were used as templates if available; otherwise, reverse-transcription was performed using total cellular mRNA to generate cDNA, which was used as a template. Since PCR products were subsequently digested using restriction endonucleases, terminal caps were added to all primers to allow for enzyme binding, according to the manufacturer's guidelines (NEB). Prior to further processing, a 5µl aliquot of PCR product was separated by gel electrophoresis to confirm the presence and approximate size of product.

2.2.4.3. Extraction and precipitation of PCR products

PCR product was purified by phenol/chloroform extraction and ethanol precipitation. Tris-EDTA (pH 8) was added to a total volume of 100µl, mixed with 100µl of phenol/chloroform/isoamyl alcohol (25:24:1), vortexed, and centrifuged at 16,000g for 5min at room temperature. The aqueous phase was transferred to a new Eppendorf tube, mixed with 270µl of ice-cold 100% ethanol and 9µl of 3M sodium acetate, vortexed, allowed to precipitate for 30min at -20°C, and centrifuged at 16,000g for 15min at 4°C. The supernatant was removed, and the pellet was washed with ice-cold 70% ethanol, vortexed, and centrifuged at 16,000g for 5min at room temperature. The supernatant was removed, and the pellet was allowed to air-dry for 15min to remove residual ethanol, and resuspended in 30µl of T0.1E buffer. DNA concentration and purity were assessed spectrophotometrically (NanoDrop).

2.2.4.4. Restriction digest

Restriction endonucleases were purchased from New England Biolabs. PCR products and vectors (1μg each) were digested in 50μl reactions, prepared as follows:

5μl	NEB buffer (10x) – selected according to manufacturer's guidelines
0.5μl	BSA (100x) – if necessary
1μl	restriction enzyme - multiple enzymes combined if reaction conditions compatible
+	DNA (1μg)
+	dH_2O to 50μl

Reactions were incubated overnight at 37°C to ensure complete digestion and avoid contamination with undigested vector. Where possible, enzymes were heat-inactivated for 20 minutes at 65°C.

2.2.4.5. DNA electrophoresis and extraction

Restriction digest products were mixed with DNA loading dye and separated by electrophoresis in 0.8% low-melting-temperature agarose supplemented with ethidium bromide. Bands were excised using a sterile scalpel over ultraviolet transillumination, and gels were imaged post-excision to confirm that bands were successfully removed. Excised fragments were trimmed and DNA was extracted using the QIAquick Gel Extraction Kit (Qiagen), according to the manufacturer's instructions, and eluted in 30μl of Buffer EB.

2.2.4.6. Ligation of vectors and inserts

Following gel extraction, the resulting vector and insert restriction digest products were ligated using T4 ligase (NEB) in 20µl reactions, prepared as follows:

2µl	vector
2-6µl	insert (various vector:insert ratios for optimization purposes)
2µl	T4 ligase buffer (10x)
0.5µl	T4 DNA ligase
+	dH_2O to 20µl

Ligation reactions were performed on a PCR block, for 90min at 16°C, followed by heat-inactivation of T4 ligase for 10min at 65°C. For vectors digested with incompatible 5' and 3' ends, vector-only ligations were performed to control for false-positive colonies due to the presence of undigested vector.

2.2.4.7. Bacterial transformation and culture

Competent *E. coli* (NEB) were transformed with ligation products to amplify DNA. For standard transformations, 5-α *E. coli* were used; for large vectors (*e.g.*, the ~10kb transgenic constructs), 10-β *E. coli* were used. Strain genotypes are listed below:

NEB 5-α (C2987H): *huA2Δ(argF-lacZ)U169 phoA glnV44 Φ80 Δ(lacZ)M15 gyrA96 recA1 relA1 endA1 thi-1 hsdR17*

NEB 10-β (C3019H): *araD139 Δ(ara-leu)7697 fhuA lacX74 galK (ϕ80 Δ(lacZ)M15) mcrA galU recA1 endA1 nupG rpsL (StrR) Δ(mrr-hsdRMS-mcrBC)*

Bacteria were thawed on ice for 10min before transformation. DNA was added to bacterial suspension and incubated on ice for 30min. Bacteria were transformed by heat-shock, at 42°C for 30s, and returned to ice for 5min. 950µl of SOC medium was added to each tube, and starter cultures were incubated for 60min at 37°C in a shaking incubator. 20-200µl aliquots of starter cultures were seeded on selective agar plates and incubated overnight at 37°C, for 24-36h at 30°C, or for 48h at room temperature. The following controls were included in all experiments: contamination control (unseeded plate), bacterial viability control (*E. coli* seeded on antibiotic-free plate), and transformation control (*E. coli* transformed with pUC19 control plasmid – for ampicillin plates only). Media composition and antibiotic concentrations are detailed in Appendix A.5.

2.2.4.8. Amplification of generated plasmids

Individual colonies of transformed *E. coli* were picked and used to inoculate 4ml suspension cultures, which were incubated for 16h at 37°C with vigorous shaking (250rpm). Bacteria were harvested by centrifugation at 5500g for 10min at 4°C. DNA was extracted using the QIAprep Spin Miniprep kit (Qiagen), according to the manufacturer's instructions, and resuspended in 50µl of Buffer EB. Products were screened by diagnostic restriction digest, and those with confirmed vector-insert ligation were sequenced (see below). Plasmids with the correct sequence were used to re-transform *E. coli*, and 4ml starter cultures were incubated for 8h at 37°C with vigorous shaking (300rpm). 200µl aliquots of starter cultures were used to inoculate 100ml cultures, which were incubated for 16h at 37°C with vigorous shaking (300rpm). Bacteria were harvested by centrifugation at 6000g for 15min at 4°C. DNA was extracted using the Endo-Free Plasmid Maxi Kit (Qiagen), and resuspended in 200µl of Buffer TE. DNA yield and purity were verified spectrophotometrically (NanoDrop), and products were stored at −20°C until further analysis. All amplified plasmids were screened by diagnostic restriction digest and sequenced before use.

2.2.4.9. DNA sequencing

Sequencing of cloned plasmids was outsourced to Source BioScience, Oxford. Sequencing primers were designed to ensure that the entire insert, including both ligation sites, was covered by at least two separate reads. Sequencing traces were analyzed using 4Peaks. Consensus sequences were constructed from the individual sequencing reads using Serial Cloner, and subsequently checked for alignment against the predicted sequence.

2.2.5. RNA extraction and quantitative RT-PCR

2.2.5.1. RNA extraction from cultured cells

RNA was extracted from cultured cells using the Qiagen RNeasy Mini Kit. Cells grown in 6-well plates were lysed in 300µl of buffer RLT supplemented with 0.1% β-mercaptoethanol, and processed according to the manufacturer's instructions. RNA was resuspended in 60µl of RNAse-free water (2x elution in 30µl each), and RNA yield and purity were determined spectrophotometrically (NanoDrop).

2.2.5.2. RNA extraction from mammalian tissues

RNA extraction from mammalian tissues was performed using a combined protocol, incorporating TRIzol extraction followed by spin-column purification. 10-20mg of tissue was homogenized in 500µl of TRIzol, using a Polytron homogenizer, and centrifuged at 12,000g for 10min at 4°C. Supernatant was transferred to a new tube, incubated for 5min at room temperature, mixed with 100µl of chloroform, incubated for 2min at room temperature, and centrifuged at 12,000g for 15min at 4°C. The aqueous phase was transferred to a new tube, mixed with an equal volume of 70% ethanol, and purified using the Qiagen RNeasy Mini Kit,

according to the manufacturer's instructions. RNA was resuspended in 60µl of RNase-free water (2x elution in 30µl each), and RNA yield and purity were determined spectrophotometrically (NanoDrop).

2.2.5.3. Quantitative RT-PCR

Quantitative RT-PCR (qPCR) was performed using the iScript™ One-Step RT-PCR Kit With SYBR® Green (BioRad). Reactions were prepared in a 10µl volume, using 2ng of RNA:

2µl	RNA (1ng/µl)
5µl	SYBR RT Master Mix (2x)
0.06µl	F primer (50µM stock)
0.06µl	R primer (50µM stock)
0.2µl	iScript reverse transcriptase
2.68µl	H_2O

qPCR was performed using a BioRad C1000 Thermal Cycler, according to the following protocol:

50°C	x 10min	(reverse transcription)
95°C	x 5min	(polymerase activation)
40 cycles:		(amplification and detection)
	95°C x 10s	
	58°C x 30s	
	{read SYBR green}	
95°C	x 10s	(final denaturation)
65-90°C, 5s per step		(gradient for melt curve analysis)

Standards were prepared by pooling RNA extracts, and a series of five 10-fold dilutions was used to construct a standard curve for each reaction (100-0.01ng/µl, 2µl per reaction). Standards and samples were run in triplicate. mRNA expression was calculated by the $2^{-\Delta\Delta C_T}$ method[155] using BioRad CFX Manager software, and normalized to expression of the reference gene *Polr2a* (RNA polymerase II, polypeptide A)[156,157] unless otherwise noted. No-template and no-reverse-transcriptase controls were included in all assays.

2.2.6. Protein extraction and western blotting

2.2.6.1. Protein extraction from cultured cells

Protein extraction was performed using ice-cold RIPA buffer supplemented with 1mM dithiothreitol (DTT) and complete protease inhibitor cocktail (Roche). Cells were washed with PBS, lysed *in situ* in supplemented RIPA buffer, and detached using a rubber cell scraper. Cell lysates were homogenized by passing through a 20-gauge needle ≥10 times, and centrifuged at 15,000g for 15min at 4°C. Supernatant was transferred to a fresh tube, and pelleted debris was discarded.

2.2.6.2. Protein extraction from mouse tissues

Powdered tissue (10-20mg) was suspended in ice-cold RIPA buffer (supplemented with 1mM DTT and complete protease inhibitor cocktail), homogenized by passing through a 20-gauge needle, and centrifuged as described above. Protein extracts were used immediately, and leftover extract was frozen at -80°C for long-term storage.

2.2.6.3. Sample preparation

Protein concentration was determined by the bicinchoninic acid assay (Pierce BCA Protein Assay Kit). Aliquots of protein extract were diluted 25-fold in unsupplemented RIPA buffer (4µl sample + 96µl RIPA), in order to reduce the concentration of DTT, which interferes with the BCA assay. Serial dilutions of bovine serum albumin were used as standards, prepared according to the manufacturer's instructions. Samples (25µl) were aliquoted into a 96-well plate, mixed with working reagent (200µl), and incubated for 30min at 37°C. Protein concentration was determined spectrophotometrically, by measuring absorbance at 562nm. Measurements were performed in triplicate, and the mean protein concentration was corrected for the initial 1:25 dilution. Once sample concentration was established, an aliquot containing 20µg of protein was mixed with 7.5µl of 4x NuPAGE LDS Sample Buffer and 3µl of 10x NuPAGE Reducing Agent (Invitrogen), supplemented with extraction buffer to a final volume of 30µl, and incubated for 5min at ≥95°C to reduce and denature protein.

2.2.6.4. Polyacrylamide gel electrophoresis

Protein extracts and molecular weight markers (BioRad) were loaded onto pre-cast 12% polyacrylamide gels (Pierce) in Tris-HEPES running buffer, and separated by electrophoresis for 45-60min at 120V. Protein was subsequently transferred to Hybond PVDF membranes, which were activated for ~2s in 100% methanol, and equilibrated in transfer buffer for 15min. Transfer was performed in transfer buffer at 4°C, with constant stirring and an ice pack in the tank, for 4hr at 200mA or overnight at 100mA.

2.2.6.5. Immunoblotting and detection

All solutions were prepared in PBS supplemented with 0.1% v/v TWEEN-20 (PBS-T). Membranes were blocked in 2% ECL Blocking Agent (GE Healthcare) for 30min, and incubated with primary antibody solution for 2hrs at room temperature, or overnight at 4°C. Membranes were washed in PBS-T (5x 5min),

incubated with secondary antibody for 1hr at room temperature, and washed in PBS-T (5x 5min). Detection was performed using ECL Advance (GE Healthcare), according to the manufacturer's instructions, and chemiluminescence was visualized using a Fluorchem 8800 digital imaging system (AlphaInnotech). Where loading controls were required, membranes were rinsed in PBS, incubated for 30min at 55°C in stripping buffer (2.5% SDS, 62.5mM Tris-HCl [pH 6.8], 100mM β-mercaptoethanol), and re-probed using the appropriate antibodies.

Antibodies and concentrations are listed in the relevant chapters, and summarized in Appendix A.4.

2.2.7. Immunocytochemistry

Cells grown in glass-bottom dishes/plates (PAA Labs) were washed in PBS, fixed in 4% paraformaldehyde in PBS (TAAB Labs) for 20min, and permeabilized in 0.5% Triton X-100 (TX; Sigma) in PBS for 30min. Blocking was performed in 10% normal goat serum (NGS; Sigma) for 30min; all subsequent solutions were prepared in PBS supplemented with 1% NGS and 0.1% TX. Cells were incubated in primary antibody overnight at 4°C, with gentle rocking, washed with PBS, and incubated with fluorescent secondary antibody for 1hr at room temperature, protected from light. Finally, cells were washed with PBS, nuclei were stained with 10μg/ml Hoechst 33258 for 5min, and cells were mounted in SlowFade Gold (Invitrogen) to preserve fluorescence.

Antibodies and concentrations are listed in the relevant chapters, and summarized in Appendix A.4.

2.2.8. Microscopy

Standard phase/contrast and epifluorescence microscopy was performed using a Nikon TE2000U microscope, equipped with a mercury lamp and standard filter sets (DAPI/FITC/TRITC). Images were recorded using a Hamamatsu black-and-white camera, using IPLab (v. 3.7, Scanalytics).

Confocal microscopy was performed using a Zeiss LSM510 MetaHead laser-scanning confocal microscope, equipped with a live-cell imaging incubator and the following lasers: diode (405nm), argon (458, 477, 488, 504nm), helium-neon (543nm), and helium-neon (633nm).

Image processing and analysis was performed using ImageJ, with additional plug-ins (v. 1.46, NIH). For mPTP assays (see section 6.3.3), changes in fluorescence were measured in real-time, using the built-in software of the Zeiss confocal microscope (Zeiss LSM510, v. 4.2).

2.2.9. Enzyme activity assays

For enzyme activity assays, 5-10mg of powdered tissue was thawed in ice buffer (0.08mM K_2HPO_4, 0.02mM KH_2PO_4, 1mM EGTA, 1mM β-mercaptoethanol) blotted on weighing paper (Schleicher & Schuell) and weighed. Samples were suspended in 1ml of ice buffer, homogenized in glass homogenization vessels, and diluted with ice buffer to a concentration of 5mg wet weight / ml. Three 50µl aliquots were removed for Lowry protein assays at this point (see below). Triton X-100 was added to the remaining sample to permeabilize cells, to a final concentration of 0.1% v/v. Samples were stored on ice and allowed to precipitate; supernatant was used for all enzyme activity assays.

2.2.9.1. Total creatine kinase activity

Total CK activity was measured using the following cascade of reactions[158,159]:

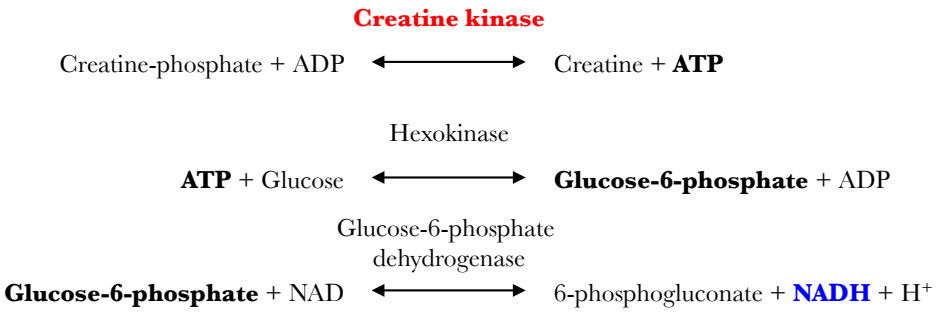


Figure 2-1: Creatine kinase assay.

Samples were diluted 1:5 in ice buffer, and 20µl of diluted sample was incubated with 1ml of CK-NAC reagent (Microgenics) at 30°C. After a 3min lag time, creatine kinase activity was quantified spectrophotometrically by measuring the increase in absorbance at 340nm over 2min as a result of NADH production. Measurements were performed in triplicate, and results were normalized to protein concentration.

2.2.9.2. Relative activities of creatine kinase isoenzymes

Sample supernatant was diluted 1:2 in 0.9% NaCl, and creatine kinase isoenzymes were separated by rapid electrophoresis (REP2, Helena Biosciences). Electrophoresis gels were incubated in CK-REP reagent supplemented with 10µM diadenosine pentaphosphate, to inhibit adenylate kinase. Gels were dried and scanned under ultraviolet light, and the relative activities of individual creatine kinase isoenzymes were quantified by integrating the area-under-curve for UV fluorescence. Absolute activities were calculated by multiplying the relative isoenzyme activity by total CK activity. Measurements were performed in duplicate.

2.2.9.3. Citrate synthase activity

Citrate synthase activity was measured as a marker of mitochondrial volume[160], using the following cascade of reactions[161]:

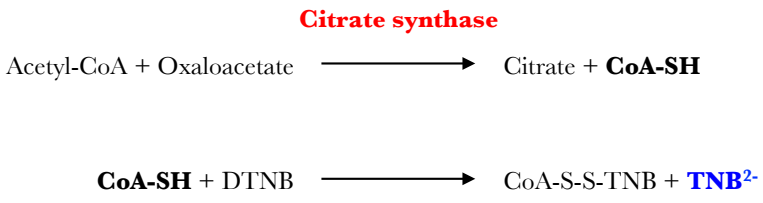


Figure 2-2: Citrate synthase assay.

Measurements were performed at 25°C. 50µl of sample supernatant was placed in a cuvette, and 850µl of reaction mixture (0.35mM acetyl-CoA, 0.12mM DTNB) was added. After 3min, 100µl of 1mM oxaloacetate

solution was added to the sample, mixed using a stirrer bar, and spectrophotometric measurement was commenced immediately. Citrate synthase activity was quantified by measuring the increase in absorbance at 412nm over 1min as a result of 5–thio–2–nitrobenzoate (TNB^{2-}) production. Measurements were performed in duplicate, and results were normalized to protein concentration.

2.2.9.4. Lowry protein assay

Protein concentration was measured in order to normalize enzyme activity results, using a modified Lowry assay[162]. After samples were weighed, homogenized, and diluted to 5mg wet weight / ml, 3x 50µl aliquots were removed, mixed with 50µl of 4% NaOH each, vortexed, and incubated for 2h at 60°C. Samples were briefly centrifuged to collect condensation, and 900µl of distilled water was added. Lowry reagent (1ml each) was added, and samples were vortexed immediately and incubated for 20min at room temperature. Folin-Ciocalteu reagent (0.5ml each) was added, and samples were vortexed immediately and incubated for 30min at room temperature. Protein concentration was determined by measuring absorbance at 650nm, and calculated from a standard curve constructed using known concentrations of BSA.

2.2.10. Statistical analysis

Statistical analyses were performed using GraphPad Prism. For experiments with two groups, means were compared using the two-tailed Student's t-test or Mann-Whitney *U* test. Experiments with ≥3 groups were analyzed using one-way ANOVA with Bonferroni's multiple comparisons test or the Kruskall-Wallis test. When parametric tests were used, Bartlett's test was applied to compare variances. If groups were being compared to a single control (*e.g.,* wild-type), Dunnett's or Dunn's multiple comparisons post-test were used. Values of $p<0.05$ were considered statistically significant.

3. *IN VITRO* MODELS OF AUGMENTED CREATINE KINASE EXPRESSION – EXPERIMENTS IN CULTURED CELLS

3.1. Introduction

This chapter describes the generation of *in vitro* models of creatine kinase overexpression. These models were used to validate the feasibility of increasing CK activity by overexpressing individual isoenzymes. This served a dual purpose, namely to generate *in vitro* models of CK overexpression for further experiments, and to validate the expression constructs prior to generation of transgenic mice.

In order to specifically detect the overexpressed proteins, all expression constructs were designed to incorporate a C-terminal hemagglutinin (HA) tag. The majority of *in vitro* experiments were performed in atrial-derived HL-1 cells. These cells maintain a cardiomyocyte-like phenotype[152], which is a significant advantage since the ultimate goal was to express similar constructs in the transgenic mouse heart. In parallel, experiments were performed in HEK293 cells, which are a widely used mammalian cell line, and are easier to passage and transfect than HL-1 cells. In addition to transient transfection, attempts were made to establish stably transfected lines for both cell types. This would allow for the production of large amounts of cells uniformly overexpressing CK isoenzymes at a stable level.

In parallel, an *in vitro* model of simulated ischemia/reperfusion injury was generated. The goal was to use this model as an objective screening tool to determine which, if any, CK isoenzymes are the most promising targets for further research into cardioprotection by augmentation of the CK system. This was performed by

transiently transfecting HL-1 cells (including fluorescent proteins as transfection markers), and evaluating cell death in response to simulated ischemia/reperfusion injury using viability dyes.

3.2. Aims and hypotheses

The goal of the experiments described in this chapter was to generate and validate *in vitro* models of creatine kinase overexpression, and use these models to test whether CK overexpression has a protective effect in simulated ischemia/reperfusion injury. Specifically, the aims were to (1) create appropriate expression vectors for the CK isoenzymes, (2) verify protein expression, activity, and subcellular localization, (3) establish a model of *in vitro* simulated ischemia/reperfusion (sI/R) injury, and (4) apply the sI/R model to determine whether overexpression of CK isoenzymes protected cells against simulated ischemia/reperfusion injury. Furthermore, since the same cDNA coding sequences were subsequently used to overexpress the CK isoenzymes *in vivo* (see sections 4.3.1.1 and 5.3.1.1), these experiments served an additional purpose, by validating expression and function of the constructs prior to generation of transgenic mice.

The experimental hypothesis of simulated ischemia/reperfusion experiments was that overexpression of CK isoenzymes reduces cell death in response to conditions which mimic myocardial ischemia/reperfusion injury.

Since the generation/validation of *in vitro* models of CK overexpression and simulated ischemia/reperfusion experiments constitute two distinct stages of this project, they are discussed as separate sections below.

3.3. Methods and results I: Overexpression of creatine kinase isoenzymes

This section describes the generation of *in vitro* models of CK overexpression, specifically the cloning and validation of HA-tagged constructs encoding each of the CK isoenzymes. In addition, further work was conducted to generate a fusion protein between mitochondrial CK and green fluorescent protein for localization and imaging experiments.

3.3.1. *In vitro* overexpression of HA-tagged creatine kinase isoenzymes

3.3.1.1. pcDNA3.1+/- expression vectors

The CK isoenzyme coding sequences were cloned into pcDNA3.1 vectors for expression in cultured cells. Depending on the required orientation of restriction sites, either pcDNA3.1+ or 3.1− was used (Figure 3-1). These vectors have different multiple cloning sites, but the plasmid backbone is otherwise identical. Expression of genes cloned into pcDNA3.1+/- is driven by the cytomegalovirus promoter-enhancer (P_{CMV}), which is constitutively active in mammalian cells.

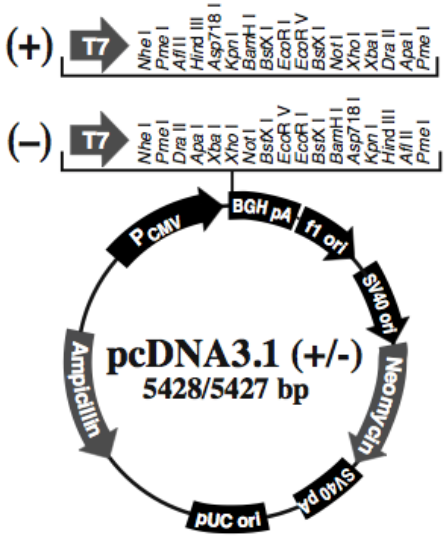


Figure 3-1: pcDNA3.1(+/-) vector.

The order of restriction sites in the multiple cloning sequence is shown for pcDNA3.1+ and pcDNA3.1-, respectively. Figure from the manufacturer's documentation (Invitrogen).

3.3.1.2. PCR amplification of CKmt, CK-M, and CK-B coding sequences

The general design of the expression vectors was analogous for all three isoenzymes. In addition to the required restriction sites, the 5' primers were used to incorporate a Kozak consensus sequence[163], and 3' primers were used to add a C-terminal hemagglutinin (HA) tag and stop codon (TAG or TGA), and remove the original stop codon (see Table 3-1 for detailed primer sequences).

Ckmt was amplified using a previously developed 5' primer (Ckmt2_F_HindIII/Kozak, a kind gift from Dr. Imre Hunyor), and a newly designed 3' primer (Ckmt2_R_HA/stop/XbaI). Cloning of *Ckm* and *Ckb* constructs was performed in parallel with cloning of vectors for *in vivo* expression, using primers designed to incorporate multiple restriction sites.

Construct	Primer name	Sequence (5'-3')
Ckmt2	**Ckmt2_F_HindIII/Kozak**	GACCAAGCTTAAGAAGAAGGATGGCCAGTGCCTTCTCAAAGTTGCT
	Ckmt2_R_HA/stop/XbaI	CTAGTCTAGATCAAAGAGCGTAATCTGGAACATCGTATGGGTACTTCCTGCCAAACTGAGGCA
Ckm	**Ckm_F_NheI/SalI/Kozak_c12t**	GGGGCTAGCGTCGACACCATGCCGTTCGGTAACACCCAC
	Ckm_R_HA/stop/XhoI	GGCCTCGAGCTATGCGTAATCTGGAACATCGTATGGGTACTTCTGCGCGGGGATCATGT
Ckb	**Ckb_F_NheI/SalI/Kozak**	CCCCGCTAGCGTCGACACCATGCCCTTCTCCAACAGCCAT
	Ckb_R_HA/stop/KpnI/HindIII	CCGAAGCTTGGTACCTATGCGTAATCTGGAACATCGTATGGGTACTTCTGGGCCGGCATGAGGTC

Table 3-1: Primers for *in vitro* expression constructs.

The underlined regions are the Kozak sequences (5' primers) and stop codons (3' primers). The restriction sites used for cloning are marked in yellow (other restriction sites, used for cloning *in vivo* constructs, are gray). The HA tag sequence (green) is different in the *Ckmt2* reverse primer, as a slightly shorter version of the HA tag sequence was used for *Ckm* and *Ckb* constructs. A silent substitution (red) was incorporated at the +12 position in the *Ckm* forward primer, as the *Ckm* sequence was predicted to cause primer hairpin formation at this site (C replaced by T, *i.e.* codon changed from GGC to GGT, both of which encode glycine).

Murine (*Mus musculus*) cDNA sequences were used as templates for all constructs, to avoid any confounding effects due to inter-species variability. *Ckmt2* was amplified from a commercially available vector (Geneservice, I.M.A.G.E clone #30296538). *Ckm* and *Ckb* were amplified from *Mus musculus* C57BL/6 total cDNA, synthesized using the Bioline cDNA synthesis kit (BIO-65025), according to the manufacturer's guidelines, using 0.5µg of mouse left ventricular RNA as a template and Oligo$(dT)_{18}$ primer mix.

cDNA was amplified by touch-down PCR, using high-fidelity Phusion DNA polymerase (NEB). PCR products were visualized by agarose gel electrophoresis (Figure 3-2), and purified by ethanol precipitation.

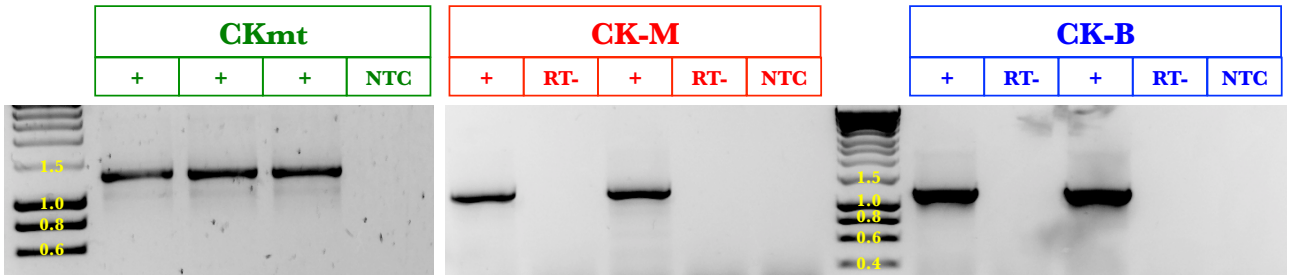


Figure 3-2: Cloning PCR.

Agarose gel electrophoresis demonstrates products of the expected size (~1.2kb) in all reactions. Negative controls were as follows: NTC, no-template control; RT-, no reverse transcriptase during cDNA synthesis (applies to *Ckm* and *Ckb* only, as *Ckmt* was amplified from an existing vector).

3.3.1.3. Cloning of expression constructs

Purified PCR products and pcDNA3.1+/- vectors were restriction-digested overnight at 37°C using the following combinations of restriction enzymes: *HindIII/XbaI* (Ckmt x pcDNA3.1+), *NheI/XhoI* (Ckm x pcDNA3.1-), *NheI/HindIII* (Ckb x pcDNA3.1-). Restriction fragments were separated by agarose gel electrophoresis (Figure 3-3), excised under ultraviolet light, and purified by gel extraction.

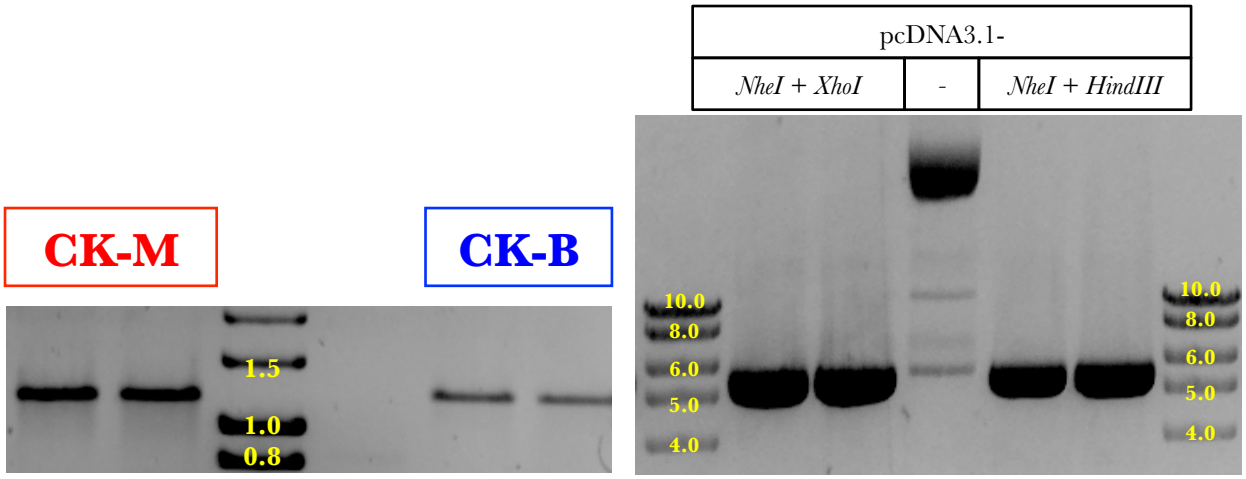


Figure 3-3: CK-M and CK-B restriction digest.

Gels demonstrate *Ckm* and *Ckb* PCR products (left) and pcDNA3.1- vector (right) prior to excision for DNA extraction.

Vector and insert digest products were ligated, and used to transform 5-α competent *E. coli* (NEB). Bacteria were cultured overnight at 37°C on ampicillin-containing LB agar, and individual colonies were picked to inoculate overnight suspension cultures in ampicillin-containing LB broth. DNA was extracted by MiniPrep (Qiagen), and purified products were analyzed by diagnostic restriction digest. Selected samples were verified by DNA sequencing, using a T7_F primer binding upstream of the 5' insertion site and a bGH_R primer binding in the polyadenylation sequence (Figure 3-4). To ensure double coverage of the coding sequence, additional construct-specific primers were used. The correct sequence was confirmed in all MiniPrep products, which were subsequently used to re-transform 10-β *E. coli*, and DNA was amplified and extracted by Endotoxin-Free MaxiPrep (Qiagen).

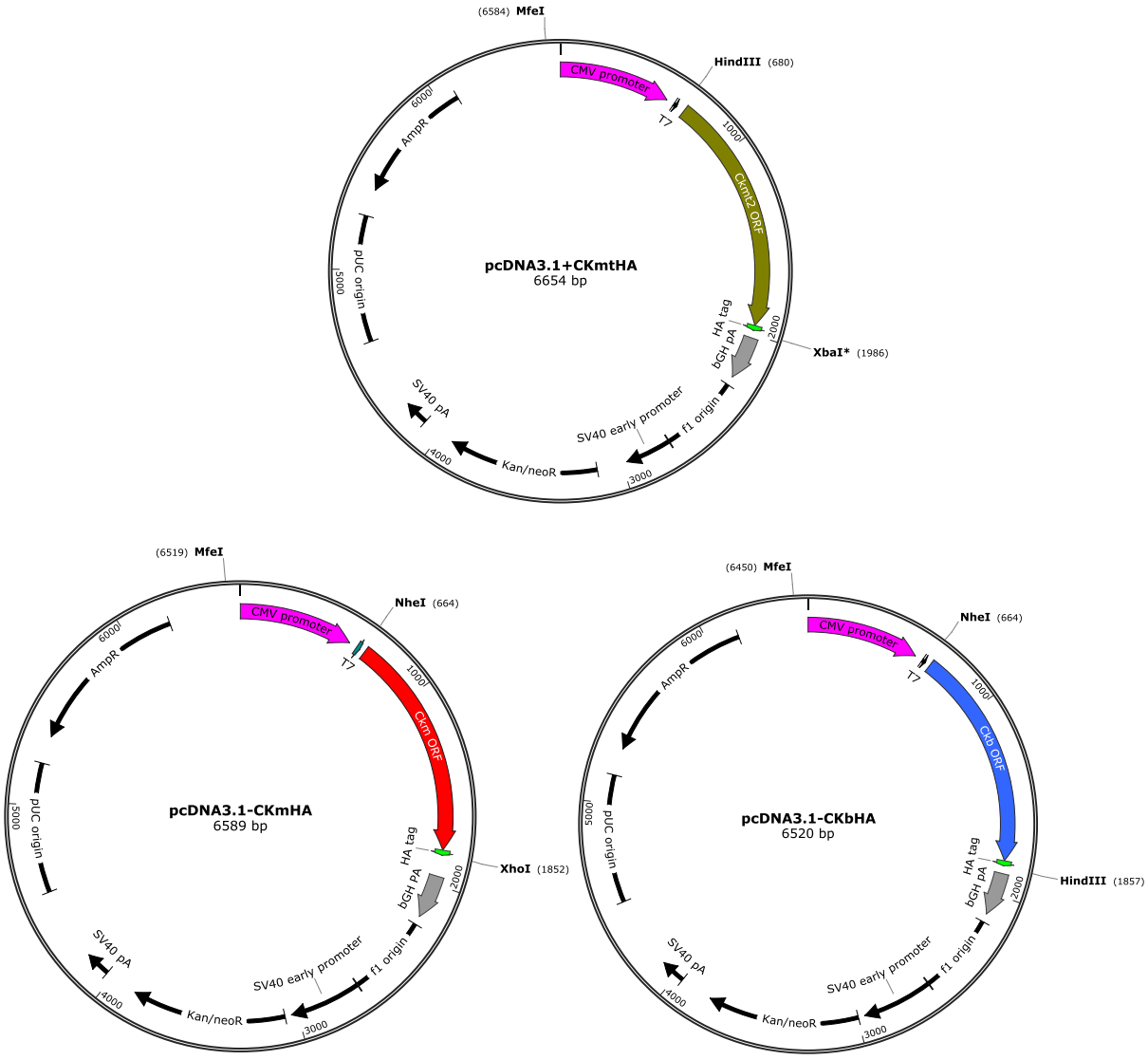


Figure 3-4: Maps of *in vitro* expression vectors.

Significant features of the plasmids are labelled, along with the restriction sites used for ligation. The *MfeI* sites were used to linearize vectors prior to stable transfections.

3.3.1.4. Transient transfection of HEK293 and HL-1 cells

Transfections were initially optimized using various reagents (GeneJuice, LipofectamineLTX, FuGENE 6, FuGENE HD). To test transfection efficiency, cells were transfected with the pEGFP-N1 vector (Figure 3-5), and enhanced green fluorescent protein (EGFP) expression was visualized by epifluorescence microscopy at 48 hours post-transfection.

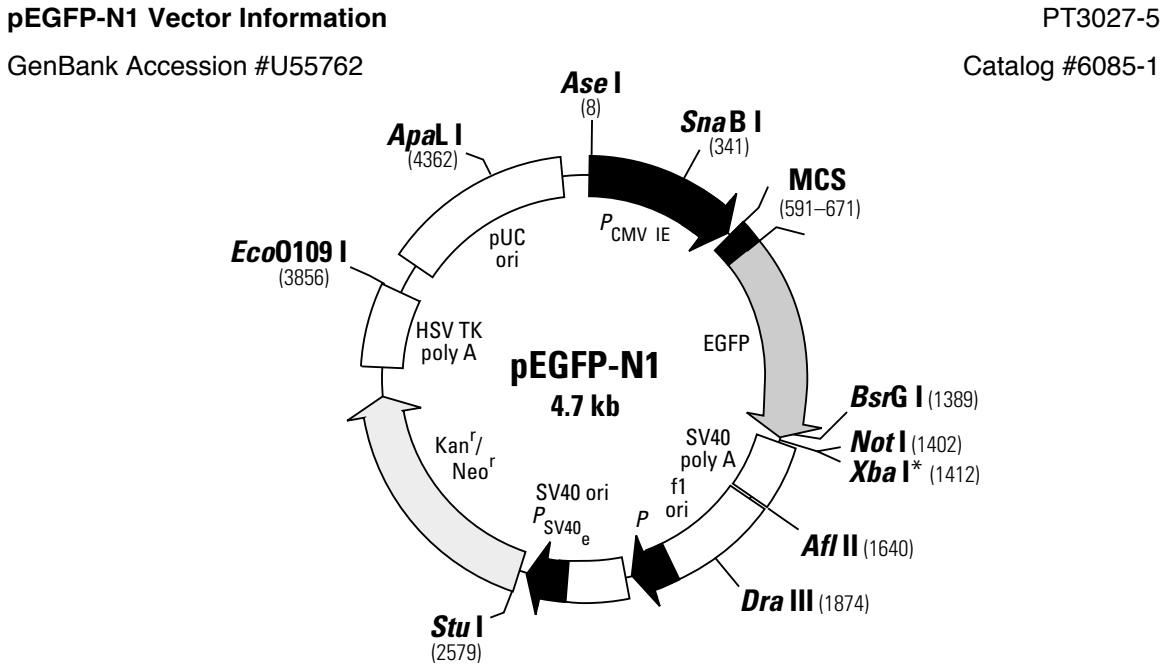


Figure 3-5: pEGFP-N1 vector map.
Figure from the manufacturer's documentation (Clontech).

HEK293 cells proved relatively easy to transfect, with >50% transfection efficiency for all reagents. FuGENE HD yielded the best results in HL-1 cells and, following optimization of conditions (transfection time, amounts and ratio of FuGENE HD and plasmid DNA), was used for all subsequent experiments.

Transfections were performed according to the FuGENE HD manufacturer's protocols (Roche). Unless otherwise noted, cells were seeded at 2.5–5.0 x $10^4/cm^2$, and transfected at 24-48 hours after plating, in freshly changed antibiotic-free media. Transfection mixtures were prepared in Opti-MEM (Invitrogen), and contained 10µl FuGENE HD and 2000ng DNA per 100µl (FuGENE HD:DNA [µl:µg] = 5:1). Mixtures

were vortexed, incubated at room temperature for 30 minutes, and added directly to the cells. Pilot experiments indicated that exposing cells to transfection mixture for 24 hours yielded a higher efficiency than shorter incubations, without evidence of significant cytotoxicity. Cells were therefore allowed to transfect for 24 hours, and culture media were replaced with complete growth media at 24 hours post-transfection. Transfection efficiency was routinely assessed at 48 hours by fluorescence microscopy in GFP-transfected controls (Figure 3-6). Despite optimization of the transfection protocol, efficiency in HL-1 cells remained relatively low – therefore, HEK293 cells were used for experiments in which a large population of transfected cells was required (*e.g.,* validation of expression constructs), while HL-1 cells were used for experiments where transfection status could be directly visualized in individual cells (see sections 3.3.1.7 and 3.4.1.5).

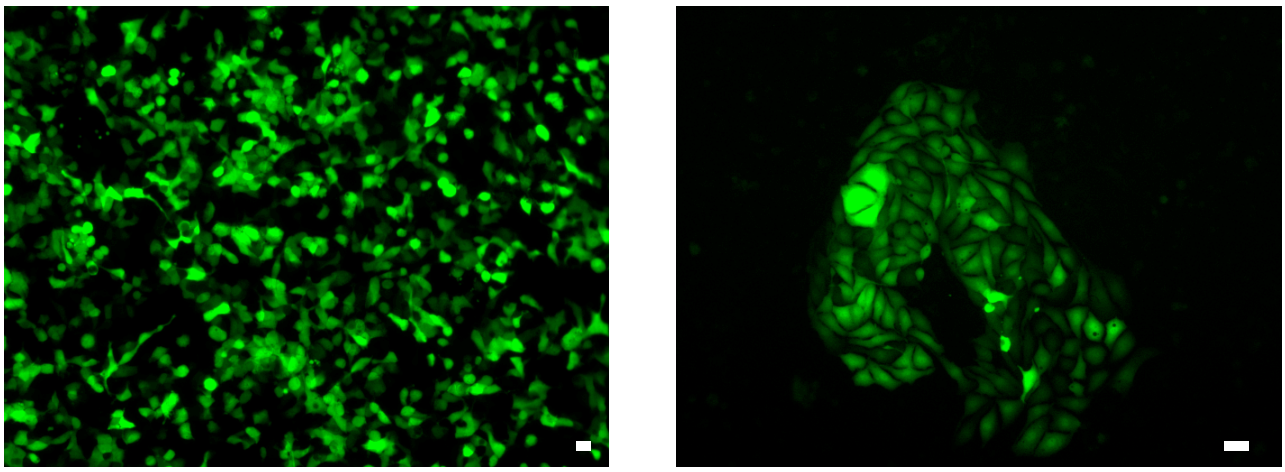


Figure 3-6: GFP expression in transiently transfected cells.

HEK293 (left) and HL-1 (right) cells were transfected with pEGFP-N1, and transfection efficiency was visualized by epifluorescence microscopy at 48 hours. Both images were acquired in confluent fields of view. Scale bars, 20μm.

3.3.1.5. Protein expression by western blot

Protein extraction and western blotting was performed in HEK293 cells transiently transfected with CKmt, CK-M, and CK-B. Membranes were probed using anti-HA antibodies to specifically detect HA-tagged proteins. All three proteins were found to be expressed, and migrated at the expected size (between 37 kDa and 50 kDa bands on molecular weight ladder – see Figure 3-7).

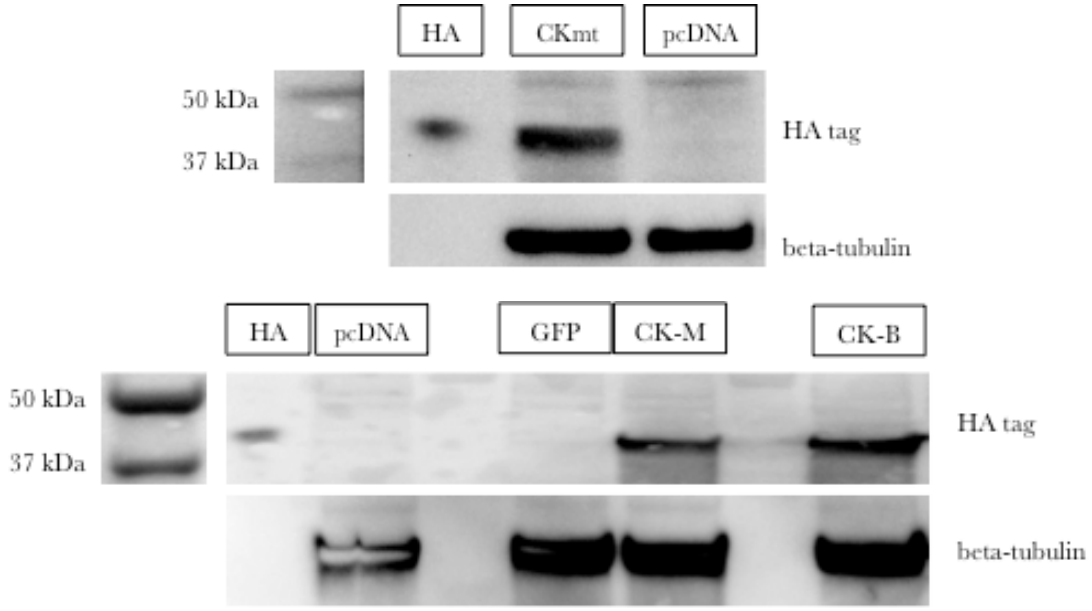


Figure 3-7: Representative *in vitro* construct western blots.

Membranes were probed using anti-HA antibodies to specifically detect HA-tagged CKmt (top), CK-M and CK-B (bottom). Antibodies: 1°: Roche rat anti-HA (1:200,000) 2°: Dako anti-rat-HRP (1:10,000). Lysate of *E. coli* expressing the HA tag sequence was included as a positive control in both blots. No HA-tagged protein was detected in negative controls, transfected with other vectors (empty pcDNA3.1+, or pEGFP-N1). Membranes were stripped and re-probed for beta-tubulin, to confirm comparable loading between lanes.

3.3.1.6. Enzymatic activity assays

Since *in vitro* expression of the constructs was confirmed at the protein level, the next step was to confirm whether they were enzymatically active. HEK293 cells transfected with either empty pcDNA3.1- or the HA-tagged CK constructs were harvested by trypsinization, and pellets were homogenized in 1ml of ice buffer using a 20-gauge needle and syringe. CK isoenzyme electrophoresis was performed as described in section 2.2.9.2 (Figure 3-8).

In control cells transfected with empty vector (pcDNA3.1-), a clear CK-BB band was detected, as well as a faint CKmt band (most likely the ubiquitous isoform of CKmt). Cells transfected with (sarcomeric) CKmt had a robust increase in CKmt activity, as expected. In cells transfected with CK-M, which is not normally expressed in HEK293 cells, activity of both CK-MM homodimers and CK-MB heterodimers was detected, suggesting that the HA-tagged protein was able to form dimers with endogenous CK-B. Densitometric

analysis revealed that the activity of CK-BB was 28% higher in cells transfected with CK-B (relative to empty pcDNA3.1- controls); if the endogenous CKmt band was used as a "loading control," normalized CK-BB activity was 41% higher in cells transfected with CK-B, relative to pcDNA3.1-. This confirms that all constructs were enzymatically active, and formed the expected homo-/heterodimers.

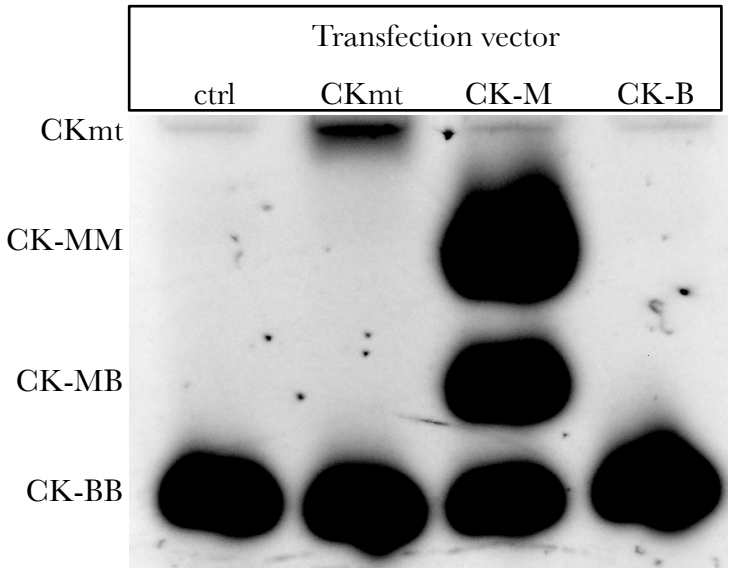


Figure 3-8: CK isoenzyme electrophoresis in transfected HEK293 cells.

The transfection vector used in each lane is listed above the gel, and migration pattern of the individual CK isoenzymes is noted on the left.

3.3.1.7. Immunocytochemical localization of CKmt-HA

Mitochondrial creatine kinase differs from the remaining CK isoenzymes in that it is closely associated with a specific subcellular compartment, specifically the mitochondrial intermembrane space. Therefore, in order to draw meaningful conclusions about the effects of CKmt overexpression, it is necessary to confirm that the protein is targeted to the mitochondria. This could be accomplished by subcellular fractionation and western blotting; however, in order to directly visualize the intracellular distribution of CKmt, immunocytochemical staining was performed to specifically detect the HA tag, and determine whether it co-localizes with a mitochondrial protein (complex IV).

HL-1 and HEK293 cells were transiently transfected with pcDNA3.1-CKmtHA and/or pEGFP-N1 (transfection control), and immunocytochemical staining was performed at 48h post-transfection as described in section 2.2.7. Mitochondria were stained using a mouse monoclonal antibody against complex IV (Abcam), and a goat anti-mouse alexa488 secondary antibody (Molecular Probes). CKmtHA was stained using the rat anti-HA antibody used for western blots (Roche), and a goat anti-rat alexa546 secondary antibody (Molecular Probes). As expected, COX-IV signal was present in all cells, and was clearly compartmentalized within cells; HA signal was detectable in only some (transfected) cells, and was also compartmentalized (Figure 3-9). Merging the COX-IV and HA images demonstrated that the signals overlapped to a significant extent, indicating that CKmt-HA was being specifically expressed in the mitochondria of HL-1 cells. The lack of fluorescence in control wells incubated without either anti-COX-IV or anti-HA primary antibody confirmed that the co-localization was not an artefact due to non-specific secondary antibody binding or spectral bleed-through between the fluorescent signals. It is worth noting that, although this clearly indicates that CKmt is being expressed in the mitochondria, this method cannot determine whether the protein is localized in the mitochondrial intermembrane space, as expected.

In parallel, individual wells were co-transfected with pcDNA3.1-CKmtHA and pEGFP-N1 (Figure 3-9F). The HA signal was only detected in GFP-positive cells, confirming that co-transfection with a fluorescent protein could serve as a marker of the transfection status of individual cells – this was necessary for identification of transfected cells in simulated ischemia/reperfusion experiments (see section 3.4.1.5).

Figure 3-9 **(see next page). (A-D)** HL-1 cells transfected with pcDNA3.1-CKmtHA, stained for nuclei (Hoechst 33258, blue), mitochondria (anti-COX-IV, green), and CKmtHA (anti-HA, red). The composite image (D) demonstrates that the distribution of CKmtHA in the transfected cell co-localizes with mitochondrial staining. Images were acquired by confocal microscopy, using a 40x air objective. **(E)** Fragment of the transfected cell, imaged using a 63x oil-immersion objective and increased optical zoom, demonstrating co-localization of HA (red) and COX-IV (green). **(F)** Representative image from a well co-transfected with pcDNA3.1-CKmtHA and pEGFP-N1, demonstrating that the transfected cell (right) is expressing both CKmtHA and EGFP, while an untransfected cell (left) expresses neither. Scale bars are either 2μm or 20μm, depending on magnification.

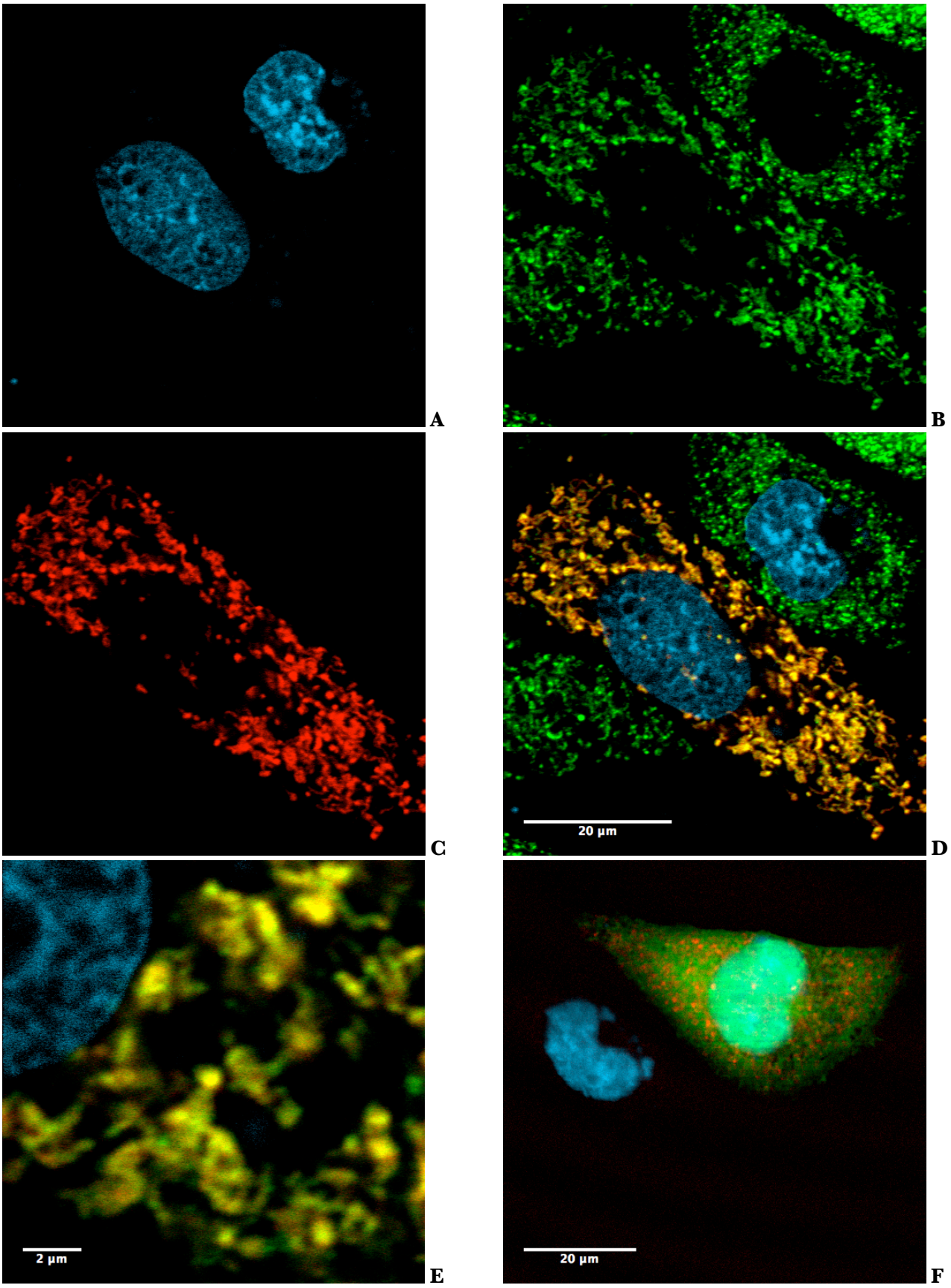


Figure 3-9: Immunocytochemical staining in HL-1 cells expressing CKmtHA.

(Detailed caption on previous page)

3.3.1.8. Generation of stably transfected cell lines

In order to determine suitable antibiotic concentrations for selection of stably transfected cells, G-418 kill curves were assessed by culturing HEK293 and HL-1 cells for 14 days in a range of G-418 concentrations (0 - 1,000µg/ml). The optimal concentration, *i.e.* the lowest concentration which did not leave any viable colonies, was determined to be 600µg/ml for HEK293 cells, and 500µg/ml for HL-1 cells, and these concentrations were used for all stable transfection experiments (Figure 3-10).

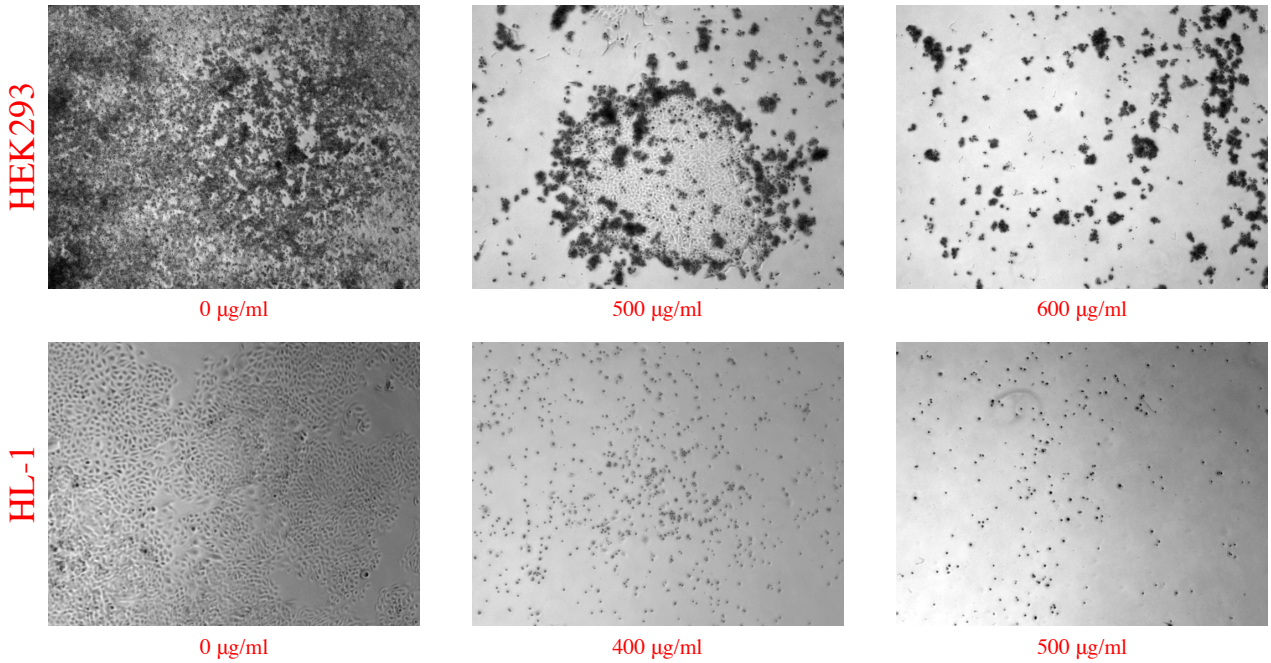


Figure 3-10: G-418 kill curves.

HEK293 (top) and HL-1 (bottom) cells were cultured for 14 days in a range of G-418 concentrations. No viable cells were observed at concentrations equal to or greater than 600µg/ml (HEK293) or 500µg/ml (HL-1), respectively.

Since circular DNA cannot directly integrate into the genome, the strand must be linearized prior to integration. If cells were transfected with circular plasmids, stable transfection would only occur in the event of spontaneous breakage of a strand, at an unpredictable locus. Since this could theoretically interrupt the transgenic expression cassette, CK expression vectors were linearized at a known site prior to transfection, by digestion with *MfeI*.

HL–1 and HEK293 cells were transfected with each of the CK expression vectors, empty pcDNA3.1- vector, or pEGFP-N1 (as a control, for visualization by microscopy). Transient transfection efficiencies, as

determined by GFP expression in controls, were 30-40% in HL-1 cells and 80-90% in HEK293. Cells were incubated in the presence of G-418 (600μg/ml for HEK293, 500 μg/ml for HL-1) from 48 hours post-transfection. After two weeks, antibiotic-resistant colonies of HEK293 cells were present, and these were expanded to form stably transfected lines; however, no viable colonies developed in HL−1 cells. Fluorescence microscopy indicated that HEK293 cells transfected with pEGFP-N1 were uniformly expressing GFP, suggesting that all surviving cells had stably integrated plasmid DNA (Figure 3-11).

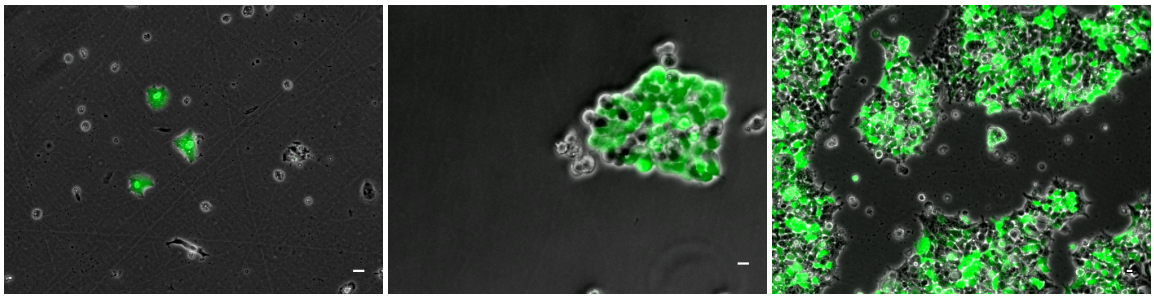


Figure 3-11: Selection of stably transfected cells.

During stable transfection experiments, representative composite images were acquired of control cells transfected with pEGFP-N1 to assess the efficiency of transfection and selection. Individual HL-1 cells (left) were found to express GFP, but these cells did not form viable colonies. HEK293 cells (center) formed GFP-positive colonies, which were resistant to G-418 toxicity were expanded to form stably transfected lines (right). Scale bars, 20μm.

3.3.2. EGFP-tagged mitochondrial creatine kinase

In addition to the HA-tagged CKmt construct described above, a vector was constructed to express CKmt fused to the enhanced green fluorescent protein (CKmt-EGFP). The goal of this experiment was to generate a model which would allow (1) easy identification of transfected cells and (2) subcellular localization of the protein in live cells. Furthermore, if successful, this model could be used for live-cell imaging, *e.g.* to determine whether expression of CKmt affects mitochondrial morphology.

3.3.2.1. Design and cloning of pCKmt-EGFP

The open reading frame of *Mus musculus* Ckmt2 cDNA was amplified by PCR, using primers designed to incorporate a *HindIII* restriction site and Kozak consensus sequence (5'), and a *KpnI* site (3'). The 3' primer was used to incorporate additional bases, in order to ensure that the EGFP coding sequence would be

translated in-frame with CKmt. PCR product and pEGFP-N1 vector were digested using *HindIII* and *KpnI*, and ligated using T4 ligase. The resulting plasmid (Figure 3-12) was amplified and purified by MiniPrep, and sequencing verified that the insert sequence was correct and in frame with eGFP, without intervening stop codons.

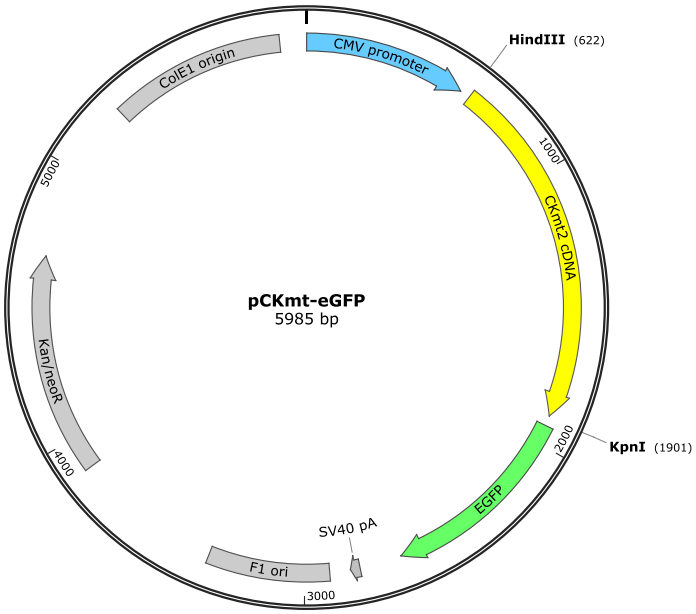


Figure 3-12: pCKmt-EGFP vector.
The *Ckmt2* open reading frame was inserted upstream of EGFP using *HindIII* and *KpnI*.

3.3.2.2. Expression of pCKmt-EGFP

Transfection were initially performed in HL–1 cells. Fluorescence microscopy indicated that cells transiently transfected with pEGFP-N1 exhibited diffuse, uniform GFP signal throughout the cytoplasm and nucleus, while CKmt-eGFP cells had a compartmentalized signal (Figure 3-13).

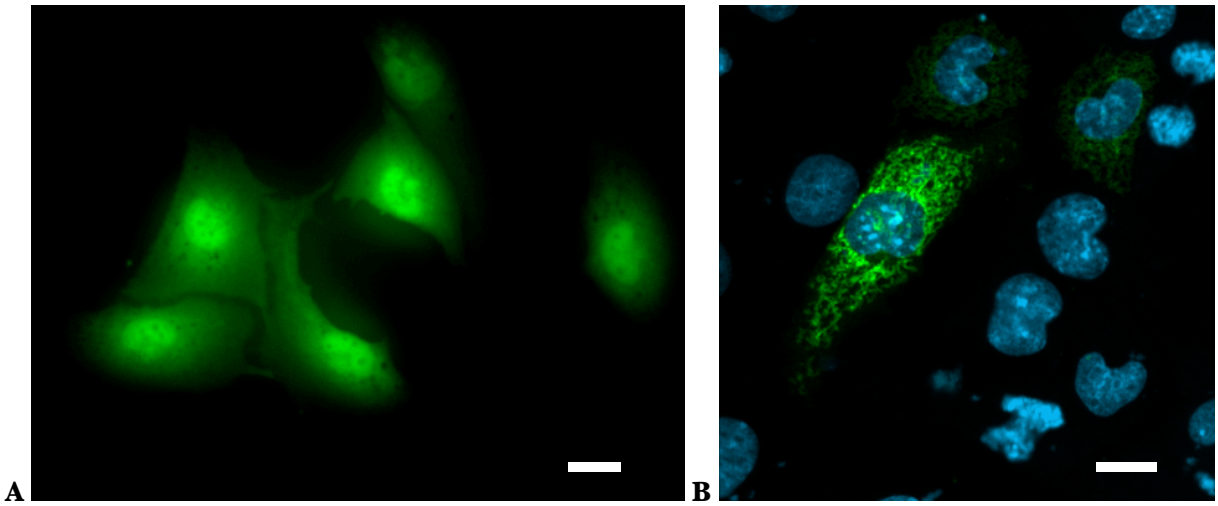


Figure 3-13: HL-1 cells transfected with GFP constructs.

(A) Epifluoresence microscopy image of cells transfected with pEGFP-N1 (nuclear counterstain not shown to avoid obscuring intranuclear GFP signal). **(B)** Confocal microscopy image of cells transfected with pCKmt-EGFP (green), demonstrating compartmentalized distribution of GFP; nuclei counterstained with DAPI (blue). Scale bars, 20μm.

Despite further optimization, transient transfection efficiency in HL−1 cells remained relatively low (≤40%). In an attempt to generate stably transfected lines, HL-1 cells were transfected and incubated in 500 μg/ml G-418 from 48 hours; however, after only 4 days, there were almost no viable cells expressing CKmt-EGFP. Controls transfected with "empty" pEGFP-N1 vector were still viable at this stage.

In parallel, HEK293 cells transfected with pCKmt-EGFP did not survive more than a week; cells transfected with pEGFP-N1 were cultured for over three weeks (Figure 3-14). This suggests that cell viability may have been adversely affected by the pCKmt-EGFP construct in both cell types.

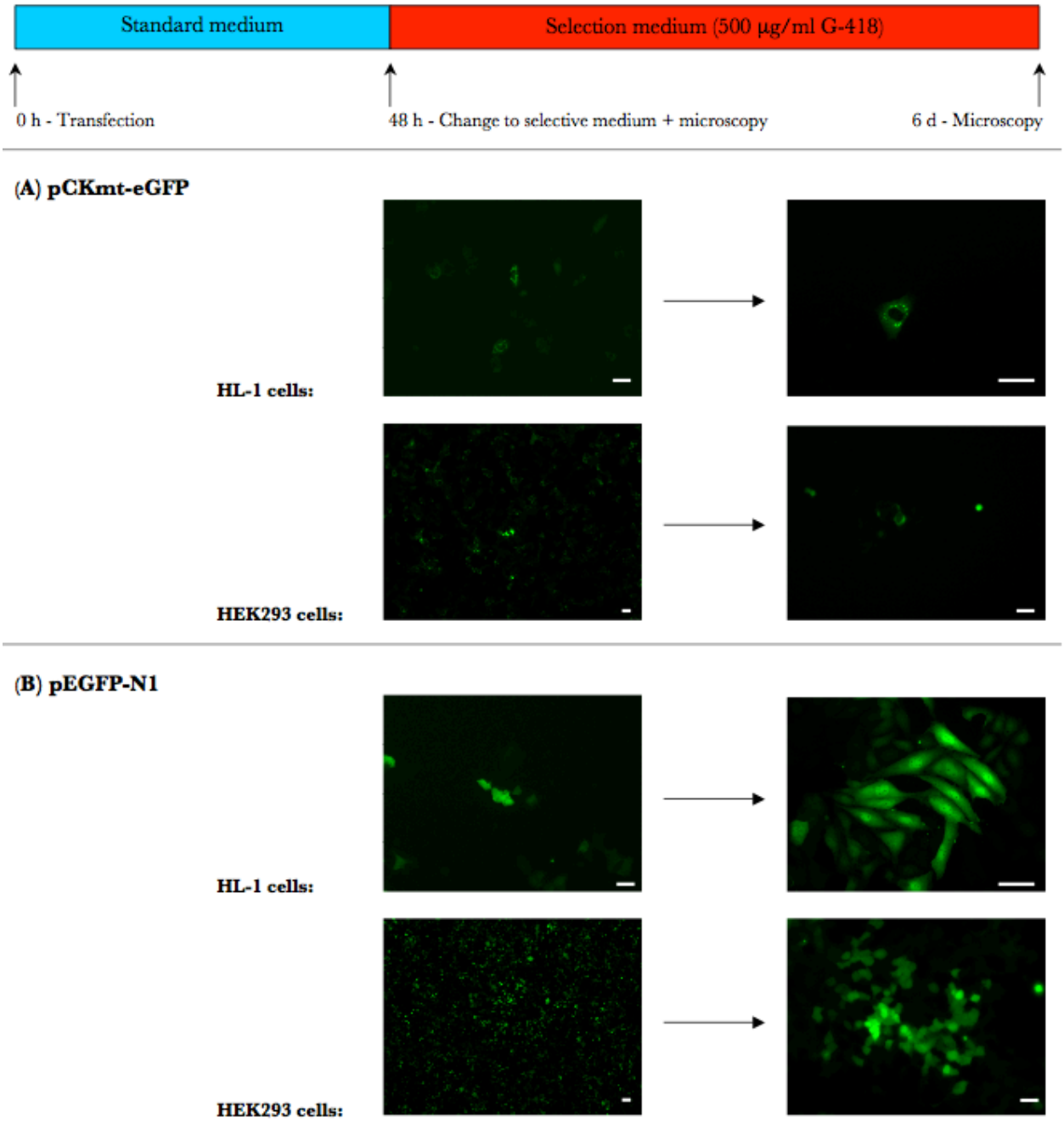


Figure 3-14: Selection of HL−1 and HEK293 cells stably transformed with pCKmt-EGFP.

(A) Cells transfected with pCKmt-EGFP did not survive antibiotic selection. **(B)** Controls transfected with pEGFP-N1 at the same timepoints, demonstrating a large number of viable, GFP-expressing cells. Scale bars, 20µm.

The lack of viable cells stably transfected with pCKmt-EGFP could be due to failed transfection, defective antibiotic resistance, or a toxic effect of GFP-tagged CKmt itself. Transfections were repeated, with similar results – transfection of HEK293 with empty pEGFP-N1 yielded multiple colonies of GFP-positive cells, while no G418-resistant colonies were developed from cells transfected with pCKmt-EGFP.

The lack of pCKmt-EGFP colonies could be due to a defective antibiotic resistance cassette (*e.g.*, due to an unexpected mutation during cloning), which would preclude positive selection of stably transfected cells. In order to determine whether the plasmid conferred antibiotic resistance as expected, a G-418 growth curve was performed in transformed *E. coli*. Since the presence of bacteria increases the turbidity of culture medium, serial measurement of culture optical density can be used to monitor bacterial growth, and whether the rate is influenced by selective antibiotics[164].

Overnight starter cultures of 5-α *E. coli* were transformed with either pEGFP-N1 or pCKmt-EGFP and diluted 1:100 into flasks of LB broth containing a range of G-418 concentrations (0–100 μg/ml). Cultures were incubated at 37°C, with agitation at 225rpm. A 1ml sample of each culture was removed every hour, and optical density was measured spectrophotometrically at 600nm, relative to a calibrator (sterile LB broth).

Bacteria seeded in non-selective media grew at similar rates, and the low G-418 concentration (10μg/ml) did not inhibit growth of bacteria transformed with either construct. The intermediate concentration (50μg/ml) slowed bacterial growth, to a similar extent for both constructs. High G-418 (100μg/ml) prevented growth entirely in both cultures (Figure 3-15). This indicates that there was no significant difference between pEGFP-N1 and pCKmt-EGFP with respect to antibiotic resistance.

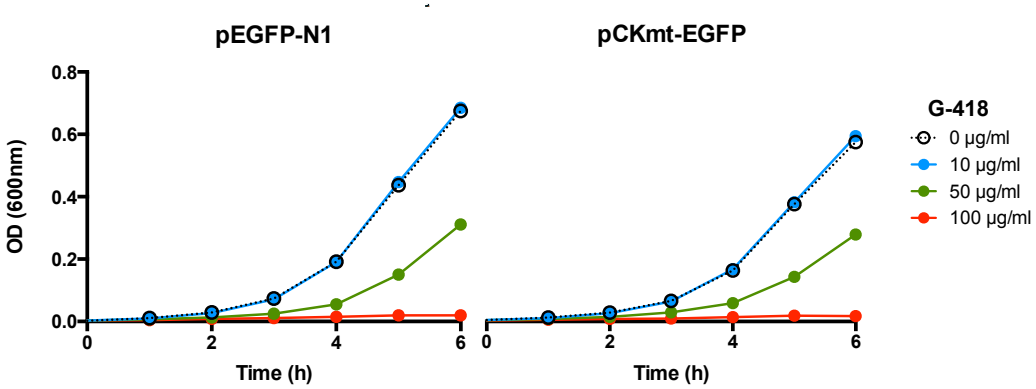


Figure 3-15: Bacterial growth curves.

Competent *E. coli* were transformed with either pEGFP-N1 (left) or pCKmt-EGFP (right), and medium turbidity was measured spectrophotometrically as an indicator of culture growth. The control samples (0μg/ml G-418) are plotted as dotted lines, as they overlap with the 10μg/ml samples.

3.4. Methods and results II: Response to simulated ischemia/reperfusion injury

The results described above confirm that functional CK isoenzymes can be overexpressed by transfecting cultured cells. The subsequent experimental goal was to apply these models to determine whether increasing CK activity can have a beneficial effect under conditions simulating cardiac disease. This section describes the validation of an *in vitro* model of ischemia/reperfusion injury in cardiomyocyte-derived HL-1 cells, and its application to determine whether overexpression of CK isoenzymes can have a protective effect.

3.4.1. Protocol optimization

3.4.1.1. Hypoxic tissue culture

In order to mimic the hypoxic state of ischemic myocardium, cells were cultured in an incubator equipped with O_2 and CO_2 sensors. All incubations were performed at 37°C, 5% CO_2; oxygen concentration was reduced by displacement with nitrogen.

3.4.1.2. Quantification of cell viability

Viability was quantified using propidium iodide (PI), a nuclear dye which is membrane-impermeant. Cell death leads to permeabilization of the plasma membrane, which allows PI to enter the cell. PI binds to nuclear DNA, and this can be visualized as fluorescence in the red spectrum, allowing for identification of dead cells. The protocol was initially optimized using epifluorescence microscopy to directly observe nuclear staining. In order to increase throughput, subsequent experiments were performed using flow cytometry to quantify cell death.

3.4.1.2.1. *Fluorescence microscopy*

Fluorescence microscopy was used to validate the staining protocol, and during initial optimization experiments. In order to determine the total number of cells in each field of view, the membrane-permeant dye Hoechst 33258 was used, which stains the nuclei of both live and dead cells. Cells were stained for 30min at 37°C with Hoechst 33258 (10 μg/ml) and propidium iodide (1 μg/ml) (Figure 3-16). Image analysis was performed in ImageJ, and cell death was expressed as the percentage of PI-positive nuclei (PI+/Hoechst+); where possible, quantification was automated using the Nucleus Counter plugin (MacBiophotonics, McMaster University).

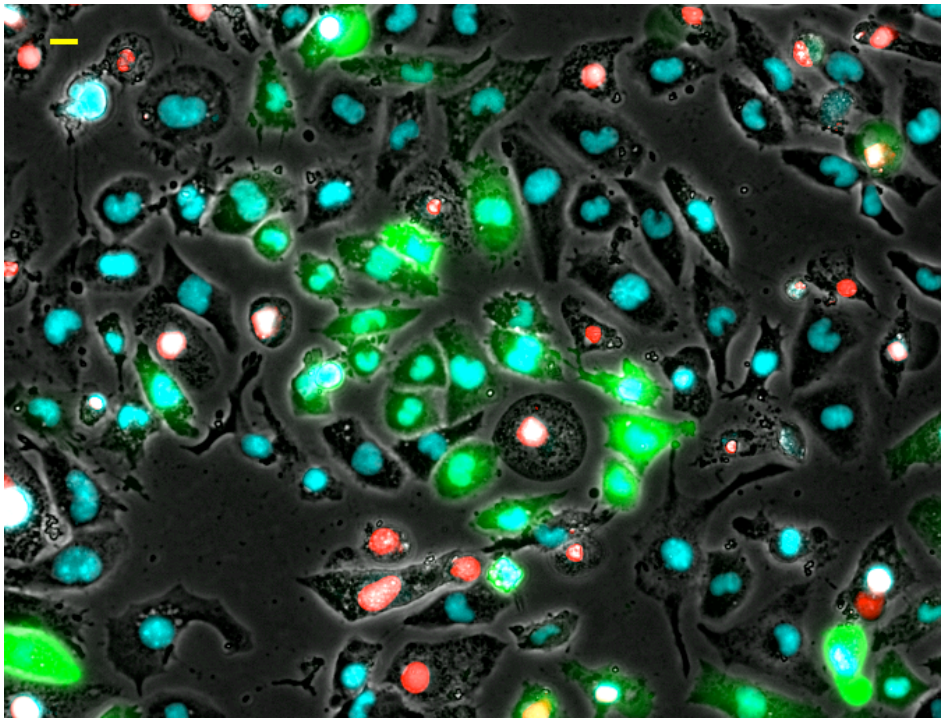


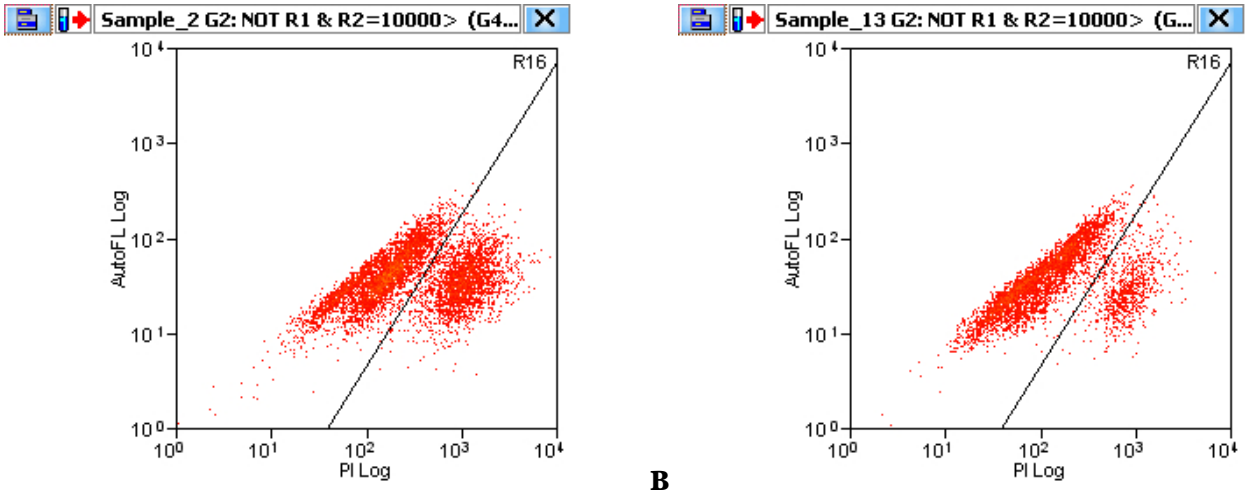
Figure 3-16: Cell viability stain.

Composite epifluorescence and phase-contrast image demonstrating viability staining in HL–1 cells, with Hoechst 33258 (cyan) and propidium iodide (red). Cells were additionally transfected with pEGFP-N1 (green), to confirm that transfection status and nuclear staining could be visualized simultaneously. Scale bar, 20μm.

3.4.1.2.2. *Flow cytometry*

To increase throughput, the protocol was adapted to quantify cell death by flow cytometry. Cells were stained with propidium iodide as described above, harvested by trypsinization, and resuspended in 0.5ml of phosphate-buffered saline. Cell death was quantified using a Beckman Coulter CyAn ADP flow cytometer

(Jenner Institute, University of Oxford). Acquisition thresholds were set using unstained controls at the beginning of each experiment, and events were gated to exclude debris and multi-cellular aggregates. A total of 10,000 cells per sample were counted, and cell death was expressed as the percentage of PI-positive cells (Figure 3-17).



A **B**

Figure 3-17: Quantification of cell death by flow cytometry with propidium iodide staining.

Scatter plots represent the logarithm of propidium iodide (PI) fluorescence (horizontal axis) and autofluorescence (vertical axis). Cells were stained with PI, and cell death was measured as the percentage of cells above a threshold determined using an unstained control. **(A)** Control sample; 41.2% cell death. **(B)** Cells treated with the caspase inhibitor zVAD-FMK (see section 3.4.1.4); 10.0% cell death.

3.4.1.3. Optimization of incubation conditions

Several groups have described models of simulated ischemia/reperfusion using HL-1 cells, but published protocols vary considerably. For example, the duration of hypoxia varies widely between sources, from 1.5[165] or 2 hours[166], to 12[167] or even 24 hours[165,168]. Since there appears to be no clear consensus, pilot studies were performed to establish the optimal incubation conditions empirically. In addition to incubation times, several other variables were optimized as described below, including composition of media, O_2 concentration, and cell plating density.

Incubation media were adapted from the protocol published by Brady *et al.*, who performed simulated ischemia/reperfusion experiments in HL-1 cells[166]. In order to approximate the conditions in the ischemic

myocardium (*i.e.*, acidosis, hyperkalemia, glucose deprivation, lactate accumulation), a modified "ischemic-mimetic" Krebs-Henseleit buffer was used for hypoxic incubations (Table 3-2); for the "reperfusion" phase, a standard Krebs-Henseleit buffer was used. All media were filter-sterilized before use, and media for hypoxic incubations were pre-equilibrated at the required O_2 concentration, overnight in filter-capped tissue culture flasks[169].

	Ischemic-mimetic buffer (pH 6.6)	**Reoxygenation buffer** (pH 7.4)
NaCl	**125.00**	110.00
KCl	**8.00**	4.70
$NaHCO_3$	6.25	**25.00**
KH_2PO_4	1.20	1.20
$MgSO_4$	1.25	1.25
$CaCl_2$	1.20	1.20
HEPES	20.00	20.00
Glucose	**-**	**15.00**
Na lactate	**5.00**	**-**

Table 3-2: Composition of buffers for simulated ischemia/reperfusion experiments.
Components which differ between ischemic-mimetic and reoxygenation buffer are highlighted in boldface. All concentrations are expressed in mM.

Since the duration of hypoxia in simulated ischemia/reperfusion experiments varies widely as described above, time-course experiments were performed to determine the optimal incubation time. In order to differentiate between the effects of hypoxia and medium composition (*e.g.*, starvation), initial experiments also included control groups incubated in complete Claycomb medium, rather than the buffers detailed above.

For initial pilot experiments, HL-1 cells were incubated at 1% O_2[168] in Claycomb medium or ischemic-mimetic buffer for 1, 3, 6, 12, or 24h. To minimize fluctuations in O_2 concentration resulting from removal of individual samples during time-course experiments, hypoxic incubations were performed in a sealed

incubator equipped with an air-lock chamber (Ruskinn Invivo$_2$ 400, courtesy of the Ratcliffe group, Centre for Cellular and Molecular Physiology, University of Oxford). After cells were removed from the hypoxic incubator, media were replaced with normoxic Claycomb medium or reoxygenation buffer, supplemented with 1μg/ml propidium iodide. Cells were transferred to a normoxic incubator, and harvested after 60, 90, or 120 minutes of reoxygenation. All media were collected at each stage of the experiment, stained with PI, and added to the final suspension for flow cytometry, in order to include cells which had died and detached during the incubations.

Pilot experiments demonstrated that hypoxic incubations up to 12h were not sufficient to cause significant cell death in HL-1 cells (Figure 3-18). At 24h, there was a clear increase in cell death, which was dependent on the duration of reoxygenation (Figure 3-19).

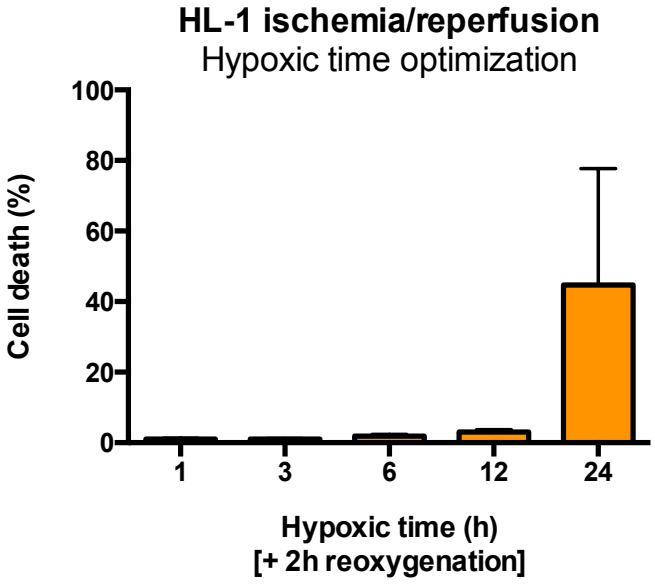


Figure 3-18: Effect of duration of hypoxia on cell viability.

Bars represent multiple wells (n>500 cells each) which were incubated at 1% O_2 for the time indicated, followed by 2h reperfusion.

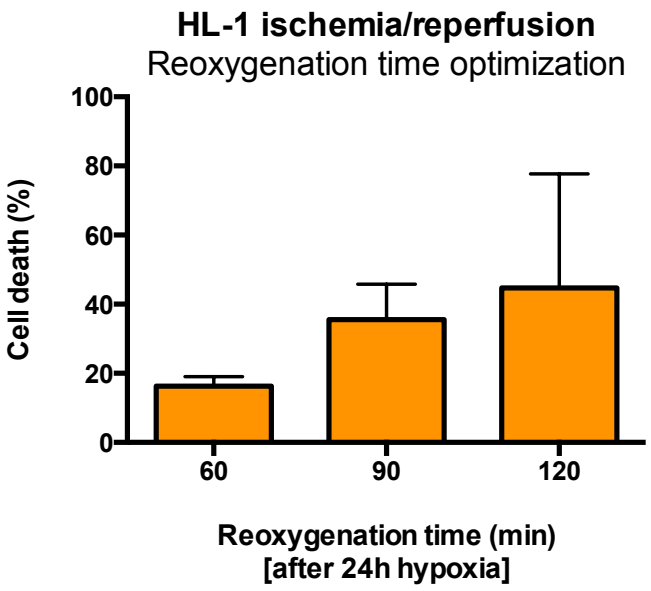


Figure 3-19: Effect of duration of reoxygenation on cell viability.

Bars represent wells which were incubated at 1% O_2 for 24h, followed by reoxygenation for the time indicated.

Since the maximal effect, observed after 24h hypoxia + 2h reoxygenation, was relatively modest (44.7% cell death), additional experiments were conducted to determine whether further increasing the duration of hypoxia, or decreasing the oxygen concentration, would have a more pronounced effect. Cells were incubated for either 24 or 48h, under normoxic conditions, moderate hypoxia (1% O_2), or severe hypoxia (0.1% O_2). In order to determine whether cell death was due to hypoxia, nutrient deprivation, or a combination of the two, samples were incubated in complete Claycomb medium (hypoxia alone), ischemic buffer supplemented with 15mM glucose, or ischemic buffer without glucose (Figure 3-20). All hypoxic media were titrated to pH 6.6 to mimic acidosis; normoxic media were pH 7.4.

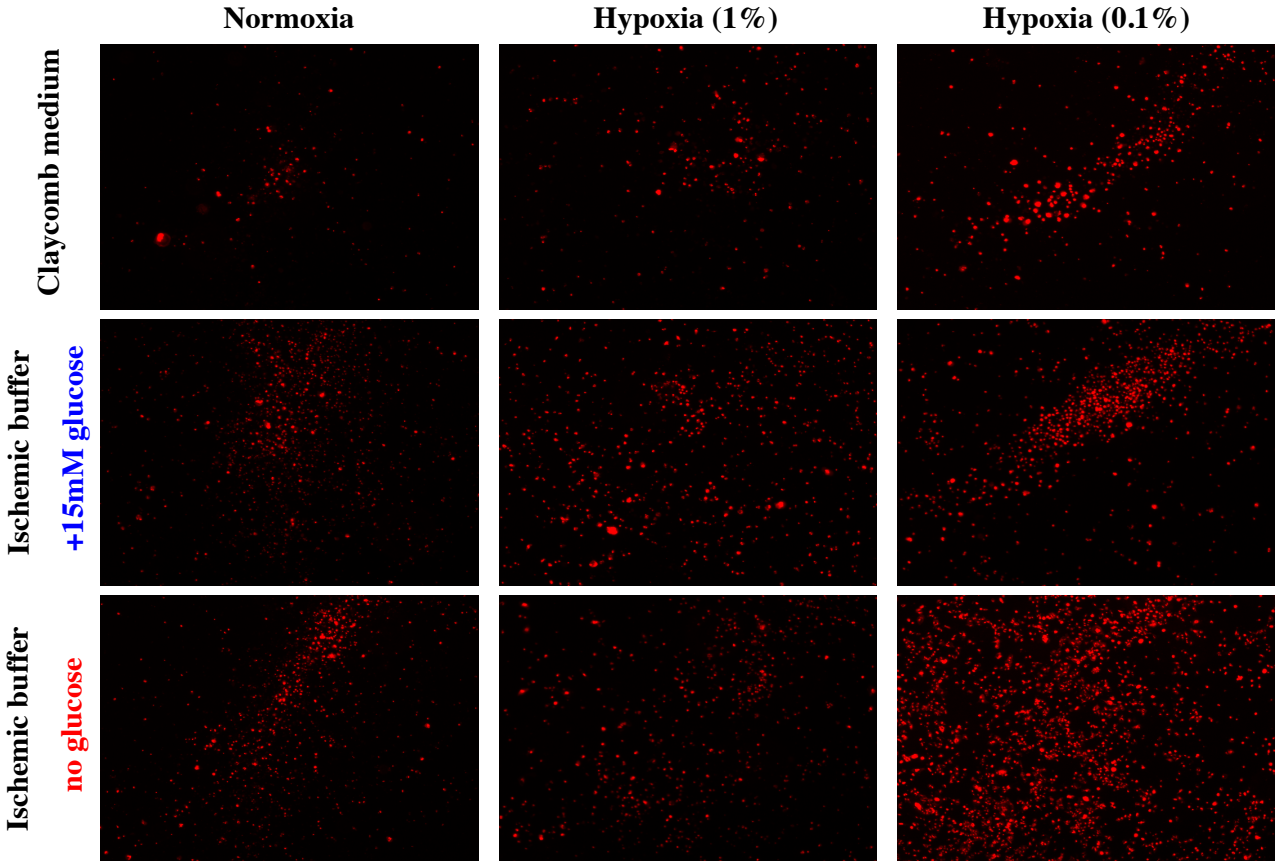


Figure 3-20: Optimization of O_2 concentration and incubation media in HL-1 cells.

Samples were incubated for 24h, reoxygenated for 2h, and stained with propidium iodide to visualize nuclei of dead cells (note that cell density by phase-contrast imaging and Hoechst staining was similar in all wells, but has not been shown for clarity of presentation). Representative images were obtained from the central field of each well.

Propidium iodide staining indicated that both severe hypoxia (0.1%) and nutrient deprivation (no glucose) were required to induce significant cell death in this model. Cell death was quantified in the groups incubated in Claycomb medium and glucose-free ischemic buffer (Figure 3-21). There was a dose-dependent

relationship between severity of hypoxia and cell death in both groups, which was particularly pronounced in cells incubated in ischemic buffer (69.1 ± 1.8% cell death at 0.1% O_2). Extending hypoxic incubation to 48h affected viability of cells incubated at 1% O_2 most severely. Since the relationship between severity of hypoxia and cell viability was most pronounced at 24h, incubation for 24h at 0.1% O_2 was deemed to be the most suitable for further experiments.

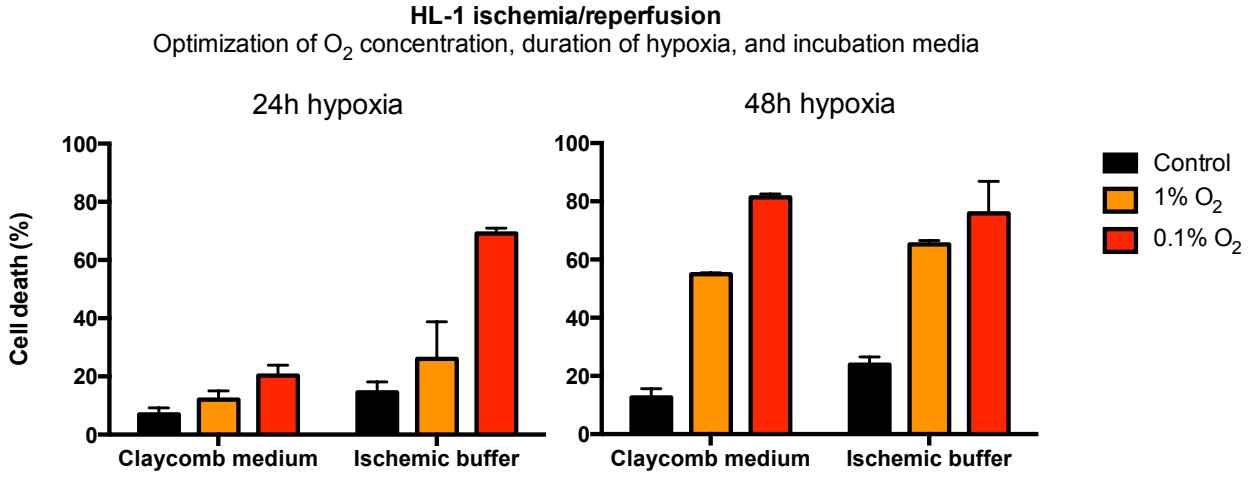


Figure 3-21: Optimization of hypoxic incubation time, O_2 concentration, and incubation media.

As expected, cell death increased with duration and severity of hypoxia, and was generally higher in cells incubated in ischemic buffer than in cells incubated in Claycomb medium. n=3 independent wells per group.

Finally, to determine whether it was preferable for cultures to be sub-confluent or confluent at the beginning of hypoxic incubation, experiments were performed in cells seeded at either 0.25 or 0.5 x 10^5 per well (in 24-well plates). No significant difference was observed, and all subsequent experiments were performed at 0.5 x 10^5 per well to maximize the number of cells for flow cytometry (Figure 3-22).

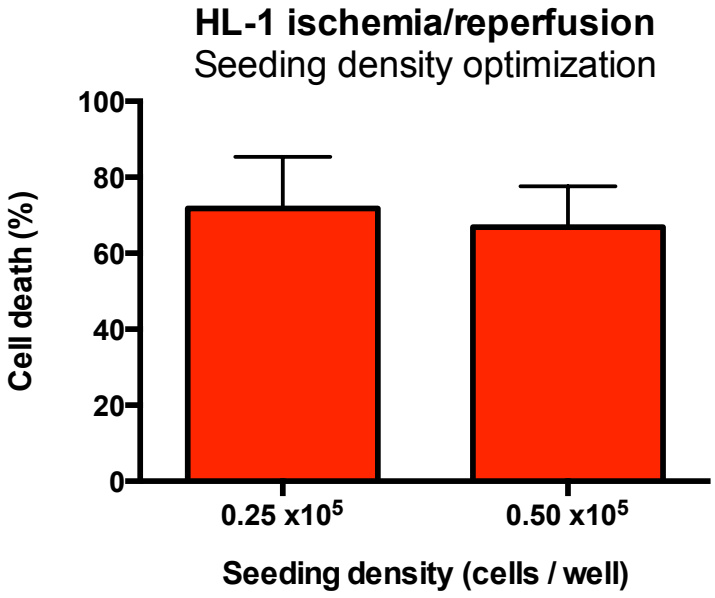


Figure 3-22: Effect of seeding density on cell viability.

Cells were plated at the densities indicated, and incubated at 0.1% O_2 for 24h.

3.4.1.4. The caspase inhibitor zVAD-FMK as a positive control for prevention of cell death

In order to determine whether the simulated ischemia/reperfusion model was suitable for detection of cardioprotective interventions, pilot experiments were performed using the non-selective caspase inhibitor benzyloxycarbonyl-Val-Ala-Asp-fluoromethylketone (zVAD-FMK).

Oligopeptide caspase inhibitors such as zVAD-FMK were initially developed when it was discovered that interleukin-1β-converting enzyme possesses cysteine protease activity; peptide-aldehyde compounds containing enzyme's substrate sequence, Tyr-Val-Ala-Asp (YVAD), were shown to inhibit its activity[170]. This enzyme was first linked to a role in apoptosis when the *C. elegans* cell death gene *ced-3* was cloned, and found to encode a protein with significant sequence similarities[171]. A fluoromethyl ketone derivative of the original inhibitors, zVAD-FMK, was subsequently found to inhibit apoptosis in thymocytes[172].

Several studies have applied zVAD-FMK to models of cardiac ischemia/reperfusion injury, primarily to determine whether apoptosis plays a significant role in cardiomyocyte death. Pre-incubation of isolated rabbit cardiomyocytes with zVAD-FMK was found to reduce cell death in response to metabolic inhibition, in a dose-dependent manner (10μM/100μM)[173]. In an *in vivo* rat model, administration of zVAD-FMK before, during, and after ischemia/reperfusion was found to improve functional recovery and reduce infarct size[174]. Most significantly, zVAD-FMK (50/100μM) was used in a model of simulated ischemia/reperfusion injury in HL-1 cells, and was associated with a ~50% reduction in cell death[175].

The pilot experiments using zVAD-FMK were performed under the conditions established above (24h in ischemic-mimetic buffer at 0.1% O_2, 2h in reoxygenation buffer). Since the ultimate goal was to apply the model to studying the effect of CK overexpression, which would be present throughout the experiment, zVAD-FMK was included during the hypoxic and reoxygenation incubations (as opposed to, for example, pre-incubation before ischemia). Previous studies have demonstrated a maximum protective effect at 100μM zVAD-FMK; in order to minimize potential toxicity, a lower dose was also tested (10μM). Control cells were

incubated with 0.1% DMSO (v/v), equivalent to the concentration present in treated cells. Cell death was quantified by flow cytometry, as described above (Figure 3-23). Incubation with 100μM zVAD-FMK significantly and reproducibly decreased cell death (60.7 ± 2.1% of control); no significant effect was observed at 10μM (96.6 ± 2.6%). Therefore, 100μM zVAD-FMK was used as a positive control for all subsequent assays.

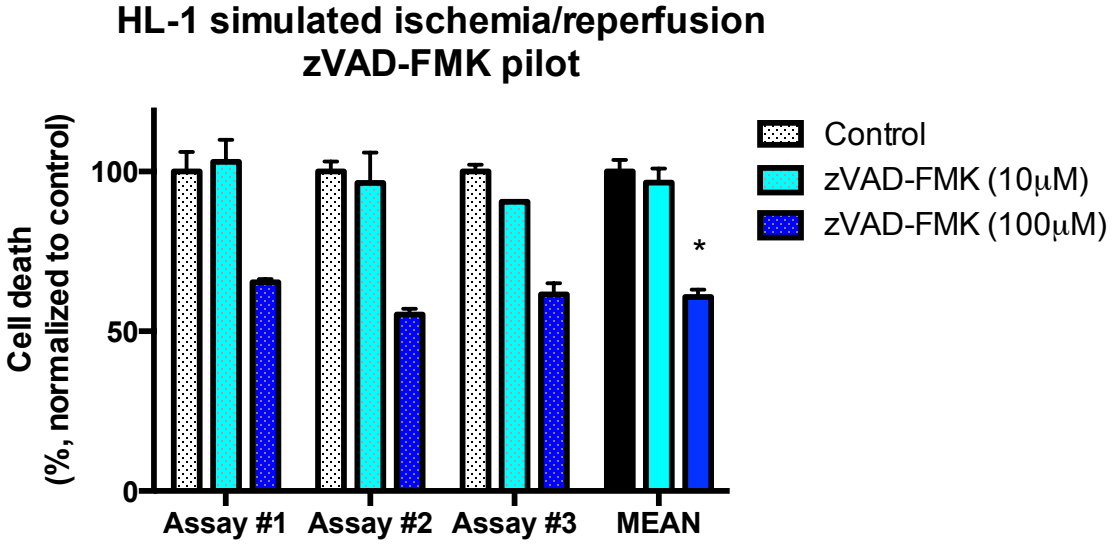


Figure 3-23: Pilot experiment to determine the effectiveness of zVAD-FMK as a positive control in HL-1 simulated ischemia/reperfusion.

Normalized results of three consecutive assays are shown (n=2 wells per treatment), followed by mean±SEM of all assays. Results were analyzed by one-way ANOVA with Dunnett's multiple comparison test. * denotes a significant difference compared to control.

3.4.1.5. Identification of transfected cells with pBFP2-nuc

Since attempts at establishing stably transfected HL-1 cells were unsuccessful, simulated ischemia/reperfusion experiments were performed in transiently transfected cells. Transfection efficiency was relatively low in HL-1 cells, and it was therefore necessary to identify which specific cells had been transfected in each experiment. Since cell death was being quantified by flow cytometry, cells could be co-transfected with a fluorescent protein, and transfected cells identified by fluorescence in the appropriate

channel. Initial experiments were performed using pEGFP-N1 as a transfection marker; however, despite the use of appropriate filters, there was a degree of spectral bleed-through between EGFP and propidium iodide in cells which were strongly positive for either signal (this was confirmed using untransfected or unstained controls, respectively). This could not be entirely eliminated by compensation, and therefore an alternative marker was sought.

In order to reduce spectral overlap between the transfection marker and propidium iodide, a blue- or cyan-fluorescent protein would be preferable to GFP. Furthermore, cell death could lead to disruption of the cell membrane and loss of cytoplasmic signal; since dead cells were being identified by nuclear propidium iodide staining, a nuclear fluorescent protein would be ideal. Therefore, the nuclear-targeted, blue-fluorescent EBFP2-Nuc was selected[176]. HL-1 cells were transfected with the expression vector pEBFP2-Nuc (a kind gift from Dr. Matthew Daniels, University of Oxford), and expression was confirmed by epifluorescence microscopy (Figure 3-24).

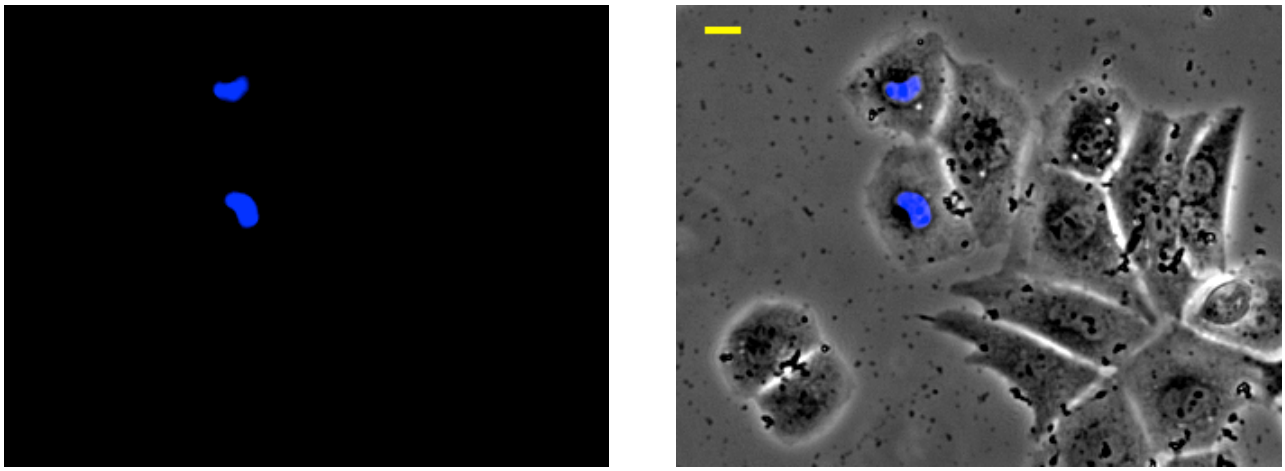


Figure 3-24: Expression of EBFP2-Nuc in HL-1 cells.

Cells were transfected with pEBFP2-Nuc, and imaged by epifluorescence microscopy to visualize EBFP2 expression (left). Phase-contrast imaging confirmed that the protein was expressed in the nucleus (overlay, right). Scale bar, 20μm.

Expression of EBFP2-Nuc did not interfere with propidium iodide signal in flow cytometry, and was therefore used as a transfection marker in all subsequent experiments.

3.4.2. Final protocol and results

HL-1 cells were seeded at a density of 0.5 x 10^5 per well in gelatin/fibronectin-coated 24-well plates. After 24h, cells were transfected with expression vectors (CKmt, CK-M, CK-B) or empty vector (pcDNA3.1-), using FuGENE HD. All constructs were co-transfected with pBFP2-Nuc as a transfection marker, and cells were cultured for 48h under standard conditions to allow for protein expression. An untransfected control group was included in all experiments, and additional untransfected wells were incubated with the caspase inhibitor zVAD-FMK (100μM), as a positive control.

Simulated ischemia was induced by culturing cells for 24h at 0.1% O_2 in ischemic-mimetic buffer, followed by 2h in reoxygenation buffer. Cells were harvested by trypsinization and resuspended in phosphate-buffered saline. Cell death was analyzed using a Beckman Coulter CyAn ADP flow cytometer. A total of 10,000 cells per well were counted, and cell death was expressed as the percentage of BFP-positive (*i.e.*, transfected) cells which were positive for propidium iodide.

Compared to cell death in untransfected controls (40.5 ± 3.7%), there was no significant difference in wells transfected with empty vector (37.0 ± 4.2%), CK-M (36.2 ± 5.9%), or CK-B (39.5 ± 4.8%). Transfection with CKmt was associated with a significant reduction in cell death (30.1 ± 3.1%). Treatment of untransfected cells with 100μM zVAD-FMK also significantly reduced cell death (23.4 ± 3.4%), as expected (Figure 3-25).

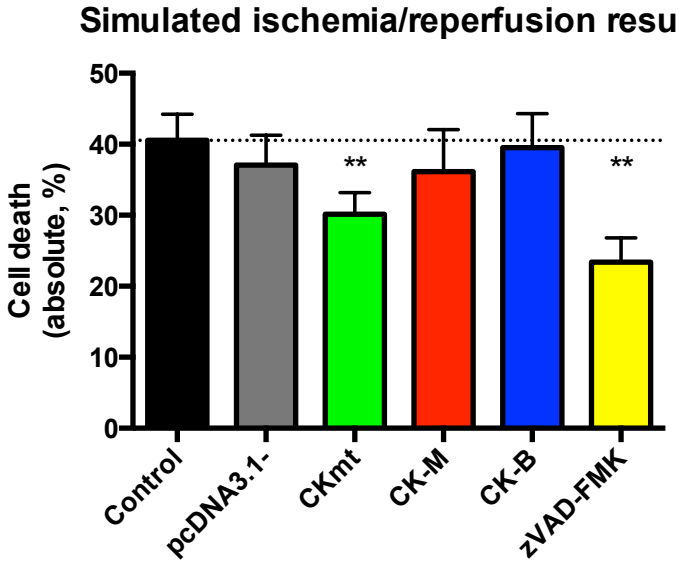


Figure 3-25: Results of simulated ischemia/reperfusion experiments in transiently transfected HL-1 cells.

Data are pooled results of six consecutive assays (n=2 wells per treatment, per assay), normalized to cell viability in untransfected controls for each assay. Results were analyzed by one-way ANOVA with Dunnett's multiple comparison test. ** denotes a significant difference compared to control.

3.5. Discussion

The goal of the experiments described in this chapter was to establish and validate models of creatine kinase (CK) overexpression in cultured cells, and determine whether CK overexpression affects viability in an *in vitro* model of simulated ischemia/reperfusion injury. Expression constructs were generated by cloning the murine open reading frames of CKmt, CK-M, and CK-B into pcDNA vectors, with incorporation of C-terminal hemagglutinin (HA) tags. HEK293 and HL-1 cells were transfected, and expression of HA-tagged protein was confirmed by western blot for all constructs. An electrophoretic assay was used to confirm the activity of the individual isoenzymes, as well as the ability of CK-M to form both CK-MM and CK-MB dimers *in vitro*. Finally, immunocytochemical experiments were performed in cells transfected with CKmt; co-localization analysis confirmed that the protein was being expressed in the mitochondria, as expected.

Stably transfected HEK293 cells were generated by antibiotic selection. Selection of HL-1 cells was performed in parallel, but no stably transfected lines were established, despite multiple attempts. Finally, transfection of cells with GFP-tagged CKmt led to compartmentalized expression of the protein, but stable cell lines could not be generated, in either cell type.

Once *in vitro* models of CK overexpression were generated, the next goal was to establish a protocol of simulated ischemia/reperfusion injury. Pilot experiments were performed to empirically determine the optimal duration of hypoxia and reoxygenation, composition of incubation media, severity of hypoxia, and cell seeding density. The caspase inhibitor zVAD-FMK was optimized as a positive control, and was included in all assays. A final protocol was established, with cells incubated in ischemic-mimetic medium at 0.1% O_2 for 24 hours, followed by 2 hours of reoxygenation with propidium iodide staining, and quantification of cell death by flow cytometry. Cell death was significantly reduced in cells transiently transfected with CKmt (by 25%), but not in cells transfected with the cytosolic isoenzymes. These results are discussed in detail below.

3.5.1. Generation of stably transfected cell lines

To empirically determine the optimal antibiotic concentrations for selection of stably transfected HEK293 and HL-1 cells, kill curves were performed. HEK293 cells formed resistant colonies for each transfection group, as expected. In contrast, no resistant HL-1 colonies were observed. There are several possible reasons for this finding. First, the antibiotic concentration may have been too high; this is unlikely, since the G-418 concentration used (500μg/ml) was determined empirically in the same cells used for stable transfections. Second, cell viability could be adversely affected by the expression construct; however, HEK293 cells transfected in parallel were viable, although it remains possible that this was a cell-type-specific effect. Third, integration of foreign DNA into the cellular genome can have a toxic effect by disrupting endogenous genes; while possible in individual clones, this is unlikely to be responsible for the lack of stable colonies in multiple groups, across several experiments. Fourth, transfection reagent toxicity may adversely affect cell viability, which is possible in this setting, particularly if HL-1 cells are more sensitive to these effects than HEK293 cells. Finally, HL-1 cells are generally difficult to transfect, compared to widely used lines such as HEK293, and require more specific culture conditions. Significantly, the health of HL-1 cultures depends on intercellular contact (*e.g.*, contractile activity is only observed at full confluence), and these cells do not grow well when plated at low densities. Since selection requires clones to be expanded from single cells which have stably integrated the expression construct, this is likely to be more difficult to achieve in HL-1 cells than other lines. Nonetheless, there are individual reports of stably transfected HL-1 lines[177-181]. The majority of these publications do not report the specific conditions used, or whether the efficiency of stable selection was verified using suitable controls (such as GFP expression in this thesis). Only one paper cites the G-418 concentration used (800μg/ml)[180], which is significantly higher than that used in this thesis (500μg/ml). This provides further evidence that the antibiotic concentration was appropriate, but indicates that stable transfection of HL-1 cells is feasible under the appropriate conditions.

Ultimately, no further optimization of stable transfection in HL-1 cells was performed, as experiments in HEK293 cells were sufficient to demonstrate that the constructs were being expressed and enzymatically active. Subcellular localization experiments were performed in transiently transfected cells, as this does not

require the entire cell population to be homogenously transfected. Finally, stably transfected cells were not required for the simulated ischemia/reperfusion assays. The protocol was designed to use transiently transfected cells, in order to avoid any potential confounding effects of using multiple cell lines in parallel, *e.g.* due to differences in plating density or passage number.

3.5.2. Expression of GFP-tagged mitochondrial creatine kinase

The CKmt coding sequence was cloned into a pEGFP-N1 vector, in order to produce a CKmt-EGFP fusion protein which could be directly visualized in live cells. The fusion protein was expressed in both HEK293 and HL-1 cells, and demonstrated subcellular compartmentalization in both cell types, suggesting that it was expressed in the mitochondria. Selection of stably transfected cells was unsuccessful in both cell types. While this is consistent with the failure to establish similar lines in HL-1 cells transfected with HA-tagged CK constructs, there were no GFP+ colonies after a week, at which point controls transfected with "empty" pEGFP-N1 vector were still viable and homogenously expressing EGFP. Significantly, a similar pattern was observed in HEK293 cells, which had previously been used to successfully generate stably transfected lines.

The fact that both HEK293 and HL-1 cells transfected with "empty" pEGFP-N1 were viable, but cells transfected with pCKmt-EGFP were not, suggests that the construct itself is having an adverse effect on cell viability. There are two likely mechanisms which could be responsible for this effect, both due to the effect of adding the relatively large EGFP peptide to CKmt. This may impede formation of CKmt octamers, which is thought to play a significant role in the enzyme's function. While octamer formation is primarily mediated by N-terminal residues (and the EGFP protein is attached at the C-terminus)[182], the overall size of the complex may interfere with higher levels of protein structure. Furthermore, CKmt is localized in the mitochondrial intermembrane space, where it is closely associated with a variety of inner and outer membrane proteins. The addition of the EGFP peptide may affect binding of CKmt to these proteins or the membrane itself – particularly since C-terminal residues are thought to play a role in membrane association[183]. Finally, the

CKmt-EGFP protein could simply be too large to fit in the relatively narrow intermembrane space. This could have knock-on effects on mitochondrial structure and function, which could in turn adversely affect cell viability.

3.5.3. CKmt overexpression reduces cell death in an *in vitro* model of ischemia/reperfusion injury

In order to study the effect of CK overexpression in ischemia/reperfusion injury, an *in vitro* model was developed and validated. Cell death was significantly reduced in wells transfected with CKmt, but not in wells transfected with empty vector or either of the cytosolic CK isoenzymes. This suggests that CKmt overexpression may protect against acute ischemia/reperfusion injury. The mechanism by which this may occur is not addressed in this model, but may be due to augmented delivery of high-energy phosphates generated by mitochondrial oxidative phosphorylation, stabilization of mitochondrial function, or inhibition of the permeability transition.

The primary limitation of these simulated ischemia/reperfusion experiments is that it may be difficult to draw strong parallels between the findings of *in vitro* assays and *in vivo* disease models. First of all, there are significant energetic and functional differences between HL-1 cells and cardiomyocytes[184]. In addition, the duration of hypoxia (24h) is significantly longer than that used in surgical models of ischemia/reperfusion injury (in our laboratory, commonly 45 minutes[144]); however, this discrepancy may be due to the markedly different metabolic requirements of a living, beating heart and cultured cells. Nonetheless, similar protocols have been previously reported for HL-1 cells[168], and the incubation conditions were determined empirically in pilot experiments. An additional limitation is that the "normoxic" oxygen concentration used in standard tissue culture is significantly higher than under physiological conditions in the heart. The concentration of O_2 in air is 21%, which at atmospheric pressure equates to a partial pressure of approximately 160 mm Hg. Extracellular oxygen *in vivo* is typically ~40 mm Hg[185], which would be equivalent to ~5% O_2 in a tissue culture incubator. Myocardial intracellular oxygen levels are even lower, estimated at 4-6 mm Hg, or ~0.5%

O_2[186] – barely higher than the level used to induce hypoxia in these experiments (0.1%). Therefore, it is difficult to assess how well this model corresponds to the conditions experienced by ischemic cardiomyocytes *in vivo*. Finally, the "reoxygenation" stage of the experiment is also a simplification, as it does not take into account the effect of arterial re-flow and reactive hyperemia – in order to address this issue, it would be preferable to use a model in which cells are incubated in a flow chamber, rather than a standard culture dish. Taken together, these factors call into question whether *in vitro* models can be a suitable approximation of ischemia/reperfusion injury. However, two of the studies referenced in this chapter report experiments in both HL-1 cells and the intact heart, and found analogous results[167,175]. This suggests that, under suitable conditions, *in vitro* models can be used to predict the results of *ex vivo* or *in vivo* experiments.

It is worth noting that transfection with CK-M did not reduce cell death in this model, in contrast to the recent finding that overexpression of CK-M in the mouse heart reduces LDH release (a marker of cell death) during *ex vivo* ischemia/reperfusion[146]. There are several reasons why this result might not be recapitulated *in vitro*, broadly falling into two categories: either (1) the *in vitro* model is not a suitable approximation of ischemia/reperfusion injury, or (2) the model is suitable, but CK-M, specifically, does not have a protective effect in this setting, due to methodological differences. While it remains possible that the *in vitro* model established in this chapter is not a valid approximation of ischemia/reperfusion injury (see above), there are specific methodological differences which could explain the apparent discrepancy in findings with respect to CK-M. The simplest explanation is that the level of overexpression was not appropriate, as it is difficult to determine whether the increase in CK-M activity *in vitro* is of a similar magnitude to the transgenic model. Alternatively, it may be that the specific mechanism by which CK-M exerts its protective effect in the intact heart does not play a role in this *in vitro* model. The authors of the CK-M study suggested that the protective effect may be due to attenuation of ischemic acidosis (pH in CK-M hearts was maintained in the 6.3-6.4 range, while pH in control hearts fell to 6.0), and more rapid restoration of neutral pH during reperfusion. In contrast, the *in vitro* model used incubation media of specific pH (6.6 for hypoxia, 7.4 for reoxygenation). While no data are available on the actual intracellular pH during these incubations, the fact that all cells were subjected to identical incubation conditions suggests that, if the protective effect of CK-M

overexpression is mediated by attenuation of ischemic acidosis, this may not have been observed in the *in vitro* model.

The fact that transfection with CKmt, but not CK-M, was found to have a protective effect should also be addressed, but this is difficult to interpret in the absence of data on *in vivo* CKmt overexpression for comparison. For example, it may be that CKmt exerts a more potent effect than CK-M. If so, the *in vitro* model may not be sufficiently sensitive to detect a (less pronounced) effect of CK-M, or the severity and duration of hypoxia used in this protocol may be too strong a stimulus for cell death to be prevented by CK-M overexpression. If so, this "false negative" would indicate that caution should be taken when excluding potential treatments based on a negative result in *in vitro* experiments.

In conclusion, while the results indicate that overexpression of CKmt may protect against ischemia/reperfusion injury, further work is required to confirm whether this is the case, and whether the *in vitro* model can be applied to screen for other cardioprotective treatments.

3.6. Conclusions and future work

The experiments performed in this chapter demonstrated that it is feasible to (over-)express the creatine kinase isoenzymes in mammalian cells, using suitable transfection vectors. Furthermore, addition of a C-terminal hemagglutinin tag does not abolish enzymatic activity of the individual isoenzymes, or interfere with mitochondrial targeting of CKmt. Finally, in a model of simulated ischemia/reperfusion injury, CKmt was found to significantly reduce cell death. This suggests that increasing CK activity, specifically that of the mitochondrial isoenzyme, may be a target for development of new therapeutic targets in acute ischemia/reperfusion injury. In order to confirm that CKmt has a protective effect, it is necessary to reproduce these findings *in vivo* in the intact heart. The following chapter discusses the generation and validation of a transgenic mouse model, overexpressing CKmt in the myocardium.

4. *IN VIVO* MODELS OF AUGMENTED CARDIAC ENERGETICS – OVEREXPRESSION OF MITOCHONDRIAL CREATINE KINASE BY TARGETED INTEGRATION AT THE ROSA26 LOCUS

4.1. Introduction

The experiments described in this chapter were performed to generate and study transgenic mice overexpressing sarcomeric mitochondrial creatine kinase (CKmt). CKmt was selected as the first CK isoenzyme for generation of an *in vivo* model, since previous studies in knockout models have demonstrated that loss of CKmt activity is particularly detrimental to the heart[126,128]. Furthermore, the results of the *in vitro* assays described in chapter 3 indicated that CKmt reduced cell death in a model of simulated ischemia/reperfusion injury, which warrants further study to confirm whether a protective effect can be reproduced *in vivo*.

This introduction describes the strategy adopted for generation of transgenic mice, using targeted PhiC31 recombination at the ROSA26 locus.

4.1.1. Targeted transgenesis at the ROSA26 locus

The ROSA26 (reverse orientation splice acceptor 26) locus was first established as a promoter trap in a study of murine developmental gene expression[187], and was subsequently targeted for site–specific transgene integration[188]. Transgene integration was not found to affect development, viability, or fertility of mice,

indicating that disruption of the locus does not have significant adverse effects. Site–specific integration at ROSA26 has two significant advantages over random chromosomal integration, as this ensures that (a) transgene insertion does not disrupt endogenous genes, and (b) transgene expression is not affected by the presence of unexpected regulatory elements around the integration site, such as promoters, enhancers, or silencers. The ROSA26 locus has been widely validated, and has been targeted for more complex models, including conditional expression in Cre–lox[188,189] or tetracycline–inducible[190] systems, as well as Gateway cloning[191,192].

The endogenous promoter at ROSA26 is constitutively active, and can be used if low–level, ubiquitous transgene expression is desired. If a different level or pattern of expression is preferable, as in this model, an alternative promoter can be inserted at the ROSA26 locus to drive transgene expression. Transcriptional regulation of the endogenous ROSA26 site is complex[193], and the level of transgene expression has been found to be orientation–dependent, possibly due to the effect of the endogenous ROSA26 promoter and other regulatory sequences[192,194]. Therefore, an H19 insulator was included in the transgenic construct, in order to minimize any potential effect of surrounding regulatory elements on transgene expression[195].

4.1.2. PhiC31 integrase–mediated cassette exchange

PhiC31 (ϕC31) integrase is an enzyme isolated from a *Streptomyces* phage, which catalyzes recombination between two specific sequences, termed *attP* and *attB*[196]. This enzyme has been adopted for use in murine transgenesis, by incorporation of *attP* sequences in a genomic docking site. Transfection of cells with a delivery vector containing an insert flanked by *attB* sequences and a vector encoding PhiC31 integrase leads to recombination between the delivery vector *attB* and genomic *attP* sites. This yields two new sites, denoted *attL* and *attR*, which are not targeted by PhiC31 integrase; therefore, no further recombination events occur (Figure 4-5). This ensures that a single copy of the transgene is inserted, and cannot be excised by the integrase. In contrast, other recombinases commonly used in murine transgenesis, such as Cre[197] or Flp[198], do not modify their recombination sites during a reaction, meaning that the sites remain a target for their respective enzymes after an integration event has occurred.

Taken together, the use of PhiC31 integrase–mediated cassette exchange targeted to the ROSA26 locus ensures that a single copy of the transgene is inserted at a known locus[199]. This negates the need for copy–number screening in founder mice, and avoids the unpredictable consequences of positional effects on transgene expression or disruption of endogenous genes.

4.1.3. Constitutive transgene expression

The construct was designed to ensure constitutively active expression of the transgene. While there are a variety of methods for inducible transgene expression, such as the Cre–lox or tetracycline–inducible systems, these models require the presence of two separate (inducer/responder) transgenic constructs, and may have unintended effects on phenotype. For example, there is evidence that expression of Cre recombinase itself can be cardiotoxic[200,201]; while the mechanism remains to be established, recent evidence suggests that it may be due to DNA damage and induction of apoptosis[202]. Furthermore, a long-term goal of the project is to cross transgenic lines, in order to simultaneously overexpress various elements of the CK system (*e.g.*, other CK isoenzymes and/or the creatine transporter). Since each inducible model requires two separate transgenic loci (inducer/responder), crossing such mice with a different line would generate triple- or even quadruple-transgenic mice, which would exponentially increase the number of mice required to breed an appropriate number of transgenics and littermate controls. One of the disadvantages of using a constitutive model is that early expression of the transgene can have unpredictable effects on development; however, there is no obvious reason to suspect that overexpression of CKmt would have a detrimental effect. This risk can be further addressed by the choice of promoter, *e.g.* to minimize prenatal expression (see below). Therefore, a constitutive model was considered appropriate for this project.

4.1.4. The alpha–myosin heavy chain promoter

The αMHC promoter was selected to drive transgene expression, based on two factors: (a) cardiac specificity and (b) developmental expression pattern. While no data have been published concerning developmental expression of CKmt in mice, studies in rats have found that expression is very low in the perinatal period, increasing during the second week post–partum[54,203]. Of the cardiac–specific genes whose promoters have been characterized, expression of αMHC follows the most similar pattern[204,205]. The αMHC promoter was therefore selected, in order to ensure cardiac–specific expression while avoiding potential confounding effects due to early developmental expression of CKmt (Figure 4-1).

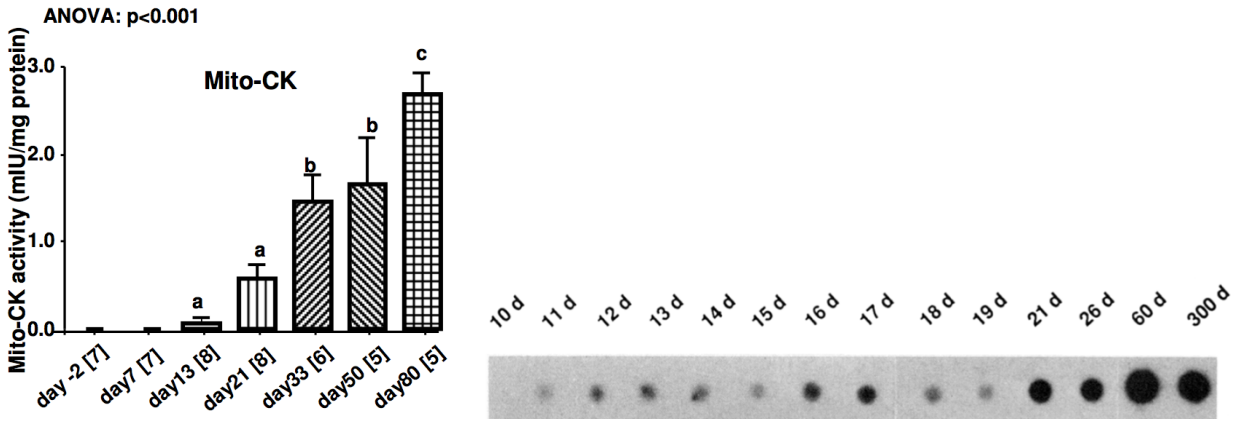


Figure 4-1: Developmental expression of CKmt and αMHC.

(A) CKmt activity in the rat heart is negligible in the perinatal period, but increases significantly over the first weeks of life. **(B)** αMHC mRNA expression in the developing mouse heart is low *in utero*, and increases rapidly after birth. Note that the legend in (A) refers to post–partum age, whereas (B) refers to days post–coitus. Figures are from Fischer *et al.*[54] and Ng *et al.*[204], respectively.

It is worth noting that there is a well–documented decrease in αMHC expression in response to cardiac hypertrophy[206], which could potentially inactivate transgene expression in disease models, abolishing any effect of CKmt overexpression. However, downregulation of αMHC–driven expression in transgenic models is modest (15–45%), and is therefore unlikely to be a significant concern[201].

4.1.5. The hemagglutinin tag

The transgenic construct was designed to incorporate a hemagglutinin (HA) tag, in order to specifically detect transgenic protein. The tag was added to the C–terminus, as the N–terminus of CKmt is known to play a role in mitochondrial targeting of the protein, as well as octamer formation[182]; therefore, adding an N-terminal tag could interfere with these processes. Furthermore, cleavage of the N–terminal mitochondrial transit peptide could lead to removal of the tag from the mature protein, making it impossible to distinguish between transgenic and endogenous CKmt.

4.1.6. Choice of background strain

Studies have demonstrated that there are significant differences between mouse strains with respect to cardiovascular physiology[207] and pathophysiology[208], and this must be taken into account when new transgenic models are being generated.

In this project, the goal was initially to generate all transgenic mice on a C57BL/6 background. This is the most widely used laboratory strain, and the mice have been well characterized, including sequencing of their complete genome[209]. Furthermore, C57BL/6 mice have been specifically used to determine the effect of genetic background on the phenotype of creatine kinase knockout models ($CKmt^{-/-}$, $CK\text{–}M^{-/-}$, and double knockouts [$M/Mt\text{–}CK^{-/-}$])[130,131].

A potential disadvantage of using the C57BL/6 strain to generate transgenic mice is that the efficiency of transgenesis can be relatively low, compared to mixed backgrounds or other strains, *e.g.* FVB; however, these statistics are primarily based on studies using pronuclear microinjection[210,211]. For blastocyst injections, the Transgenics Core in our institute has found that the best results are achieved by using hybrid F1 embryonic stem cells (ES), which are derived on a mixed 129 x C57BL/6 background, into C57BL/6 blastocysts (personal communication, Dr. Ben Davies)[212,213]. It is worth noting that the ES cells, rather than the blastocyst they are injected into, define the background of transgenic mice generated by this method.

Chimeric founder mice are derived from a mixture of the transgenic ES cells and wild–type cells in the blastocyst, and transgenic offspring were produced by mating the chimeric founders with wild–type C57BL/6 females. Since any germ cells carrying the transgene must have been derived from the ES cells (F1), this effectively constitutes a $F1^{129/C57BL/6}$ x C57BL/6 cross, and first–generation transgenic pups can therefore be considered 75% congenic with the C57BL/6 strain, necessitating further backcrossing onto a pure C57BL/6 background.

4.2. Aims and hypotheses

The goal of the experiments described in this chapter was to determine the effect of increasing myocardial CKmt activity *in vivo*, using transgenic mice. Specifically, the goal was to (1) establish the transgenic model, (2) validate expression and activity of transgenic CKmt, and (3) determine the effect of CKmt overexpression on cardiovascular phenotype.

The experimental hypothesis was that overexpression of CKmt in the heart would increase the capacity of the myocardial CK system to regenerate ATP, particularly under conditions of increased demand, and consequently render hearts more resistant to cardiovascular disease, including acute ischemia/reperfusion injury and chronic heart failure.

4.3. Methods and Results

4.3.1. Generation of transgenic mice

This section describes the generation of an *in vivo* model of CKmt overexpression, by targeted integration of the αMHC–CKmt–HA construct at the ROSA26 locus.

4.3.1.1. Cloning of vectors for transgenesis

The open reading frame of *Mus musculus* sarcomeric mitochondrial creatine kinase (*Ckmt2*) cDNA was amplified by PCR from a commercially available vector (Geneservice, I.M.A.G.E clone #30296538). Primers were designed to amplify the entire coding sequence, and incorporate a *SalI* restriction site and Kozak consensus sequence (5'), as well as a C–terminal hemagglutinin (HA) tag for protein identification, stop codon (TGA) and *HindIII* site (3'). Poly-guanine caps (GGGG) were appended to both primers, to facilitate binding of restriction endonucleases to the terminal restriction sites of PCR products, according to the enzyme manufacturer's guidelines (NEB). Primer sequences are detailed in Table 4-1.

Primer name	Sequence (5'–3')
Ckmt2_F_SalI/Kozak	GGGGGTCGACACCATGGCCAGTGCCTTCTC
Ckmt2_R_HA/stop/HindIII	GGGGAAGCTTCATGCGTAATCTGGAACATCGTATGGGTACTTCCTGCCAAACTGAGG

Table 4-1: Primers used for generation of the CKmt overexpression construct.

The underlined regions are the Kozak sequence (forward primer) and stop codon (reverse primer). The restriction sites used for cloning are marked in yellow, and the HA tag sequence is marked in green.

The *Ckmt2* cDNA was amplified using high–fidelity Phusion polymerase (NEB). PCR product was purified by ethanol precipitation and cloned into a pBluescriptII–based vector containing the αMHC promoter (a kind gift from Dr. Arash Yavari). Briefly, PCR product and vector were digested with *SalI–HF* and *HindIII*, to generate compatible ends for ligation. Restriction fragments were separated by agarose gel electrophoresis, and bands were excised and extracted (Figure 4-2).

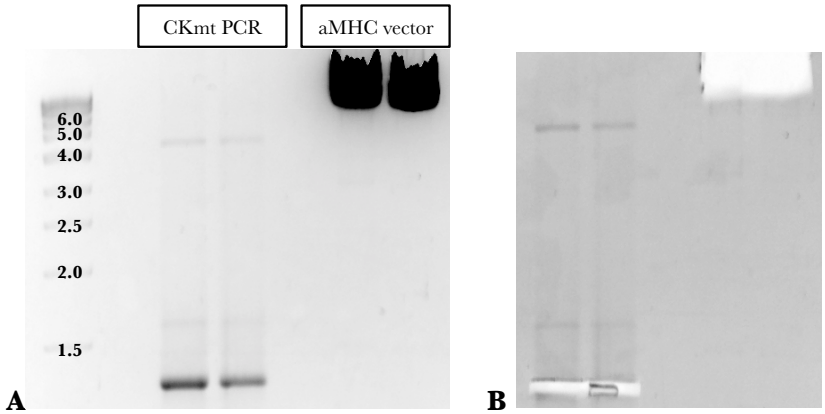
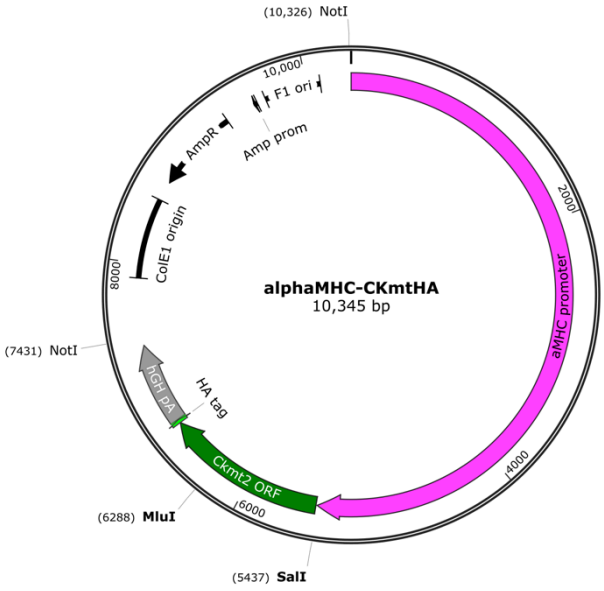


Figure 4-2: Restriction digest of *Ckmt2* PCR product and αMHC vector.

(A) Agarose gel electrophoresis of restriction digest products. **(B)** Gel re–imaged after excision of bands required for cloning.

Digested vector and PCR product were ligated using T4 ligase (NEB), and the ligation product was used to transform competent *E. coli*. Resistant colonies were selected by plating transformed bacteria on ampicillin–containing LB agar and amplified in suspension culture. DNA was extracted and purified by MiniPrep, and diagnostic restriction digest was performed to confirm insertion of a single copy of the PCR product, in the correct orientation (Figure 4-3).



A

B

Restriction enzyme(s)	*SalI*	*SalI* *MluI*	*SalI* *MluI* *NotI*
Expected restriction fragment size (bp)	10331	9480 851	 5456 2878 1146 851

C

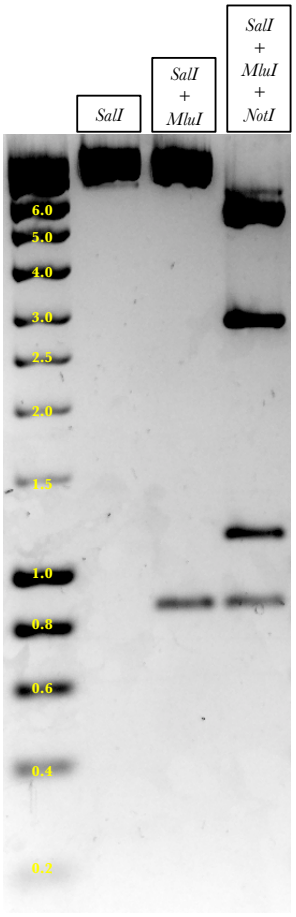


Figure 4-3: Restriction digest of αMHC–CkmtHA MiniPrep products.

(A) Map of the vector, showing the restriction sites used (*SalI*, *MluI*, 2x *NotI*). **(B)** Expected product sizes for single, double, and triple digest. **(C)** Agarose electrophoresis of products, demonstrating that the expected restriction fragments were present.

Both insertion sites and the entire *Ckmt2* open reading frame were sequenced. The verified plasmid was amplified and purified by Endotoxin–Free MaxiPrep (Qiagen), re–sequenced, and subcloned into a CB92 delivery vector (Figure 4-4) for transfection of embryonic stem cells (performed by the Wellcome Trust Centre for Human Genetics Transgenics Core).

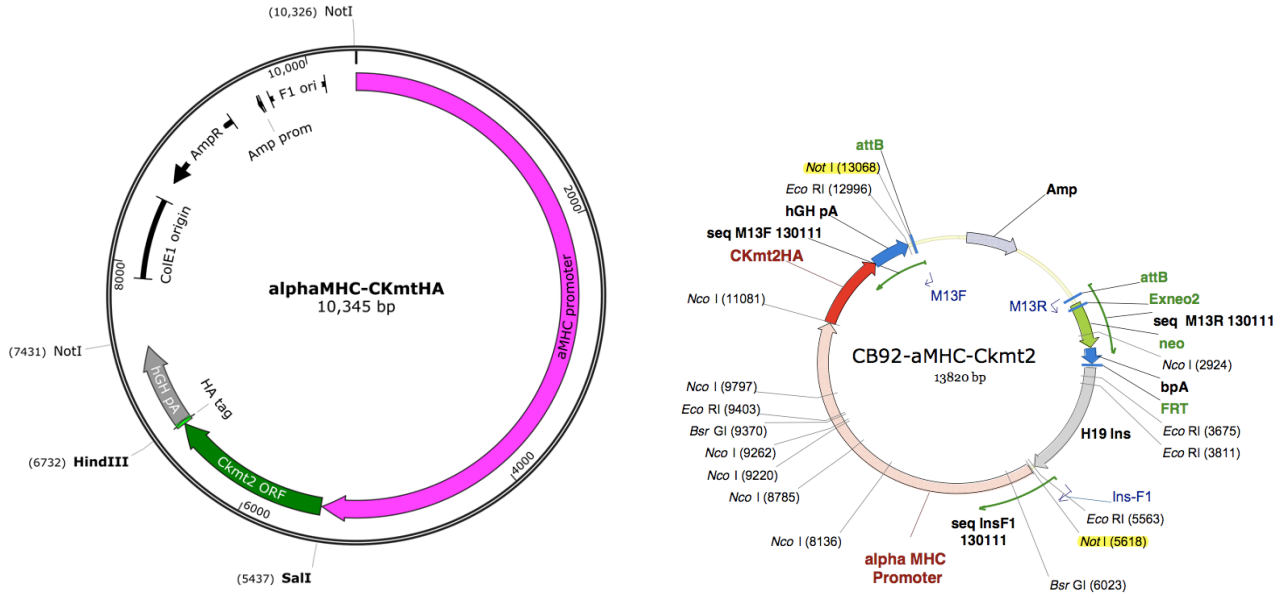


Figure 4-4: αMHC–CKmt–HA cloning for generation of the transgenic model.

(A) αMHC–CKmt–HA construct, with key features and restriction sites used for ligation (*SalI*/*HindIII*). The labelled 7,449bp fragment containing the αMHC promoter, Ckmt coding sequence, and polyadenylation signal was excised using *NotI* for cloning into the delivery vector. **(B)** CB92–αMHC–Ckmt2 delivery vector, with recombination sites for PhiC31–mediated integration (attB), neomycin resistance cassette for selection of stably transfected stem cells (neo), and insulator (H19 Ins). Note the *NotI* sites (highlighted yellow) flanking the integrated construct. Vector map (B) courtesy of Dr. Ben Davies.

4.3.1.2. Generation of chimeric founder mice by blastocyst injection of embryonic stem cells

Transgenic mice were generated by injecting C57BL/6 blastocysts with hybrid F1 embryonic stem cells (129 x C57BL/6) [212,213]. The choice of strain is discussed in detail in section 4.1.6.

Embryonic stem cells carrying the transgenic construct were generated by integration at the ROSA26 locus using PhiC31 integrase, as described above. This was accomplished by co–electroporation of the CB92 delivery vector and a vector encoding PhiC31 into ES cells containing an acceptor construct at ROSA26[214]. The CB92 vector contains a promoter–less 5' neomycin–resistance cassette, while the acceptor locus contains a constitutively active phosphoglycerate kinase (PGK) promoter. Integration in the correct (sense) orientation places the neomycin–resistance cassette downstream of the PGK promoter, driving its expression (Figure 4-5). Therefore, ES cells in which integration was successful could be selected for antibiotic resistance

(350μg/ml G–418). To exclude ES cells in which a larger fragment, *e.g.* a portion of the vector backbone, had integrated, resistant colonies were screened by PCR to confirm that integration was successful at both the 5' and 3' sites. These ES cells were subsequently microinjected into C57BL/6 blastocysts, which were implanted into pseudopregnant females to generate chimeric founder mice. A detailed report, provided by the Transgenics Core, can be found in Appendix B.1.

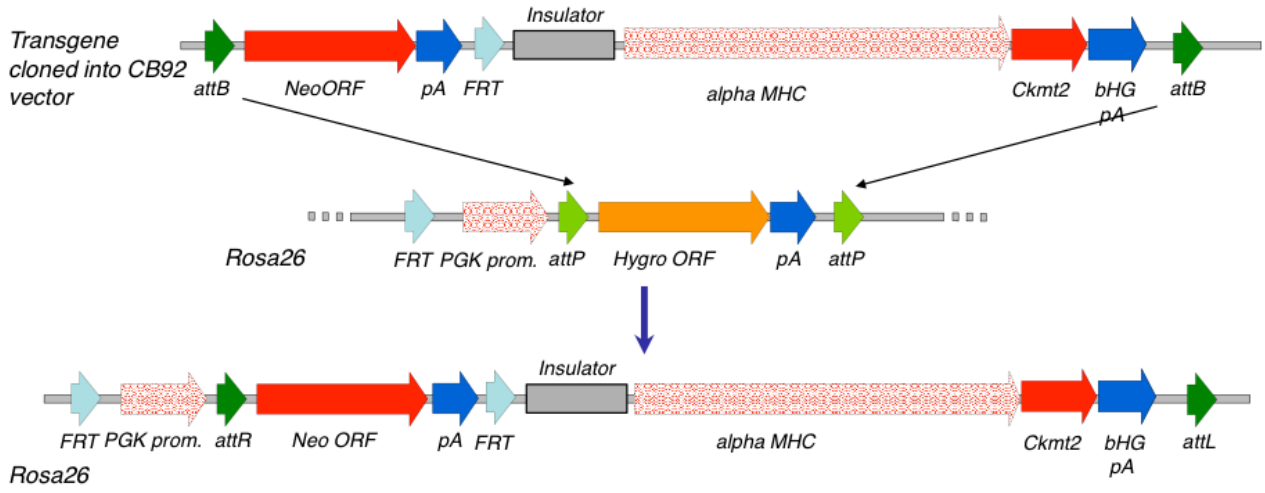


Figure 4-5: *ROSA26* recombination using PhiC31 integrase.

The PhiC31 recombination sites (*attB* on the CB92 vector, *attP* on the ROSA26 acceptor site) are modified as a result of integration, generating *attL*/*attR*, which are not substrates for further reactions. This prevents integration of additional copies of the transgene. The neomycin resistance cassette (*NeoORF*, red) confers aminoglycoside resistance for selection of cells in which the construct has integrated downstream of the PGK promoter. The 3' HA tag attached to the *Ckmt2* coding sequence is not shown. Figure courtesy of Dr. Ben Davies.

4.3.1.3. *In vitro* differentiation to confirm promoter activity in embryoid bodies

The ROSA26–αMHC expression construct is a relatively novel approach, and no data on *in vivo* expression were available at the time the model was being generated. It was therefore considered prudent to confirm functionality of the construct prior to generation of transgenic mice. This was accomplished by *in vitro* differentiation of the ES cell clones used for blastocyst microinjections. Under appropriate conditions, ES cells can spontaneously differentiate into several cell types, including the cardiomyocyte lineage[215].

Significantly, differentiated ES cells have been shown to express αMHC, suggesting that transgene expression under the control of the αMHC promoter could be observed using this technique[215,216]. This provided an opportunity to assess the presence and "tissue specificity" of transgene expression several months before transgenic mice were expected to be available.

Embryonic stem cells cultured in hanging drops aggregate under the influence of gravity, forming clusters termed embryoid bodies (EB, Figure 4-6). EBs can be grown in adherent culture, and differentiate spontaneously when cultured in medium without leukemia inhibitory factor, which inhibits differentiation. Differentiation into cardiomyocyte–line cells can be verified by observation of spontaneous contractile activity. EBs can then be fixed and stained to detect the protein of interest (CKmt–HA) and a cell–type marker (αMHC), which should coincide if expression follows the expected pattern.

4.3.1.3.1. *Spontaneous differentiation of cardiomyocyte–lineage cells*

Confluent ES cell clones which had survived antibiotic selection were washed with PBS, trypsinized, centrifuged, and resuspended in complete medium. Hanging drops (20μl, 400 cells each) were seeded onto the lids of plastic tissue culture dishes, inverted onto PBS–filled dishes (to maintain humidity within the dish), and incubated at 37°C for 48 hours, to induce formation of embryoid bodies. EBs were washed into uncoated plastic Petri dishes and cultured in suspension, in complete cell medium. After 5 days, individual EBs were plated into gelatin–coated glass–bottom 24–well plates for adherent culture, in differentiation medium (without leukemia inhibitory factor). Spontaneous contractile activity, which indicates differentiation of cells into the cardiomyocyte line, was observed after 1–2 weeks in the majority of EBs, and video microscopy recordings of beating cell clusters were obtained. Finally, EBs were fixed for immunocytochemistry to confirm transgene expression.

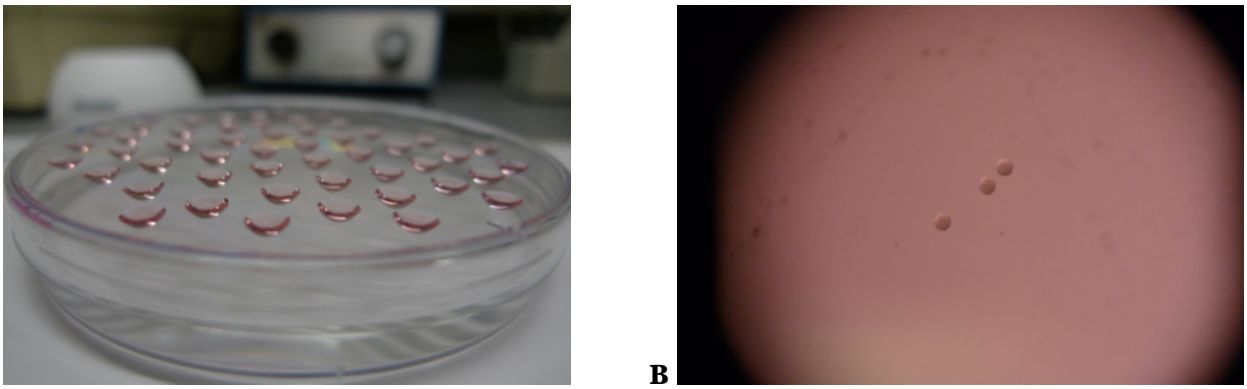


Figure 4-6: Generation of embryoid bodies.

(A) Embryonic stem cells cultured in 20µl hanging drops. **(B)** Phase–contrast image of three embryoid bodies in suspension culture, after 48 hours in hanging drops. No scale bar is provided, as this image was acquired using a standard tissue culture light microscope and (uncalibrated) digital camera.

4.3.1.3.2. *Optimization of immunocytochemical staining protocol*

Before immunocytochemistry was attempted in differentiated EBs, antibody concentrations were optimized in cardiac–derived HL–1 cells, since these cells are known to express αMHC[152] and could be transfected to express CKmt–HA. Since the anti–HA stain has been previously optimized (Figure 3-9), experiments were initially performed using single–staining for αMHC in untransfected HL–1 cells. The sarcomeric structure of HL–1 cells does not exhibit the degree of organization observed in primary cardiomyocytes[152]; however, staining of linear myosin filaments could be observed in the cytoplasm (Figure 4-7A).

To optimize αMHC/HA co–staining, experiments were repeated in HL–1 cells transiently transfected with pcDNA3.1–CKmt–HA (Figure 4-7B). Both proteins were successfully visualized, and there was no apparent co–localization of the αMHC and HA signals - αMHC staining was observed in linear strands at the periphery of the cell, while HA staining followed a punctate distribution throughout the cytoplasm. This confirms that the protocol can be used to demonstrate expression of these proteins, and distinguish between αMHC as a marker of cardiac lineage, and HA as a marker of transgene expression.

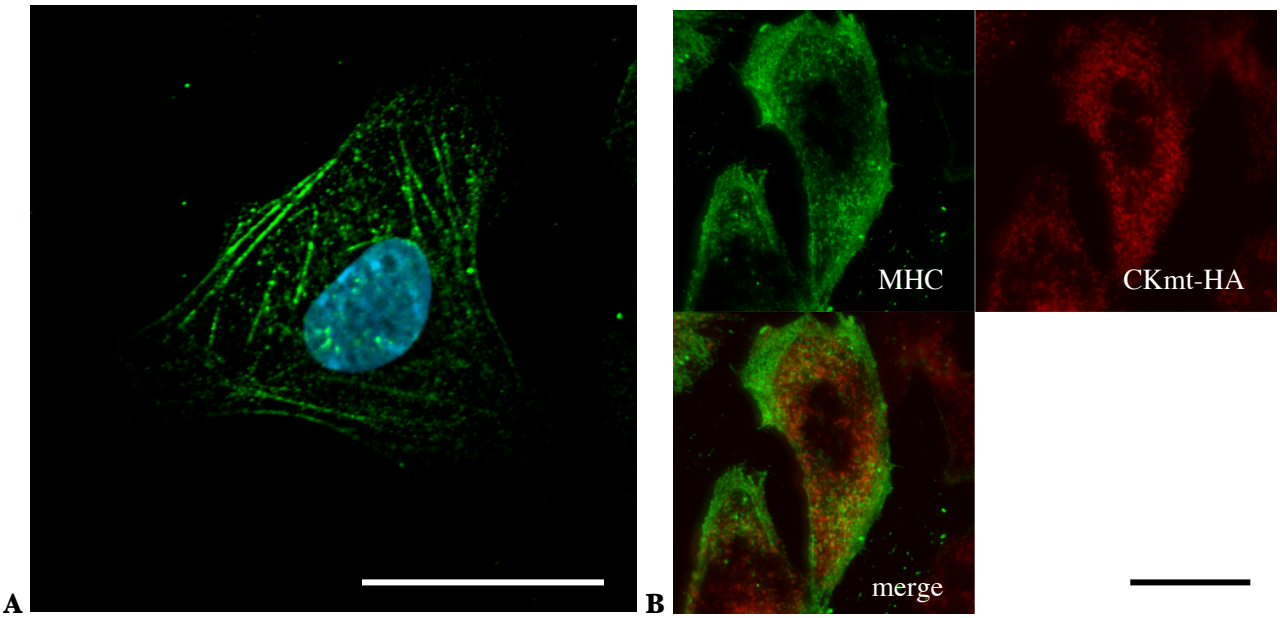


Figure 4-7: Optimization of αMHC/HA immunocytochemistry.

(A) Confocal image of an HL–1 cell stained for αMHC (green); nucleus counterstained with DAPI (blue). **(B)** Confocal image of HL–1 cells transfected with pcDNA3.1–CKmt–HA and co–stained for αMHC (green) and HA (red). No significant co–localization was observed between stains. Scale bars, 20μm.

4.3.1.3.3. *Immunocytochemistry in differentiated embryoid bodies*

Embryoid bodies were washed in PBS and fixed using 4% paraformaldehyde. Immunocytochemical staining was performed using the following antibodies:

	Target	Host species	Fluorophore	Manufacturer	Product number	Dilution
Primary antibodies	HA tag	Rat	–	Roche	11867431001	1:1500
	α–MHC	Mouse	–	Abcam	ab50967	1:200
Secondary antibodies	Rat IgG	Goat	Alexa546	Molecular Probes	A–11081	1:200
	Mouse IgG	Goat	Alexa488	Molecular Probes	A–11001	1:400

Table 4-2: Antibodies used for immunocytochemical staining of embryoid bodies.

Since embryoid bodies were seeded in rectangular 24–well plates, the fixed orientation of the plate and small surface area of each well made it possible to note the approximate location and shape of contractile patches prior to fixation, without marking the plate. These regions were subsequently found to express αMHC, as would be expected in cells capable of cardiomyocyte–like contraction. Significantly, HA signal was observed in the same patches of cells, indicating that the transgene was being expressed (Figure 4-8). There was

negligible HA staining in other, non–contracting regions of embryoid bodies, suggesting that transgene expression was being driven by the αMHC promoter, without leaky expression in other cell types.

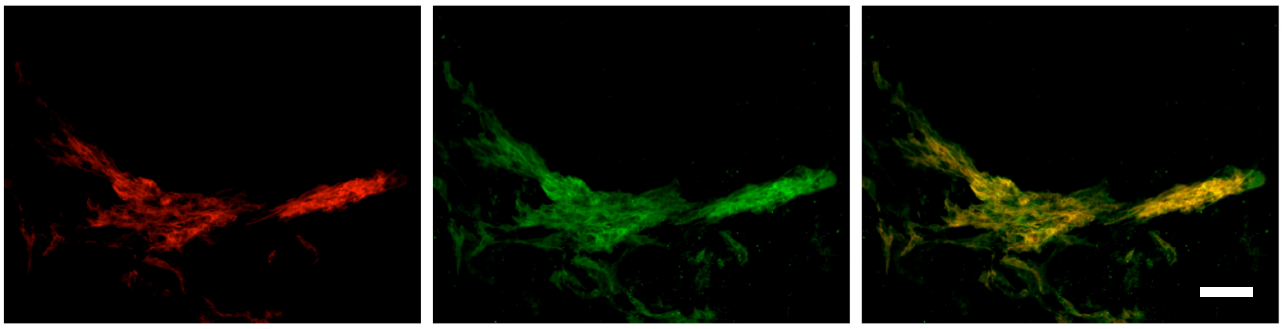


Figure 4-8: Immunocytochemistry in differentiated embryoid bodies.

Staining against the HA tag (red) and αMHC (green) confirmed that transgene expression was present in, and restricted to, cells which expressed αMHC (merge, yellow). Scale bar, 200μm.

4.3.1.4. Mouse husbandry and genotyping

4.3.1.4.1. *Chimeric founder mice*

Chimeric founder mice were generated by blastocyst injection of stably transfected embryonic stem cells (see Appendix B.1 for a detailed technical report). During the initial rounds of experiments, a total of 69 blastocysts were injected and transferred to pseudopregnant females. One female did not give birth to any viable offspring, most likely due to technical failure, and these injections were therefore excluded from analyses (n=10 blastocysts). The remaining females produced a total of 24 viable pups (40.7% of transferred blastocysts), of which 2 were male chimeras, identified as BI525 and BI541 (8.3% of viable pups, or 3.4% of all blastocysts injected).

The degree of chimericity of individual founder mice was estimated by assessing coat color. While mice were derived from wild–type (non–agouti) blastocysts, the transgenic ES cells are heterozygous at the agouti locus (A/a). Since the agouti allele (A) is dominant with respect to the non–agouti allele (a), regions of fur derived from these cells are phenotypically agouti. The percentage of agouti coat color in a founder mouse is therefore a rough indicator of the proportion of cells derived from transgenic ES cells, and is expected to

indicate the likelihood of germline transmission of the transgene. In this case, the percentage of agouti coat in both founders was estimated at 30–40% (Figure 4-9).

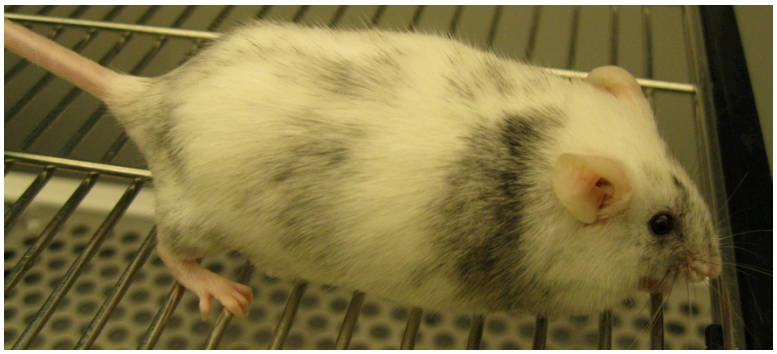


Figure 4-9: Chimeric founder.

This mouse (BI525) was generated on an albino background, and clearly demonstrates patches of agouti fur, which are derived from transgenic ES cells.

4.3.1.4.2. *Breeding of transgenic mice*

Male chimeric founders were mated with wild–type C57BL/6 females (obtained from Harlan) at 6 weeks. Both founders produced viable offspring, and the first–generation (F_1) pups were weaned and ear biopsies were obtained for identification and as material for genotyping at 3 weeks.

1.1.1.1.1. *Coat color as an indicator of chimericity in founder mice and germline transmission*

Coat color was noted in all litters derived from chimeric founders, as the presence of agouti F_1 pups indicates that germline transmission has occurred (*i.e.*, that these mice were derived from the transgenic embryonic stem cells). All F_1 pups from the two initial founders had black coats, suggesting that germline transmission of transgenic DNA was unlikely. However, since the embryonic stem cells were heterozygous at the agouti locus (A/a), any germ cells derived from these cells would have a 50% chance of carrying either the agouti (A) or non–agouti (a) allele, and therefore only 50% of pups would be expected to be phenotypically agouti (A/a), with 50% black (a/a). Therefore, the lack of agouti pups did not unequivocally preclude the possibility of germline transmission, and all F_1 pups were genotyped without regard to coat color.

4.3.1.4.3. *Genotyping strategy and validation*

A single pair of genotyping primers was designed to simultaneously amplify both the wild–type *Ckmt2* gene (gDNA) and transgenic *Ckmt2* (cDNA), with the gDNA band serving as an internal control (*i.e.*, while the cDNA band would serve to identify transgenics, the gDNA band should be present in all mice). In order to distinguish between gDNA and cDNA, primers were designed to span a genomic intron. Since cDNA is reverse–transcribed from mRNA, it does not contain introns, and the same PCR will therefore produce a smaller product. The shortest intron of *Ckmt2*, intron 4 (393bp), was selected, in order to minimize amplicon size. Primers were therefore designed to bind to sequences in exon 4 (sense primer, CKmt_ex4_F) and exon 5 (antisense primer, CKmt_ex5_R), respectively. Primer specificity was confirmed by PrimerBLAST search of the C57BL/6 genome. Amplicon lengths for gDNA and cDNA were predicted to be 523bp and 130bp (Figure 4-10).

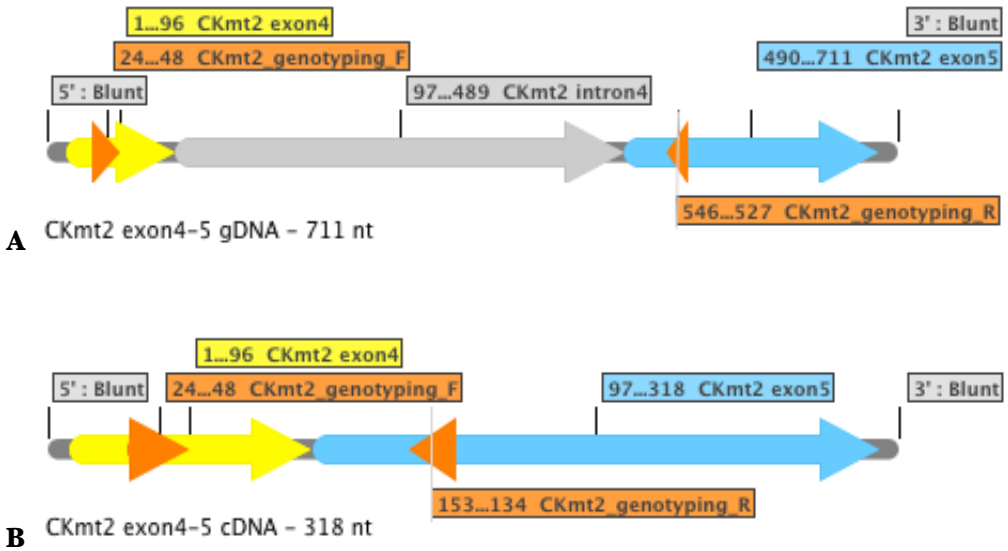


Figure 4-10: Genotyping primer binding sites in exons 4/5 of *Ckmt2*.
(A) Genomic *Ckmt2* DNA. **(B)** Transgenic *Ckmt2* cDNA. The presence of intron 4 (grey) in the genomic sequence makes it possible to distinguish between gDNA and cDNA using a single pair of primers (orange).

Genotyping PCR was optimized and tested using wild–type mouse gDNA and the αMHC–CKmt–HA vector DNA as wild–type and transgenic templates, respectively. In single–template PCRs, the wild–type and transgenic bands were produced as expected. When both templates were combined, the reaction was expected to yield two products; however, only the transgenic band was observed (Figure 4-11).

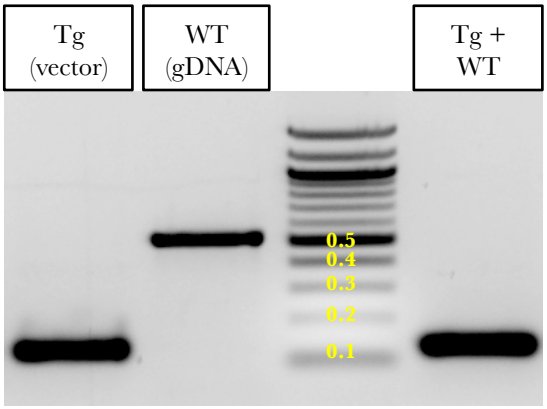


Figure 4-11: Test CKmt–OE genotyping PCR.

The expected wild–type and transgenic bands were detected in reactions loaded with a single template; when both templates were combined, only the transgenic band was observed (right).

The most likely explanation for this discrepancy is competition between the two alleles for primer binding. Since the same primer pair is used to generate both products, a significant difference in template copy number would favor one reaction over the other. Assuming that the mass of the haploid mouse genome is approximately 3pg[217], the amount of genomic DNA loaded in the initial PCR (100ng) contains ~3.3 x 10^4 copies of the genome (100,000 pg / 3 pg = 33,333), and therefore ~3.3 x 10^4 copies of wild–type *Ckmt2*. The amount of αMHC–CKmt–HA vector used (10 ng, m.w. 6,392,403) corresponds to ~1.6fmol (10^{-8} g / 6,392,403 g/mol = 1.6 x 10^{-15} mol); multiplying by Avogadro's constant (6.022 x 10^{23}) gives a total of ~9.6 x 10^8 molecules of the vector, *i.e.* ~9.6 x 10^8 copies of *Ckmt2* – over four orders of magnitude more than the number of genomic DNA copies loaded in each reaction. This suggests that, although the PCR could amplify both alleles, under the conditions used the transgenic template was outcompeting the genomic locus for primer binding.

In order to determine whether the reaction could amplify both alleles when their relative copy numbers were similar, PCR was repeated using lower amounts of the αMHC–CKmt–HA vector (Figure 4-12). The expected stoichiometry in a hemizygous transgenic mouse (*i.e.*, 1 copy of transgenic *Ckmt* cDNA : 2 copies of wild–type *Ckmt* gDNA) is approximately equivalent to loading 1pg of cDNA with 100ng of gDNA (3.3 x 10^4 and 9.6 x 10^4 copies, respectively). To test this, 10–fold serial dilutions of αMHC–CKmt–HA vector spanning two orders of magnitude either side of 1pg were used as template, with or without 100ng of

genomic DNA. As expected, there was a dose–dependent shift between production of the wild–type and transgenic bands; significantly, under the target loading conditions (1pg transgenic vector + 100ng gDNA), both bands were observed, confirming that the protocol could be used for genotyping CKmt–OE mice.

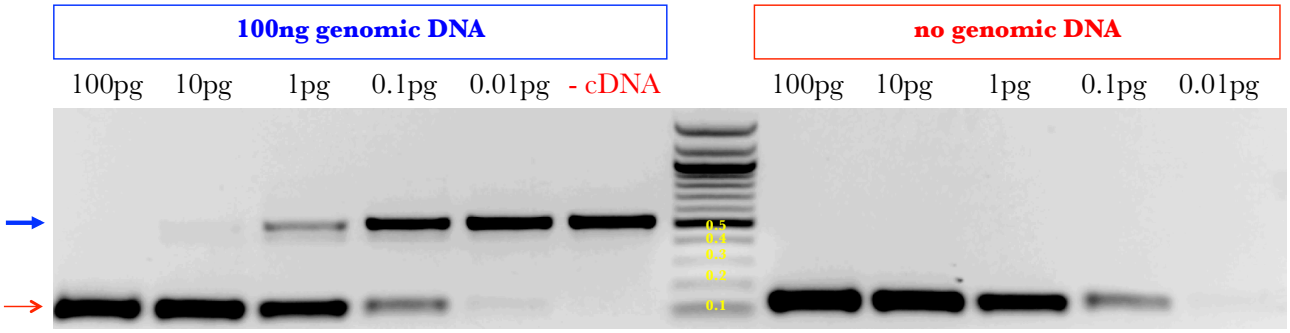


Figure 4-12: CKmt–HA genotyping – troubleshooting.

PCR was performed using 10–fold dilutions of transgenic cDNA vector as template (total amount labelled above image), with or without 100ng of genomic DNA. The lack of wild–type bands in the reactions with high cDNA content (lanes 1/2) is most likely a result of competition due to differences in copy number. Lanes 3 and 4 produced two clear bands of the expected sizes, confirming that the protocol is capable of simultaneously detecting both genes. Blue arrow, 523bp wild–type fragment. Red arrow, 130bp cDNA fragment.

4.3.1.4.4. *Genotyping results*

All F_1 pups from the initial founders were screened, but no transgenics were identified. A sample genotyping result is presented in Figure 4-13.

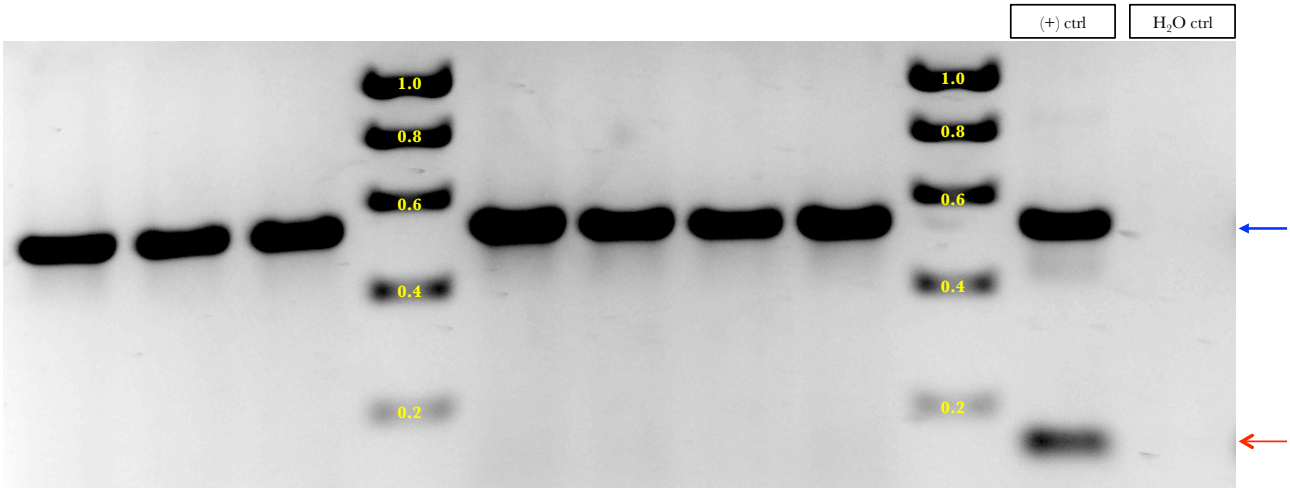


Figure 4-13: Results of F_1 genotyping.

Note presence of wild–type bands (523bp, blue arrow) and lack of transgenic bands (130bp, red arrow) in all samples. αMHC–CKmt–HA cloning vector was used as a "transgenic" positive control (1pg co–loaded with wild–type DNA) and produced the expected 130bp band.

4.3.1.4.5. *Generation of additional founder mice*

Since no transgenic mice were identified despite screening a relatively large number of pups (n=89), additional blastocyst injections were performed to generate new founders. While the two initial founder mice had relatively low degrees of chimericity (30–40%), the second round of blastocyst injections yielded three potential founders, with 40–50% chimeric coat color. These mice were mated with wild–type females and were all fertile, but failed to produce transgenic offspring (Table 4-3). No agouti pups were produced, indicating that germline transmission, and not embryonic lethality of the transgene, remained the problem.

	BI 525	**BI 541**	**Fo B1**	**Fo B2**	**Fo B3**	**Total**
Total mice	56	33	16	32	58	**195**
Transgenics	0	0	0	0	0	**0**
% Tg	n/a	n/a	n/a	n/a	n/a	**n/a**

Table 4-3: Breeding statistics for CKmt–OE founder mice derived from the first two rounds of blastocyst injections.

A total of 195 pups were genotyped, and no transgenic mice were identified.

Since the second batch of founder mice also failed to produce transgenic offspring, a further round of blastocyst injections was performed. A third batch of founder mice were generated, and included three mice with significantly higher proportions of agouti coat, including two (2606 and 2607) which were >90% agouti. All three founders were mated with wild–type females. Founders 2606 and 2607 both produced litters which were a mixture of black and agouti pups, indicating that germline transmission had occurred (Figure 4-14).



Figure 4-14: CKmt-OE F_1 pups.

The presence of agouti pups indicates that germline transmission has taken place.

Mice were genotyped at 2 weeks, and PCR revealed the presence of transgenic pups in litters derived from founders 2606 and 2607 (Figure 4-15). Additional litters were generated, and the overall proportion of transgenic pups from these founders was 48% (Table 4-4). Transgenic F_1 pups from both founders were mated with wild–type mice to generate additional transgenics.

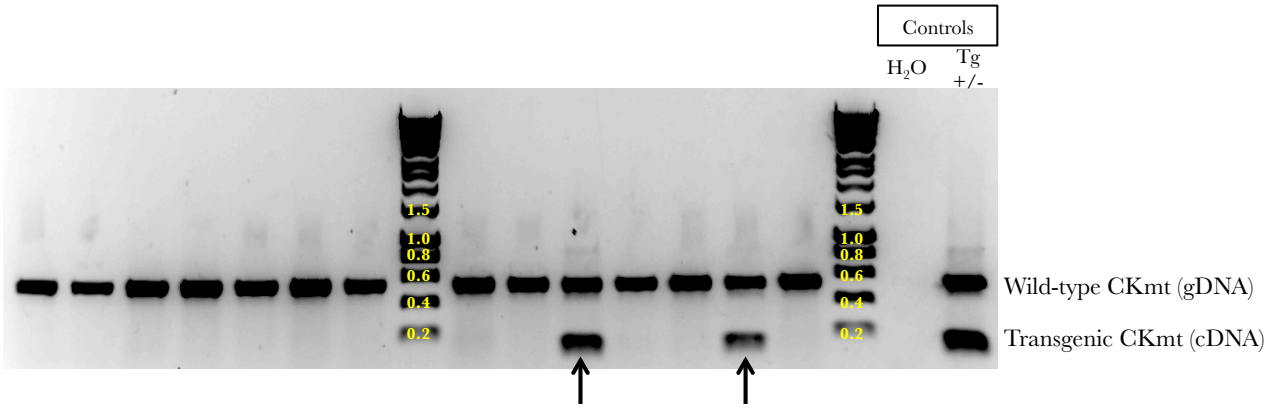


Figure 4-15: Genotyping of transgenic CKmt–OE F_1 pups.

Two transgenic pups were identified (arrows).

	2605	2606	2607	Total	Total (2606+2607)
Total mice	25	58	55	**138**	**113**
Transgenics	0	27	27	**54**	**54**
% Tg	0%	47%	49%	**39%**	**48%**

Table 4-4: Breeding statistics for CKmt–OE founder mice derived from the third round of blastocyst injections.

Founders 2606 and 2607 both produced transgenic offspring.

4.3.2. Validation of the transgenic model

Once transgenic mice were generated, the next step was to perform molecular validation to confirm that the transgene was expressed and functional. Tissues were harvested from mice at 8–10 weeks, snap–frozen in liquid nitrogen, powdered on dry ice using a percussion homogenizer, and stored at −80°C for molecular and biochemical assays.

4.3.2.1. Detection of transgenic mRNA by qRT–PCR

4.3.2.1.1. *Methods and primer design*

RNA was extracted from left ventricular tissue, and qRT–PCR was performed using primers designed to specifically amplify the transgenic transcript. The *Ckmt2* coding sequences of endogenous and transgenic mRNA are identical, but the latter contains an additional 3' sequence encoding the C–terminal HA tag. Therefore, an antisense primer complementary to the HA tag sequence was designed (HA_R), and paired with a sense primer spanning the final exon–exon junction of *Ckmt2* (Ckmt2_ex9–10_F). Since the sequence of transgenic cDNA is identical to the mRNA it produces, this primer pair could also theoretically amplify DNA in transgenic mice, which could yield a false–positive result; therefore, control reactions without reverse transcriptase were included in all experiments to exclude DNA contamination.

4.3.2.1.2. *Detection of transgenic mRNA in left ventricular tissue*

Left ventricles were harvested from 10 mice (5 wild–type, 5 transgenic). Transgenic mRNA was detected in all transgenic mice, but not in wild–type mice (Figure 4-16). No amplification was observed in transgenic samples incubated without reverse transcriptase, indicating that this result was due to genuine expression of transgenic mRNA, rather than contamination with transgenic DNA.

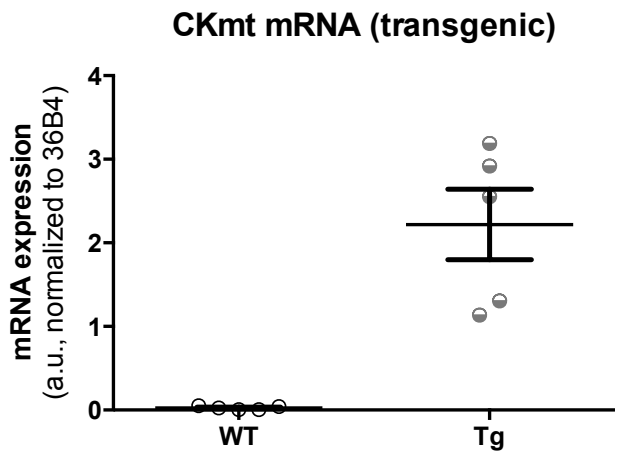


Figure 4-16: Expression of transgenic mRNA in left ventricles from CKmt–OE mice.

The transcript was detected in all transgenic mice, but not in wild-type mice. Expression of the reference gene *36B4* was detected in all samples, but levels were variable and *Polr2a* was used for subsequent assays.

4.3.2.1.3. *Tissue specificity of transgenic mRNA expression*

Since the ROSA26–αMHC expression construct used to generate CKmt–OE mice was previously untested in our group, it was necessary to demonstrate that transgene expression was cardiac–specific. A panel of tissues was harvested from two transgenic mice (1 male, 1 female), and RNA extraction and qRT–PCR were performed as described above. In both mice, transgenic mRNA was detected in all four cardiac chambers, and absent in all other tissues (Figure 4-17), confirming that the transgene is expressed in a cardiac–specific manner.

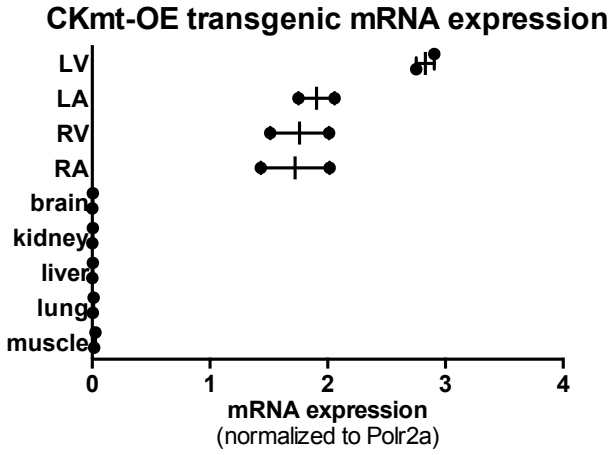


Figure 4-17: Tissue specificity of CKmt–HA transgenic mRNA expression.

qPCR was performed in RNA extracted from two CKmt–OE mice. Expression of the reference gene *Polr2a* was detected in all tissues, while transgenic mRNA was only present in the cardiac atria and ventricles.

4.3.2.2. Detection of transgenic protein by western blot

4.3.2.2.1. *Methods*

Protein was extracted from left ventricular tissue, followed by western blotting to determine whether CKmt–HA was expressed at the protein level. Membranes were probed with either an anti–HA antibody to specifically detect transgenic protein, or an anti–CKmt antibody to measure total CKmt protein expression.

4.3.2.2.2. *Detection of transgenic protein in left ventricular tissue*

Protein lysates were prepared from 6 mice (2 wild-type, 4 transgenic), and western blotting was performed using the anti–HA primary antibody to specifically detect transgenic protein. A commercially available lysate of *E. coli* expressing the HA tag was included as a positive control (Abcam, ab5395). An HA–tagged protein of the expected size (~47 kDa) was observed in all transgenic mice, and no HA staining was detectable in wild–types (Figure 4-18). Finally, the membrane was stripped of antibodies and re–probed against beta–tubulin as a loading control, which confirmed comparable protein loading between wild-type and transgenic samples.

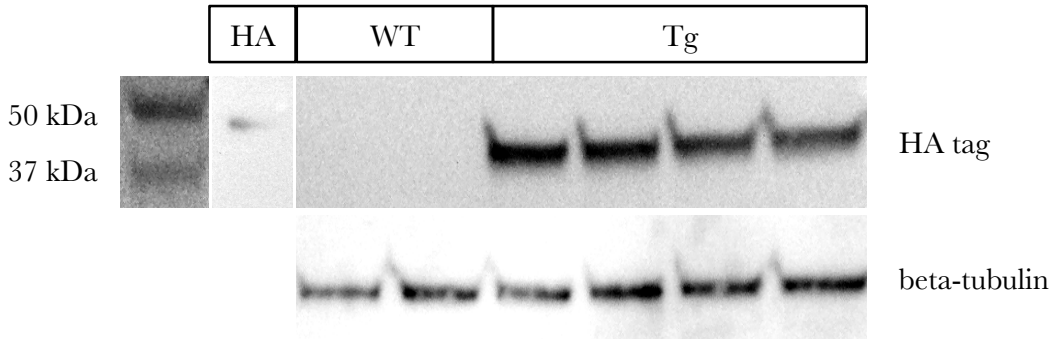


Figure 4-18: Western blot for transgene expression in CKmt-OE mice (anti-HA).
HA, HA-tag positive control. WT, wild-type. Tg, transgenic.

4.3.2.2.3. *Measurement of total CKmt protein in left ventricular tissue*

In parallel, additional membranes were probed using an anti–CKmt antibody. Following imaging, membranes were stripped and re–probed against β–tubulin, and the CKmt/β–tubulin ratio was used as a measure of total CKmt expression. There was no clear difference between groups (Figure 4-19), and western blotting was therefore repeated in additional samples. Total CKmt expression was quantified in a total of 15 mice (8 wild–type, 7 transgenic), and was not significantly different between groups (mean CKmt/β–tubulin in WT, 2.22 ± 0.30 a.u.; Tg, 2.55 ± 0.21; p=0.38).

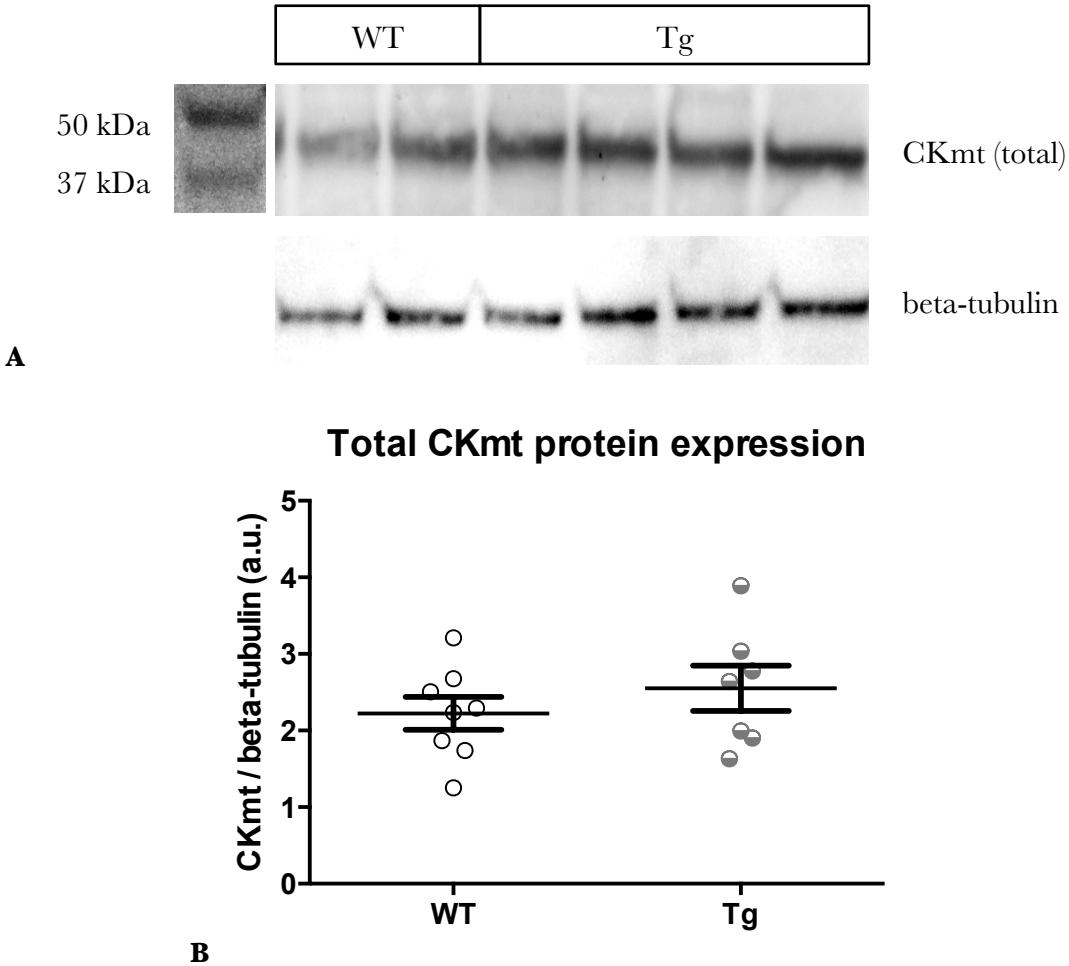


Figure 4-19: Western blot for total CKmt expression in CKmt-OE mice (anti-CKmt).

(**A**) Representative western blot result. (**B**) Quantification of CKmt expression, relative to beta-tubulin. WT, wild-type. Tg, transgenic. Results were analyzed by Student's t test. There was no significant difference between groups.

4.3.2.3. Creatine kinase activity

The results of qPCR and western blot experiments confirmed that the CKmt transgene was being expressed at the mRNA and protein levels. Biochemical assays were performed in left ventricular homogenates to determine whether enzymatic activity of CKmt was higher in transgenic mice. Tissues were harvested from 16 mice (7 wild–type, 9 transgenic), and assays for total CK and isoenzyme activities were performed, with results normalized to protein concentration, as determined by the Lowry assay (Figure 4-20). Total CK activity (WT, 4.65 ± 0.40 IU / mg protein; Tg, 5.20 ± 0.21, p=0.22) and CKmt activity (WT, 1.61 ± 0.19; Tg, 1.98 ± 0.10; p=0.09) were not significantly different between groups.

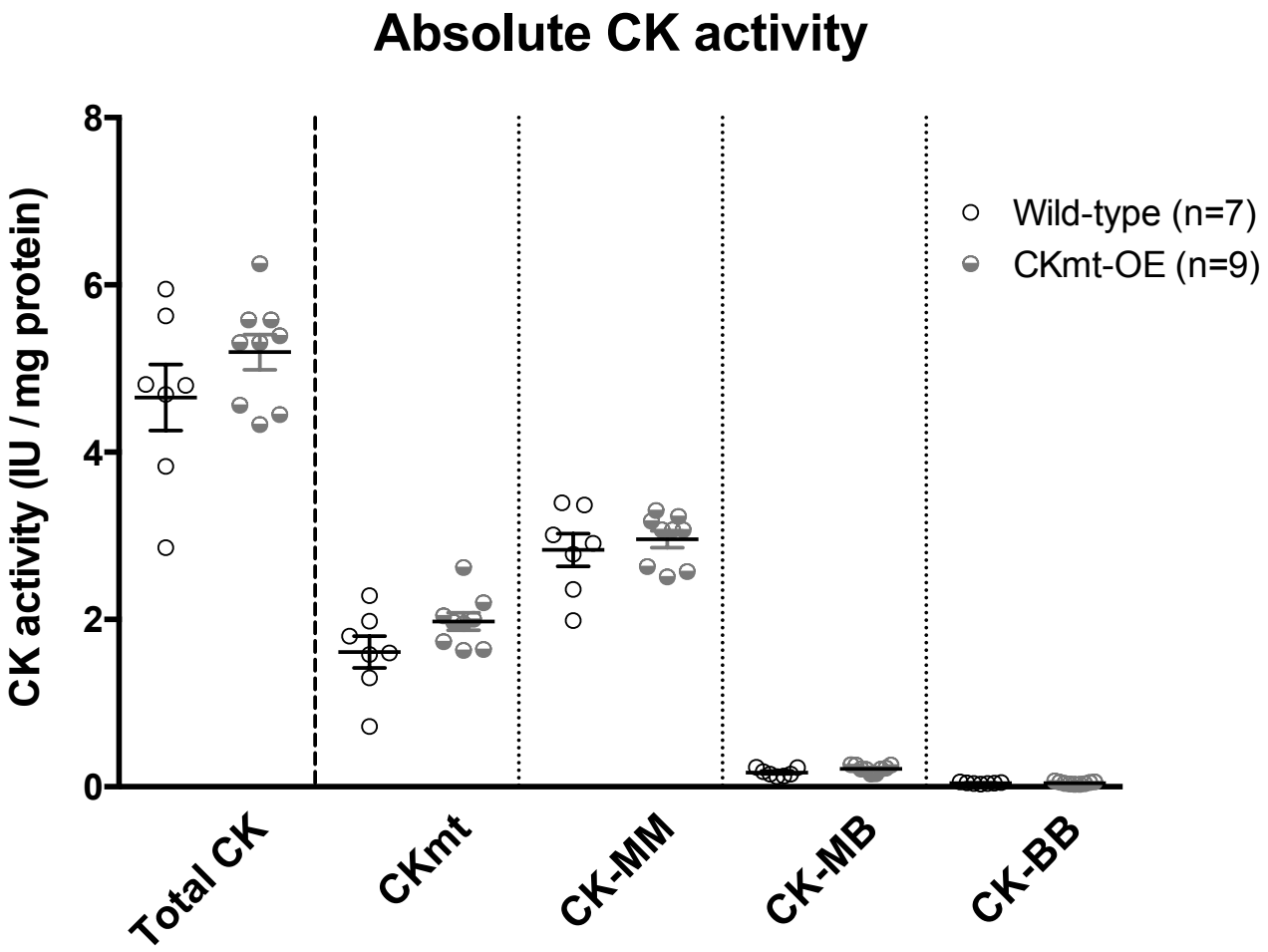


Figure 4-20: Creatine kinase activity in CKmt–OE mice.

Results were analyzed by Student's t test; no significant differences were observed between groups.

When CKmt activity was expressed as a percentage of total CK, there was a significant difference between wild–type and transgenic mice (WT, 35.30 ± 0.87%; Tg, 37.98 ± 0.60%; p≤0.05; Figure 4-21).

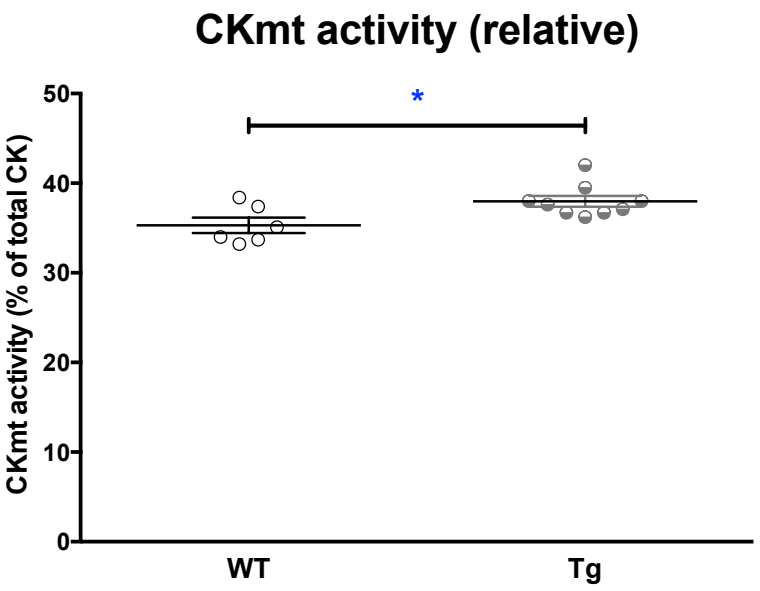


Figure 4-21: CKmt activity in CKmt–OE mice (relative).
Results were analyzed by Student's t test. * denotes a significant difference between groups (p≤0.05).

4.3.2.4. Quantification of transgenic, endogenous, and total mRNA transcripts

The results of qRT–PCR, western blotting, and activity assays indicated that the transgene was being expressed at the mRNA and protein levels, but this was not sufficient to drive a pronounced increase in total CKmt protein or activity. Since this could be due to downregulation of endogenous CKmt expression, allele–specific qRT–PCR was performed to quantify expression of transgenic, endogenous, and total CKmt mRNA. Transgenic mRNA levels had already been measured (see section 4.3.2.1); therefore, additional reactions were performed using samples from the same mice (5 wild–type, 5 transgenic) to evaluate endogenous and total CKmt mRNA transcript levels.

4.3.2.4.1. *Primer design*

In order to specifically amplify endogenous CKmt mRNA, the exon–spanning sense primer previously used for detection of transgenic mRNA (Ckmt2_ex9–10_F) was paired with an antisense primer designed to bind in the 3' untranslated region, which is not present in the transgenic sequence (Ckmt2_UTR_R). Total mRNA was measured using a pair of primers which bind within the coding sequence, and therefore amplify both the endogenous and transgenic transcripts (CKmt2_ex8–9_F and CKmt2_ex9_R).

4.3.2.4.2. *Results*

Total CKmt mRNA expression was approximately 60% higher in transgenics, but this difference was not statistically significant (WT, 1.20 ± 0.18; Tg, 1.92 ± 0.29; p=0.07; Figure 4-22). There was no difference in mean endogenous CKmt mRNA expression between wild–type and CKmt–OE mice (WT, 1.54 ± 0.23; Tg, 1.54 ± 0.28; p=0.99).

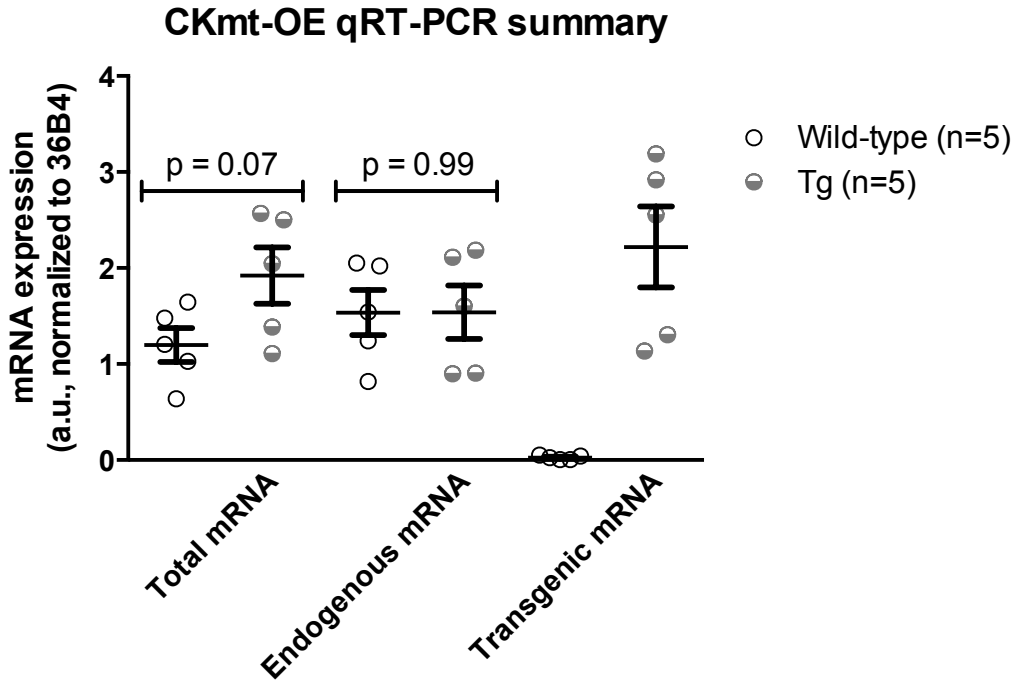


Figure 4-22: Summary of qRT–PCR results in CKmt–OE mice.

Results were analyzed by Student's t test, and P values are indicated in the figure. Transgenic mRNA expression results are reproduced from Figure 4-16, and presented for comparison (note that no transgenic mRNA was detected in wild-types).

4.3.3. Generation of homozygous transgenic mice

The results of molecular validation in CKmt–OE mice suggest that transgene expression in hemizygous ($Tg^{+/-}$) mice was not sufficient to drive a large increase in CKmt protein expression and activity. In an attempt to increase expression levels, CKmt–OE mice were bred to homozygosity ($Tg^{+/+}$) by hemizygote x hemizygote breeding.

4.3.3.1. Genotyping of transgene zygosity

$Tg^{+/-}$ x $Tg^{+/-}$ breeding was expected to produce Mendelian inheritance ratios with respect to the CKmt transgene, *i.e.* the anticipated distribution of offspring was 25% wild–type / 50% $Tg^{+/-}$ / 25% $Tg^{+/+}$. In order to distinguish between $Tg^{+/-}$ and $Tg^{+/+}$ mice, a transgene–zygosity genotyping strategy was required. Transgenic DNA copy number qPCR was performed; in parallel, a standard PCR protocol was established to determine zygosity at the ROSA26 locus, and the results of both methods were compared to ensure that it was possible to reliably determine transgene zygosity in CKmt–OE mice.

4.3.3.1.1. *Determination of transgene copy number by genomic DNA qPCR*

In order to determine the number of transgene copies in mice produced by $Tg^{+/-}$ x $Tg^{+/-}$ breeding, genomic DNA was amplified by quantitative PCR (without reverse transcription)[218]. DNA was extracted by the Hot–SHOT method used for routine genotyping, as it has been demonstrated that relatively crude DNA extracts are suitable for genotyping by qPCR[219]. In order to ensure equal template loading in all reactions, DNA concentration was measured spectrophotometrically (NanoDrop), and samples were diluted to a concentration of 2.5ng/μl. A series of five two–fold dilutions of pooled DNA from all samples (10 – 0.625 ng/μl) was used to generate standard curves. Results were normalized to the copy number of the apolipoprotein B gene (*Apob*).

Copy number values were calibrated against a known hemizygous control from $Tg^{+/-}$ x wild–type breeding (mouse #3247, set to Tg = 1). Since no mice had been identified as $Tg^{+/+}$ at this point, a mock "homozygote" control (Tg = 2) was generated using the same mouse, by loading twice the concentration of DNA (10ng) in the transgene–specific reaction, with the standard amount (5ng) in the reference *Apob* reaction (*i.e.,* theoretically twice as many transgene copies as in the Tg = 1 control, relative to the reference wells). A known wild–type was included as a negative control (#3251, Tg = 0).

Transgene zygosity qPCR identified two mice as homozygous transgenics (Figure 4-23). In order to confirm the validity of these results and develop a more rapid method of genotyping mice derived from $Tg^{+/-}$ x $Tg^{+/-}$ breeding, a zygosity–specific PCR was established, as described below.

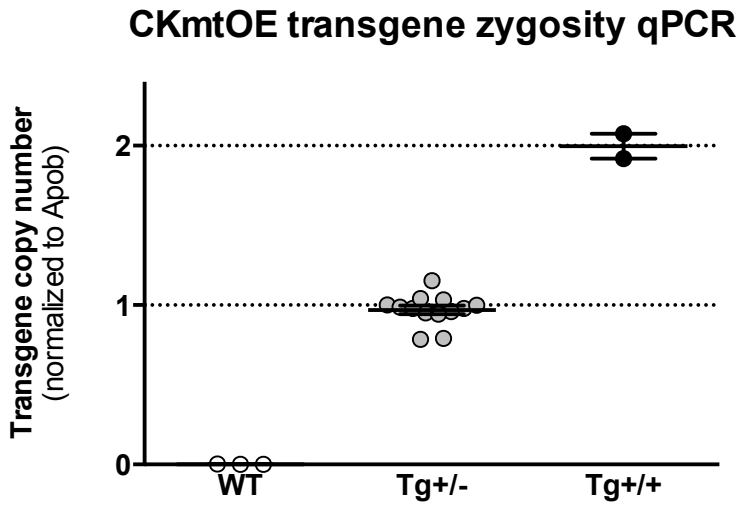


Figure 4-23: Transgene zygosity qPCR.

Mice were grouped according to results of qPCR, demonstrating three distinct levels of copy number corresponding to wild–type (n=3; mean, 0.00 copies; range, 0.00–0.00), $Tg^{+/-}$ (n=13; mean, 0.97 copies; range, 0.79–1.15), and $Tg^{+/+}$ (n=2; mean, 2.00 copies; range, 1.92–2.08).

4.3.3.1.2. *Determination of transgene zygosity by standard PCR*

The genotyping PCR initially established in CKmt–OE mice was designed to identify transgenic mice by amplifying an additional, shorter *Ckmt* band which was not present in wild–types; however, this would not be able to differentiate between hemi– and homozygous transgenics. Therefore, a new protocol was designed, in order to determine whether a given mouse was carrying two copies of the wild–type allele (wild–type), two copies of the transgenic allele ($Tg^{+/+}$), or one copy of each ($Tg^{+/-}$).

In order to detect transgenic DNA, the pair of transgene–specific primers originally designed for mRNA qPCR was used (Ckmt2_ex9–10_F x HA_R). Since the transgenic DNA does not contain introns, its nucleotide sequence is identical to the mRNA transcript, and the same primers can be used to amplify transgenic DNA or cDNA cloned from mRNA. These primers amplify a 158bp fragment at the 3' end of the transgene, and Primer–BLAST search confirmed that they would not amplify any other sequence in the mouse genome.

The transgene–specific PCR would be expected to produce a band in the presence of at least one copy of the transgene; however, this alone would not distinguish between $Tg^{+/-}$ and $Tg^{+/+}$ mice. Since the transgene is integrated at a known locus (ROSA26), a pair of primers binding either side of this site were used (ROSA26_F and ROSA26_R). On the wild–type ROSA26 allele, these primers amplify a 508bp fragment. On the transgenic allele, however, the primer binding sites would be separated by the >10kbp transgene insert. As a result, the primers would still anneal to their binding sites (as these sites were not modified by transgene integration), but would not be expected to produce a product under standard PCR conditions, due to the length of the intervening sequence. Therefore, the 508bp ROSA26 band could be used to identify mice which contained at least one copy of the wild–type allele.

Combining the two pairs of primers described above into a single PCR would be expected to yield the following possible products:

1. Wild–type mice: 508bp band (wild–type ROSA26) only
2. Tg+/– mice: 508bp band (wild–type ROSA26) and 138bp band (transgene)
3. Tg+/+ mice: 138bp band (transgene) only

PCR conditions were optimized using DNA from known wild–type and $Tg^{+/-}$ mice, as well as a mouse which was identified as $Tg^{+/+}$ by qPCR. The reaction was found to produce the expected bands for each template (Figure 4-24).

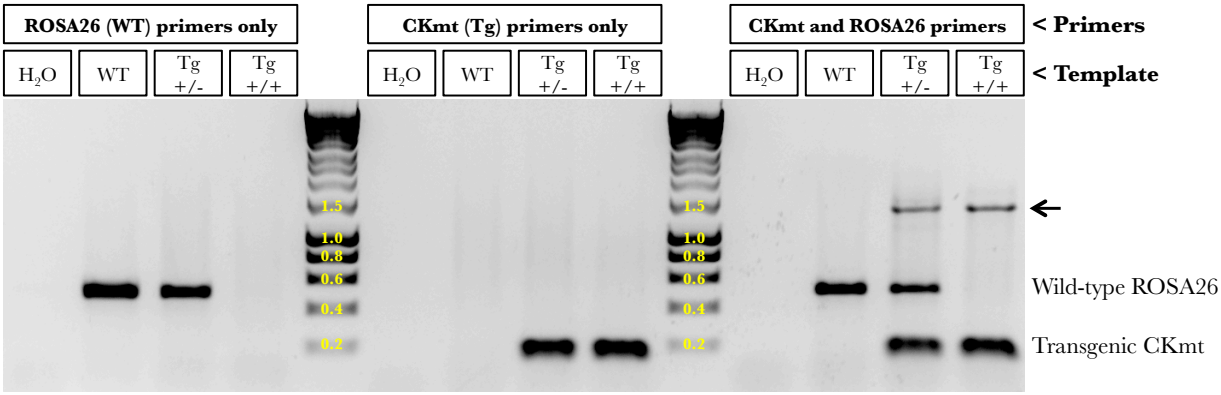


Figure 4-24: CKmt-OE transgene zygosity PCR.

Primers and DNA template for each lane are indicated above the gel. The ROSA26 primers amplify a ~500bp band in mice carrying the wild-type allele (*i.e.*, wild-type and $Tg^{+/-}$), while the CKmt primers amplify a <200bp band in mice carrying the transgene (*i.e.*, $Tg^{+/-}$ and $Tg^{+/+}$). When both primer pairs were combined, all expected bands were observed, as well as an unexpected ~1.5kbp band in transgenic mice (arrow) – this is most likely produced by the CKmt forward primer and ROSA26 reverse primer. H_2O, water (no-template) control. WT, wild-type. Ladder markers are in kbp.

Finally, PCR was performed in the same mice used in transgene copy number qPCR, and yielded identical results (Table 4-5). Since the standard PCR is a more rapid and cost–effective method, this protocol was used for genotyping all subsequent CKmt–OE mice.

Mouse #	Copy number by PCR	Copy number by qPCR	
		Mean	SEM
3340	1	0.79	0.06
3341	0	0.00	0.00
3342	1	0.95	0.07
3343	1	1.00	0.14
3344	1	1.03	0.07
3345	1	0.99	0.05
3346	1	0.98	0.09
3347	1	0.98	0.07
3382	0	0.00	0.00
3383	2	1.92	0.25
3384	1	1.00	0.13
3385	1	1.04	0.10
3386	1	0.79	0.03
3387	1	0.96	0.12
3388	0	0.00	0.00
3389	1	1.15	0.11
3390	1	0.94	0.05
3391	2	2.08	0.10
3251 (WT)	n/a	0.00	0.00
3247 (Tg+/–)	n/a	1.00	0.09
3247 (2x conc)	n/a	1.72	0.14

Table 4-5: Comparison of PCR and qPCR for genotyping transgene zygosity.

Mice were identified as wild–type (white), $Tg^{+/-}$ (yellow) or $Tg^{+/+}$ (red) by both PCR and qPCR, with both methods producing equivalent results. Samples in blue are controls; qPCR results were calibrated against #3247 (Tg = 1).

4.3.3.2. Breeding statistics

In order to determine whether transgenic status was affecting viability, detailed breeding statistics were calculated for $Tg^{+/-}$ x $Tg^{+/-}$ mating. Five breeding pairs were established, and all pairs were fertile, with a median litter size of 9 pups (range, 4–12). Overall, a total of 293 second-generation (F_2) pups were generated, and the distribution of genotypes approximated the expected Mendelian ratio (Table 4-6 and Figure 4-25).

Breeding pair		Litter size (median)	Number of pups			% of pups by genotype		
Male	Female		WT	Tg+/–	Tg+/+	WT	Tg+/–	Tg+/+
3050	3053	8	10	30	9	20%	61%	18%
3146	3151	9	24	44	29	25%	45%	30%
3340	3346	9	12	22	11	27%	49%	24%
3343	3345	7	15	23	7	33%	51%	16%
3342	3347	10	11	34	12	19%	60%	21%
Overall		**9**	**72**	**153**	**68**	**25%**	**52%**	**23%**

Table 4-6: Breeding statistics for CKmt-OE $Tg^{+/-}$ x $Tg^{+/-}$ breeding pairs.

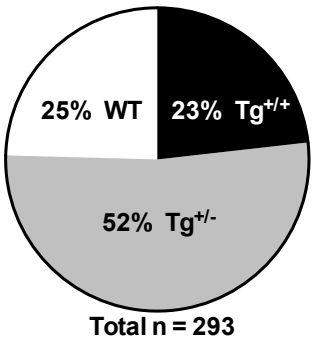


Figure 4-25: Results of $Tg^{+/-}$ x $Tg^{+/-}$ breeding.

All mice generated by hemizygous breeding were pooled. The percentage of each genotype is indicated in the corresponding sector.

4.3.3.3. Confirmation of increased transgene activity in homozygous mice

4.3.3.3.1. *mRNA expression*

In order to determine whether the presence of an additional copy of the transgene was associated with a further increase in *Ckmt* mRNA expression, qRT–PCR was performed (Figure 4-26). Transgenic mRNA expression was approximately 2.5–fold higher in $Tg^{+/+}$ mice, relative to $Tg^{+/-}$ ($p \leq 0.05$). Total *Ckmt* mRNA expression was significantly higher in both $Tg^{+/-}$ (141%) and $Tg^{+/+}$ (186%), relative to wild–type mice ($p \leq 0.05$). Finally, endogenous *Ckmt* mRNA expression was similar across all groups, indicating that there were no compensatory changes in endogenous gene expression in transgenic mice.

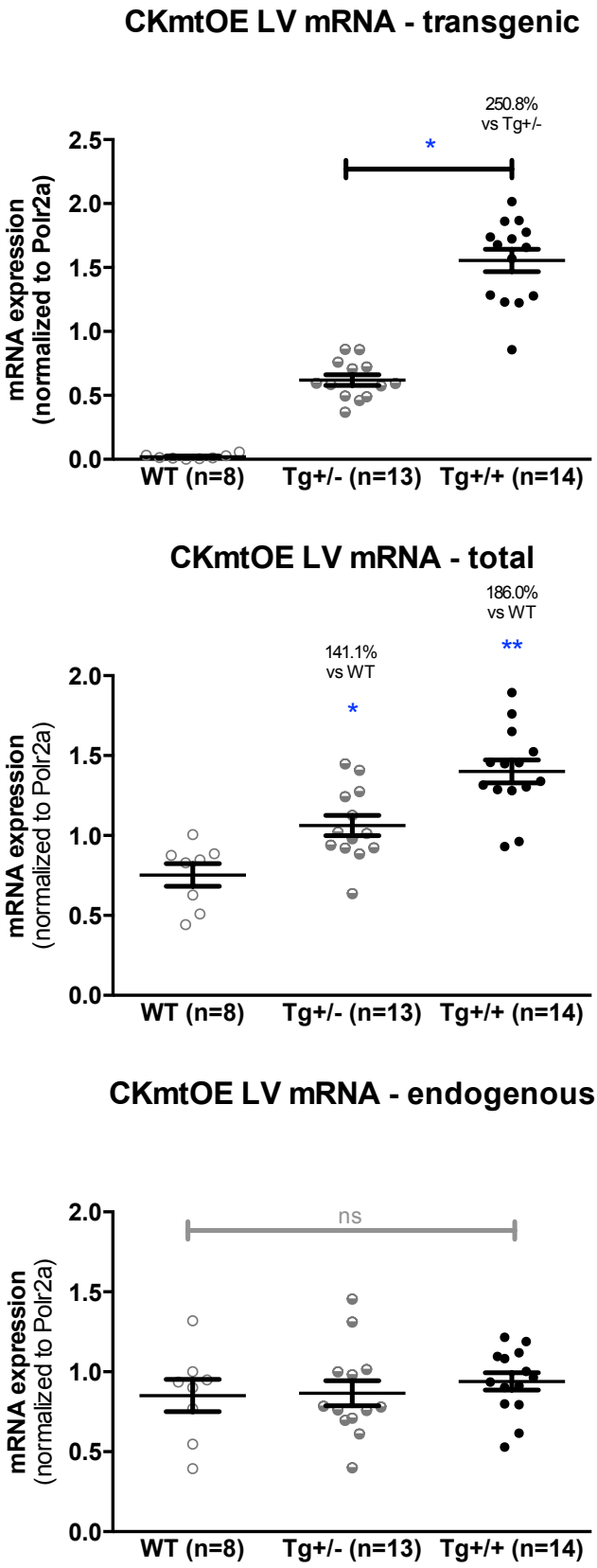


Figure 4-26: Allele–specific qRT–PCR in hemi– and homozygous CKmt–OE mice.

Results were analyzed by one–way ANOVA with Bonferroni's multiple comparison test. * denotes a significant difference between groups ($p \leq 0.05$); **, $p \leq 0.01$; ns, no significant difference.

4.3.3.3.2. *Protein expression*

Protein expression was measured by western blotting, as described above, and expressed relative to beta-tubulin expression (Figure 4-27). In order to compare results across multiple experiments, results were normalized to the wild-type mean for each blot. There was a progressive increase in total CKmt protein expression from wild-type mice (100.0 ± 12.4%, n=11), to Tg+/- (114.8 ± 13.3%, n=7), and Tg+/+ (n=6, 135.2 ± 20.5%, n=6), but no statistically significant differences were observed.

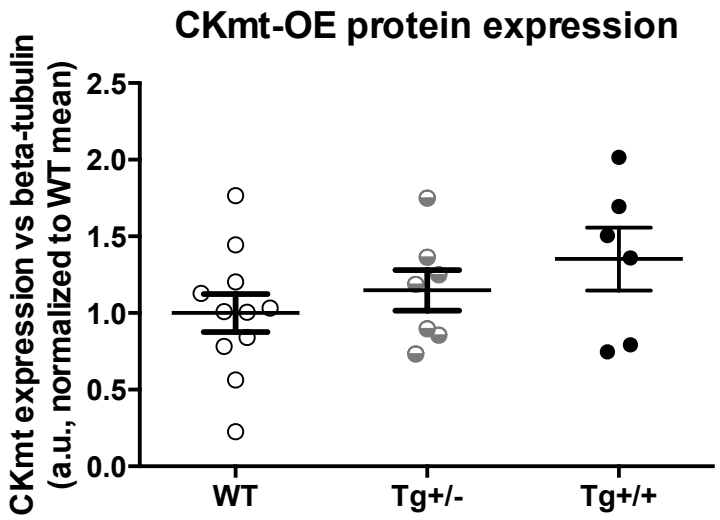


Figure 4-27: Total CKmt protein expression.

Results were analyzed by one–way ANOVA with Bonferroni's multiple comparison test, and no significant differences were observed.

4.3.3.3.3. *Enzymatic activity*

Total CK and isoenzyme activities were measured in wild–type (n=25), $Tg^{+/-}$ (n=28), and $Tg^{+/+}$ (n=15) mice (Figure 4-28). Total CK activity was not significantly increased in either transgenic group (WT, 4.66 ± 0.17 IU / mg protein; $Tg^{+/-}$, 4.93 ± 0.13; $Tg^{+/+}$, 5.08 ± 0.22; p=0.23). CKmt activity was significantly increased in $Tg^{+/+}$ mice, relative to wild–types (WT, 1.63 ± 0.09 IU / mg protein; $Tg^{+/-}$, 1.84 ± 0.08; $Tg^{+/+}$, 2.07 ± 0.12; $Tg^{+/+}$ vs WT, $p \leq 0.01$).

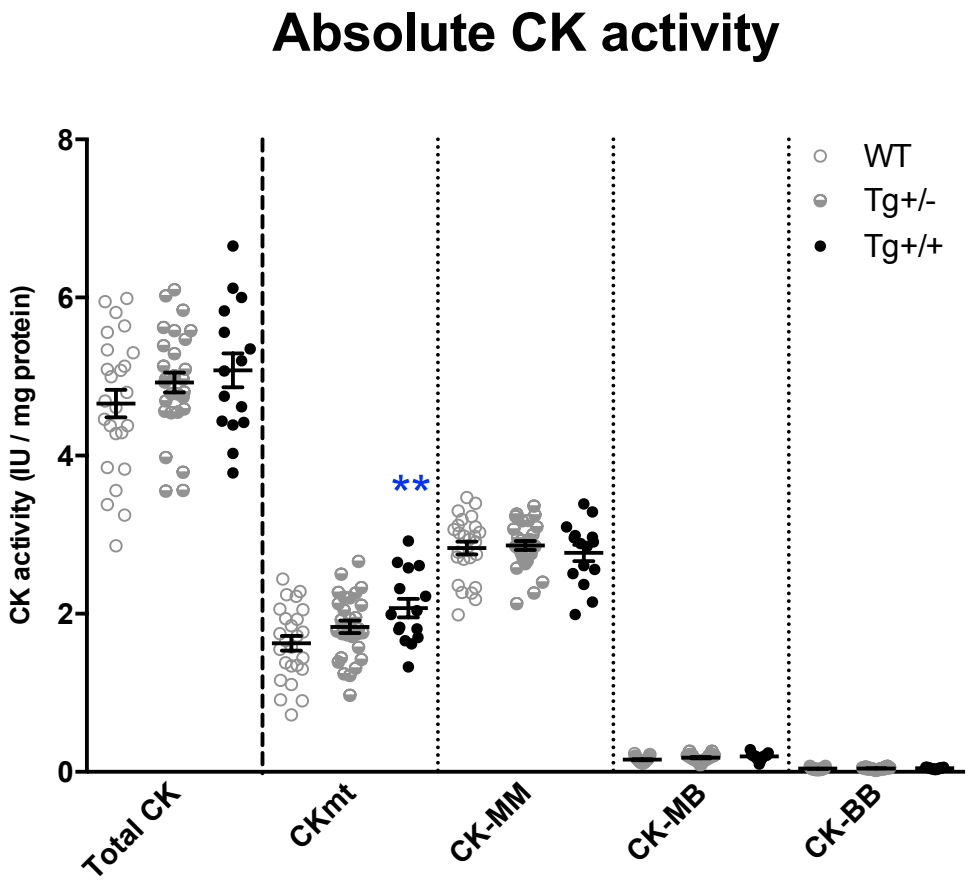


Figure 4-28: Creatine kinase activity in $Tg^{+/-}$ and $Tg^{+/+}$ CKmt–OE mice.

Results were analyzed by one–way ANOVA with Bonferroni's multiple comparison test. ** denotes a significant difference with respect to wild–type ($p \leq 0.01$).

CKmt activity, expressed as a percentage of total CK (Figure 4-29), was significantly higher in both $Tg^{+/-}$ and $Tg^{+/+}$ compared to wild–types, and significantly higher in $Tg^{+/+}$ than $Tg^{+/-}$ (WT, 34.38 ± 0.79%; $Tg^{+/-}$, 37.12 ± 0.72%; $Tg^{+/+}$, 40.57 ± 0.97%).

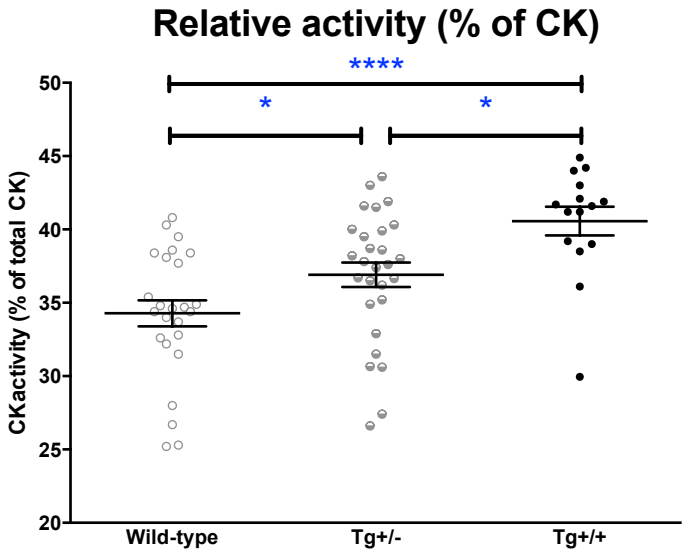


Figure 4-29: CKmt activity in $Tg^{+/-}$ and $Tg^{+/+}$ CKmt–OE mice (relative).

Results were analyzed by one–way ANOVA with Bonferroni's multiple comparison test. * denotes a significant difference with respect to wild–type ($p \leq 0.05$); ****, $p \leq 0.0001$.

4.3.3.4. Subcellular localization of transgenic protein by transmission electron microscopy

In vitro validation of the Ckmt–HA construct demonstrated that the protein was expressed in the mitochondria of cultured cells. In order to confirm that mitochondrial targeting was successful *in vivo*, transmission electron microscopy with immunogold staining was performed in perfusion-fixed left ventricular samples.

4.3.3.4.1. *Sample preparation*

Samples were perfusion–fixed, using a protocol based on published methods for fixation of rodent hearts for electron microscopy[220,221]. Experiments were performed in $Tg^{+/+}$ mice at 30 weeks, using wild–type littermates as negative controls (n=3 per group). Mice were anesthetized by intraperitoneal injection of pentobarbital, and the heart and lungs were rapidly excised and submerged in a dish filled with room–temperature Krebs–Henseleit buffer (composition in mM: 118 NaCl, 4.8 KCl, 25 HEPES, 1.25 K_2HPO_4, 1.25 $MgSO_4$, 11 glucose; pH 7.4). The heart was allowed to beat in the dish to expel blood from the ventricles and prevent clot formation, and trimmed to remove attached tissues. The ascending aorta was cut, and the heart was mounted on a Langendorff perfusion rig. All subsequent steps were performed by retrograde aortic perfusion of solutions into the coronary vasculature, using gravitational feeding under a pressure of 80 cm H_2O (approx. 60 mm Hg). The heart was perfused with Krebs–Henseleit buffer (10–20ml) to wash out residual blood, until the buffer exiting the coronary sinus ran clear. Hearts were subsequently perfused with 15ml of room–temperature fixative (3% paraformaldehyde, 0.2% glutaraldehyde, 0.1 M sodium cacodylate, 4.5mM $CaCl_2$, 0.1 M sucrose, pH 7.4). Upon completion of perfusion, the heart was immediately transferred to a dish containing the pre–chilled fixative solution (4°C), and the left ventricular free wall was dissected into ~1mm^3 fragments using a scalpel. Samples were immediately transferred to vials containing pre–chilled fixative, and fixed overnight at 4°C.

4.3.3.4.2. *Immunogold staining*

Sample processing, immunogold staining, and imaging by transmission electron microscopy was performed by Dr. Errin Johnson (Dunn School of Pathology, University of Oxford), according to the following protocol.

Samples were rinsed thoroughly in water, and incubated in 0.5% aqueous uranyl acetate overnight at 4°C. Samples were then taken through a dehydration series: 30% ethanol, 50% ethanol (20 min each at room temperature), 70% ethanol overnight at 4°C, followed by 20 min each of 80%, 90% and 95% ethanol, and 3x 100% ethanol for 30 min each. Samples were then infiltrated with HM20 monostep acrylic resin starting at 0°C and gradually cooling to −50°C at a rate of 5°C per hour. The infiltration was as follows: 25% resin in ethanol for 1 hr, 50% resin for 3 hrs, 75% resin for 2 hrs, 100% resin overnight, 100% resin for 8 hrs, 100% resin overnight, 100% resin for 8 hrs. Samples were embedded in fresh resin in gelatin capsules and polymerised under UV for 48hrs at −50°C, warmed to 0°C, and polymerised with UV for a further 24 hrs.

Blocks were sectioned on a Leica UC7 ultramicrotome using a diamond knife (Diamtome). 90nm sections were transferred to 200 mesh nickel grids. Grids were floated section side down on a 20 μl droplet of blocking solution (10% goat serum in TBS) for 10 min, then blotted and incubated on a droplet of primary antibody (Roche rat anti−HA, diluted 1:100) for 3 hrs at 37°C. Grids were washed by passing them over 5 droplets of buffer A, 5 min each, incubated with secondary antibody (Abcam goat anti−rat conjugated to 5 nm gold [ab81411], diluted 1:20) for 90 min at 37°C, and washed by passing over 3 droplets of water. Sections were post−stained with uranyl acetate and Reynold's lead citrate, and imaged in a FEI Tecnai 12 TEM at 120 kV.

4.3.3.4.3. *Results*

Immunogold staining was detected in samples from $Tg^{+/+}$ mice, but not wild−type controls. Gold particles were detected inside the mitochondria, but not in the cytosol or other organelles (Figure 4-30). No staining was detected in transgenic samples incubated without the primary antibody (Figure 4-30D), confirming that the signal was not due to non−specific binding of the secondary antibody.

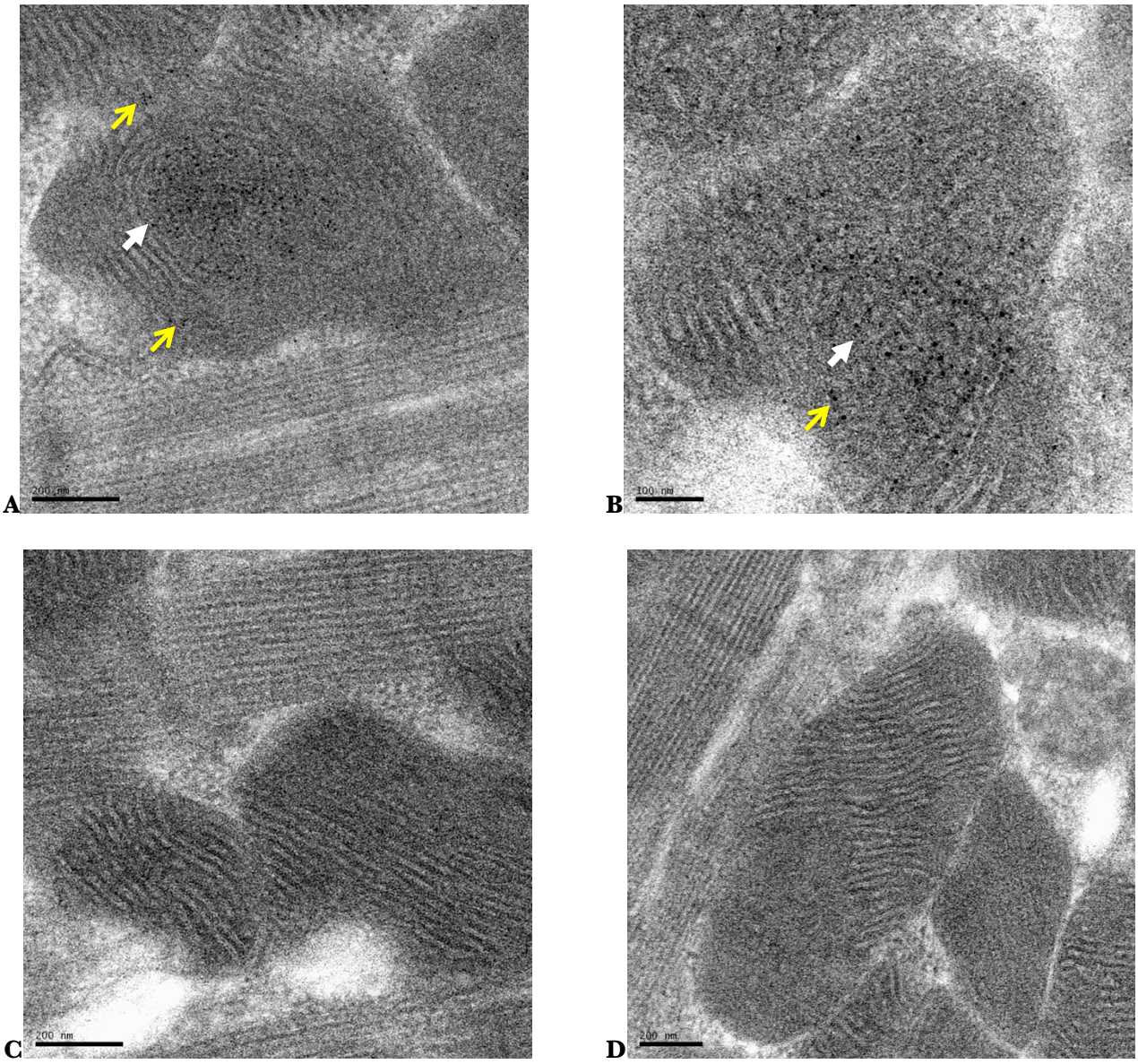


Figure 4-30: Transmission electron microscopy with immunogold staining of CKmt–HA in left ventricular tissue.

(A, B) Representative images from transgenic mice, demonstrating the presence of gold particles at the mitochondrial membrane (yellow arrows), as well as inside the mitochondria (white block arrow), but not in the adjacent sarcomere. **(C)** Sample from a wild–type mouse, stained under the same conditions as (A) and (B). **(D)** Sample from a transgenic mouse, incubated without primary (anti–HA) antibody. Scale bar is 100nm in (B), 200nm in other images.

Ultrastructural microscopy was attempted in parallel to assess mitochondrial morphology and volume, but the sections were of relatively poor quality and could not be reliably quantified. Therefore, additional experiments are required to determine whether overexpression of CKmt affects mitochondrial structure *in vivo*. Immunogold staining will also be repeated using a secondary antibody conjugated to a larger (10 nm) gold particle, to improve visualization of HA-tagged CKmt and pinpoint its intramitochondrial localization.

4.3.4. Phenotyping studies

4.3.4.1. Growth curves

In order to determine whether overexpression of CKmt had an effect on the early stages of development, 11 consecutive litters of mice from $Tg^{+/-}$ x $Tg^{+/-}$ breeding (n=110) were weighed on a weekly basis, from the age of weaning (3 weeks) until 10 weeks (Figure 4-31). Male pups grew more rapidly and reached higher weights than their female littermates, as expected; however, there were no significant differences between genotypes within gender groups.

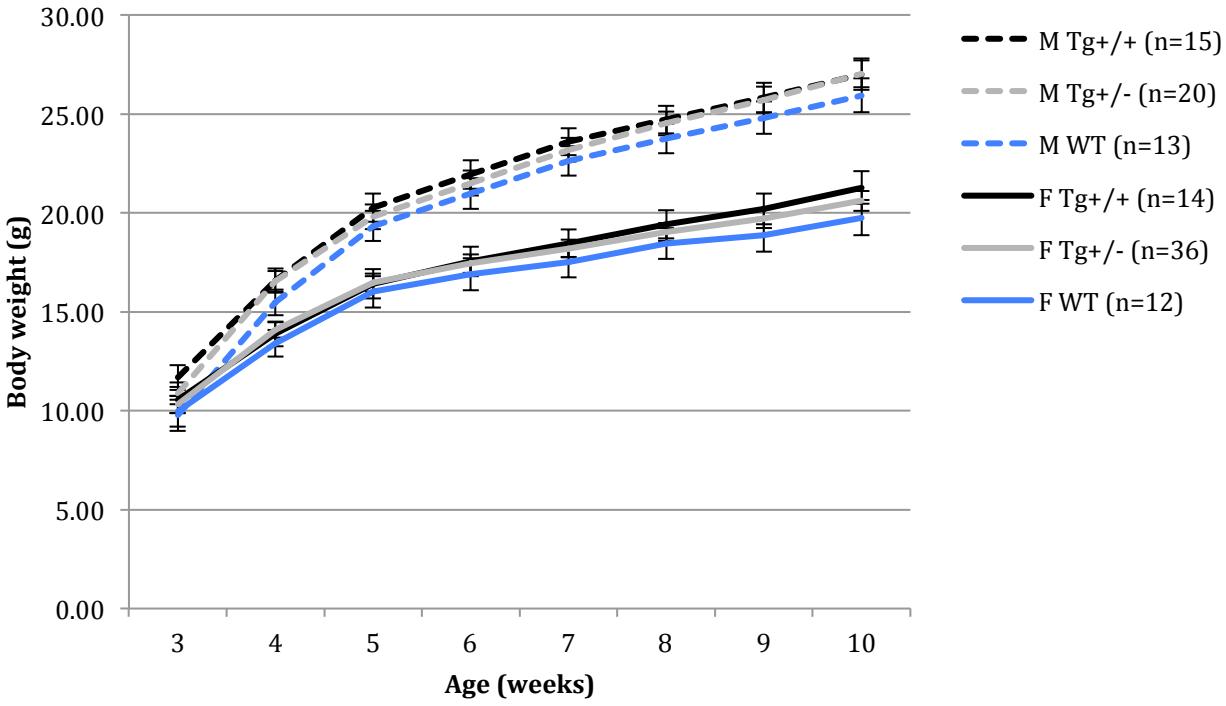


Figure 4-31: Growth curves in CKmt-OE mice.

Mice are grouped by gender (male, dashed lines; female, solid lines), and genotype. No significant differences were observed between genotypes.

In addition, adult body weights were obtained from mice at 20-30 weeks (n=147), and no significant differences were observed between groups (Figure 4-32).

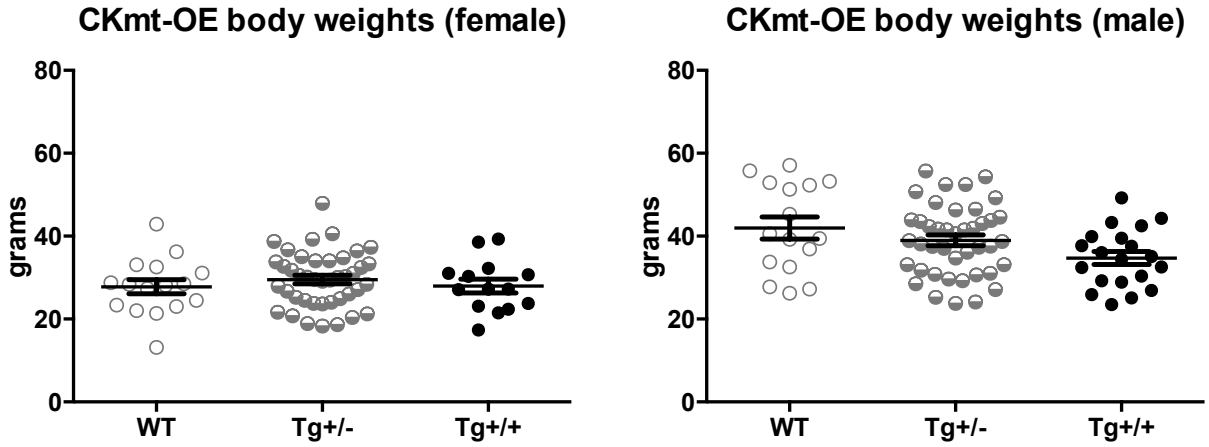


Figure 4-32: Adult body weights in CKmt-OE mice.

No significant differences were observed between genotypes (n=147 overall).

4.3.4.2. Organ weights

In order to determine whether signs of cardiac hypertrophy or pulmonary congestion were present in transgenic mice, heart and lung weights were obtained in animals undergoing cardiovascular phenotyping at 12 weeks, following completion of experiments (Figure 4-33). There was no significant difference in LV weight, RV weight, or lung weight, whether these parameters were expressed as absolute values, or indexed to body weight or tibial length (not shown).

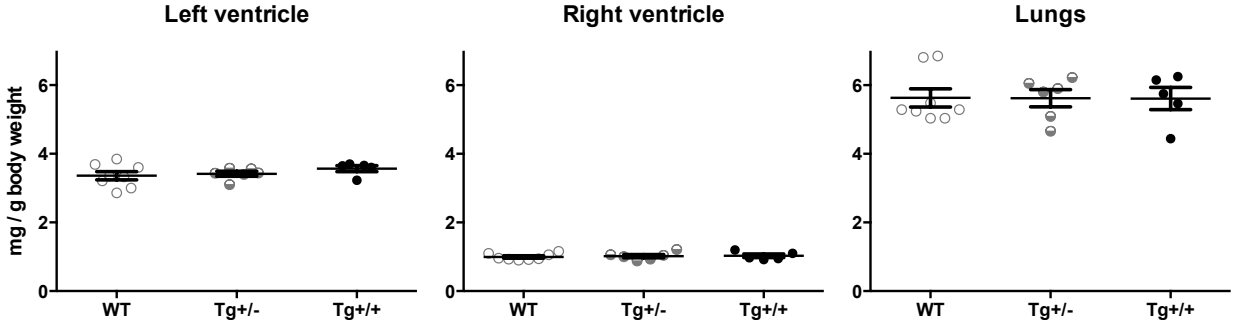


Figure 4-33: Organ weights in CKmt-OE mice.

Values are indexed to total body weight. Results were analyzed by one–way ANOVA with Bonferroni's multiple comparison test. There were no significant differences between groups.

4.3.4.3. Cardiac cine–MR imaging

Cardiac magnetic resonance cine imaging (cine-MR) was performed in mice at 12 weeks of age. Following induction of anesthesia (1% isoflurane), subcutaneous electrodes were inserted into the forelimbs for ECG gating, and mice were placed on a pressure-sensitive pad in a dedicated cradle, and transferred to a 9.4T MR scanner for imaging (Varian). Representative cine-MR images are shown in Figure 4-34.

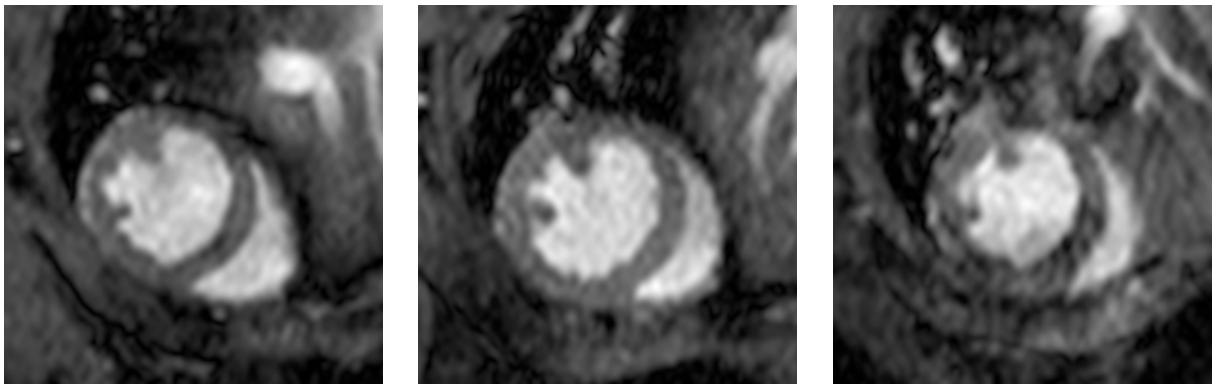


Figure 4-34: Cardiac cine-MR in CKmt-OE mice.
Images are representative mid-ventricular short-axis slices from female mice of each genotype, demonstrating normal cardiac structure in all groups.

Left ventricular mass and volumes were measured using a previously published three-dimensional guide-point modeling protocol[222]. Image processing and quantification was performed by Dr. Leonie Diffley, and statistical analyses were conducted by the author. There were no statistically significant differences between groups (Figure 4-35). Although there was a trend towards increased cardiac index in $Tg^{+/+}$ mice (WT, 11.8 ± 1.5 ml / min / g; $Tg^{+/-}$, 12.6 ± 1.0; $Tg^{+/+}$, 15.1 ± 1.5), the difference was driven by higher heart rates in these mice, while stroke volumes were similar across groups.

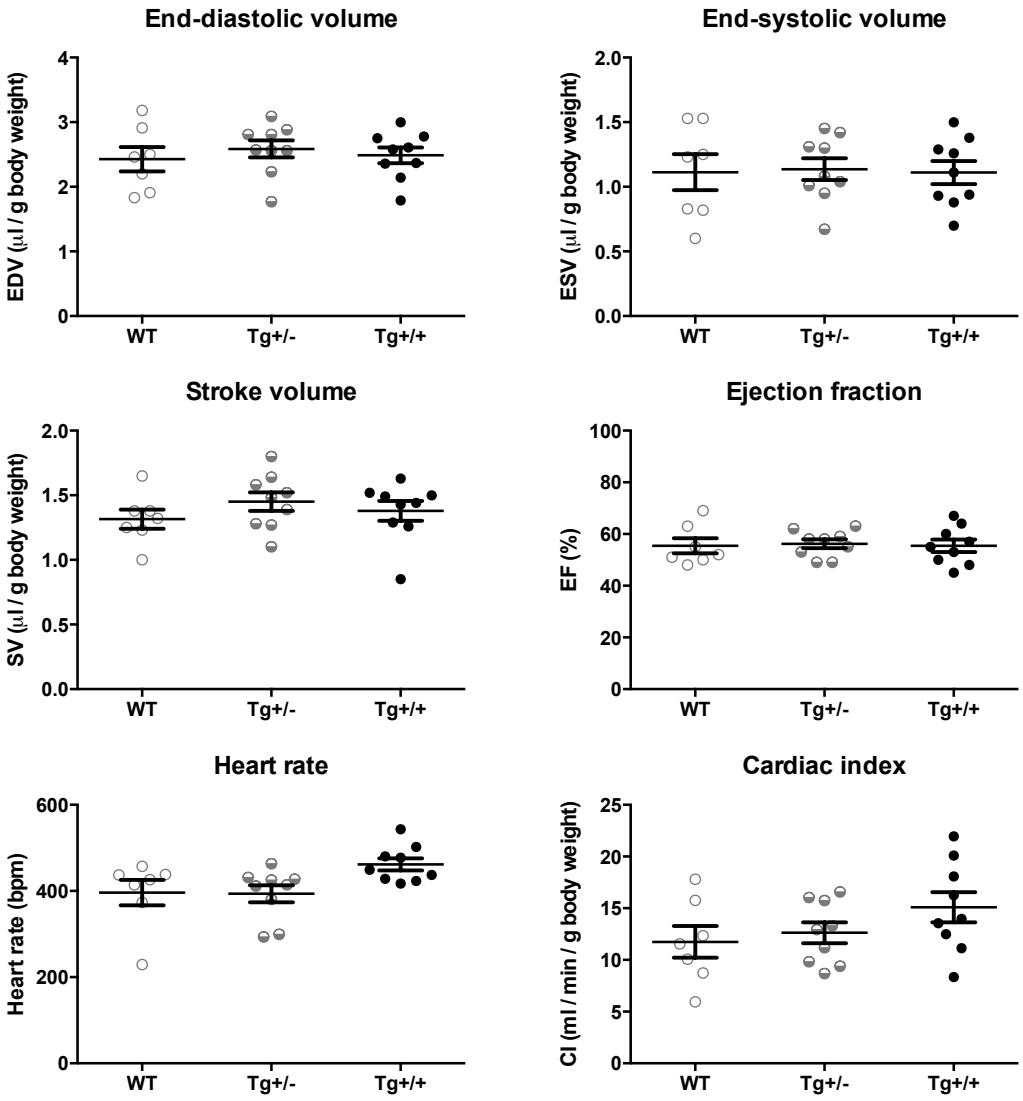


Figure 4-35: Left ventricular volumes and cardiac index in CKmt-OE mice.

LV volumes and cardiac output are indexed to total body weight, as indicated. Results were analyzed by one–way ANOVA with Bonferroni's multiple comparison test. There were no significant differences between groups.

Finally, there were no significant differences in left ventricular mass index measured by cine-MR (Figure 4-36), and values were comparable to *ex vivo* wet weights described above (WT, 3.34 ± 0.22 mg / g; $Tg^{+/-}$, 3.56 ± 0.17; $Tg^{+/+}$, 3.48 ± 0.26).

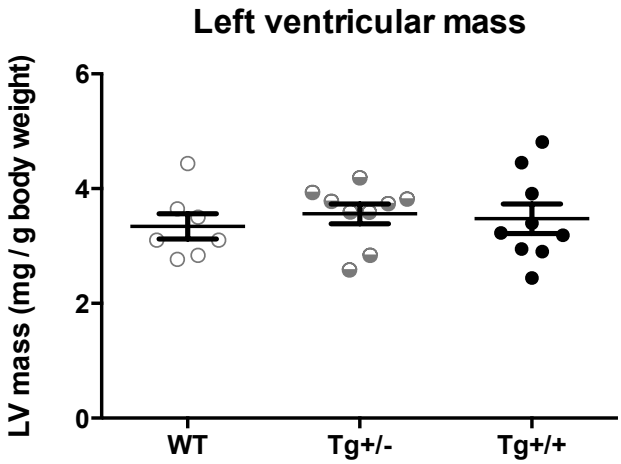


Figure 4-36: Left ventricular mass in CKmt-OE mice, measured by cine-MR.

Values are indexed to total body weight. Results were analyzed by one–way ANOVA with Bonferroni's multiple comparison test. There were no significant differences between groups.

4.3.4.4. *In vivo* left ventricular hemodynamics

Left ventricular hemodynamic measurements were acquired by Ms. Debra Medway, and data were quantified and analyzed by the author.

12-week-old mice were anesthetized using 4% isoflurane, weighed, and transferred to a homeothermic blanket (Harvard Apparatus). Mice were positioned supine with the neck hyper–extended, with anesthesia maintained using 2% isoflurane administered via a nose cone. A skin incision was made above the thyroid gland, and subcutaneous tissues were dissected to access the right common carotid artery. The artery was dissected free from the surrounding connective tissue and rinsed with 0.9% NaCl. A suture was placed at the distal end of the prepared segment and tied to occlude blood flow; an additional suture was placed at the proximal end and tightened to occlude blood flow, but not tied. A small transverse incision was made, and a 1.4F pressure–volume catheter was introduced (Millar Instruments, SPR–839) into the artery and advanced into the aorta. A third suture was placed over the incision site and tied, and the proximal suture was tied. The catheter was advanced into the left ventricle under echocardiographic guidance (Agilent Sonos 5500). Simultaneous pressure and volume measurement was commenced. A catheter was inserted into the right internal jugular vein and flushed with 0.9% NaCl. Isoflurane concentration was reduced to 1.5%, and

baseline recordings were obtained following a 15–minute equilibration period. Dobutamine (16ng/g body weight/min) was infused intravenously using a Graseby MS 16A syringe driver, and recordings were obtained following stabilization of pressure/volume traces. Once recordings were complete, the pressure catheter was returned to a calibration syringe, and the pressure readout was noted to correct for baseline drift in data analysis. Finally, mice were culled by removal of the heart under terminal anesthesia. Organ wet weights (whole heart, LV, RV, lung) and tibial length were measured, and the LV was snap–frozen in liquid nitrogen and stored at –80°C.

Results of selected left ventricular hemodynamic measurements are presented in Figure 4-37. There were no significant differences between groups with respect to heart rate or indices of systolic and diastolic function. Both wild–type and transgenic mice demonstrated a robust inotropic response to dobutamine infusion, with a significant increase in heart rate and the maximal rates of contraction (dP/dt_{max}) and relaxation (dP/dt_{min}).

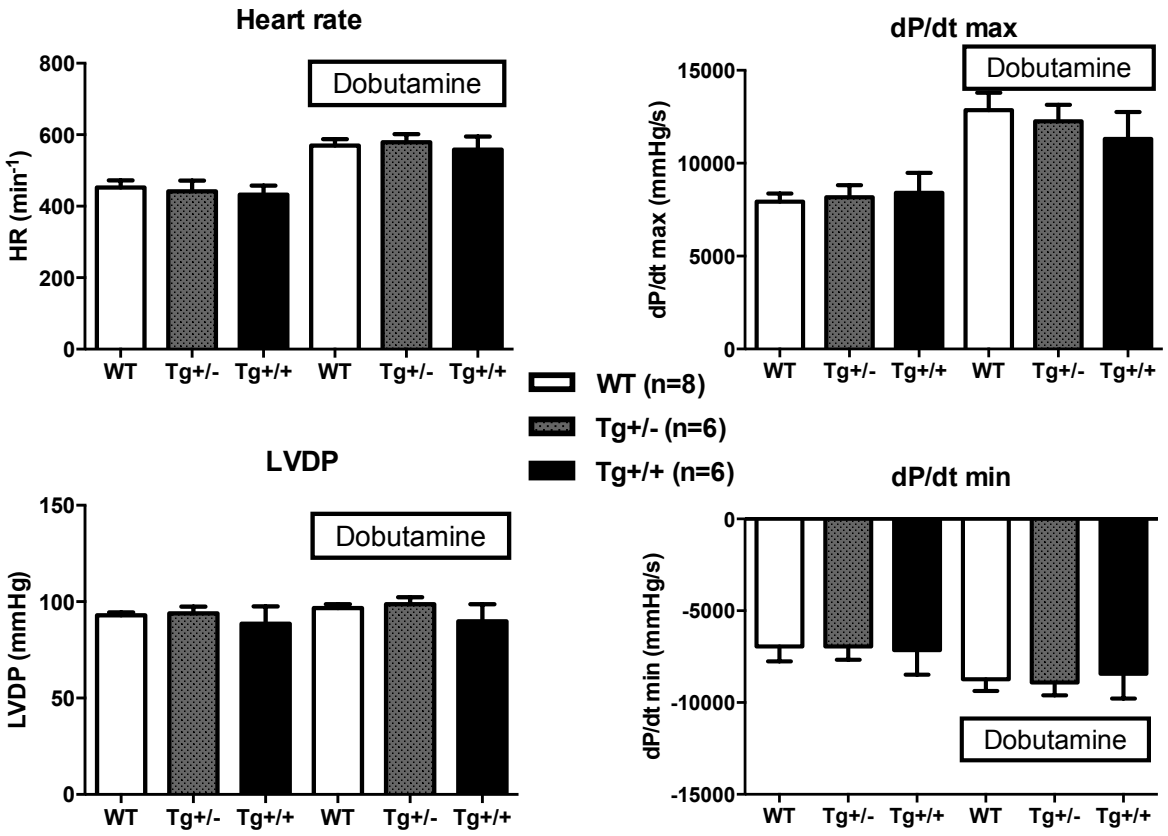


Figure 4-37: Left ventricular hemodynamics in CKmt-OE mice.

No significant differences were observed in heart rate, left ventricular developed pressure (LVDP), or maximal rates of contraction (dP/dt max) and relaxation (dP/dt min). In each graph, bars marked "Dobutamine" represent values during infusion of dobutamine (16ng/g/min).

4.3.4.5. Citrate synthase activity

Since changes in mitochondrial CK activity have been found to affect mitochondrial volume in certain studies[130,134], myocardial citrate synthase activity was measured in samples processed for CK assays (Figure 4-38). Citrate synthase activity was found to be significantly lower in both $Tg^{+/-}$ (0.97 ± 0.02 IU/mg protein) and $Tg^{+/+}$ (0.95 ± 0.03) groups, compared to wild–type controls (1.06 ± 0.03).

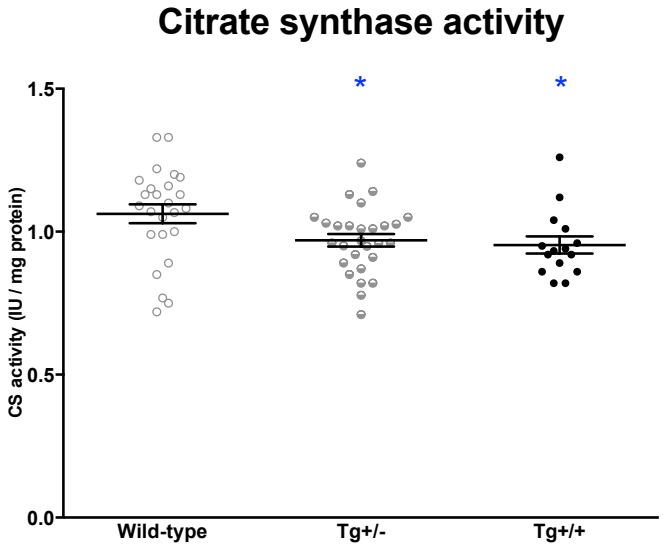


Figure 4-38: Citrate synthase activity in CKmt–OE mice.

Results were analyzed by one–way ANOVA with Bonferroni's multiple comparison test. * denotes a significant difference compared to wild–type. There was no significant difference between transgenic groups.

4.4. Discussion

To study the effects of CKmt overexpression in the heart, a line of transgenic mice was generated by targeted integration of an expression construct driven by the αMHC promoter at the ROSA26 locus in embryonic stem cells, followed by blastocyst injection. Expression of the transgene was confirmed by *in vitro* differentiation of embryonic stem cells, followed by immunocytochemical staining for αMHC and the transgenic HA tag. After several unsuccessful attempts, chimeric founder mice capable of producing transgenic offspring were generated. Transgene expression was restricted to the heart, and detectable at the mRNA and protein levels, but did not lead to a significant increase in total CKmt protein in left ventricular

tissue. Similarly, transgenic mice did not have significantly elevated CKmt enzymatic activity, although there was an increase in relative CKmt activity (expressed as a percentage of total CK), suggesting that the transgenic protein was enzymatically active.

In order to determine whether a more robust increase in CKmt activity could be achieved by increasing the transgene copy number, homozygous transgenic mice were generated. These mice were viable, and the transgene was inherited in a Mendelian ratio. Left ventricular mRNA expression was higher in homozygous mice than in wild–types and hemizygous transgenics, with respect to both transgenic mRNA and total CKmt mRNA. CKmt activity was significantly higher in homozygous transgenics than in wild–types, by 27%. Electron microscopy confirmed that the transgene was being expressed in the mitochondria.

Hemi– and homozygous transgenic mice did not differ significantly from wild–types with respect to growth in the post–weaning phase, or adult body weight. Similarly, there was no difference with respect to the weight of the whole heart, individual cardiac chambers, or lungs. Left ventricular volumes and pressures were determined *in vivo* by cine-MR and invasive hemodynamic measurement, respectively, and no significant differences were observed at baseline or under maximal inotropic stimulation. Finally, citrate synthase activity was significantly lower in both hemi– and homozygous transgenics.

The following sections will discuss the process of generating and validating the transgenic model, results of initial phenotyping, and possible future experiments.

4.4.1. Generation of transgenic mice

4.4.1.1. Chimeric founder mice

Chimeric founder mice were generated by targeted integration of the transgene at the ROSA26 locus in embryonic stem cells, which were selected for antibiotic resistance, screened by PCR, and injected into

C57BL/6 blastocysts. After several rounds of blastocyst injections, only two chimeric founders were identified (3.4% of transferred blastocysts). This could indicate that transgene expression was adversely affecting viability; however, the efficiency of murine transgenesis by blastocyst injection of embryonic stem cells is generally relatively low. In the original publication describing the method[223], the yield of viable pups was 30.3%, of which 15.0% were chimeric (4.5% of blastocysts). Subsequent studies using C57BL/6 blastocysts for injections, as in this model, observed similar results (Table 4-7). Therefore, it seems likely that the difficulties encountered in producing founder mice were due to the nature of the technique itself, rather than any factors related to the transgenic construct.

Study	Blastocysts implanted	Viable pups		Chimeric males		
		n	%	n	% (of viable pups)	% (of all blastocysts)
Gossler *et al.*[224]	471	136	28.9%	26	19.1%	5.5%
Schwartzberg *et al.*[225]	331	106	32.0%	21	19.8%	6.3%
CKmt–OE	59	24	40.7%	2	8.3%	3.4%

Table 4-7: Success rates of transgenesis by blastocyst injection.

4.4.1.2. Breeding of transgenic mice

4.4.1.2.1. *Breeding of first-generation (F_1) transgenics*

Chimeric founder (F_0) mice were mated with wild–type C57BL/6 females to generate first–generation offspring (F_1). The first five F_0 mice were all fertile, but failed to produce transgenic offspring (n=195 F_1 pups screened). The fact that no transgenic mice were identified from these founders could be due to failed genotyping PCR; however, the reaction was extensively validated before it was used. Since the wild–type control band was detected in all mice, DNA extracts and PCR conditions were adequate for genotyping purposes – particularly since the transgene would be amplified by the same pair of primers, and would produce a shorter band than the wild–type gDNA. Therefore, even if reaction conditions were suboptimal, the transgenic band would be more likely to be successfully amplified if any mice were transgenic. Furthermore, transgene–positive controls were generating the expected product; therefore, the observed lack of transgenic mice was not due to a failure of the genotyping protocol.

Several possible causes for the lack of transgenic mice were considered. Failed integration of the transgene is a possibility; however, embryonic stem cells were screened by PCR prior to blastocyst injection, and clones with failed or partial integration were excluded. Therefore, two explanations were most likely: (1) that germline transmission of the transgene was not occurring in the chimeric founder mice, or (2) that germline transmission was taking place, but the transgene was embryonically lethal, and therefore no transgenic pups were reaching the age at which mice were genotyped (2-3 weeks).

The difference in genotype at the agouti locus between the blastocysts and transgenic embryonic stem cells can be used to resolve this question. The blastocysts used for injections were genetically non–agouti (a/a); since founder mice were bred with wild–type, non-agouti C57BL/6 females (a/a), all offspring derived from the blastocyst cells would necessarily be non-agouti (a/a). In contrast, the transgenic ES cells are heterozygous at the agouti locus (A/a), and hemizygous for the *CKmt* transgene (+/–); significantly, these genes are inherited independently. Therefore, if the embryonic stem cells were to contribute to the germline in the chimeric founders, this would yield a variety of genotypes in their spermatozoa (25% each of A+, A–, a+, and a–). If the transgene was lethal, embryos derived from A+ and a+ spermatozoa would die *in utero*; however, both A– and a– embryos would develop normally. Therefore, if germline transmission was taking place, one would expect to see a certain amount of pups derived from A– spermatozoa (theoretically 50% of all pups derived from the ES cells). These A– mice would be wild–type with respect to the *Ckmt* transgene, but heterozygous at the agouti locus (A/a), and therefore phenotypically agouti. Since a large number of pups were produced by the original chimeric founders, but no agouti mice were observed, it is unlikely (although not impossible) that germline transmission was taking place. The most likely explanation for the lack of transgenic pups was therefore a lack of germline transmission.

In an effort to overcome this problem, further blastocyst injections were performed to generate additional founders with a higher proportion of ES cell-derived germ cells. Ultimately, germline transmission was observed in two founders, with 54/113 transgenic pups (47.8%). Assuming Mendelian inheritance of the transgene, the percentage of transgenic pups would be determined by the percentage of germ cells in these founders which were derived from transgenic ES cells (*i.e.*, the probability of a given germ cell being derived

from a cell carrying the transgene), multiplied by 50% (*i.e.*, the probability that, for any germ cell derived from a transgenic ES cell, meiotic division resulted in the germ cell carrying the transgene). This indicates that (1) the majority of germ cells in these founders were derived from transfected ES cells, and (2) transgenic status was not affecting embryonic viability, as this would decrease the percentage of transgenic pups.

4.4.1.2.2. *Breeding of homozygous ($Tg^{+/+}$) mice*

Homozygous transgenic ($Tg^{+/+}$) mice were generated by breeding F_1 $Tg^{+/-}$ males with F_1 $Tg^{+/-}$ females. Inheritance of the transgene was found to follow the expected Mendelian ratio (25% wild–type, 52% $Tg^{+/-}$, 23% $Tg^{+/+}$). This provides further evidence that the transgene does not adversely affect viability, as if this was the case, a lower proportion of $Tg^{+/-}$ and $Tg^{+/+}$ pups would be observed.

4.4.2. Validation of transgene expression

4.4.2.1. Initial validation by *in vitro* differentiation in embryoid bodies

Prior to generation of transgenic mice by blastocyst injection of embryonic stem cells, transgene expression was validated *in vitro* by inducing differentiation of ES cells into cells of the cardiomyocyte line. Expression and tissue–specificity of the transgene would still need to be confirmed *in vivo*, but the results of *in vitro* differentiation experiments provided a valuable early indication that the construct was functioning as expected.

4.4.2.2. Transgene expression and activity

4.4.2.2.1. *Expression of transgenic mRNA*

Transgenic mRNA expression was detected in all four cardiac chambers, but not in other organs. There is evidence that the αMHC promoter is active in the lungs, specifically in the walls of pulmonary venules[226]; however, in the original study the level of pulmonary expression was found to be significantly lower than in cardiac tissue. Therefore, while it remains possible that CKmt–HA transgene is also expressed in the lungs, this is unlikely to have a significant effect on phenotype.

4.4.2.2.2. *Expression of transgenic protein*

Transgenic protein expression was confirmed in left ventricular tissue, by detection of a <50 kDa HA–tagged protein in transgenic mice, which was not present in wild–types. This confirms that the transgenic mRNA was being translated to produce CKmt–HA protein. Western blotting for transgenic protein expression in non–cardiac tissues was not performed, since the results of qRT–PCR demonstrated the lack of transgenic mRNA in other organs.

4.4.2.3. Total CKmt mRNA, protein and enzymatic activity

4.4.2.3.1. *Confirmation of increased CKmt expression and enzymatic activity*

Although transgene expression was confirmed at the mRNA and protein levels, neither total CKmt protein nor activity was significantly increased in hemizygous transgenics. Mice were therefore bred to homozygosity in an attempt to achieve higher levels of CKmt expression. There was a further increase in CKmt mRNA, protein, and activity, confirming that the transgenic protein is enzymatically active in proportion to its expression levels.

4.4.2.3.2. *CKmt protein overexpression is not as pronounced as mRNA overexpression*

There is a slight discrepancy between the magnitude of the increase in total CKmt mRNA (41%) and protein (15%) in $Tg^{+/-}$. This is most likely due to differences in sensitivity between qPCR and western blotting, but there are other possible causes. For example, impaired translation of transgenic mRNA would lead to a relatively lower level of protein expression; however, this is unlikely to be the case, as the transgene was clearly detectable at the protein level, and the construct included a suitable Kozak sequence for initiation of translation[163]. There is a large body of evidence suggesting that the correlation between mRNA and protein levels is perhaps weaker than could be expected (reviewed in[227,228]). A study comparing relative mRNA and protein expression in two types of murine myeloid cells found that there was actually a negative correlation in some instances, particularly for mitochondrial proteins[229]. This suggests that, in addition to the level of mRNA expression, other mechanisms play a significant role in regulation of protein expression, which may explain the difference in the relative levels of CKmt mRNA and protein overexpression.

4.4.2.4. Possible causes for the relatively modest increase in total CKmt activity

The results of enzyme activity assays, in conjunction with data on mRNA and protein expression, suggest that transgenic CKmt is expressed in the hearts of CKmt–OE mice, and is associated with a step–wise increase in CKmt activity in $Tg^{+/-}$ and $Tg^{+/+}$ hearts. However, the overall level of CKmt overexpression remained relatively low (28% increase in activity in $Tg^{+/+}$). The following possible causes were considered: (1) insufficient expression of the transgene, (2) impaired enzymatic activity of the transgenic protein, (3) compensatory downregulation of endogenous CKmt expression, or (4) degradation or inactivation of CKmt protein.

4.4.2.4.1. *Transgene expression levels*

The most probable explanation for the modest increase in CKmt activity is that the transgene is not being expressed to sufficient levels to drive a pronounced increase. This could be due to low activity of the αMHC promoter itself, or an effect of integration at the ROSA26 locus.

The murine αMHC promoter was first characterized by Robbins's group[230]. A variety of *cis*– and *trans*–acting regulatory elements have been identified[231-233], including a pair of GATA–4 binding sites, which are thought to be responsible for the cardiac–specific expression pattern[234]. Truncated forms of the promoter may be inactive[226]; however, the promoter used to generate CKmt–OE mice was the full–length (~5.5kb) murine αMHC promoter. Since the complete, species–matched promoter sequence was used, there is no reason to suspect that the αMHC promoter was not functional in CKmt–OE mice, unless expression was affected by regulatory elements at the integration site.

To date, no transgenic models have been published using the αMHC promoter at the ROSA26 locus. Therefore, it is possible that activity of the αMHC promoter is relatively low at ROSA26, due to site–specific effects. A recent study sought to examine the activity of ubiquitous promoters at ROSA26 in murine ES cells[199], and activities of various promoters were found to vary by two orders of magnitude. This is not a surprising finding in itself, but parallel experiments in transiently transfected ES cells (*i.e.*, cells in which the constructs were being expressed directly from plasmid vectors, without integration at ROSA26) yielded some conflicting results. For example, the activity of the EF1α promoter was similar to that of the CAG promoter in transiently transfected cells, but 75% lower than CAG when the promoters were integrated at ROSA26. While no definitive conclusions can be drawn based on the results of this study, it is possible that activity of the αMHC promoter may be unpredictably affected by integration at the ROSA26 locus in this model.

4.4.2.4.2. *Enzymatic activity of transgenic protein*

Since the transgene was derived from murine *Ckmt2* cDNA, its amino acid sequence should be identical to the endogenous protein. The notable exception is the C–terminal hemagglutinin (HA) tag, which was incorporated in order to distinguish between endogenous and transgenic protein. The HA tag is a relatively short sequence (9 amino acids, compared to the 419aa endogenous protein); however, it is possible that even minor alteration of secondary or tertiary structure could affect enzymatic function.

Expression and function of HA-tagged CKmt was initially validated *in vitro* (see section 3.3.1), and was associated with a large increase in enzymatic activity, relative to control cells. It is difficult to evaluate the precise magnitude of this increase, as activity assays was performed in HEK293 cells, which express a relatively small amount of creatine kinase. Nonetheless, the fact that an increase in CKmt activity was observed *in vitro* suggests that the HA–tagged protein does not lose its enzymatic activity.

The fact that CKmt–HA is enzymatically active *in vitro* does not, however, confirm that its activity is equal to that of endogenous, untagged CKmt. If this was the case, one would expect to see a discrepancy between total CKmt protein expression and activity, since CKmt–HA protein would be present, but contribute proportionally less to enzymatic activity. This does not appear to be the case, as the observed increase in total CKmt protein expression (~15% in $Tg^{+/-}$) is similar to the increase in enzymatic activity (~13%). Therefore, it seems reasonable to conclude that it is the amount of CKmt protein present, rather than its enzymatic activity, which is responsible for the modest increase in CKmt activity in transgenic mice.

4.4.2.4.3. *Effect of transgene expression on endogenous CKmt*

Another possible explanation is downregulation of endogenous CKmt expression by expression of the transgene, via an undefined negative–feedback mechanism aimed at keeping total CKmt expression constant. If this was the case, it would reconcile the contradictory findings that the transgene is expressed at both mRNA and protein levels, but does not lead to a significant increase in total CKmt protein or enzymatic activity, as a decrease in endogenous CKmt would negate the effect of transgenic protein

expression. To address this possibility, allele–specific qRT–PCR was performed, and demonstrated that endogenous CKmt mRNA expression was unchanged in both hemi– and homozygous transgenics. This suggests that, at the mRNA level, expression of the transgene is not associated with compensatory suppression of the endogenous transcript.

4.4.2.4.4. *Degradation or inactivation of transgenic and/or endogenous protein*

Transgene expression is not associated with a reduction in endogenous CKmt mRNA levels; however, this does not exclude an effect at the protein level. It is possible that expression of CKmt could be subject to negative–feedback regulation at the protein level (*e.g.,* due to post–translational modification or degradation of endogenous CKmt). Post-translational modification does not seem to be a likely cause, as this would be expected to yield a discrepancy between high protein levels and low enzymatic activity, which does not appear to be the case. Degradation of transgenic and/or endogenous CKmt is a possibility, and ubiquitination of CKmt has been demonstrated[84,86]. If required, this could potentially be confirmed by a ubiquitination assay; however, this seems unlikely, since the low level of transgene expression remains the most likely cause for the modest increase in CKmt activity.

4.4.2.5. Subcellular localization of CKmt–HA

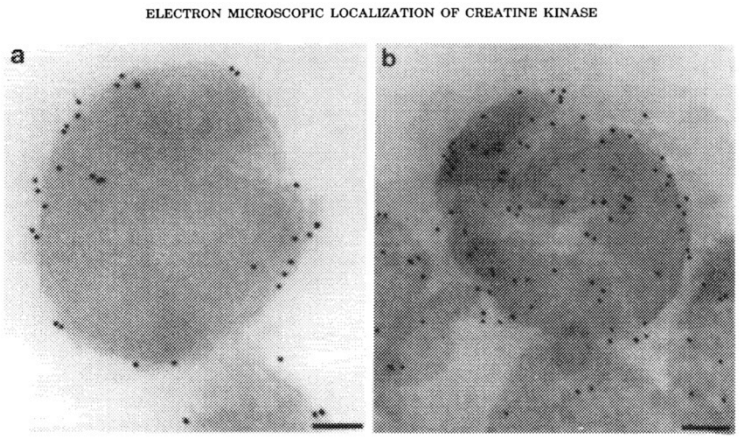
The subcellular localization of CKmt plays a key role in its function, and it was therefore necessary to confirm whether the transgenic protein was being expressed in the mitochondria. This was previously demonstrated *in vitro* in HL-1 cells, confirming that the C–terminal HA tag does not affect mitochondrial targeting of the protein.

In order to verify this finding *in vivo*, transmission electron microscopy with immunogold staining was performed in left ventricular tissue, and demonstrated that the HA tag was expressed in the mitochondria, and not in other regions of the cell. CKmt is normally expressed in the mitochondrial intermembrane space, and one could therefore expect that HA labeling would be observed at the edges of mitochondria; in

contrast, HA signal appeared to be distributed throughout the mitochondrion. This is, however, in accordance with previous studies on the localization of CKmt in brain mitochondria, which found a significant degree of intramitochondrial expression, most likely associated with the cristae membranes (Figure 4-39)[65,235]. Nonetheless, further experiments are warranted to increase the number of samples analyzed, and potentially improve imaging quality. Furthermore, anti-CKmt immunogold staining could be conducted to determine whether the expression of endogenous CKmt in these mice follows a similar distribution.



A



B

Figure 4-39: Transmission electron microscopy with immunogold labeling of CKmt.

(A) Immunogold labeling of CKmt in isolated brain mitochondria, from Wegmann *et al.*[235]. **(B)** Immunogold labeling of VDAC (left) and CKmt (right) in isolated brain mitochondria, from Kottke *et al.*[65]. Note that, while the distribution of VDAC, which is an outer membrane protein, appears confined to the edges of the mitochondrion, CKmt is detectable throughout the mitochondrion.

4.4.3. Baseline phenotyping

4.4.3.1. Cardiovascular phenotype

No significant differences were observed in CKmt-OE mice with respect to cardiac pressures or volumes, either at baseline or under maximal inotropic stimulation. There was a trend towards increased cardiac index in $Tg^{+/+}$ mice at the time of cine-MR imaging, which was driven by differences in heart rate. It is worth noting that heart rate was also assessed in these mice at the time of *in vivo* hemodynamic measurements, and no differences were observed between groups. Therefore, it is likely that the trend

towards increased heart rate and cardiac index in $Tg^{+/+}$ mice at the time of cine-MR imaging was due to other factors, such as depth of anesthesia. Nonetheless, this should be addressed by performing ECG measurements in conscious mice.

Overall, the results of baseline cardiac phenotyping indicate that overexpression of CKmt does not adversely affect cardiac function under physiological conditions, which is an expected, but nonetheless significant finding. Further experiments are required to determine whether increasing CKmt can be beneficial in pathological models of heart disease.

4.4.3.2. Citrate synthase activity is decreased in CKmt–OE mice

The experiments summarized above indicate that overexpression of CKmt does not significantly affect viability or baseline cardiovascular phenotype. The only difference observed in transgenic mice was a decrease in citrate synthase (CS) activity, which is a marker of mitochondrial volume[160]. This is an interesting finding, as previous studies have shown that ablation of CKmt activity may have the opposite effect. In our group's study on the effect of genetic background on the cardiac phenotype of $CKmt^{-/-}$ mice, CS activity was found to be increased by 18%, and it was suggested that this may be a compensatory adaptation to CKmt deficiency[130]. Dzeja *et al.* observed a 16% increase in CS activity in M/Mt–$CK^{-/-}$ mice on a mixed genetic background[134]. Similar increases in CS activity were observed in skeletal muscle from M/Mt–$CK^{-/-}$ mice[134], but not in $CKmt^{-/-}$[130]. In contrast, other studies have not observed a difference in myocardial CS activity in $CKmt^{-/-}$ mice[126,135], or in M/Mt–$CK^{-/-}$ mice backcrossed onto a pure C57BL/6 background[131]. The methodological differences between these studies may explain the lack of a consistent effect, and other measures of mitochondrial volume (*e.g.* ultrastructural electron microscopy, mitochondrial DNA copy number) should be assessed to provide a definitive answer.

The studies described above did not provide a mechanistic explanation for potential changes in CS activity. The recent discovery that activity of the metabolic sensor protein AMP–activated protein kinase (AMPK) is regulated by changes in ADP, in addition to AMP, may provide a possible link[236]. Studies in CK knockout

models have consistently demonstrated an increase in free ADP levels in CKmt$^{-/-}$[126] and M/Mt–CK$^{-/-}$[134,237,238] mice, but not in isolated M–CK$^{-/-}$[134,237,238]. While there are no previously published models of CKmt augmentation in the heart, expression of CKmt in the liver leads to a *decrease* in ADP, which is proportional to CKmt activity[239]; this effect was not observed in earlier studies of hepatic CK–B expression, suggesting that it is specifically CKmt, rather than CK activity in general, which is responsible for lower ADP levels[240]. Therefore, it is reasonable to suspect that cytosolic ADP levels may be decreased in the myocardium of CKmt–OE mice.

If ADP levels are lower in CKmt–OE mice, this could lead to a decrease in AMPK activity[236], which could be responsible for the observed difference in CS activity. AMPK can stimulate mitochondrial biogenesis by upregulating the transcriptional coactivator peroxisome proliferator–activated receptor γ coactivator 1–α (PGC–1α, reviewed in[241]). PGC–1α is a key regulator of mitochondrial biogenesis, and PGC-1α activation stimulates production of mitochondrial proteins encoded by nuclear genes[242], as well as mitochondrial transcription factor A (mtTFA/TFAM), which increases replication/transcription of mitochondrial DNA[243]. The most convincing evidence for a link between AMPK and mitochondrial biogenesis was provided by Zong *et al.*, who developed transgenic mice expressing a dominant–negative form of AMPK (dnAMPK)[244]. In wild–type mice, energy depletion (by inhibition of the CK system) led to an increase in PGC–1α expression and mitochondrial density. These effects were not observed in dnAMPK mice, confirming that AMPK is required for induction of mitochondrial biogenesis in response to changes in cellular energetic status. The fact that CK inhibition was found to activate PGC–1α provides further evidence that CKmt overexpression may decrease mitochondrial volume by inducing the opposite effect.

4.5. Conclusions and future work

A line of transgenic mice overexpressing mitochondrial creatine kinase (CKmt) was generated by targeted integration of an expression construct, under the control of the αMHC promoter, at the ROSA26 locus. Transgene expression was confirmed, but the level of CKmt overexpression was found to be relatively low in

hemizygous ($Tg^{+/-}$) mice. Mice were therefore bred to homozygosity ($Tg^{+/+}$), and increased CKmt activity was confirmed in $Tg^{+/-}$ and $Tg^{+/+}$ mice. Subcellular localization experiments confirmed that transgenic CKmt was being expressed in the mitochondria. Cardiovascular phenotyping did not reveal any structural or functional changes, and the response to adrenergic stimulation was normal. This indicates that CKmt overexpression does not have any detrimental effect at baseline, and the model is suitable for further studies.

The only significant difference observed in CKmt–OE mice was lower citrate synthase activity, which may indicate a reduction in mitochondrial volume. This finding requires validation by transmission electron microscopy, to directly visualize mitochondrial density and structure. Further experiments could be conducted to determine whether downregulation of the AMPK/PGC–1α pathway plays a role by inhibiting mitochondrial biogenesis in this model. This is a readily testable hypothesis, which could be assessed by measuring AMPK activity and PGC–1α expression in the CKmt–OE myocardium. Finally, the argument that this effect may be mediated by decreased ADP could be evaluated by ^{31}P–MRS measurement of high–energy phosphate levels. While our group is not currently able to perform these measurements *in vivo*, experiments could be conducted in the *ex vivo* perfused heart.

Finally, further experiments are being planned to determine whether CKmt overexpression protects the heart against acute ischemia/reperfusion injury and/or chronic heart failure. This is of particular interest, given the reduction in cell death in response to simulated ischemia/reperfusion injury in cultured cells overexpressing CKmt, described in section 3.4.2. If this effect is reproduced *in vivo*, it would provide a target for development of novel therapeutic approaches in heart disease. It is worth noting that transgenic mice were generated on a mixed background, and must first be backcrossed onto a pure C57BL/6 background before these experiments can be conducted (Figure 4-40).

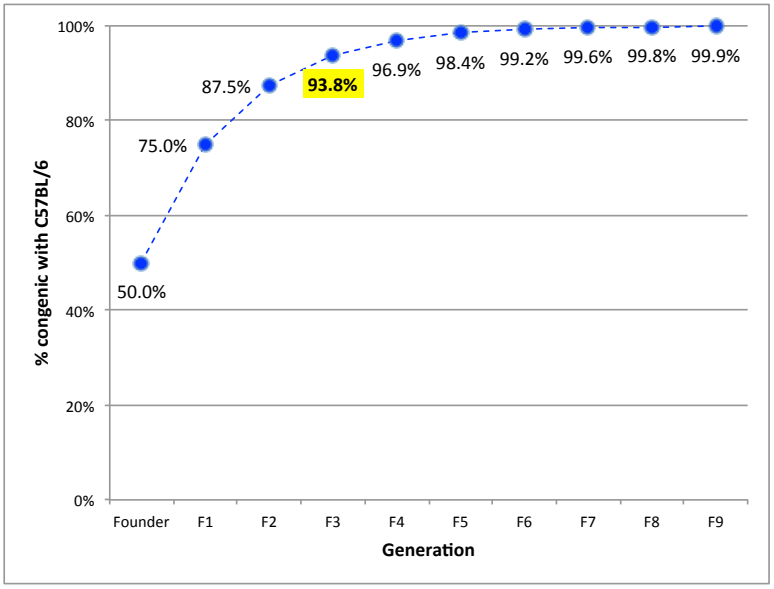


Figure 4-40: Backcrossing CKmt-OE mice onto a pure C57BL/6 background.

At the time of writing, mice have been backcrossed for three generations, and are theoretically ~94% congenic with C57BL/6 (yellow). Six further generations are required to reach ≥99.9% congenicity.

This work is in progress, and mice have currently been backcrossed for three generations; it is estimated that six further generations will be required for mice to be ≥99.9% congenic with C57BL/6 (Figure 4-40), although an additional generation will be required to generate homozygous transgenics at this point, taking the total to seven generations. Once this is complete, it will be possible to conduct further studies to determine whether increasing CKmt activity is a viable therapeutic target in cardiac disease.

5. *IN VIVO* MODELS OF AUGMENTED CARDIAC ENERGETICS – OVEREXPRESSION OF CK-M AND CK-B BY RANDOM-INTEGRATION TRANSGENESIS

5.1. Introduction

This chapter describes the generation and validation of transgenic mouse models, overexpressing the M- and B-type creatine kinase isoenzymes in the myocardium. The design and cloning of expression constructs is discussed, followed by generation and breeding of transgenic mice, and finally molecular phenotyping of these *in vivo* models.

5.1.1. Choice of transgenesis strategy

Based on the results of initial validation of the CKmt-OE mice, which demonstrated a relatively modest increase in CKmt activity using targeted integration at ROSA26, the decision was made to use an alternative strategy for generation of mice overexpressing the remaining CK isoenzymes (CK-M and CK-B). Since the alpha-MHC promoter was confirmed to ensure cardiac-specific expression of the CKmt transgene *in vivo*, the same promoter was used for CK-M and CK-B mice. In an attempt to achieve a more robust level of transgene expression than that observed in CKmt-OE mice, the initial strategy (targeted integration at the ROSA26 locus) was replaced by a random chromosomal integration-based method of transgenesis.

5.1.2. Random integration of transgenic DNA

Transgenic mice overexpressing CK-M and CK-B were generated by pronuclear microinjection of expression constructs into fertilized C57BL/6 oocytes[245-248]. There are several key differences between this method and that used to derive the CKmt-overexpressing mice described in Chapter 4. First, multiple copies of the transgene can integrate simultaneously. The exact number is unknown *a priori*, but increasing the number of transgene copies may lead to higher expression levels. Second, the transgene integration site is random. This would overcome limitations due to possible positional effects at ROSA26; however, random integration could have unexpected phenotypic effects, due to (1) disruption of endogenous genes by the transgene, or (2) the presence of regulatory elements (*e.g.*, promoters, enhancers or silencers) which could affect expression of the transgene itself. Such positional effects could have an effect on phenotype, which would be difficult to distinguish from the effect of transgene expression. Consequently, it is necessary to generate multiple transgenic lines for each model, to avoid drawing conclusions based on the phenotype associated with a particular transgene integration event. Finally, pronuclear microinjection does not allow for screening or selection of cells prior to implantation; therefore, the efficiency of transgenesis can be relatively low, and it is impossible to determine whether transgenic DNA has integrated into the genome until founder mice are born. Therefore, this strategy is likely to require a larger number of mice to be generated, as transgene integration cannot be verified *in vitro*, and multiple founder lines must be established for each model.

5.2. Hypotheses and aims

The goal of the experiments described in this chapter was to generate and validate two lines of mice overexpressing the cytosolic creatine kinase isoenzymes, CK-M and CK-B, in the heart. While it was not possible to perform cardiovascular phenotyping experiments in these in mice during the timescale of this thesis, the ultimate goal of the project is to determine whether myocardial overexpression of CK-M and/or

CK-B improves CK-mediated phosphotransfer, and whether this intervention would be beneficial in models of heart disease. Therefore, the experimental hypotheses are discussed in this long-term context.

The experimental hypothesis for mice overexpressing CK-M is that increased flux through the CK reaction will accelerate regeneration of ATP, and improve cardiac function in models of disease. During the course of this project, a similar transgenic line has been generated by the Weiss group, who demonstrated that overexpression of CK-M can protect the heart against the effects of ischemia/reperfusion injury and chronic heart failure[145,146]. In addition to recapitulating these findings in an independent transgenic line, a further long-term aim of the project is to develop double-transgenic mice, *e.g.* overexpressing multiple CK isoenzymes and the creatine transporter, to test the effects of increased enzymatic activity *and* substrate availability. This provides further rationale for generating a constitutive model of CK-M overexpression, which would be significantly easier to maintain than the Weiss group's tetracycline-inducible model.

Unlike CKmt and CK-M, CK-B is thought to play a relatively minor role in myocardial energetics due to its low activity in the heart (≤2% of total CK). Nonetheless, studies in transgenic mice overexpressing CK-B in the liver found that this was associated with reduced susceptibility to hypoxic injury[148]. Furthermore, transgenic expression of CK-B in the skeletal muscle of CK-M$^{-/-}$ mice was found to restore the energetic phenotype, suggesting that CK-B may be able to compensate for CK-M deficiency by assuming its function (despite not being directly associated with the contractile apparatus)[249]. It is therefore possible that CK-B overexpression may also have beneficial effects in the heart, similar to those observed in CK-M mice.

5.3. Methods and results

5.3.1. Design and cloning of expression vectors

5.3.1.1. Design of expression vectors

In order to achieve cardiac-specific expression of transgenic *Ckm* and *Ckb*, constructs were designed to incorporate the respective coding sequences downstream of the alpha-MHC promoter, using the αMHC vector previously generated for CKmt-OE mice (Figure 4-4).

5.3.1.1.1. *CK-B*

Primers for amplification of *Ckb* were designed to incorporate a 5' Kozak consensus sequence and a 3' HA tag (removing the native stop codon, and replacing it with a new stop codon downstream of the HA tag). In order to allow cloning of PCR product into the alpha-MHC vector, the appropriate restriction sites were included (5' *SalI* and 3' *HindIII*). Since constructs for *in vitro* expression of *Ckb* and *Ckm* were being generated in parallel, an additional 5' *NheI* site was included to allow for cloning into pcDNA3.1- (Figure 3-1).

5.3.1.1.2. *CK-M*

The strategy for amplification of *Ckm* was similar, with the exception of the 3' restriction site used. Unlike *Ckmt2* and *Ckb*, the *Ckm* coding sequence contains *HindIII* sites, and an alternative enzyme was therefore required for ligation at the 3' terminus. Since the alphaMHC-CKmtHA vector does not contain additional restriction sites at the required locus, a 3' *KpnI* site was incorporated into the *Ckb* construct, between the stop codon and *HindIII* site. Insertion of the *Ckb* construct into the vector would therefore incorporate a 3' *KpnI* site into the vector, which could subsequently be used for ligation with *Ckm*. Cloning was therefore performed

in a two-step process, with the intention of using the final alphaMHC-CKbHA vector as a template for insertion of *Ckm*:

1. Generate inserts by PCR:	CK-B	(5' *NheI*+*SalI* / 3' *KpnI/HindIII*)	
	CK-M	(5' *NheI*+*SalI* / 3' *KpnI*)	
2. Round I cloning:	Insert CK-B into:	alphaMHC-CkmtHA	(*SalI/HindIII)*
		pcDNA3.1-	(*NheI/HindIII)*
	Insert CK-M into:	pcDNA3.1-	(*NheI/KpnI)*
3. Round II cloning:	Insert CK-M into:	alphaMHC-CKbHA	(*SalI/KpnI)*

5.3.1.2. PCR amplification of *Ckb* and *Ckm* cDNA

PCR was performed to amplify the *Ckb* and *Ckm* open reading frames, using Phusion high-fidelity polymerase and cDNA as a template. PCR was initially attempted following the protocol previously used for generation of the CKmt transgene, but this was unsuccessful. The reaction was optimized, and results were significantly improved by addition of dimethyl sulfoxide (10% v/v) and increasing the magnesium concentration to 2.0mM (note that the reaction buffer for Phusion polymerase already contains 1.5mM $MgCl_2$; Table 5-1, Figure 5-1).

Ckb and *Ckm* cloning PCR								
Reaction mixture					**Cycling conditions**			
Component	**Unit**	**Stock**	**Final**	**Volume (µl)**	**Step**	**Temperature**	**Time (mm:ss)**	**Cycles**
HF Buffer	-	10x	1x	5.00	Activation	95°	10:00	
F primer	µM	100	0.5	0.25	Denaturation	95°	00:30	15
R primer	µM	100	0.5	0.25	Annealing	67.5-60.5° (-0.5°/cycle)	00:30	
dNTP	mM (ea.)	25	0.2	0.40	Extension	72°	00:45	
Phusion polymerase	U/µl	2	1 U	0.50	Denaturation	95°	00:30	13
$MgCl_2$	mM	50	0.5	0.50	Annealing	60°	00:30	
DMSO	%	100	10	5.00	Extension	72°	00:45	
cDNA				2.00	Final extension	72°	10:00	
H_2O				36.10				
Total				**50.00**				

Table 5-1: Optimized PCR protocol for *Ckb* and *Ckm* cloning.

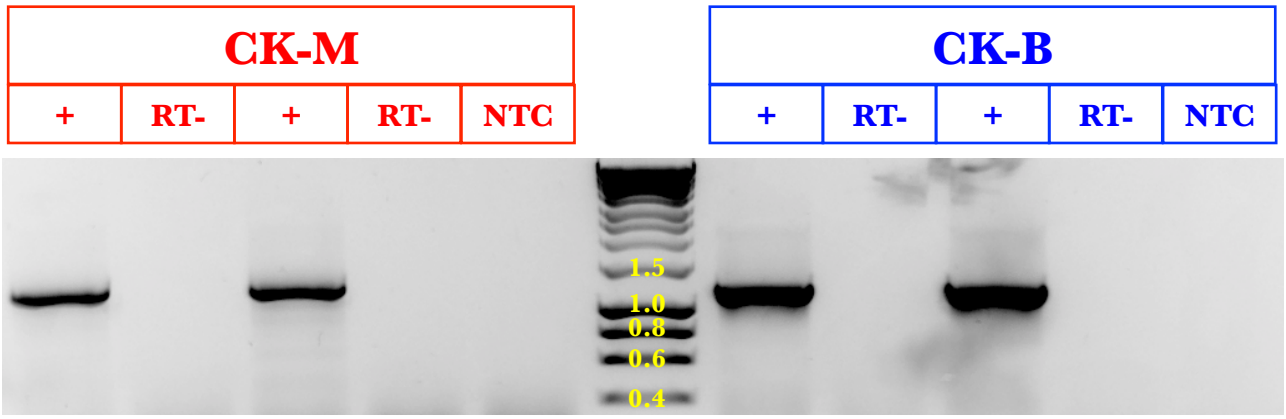


Figure 5-1: PCR amplification of *Ckb* and *Ckm* for expression vectors.

Gel electrophoresis of 5µl aliquots of PCR product (note that this is the same PCR as used for *in vitro* constructs; see Figure 3-2).

5.3.1.3. Cloning of expression vectors

5.3.1.3.1. *CK-B*

PCR products were purified by phenol/chloroform extraction and ethanol precipitation. The alphaMHC-CKmtHA vector and *Ckb* PCR product were digested using *SalI* and *HindIII* and separated by agarose gel electrophoresis (Figure 5-2). The appropriate bands were excised, and DNA was extracted.

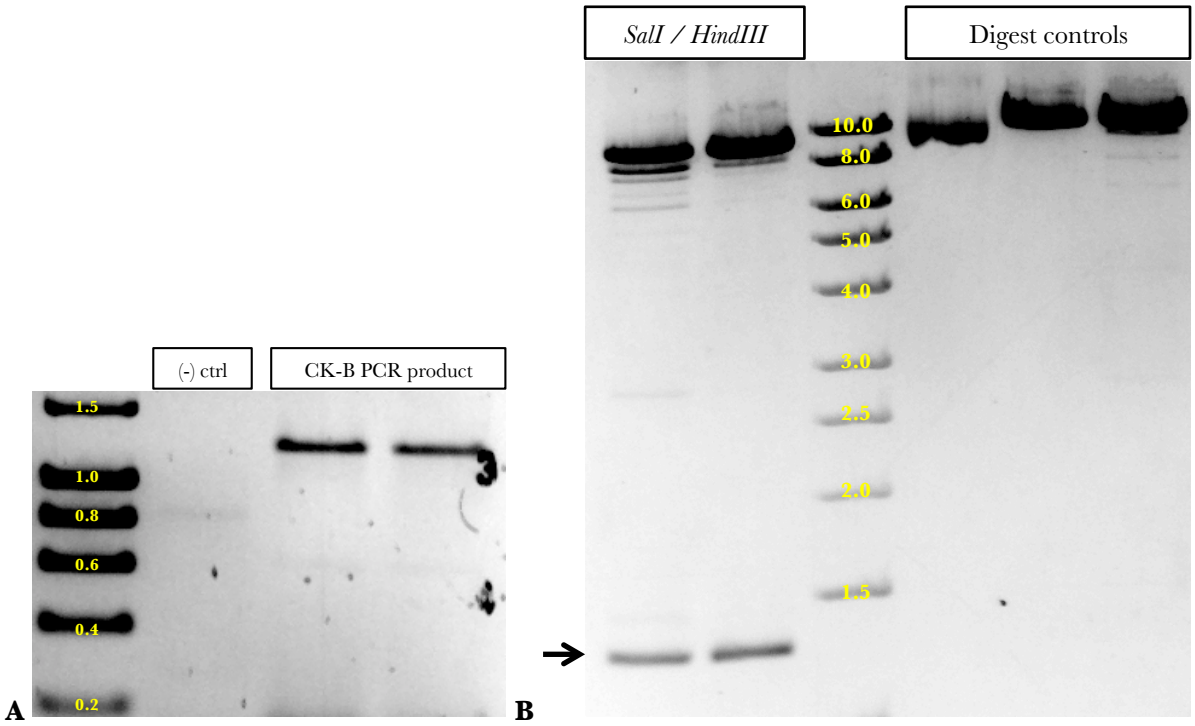


Figure 5-2: Restriction digests for CK-B cloning.

(A) CK-B PCR product. **(B)** αMHC-CKmtHA vector. The ~1.2kb fragment (arrow) is the excised CKmtHA coding sequence. Additional lanes are controls (undigested, *SalI*, *HindIII*).

Vector and insert digest products were ligated, and used to transform 10-β competent *E. coli* (NEB). Bacteria were cultured overnight at 37°C on ampicillin-containing plates, and individual colonies were picked to seed cultures, which were amplified in suspension and harvested for DNA extraction by MiniPrep (Qiagen). Purified products were analyzed by diagnostic restriction digest using *SalI* and *KpnI*; CK-M PCR product was digested simultaneously using the same enzymes, in order to generate the fragments required for cloning of the alphaMHC-CKmHA vector (Figure 5-3).

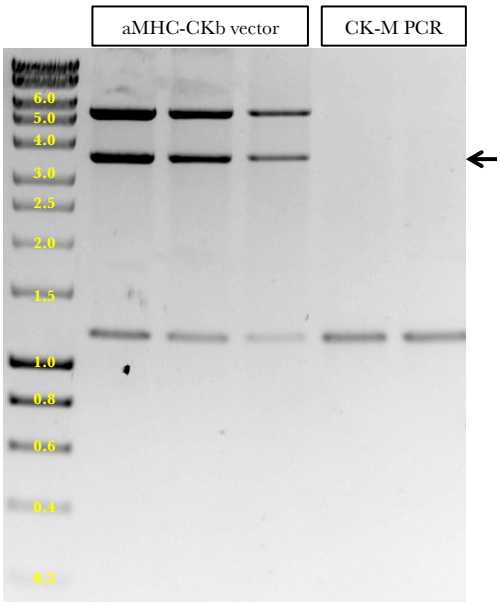


Figure 5-3: Restriction digest of alphaMHC-CKbHA MiniPrep products and *Ckm* PCR product.

Restriction digest using *SalI* and *KpnI* confirmed the presence of the CK-B insert in all MiniPrep products, but there was an unexpected additional band in all lanes (arrow). This was subsequently found to be due to an unexpected *KpnI* site in the vector backbone (see Figure 5-5 and Figure 5-6).

All alphaMHC-CKbHA MiniPrep products were found to contain the *Ckb* insert, and selected samples were verified by DNA sequencing. Sequencing was performed using a pair of primers which bind to both the *Ckb* and *Ckm* coding sequences (CKb&m_seqF and CKb&m_seqR); to ensure double coverage of the coding sequence and insertion sites, a sense primer binding towards the end of the alphaMHC promoter sequence and an antisense primer (T3) binding downstream of the polyadenylation signal were used. The correct sequence was confirmed in all DNA samples amplified by MiniPrep, which were subsequently used to re-transform 10-β *E. coli*, and DNA was amplified and extracted by Endotoxin-Free MaxiPrep (Qiagen). The final construct (Figure 5-4) was re-sequenced, and used by the Transgenics Core for microinjection into fertilized B6CBAF1 (C57BL/6 x CBA) oocytes to generate transgenic mice.

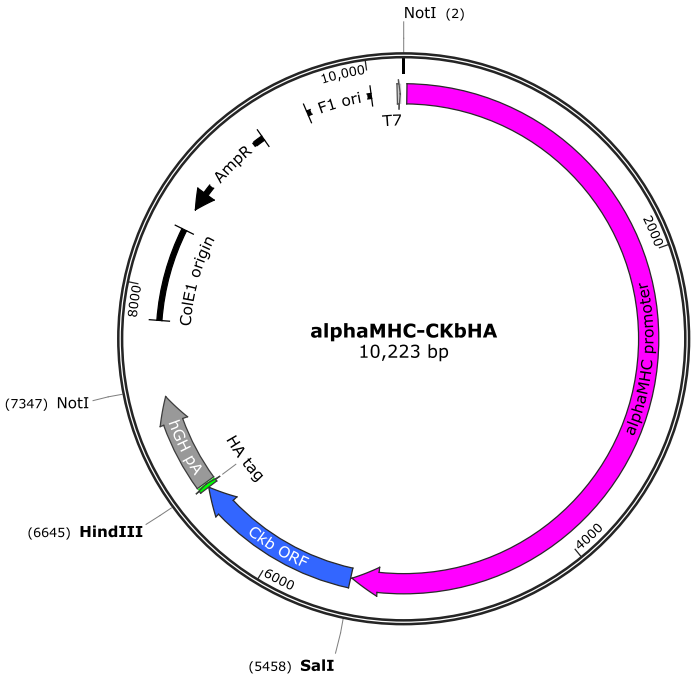


Figure 5-4: αMHC-CKbHA vector for generation of transgenic mice.

The restriction sites used for insertion of the transgene are labeled (*SalI/HindIII*).

5.3.1.3.2. *CK-M*

The initial cloning strategy involved generation of a 3' *KpnI* site during alphaMHC-CKbHA cloning, and subsequently using *SalI* and *KpnI* for insertion of *Ckm* PCR product. However, when *SalI*/*KpnI* digest was performed in alphaMHC-CKbHA MiniPrep products, the vector was unexpectedly cut at an additional site. Since *SalI* was successfully used during generation of the alphaMHC-CKbHA construct, it was most likely that the additional band was due to an unexpected *KpnI* site (Figure 5-5).

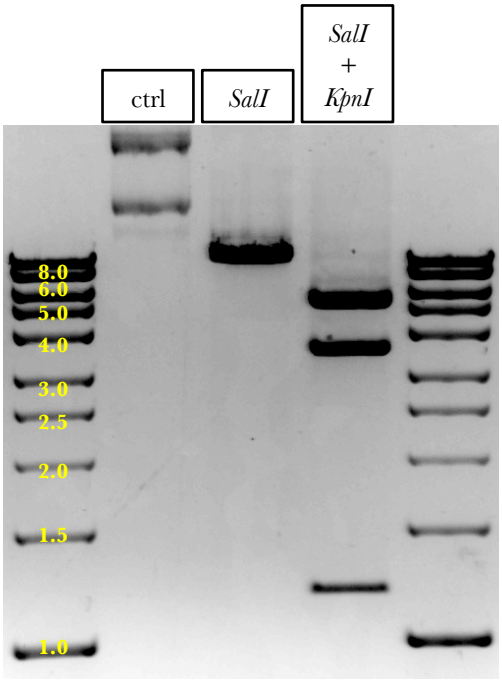
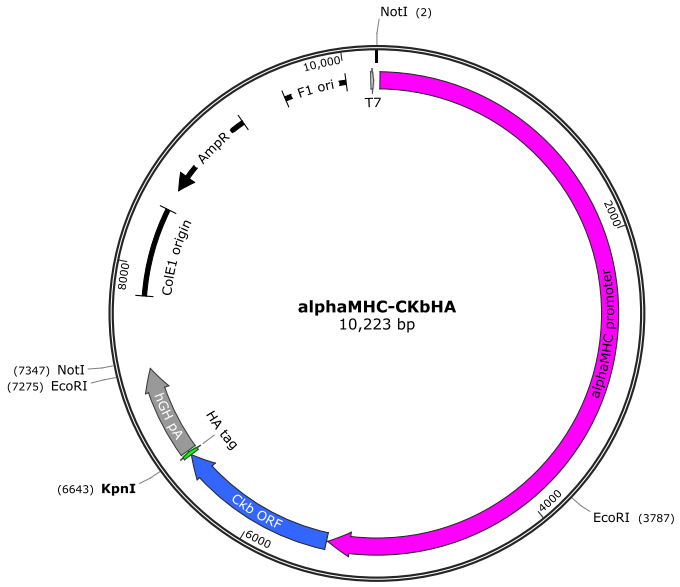


Figure 5-5: Diagnostic restriction digest of alphaMHC-CKbHA.

Digestion with *SalI* alone leads to linearization of the vector, producing a single (>10kbp) band as expected. Addition of *KpnI* produces three restriction fragments, indicating that there are two *KpnI* sites, rather than the expected single site.

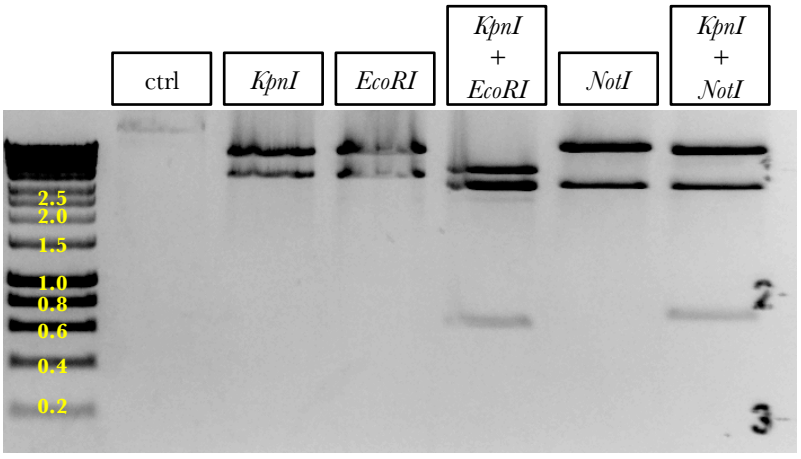
A further diagnostic digest was performed to identify the approximate location of the additional *KpnI* site, and indicated that there was a site in the vicinity of the *NotI* site upstream of the alpha-MHC promoter (Figure 5-6). The presence of this site was subsequently confirmed by sequencing.



A

	uncut	*KpnI*	*EcoRI*	*EcoRI/KpnI*	*NotI*	*NotI/KpnI*
Expected fragments (bp)	**10,223** (circular)	**10,223** (linear)			**7345**	
			6735	**6735**		**6638**
			3488			
				2852	**2878**	**2878**
				636		**707**

B



C

Figure 5-6: Diagnostic restriction digest of the alphaMHC-CKbHA vector.

(**A**) Map of vector, with restriction sites used. (**B**) Expected restriction fragments. (**C**) Gel electrophoresis of digest products. The presence of additional bands in the lanes containing *KpnI* confirms that an unexpected *KpnI* site is present; based on the fragments produced by double digestion with *KpnI* and *EcoRI* or *NotI*, this site is most likely in the vicinity of the 5' *NotI* site.

Since *KpnI* was found to cut the vector at an additional site, an alternative strategy was sought. In parallel, a new alpha-MHC vector containing a polylinker sequence with multiple restriction sites had been developed by the Transgenics Core (alphaMHC-Linker). While the original vector contained relatively few restriction sites suitable for transgene insertion, the new αMHC-Linker vector provided additional restriction sites. Specifically, in addition to the original 5' *SalI* and *NheI* sites, this vector contained a 3' *XhoI* site which could be used for insertion of *Ckm*, as the *Ckm* coding sequence does not contain *XhoI* sites.

In order to generate a 3' *XhoI* site in *Ckm*, a new reverse primer was designed and PCR was performed as described above, using 2µl of the original *Ckm* PCR product as a template (Figure 5-7).

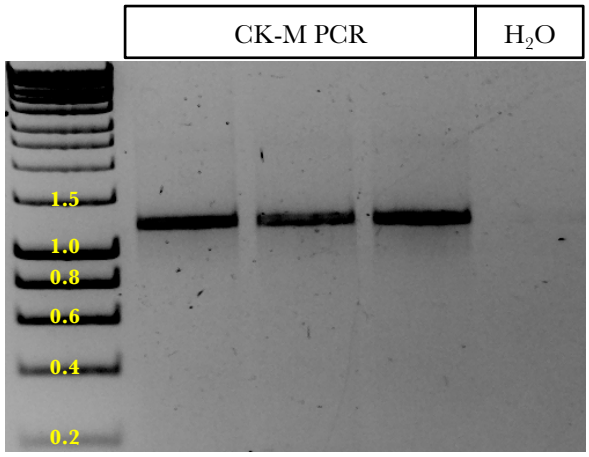
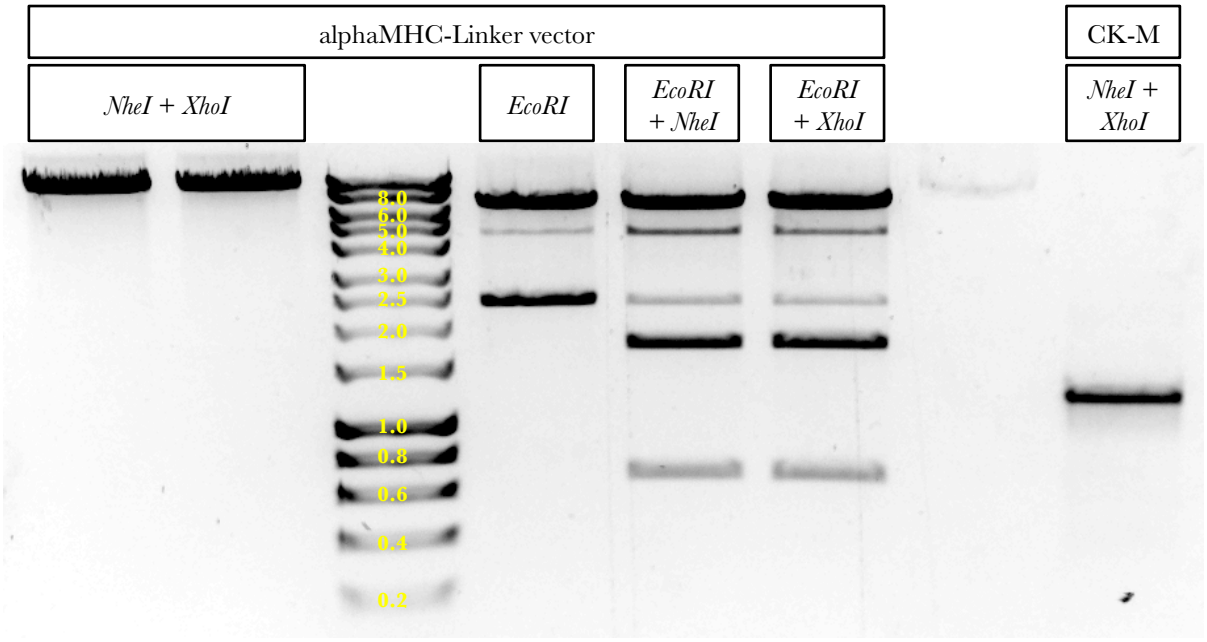


Figure 5-7: Gel electrophoresis of *Ckm* PCR product.
The expected band was present in all samples, and absent in the negative (no-template) control.

The alphaMHC-Linker vector and *Ckm* PCR product were digested using *NheI* and *XhoI*, and separated by agarose gel electrophoresis. Additional diagnostic digests were performed simultaneously using *EcoRI*, to confirm that the alphaMHC-Linker was being cut at the expected sites (Figure 5-8).

DNA	aMHC-Linker				Ckm PCR
Enzymes	*NheI/XhoI*	*EcoRI*	*EcoRI/NheI*	*EcoRI/XhoI*	*NheI/XhoI*
Expected fragments (bp)	9097				
		6752	6752	6752	
		2351			
			1695	1701	1182
			656	650	
	6				

A



B

Figure 5-8: Cloning/diagnostic restriction digest of alphaMHC-Linker vector and *Ckm* PCR product.

(A) Expected fragment sizes for each combination of enzymes, with fragments used for cloning highlighted in yellow. **(B)** Agarose gel electrophoresis demonstrating the presence of the expected restriction fragments. Faint additional bands in lanes 5 (*EcoRI/NheI*) and 6 (*EcoRI/XhoI*) are most likely partial digestion products, as they align with the ~2.5kb band in lane 4 (*EcoRI*).

The appropriate bands were excised, and DNA was extracted, ligated, and amplified by MiniPrep as described above. MiniPrep products were digested using *NheI* and *XhoI* to confirm the presence of the insert, which was detected in most samples (Figure 5-9 – note that individual samples were negative for the insert, most likely due to incomplete digestion of the alphaMHC-Linker vector prior to gel extraction).

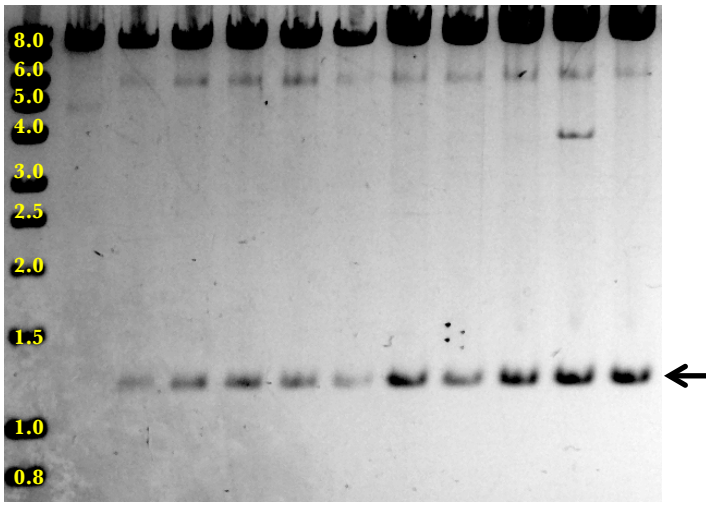


Figure 5-9: Restriction digest of alphaMHC_L-CKmHA MiniPrep products.
DNA was digested using *NheI* and *XhoI*, confirming the presence of the transgenic insert (arrow).

Finally, selected MiniPrep products were sequenced as described above, and used to re-transform 10-β *E. coli* for amplification by Endotoxin-Free MaxiPrep. The final construct (Figure 5-10) was re-sequenced, and transferred to the Transgenics Core for microinjection to generate transgenic mice by random chromosomal integration.

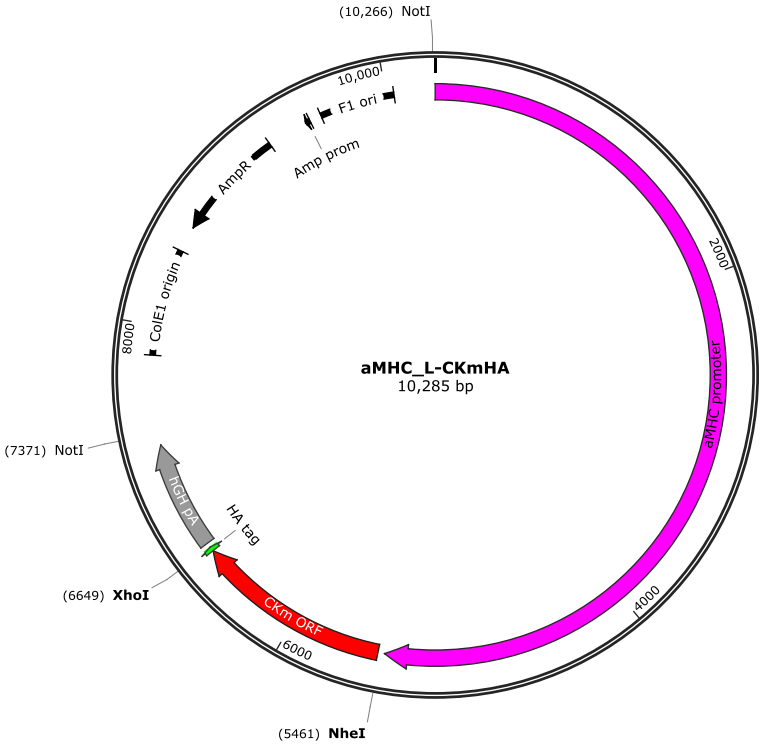


Figure 5-10: Final alphaMHC_L-CKmHA vector.

5.3.2. Generation of founder mice by pronuclear microinjection

Transgenic mice overexpressing CK-M and CK-B were generated by pronuclear microinjection of expression constructs into fertilized B6CBAF1 oocytes. Briefly, wild-type female C57BL/6 mice were superovulated and mated with wild-type C57BL/6 males, and fertilized oocytes were harvested directly from the oviduct and transferred to *in vitro* culture. Linearized expression vectors were resuspended in injection medium, and microinjected directly into the male pronucleus of the fertilized oocyte. The post-injection oocytes were cultured overnight, and implanted into pseudopregnant females.

5.3.3. Mouse husbandry and genotyping

5.3.3.1. Founder mice

Founder mice were generated by direct microinjection of expression constructs into fertilized oocytes, as described above. Unlike *in vitro* transfection of embryonic stem cells in the CKmt-OE model, this does not permit antibiotic selection or PCR screening for cells in which the transgene has integrated, and therefore is expected to yield a mixture of wild-type and transgenic (founder) mice. Tail tips were therefore obtained from all mice derived from microinjections, in order to identify those which could be bred to generate a transgenic line.

5.3.3.2. Genotyping protocols

5.3.3.2.1. *CK-M*

CK-M mice were genotyped using a pair of transgene-specific primers, binding at the final exon-exon junction (CKmb_ex7-8_F) and HA tag sequence (HA_R), respectively. The ROSA26 primers used for allelic

discrimination of homozygous CKmt mice (see section 4.3.3.1.2) were included as a quality control (note that, since the transgene in this model was not integrated at ROSA26, this PCR would be expected to produce the expected band in all samples, *i.e.,* both wild-type and transgenic). The expected product sizes were 209bp (Ckm transgene) and 508bp (ROSA26 control). PCR was performed using the standard TD_3x30 protocol, and $MgCl_2$ concentration was optimized empirically.

5.3.3.2.2. *CK-B*

CK-B mice were genotyped by a similar strategy to that used for CKmt mice in section 4.3.1.4.3, using a single pair of primers to amplify transgenic as well as endogenous (control) *Ckb*. Sense (CKb_ex3_F) and antisense (CKb_ex4_R) primers were designed to bind in exons 3 and 4 of *Ckb*, respectively. The presence or absence of an intervening intron was expected to generate products of two different sizes, namely 240bp for the wild-type allele, and 163bp for the transgenic allele. PCR was performed using the standard TD_3x30 protocol, and $MgCl_2$ concentration was optimized empirically.

5.3.3.3. Breeding transgenic mice

Tail tips were obtained by Transgenics Core staff for DNA extraction and genotyping of all litters from microinjection experiments, as described above.

5.3.3.3.1. *CK-M*

In the first round of CK-M microinjections, two potential founders were identified. These mice were named M_1 and M_2, and mated with wild-type C57BL/6 mice; however, neither of these mice was fertile, despite breeding for several months with different partners.

A second round of microinjections was performed, yielding 11 pups. The transgene was detected in two mice (18%), which were identified as founders M_3 and M_4. Transgene-specific PCR produced a relatively faint band in founder M_3, compared to M_4 (Figure 5-11). This could be due to a significantly higher number of

transgene copies in mouse M_4, and/or mosaicism in mouse M_3. An ear biopsy was additionally obtained from mouse M_3, and was negative for the transgene, suggesting that mosaicism was the most likely cause for this finding.

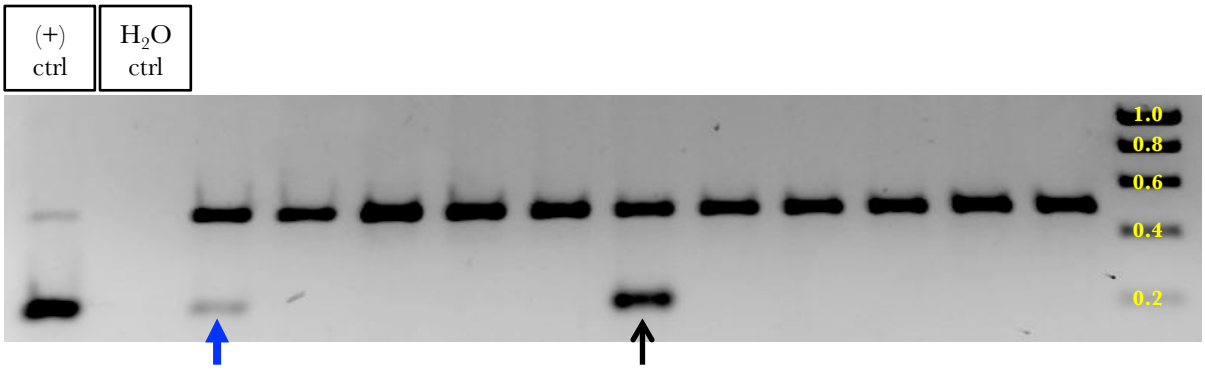


Figure 5-11: PCR genotyping of potential CK-M founders.

The transgene was detected in two mice, which were identified as founders M_3 and M_4. Note the difference in transgenic band intensity between M_3 (blue solid arrow) and M_4 (black arrow), despite comparable control bands.

Founders M_3 and M_4 were bred with wild-type C57BL/6 mates; both were fertile, but only M_4 produced transgenic offspring (41 pups were screened from founder M_3, and no transgenics were identified).

5.3.3.3.2. *CK-B*

In the first round of microinjections, three potential founders were identified. These mice were named B_1, B_2 and B_3, and mated with wild-type C57BL/6 mice. Founders B_1 and B_2 were fertile, but did not produce any transgenic offspring (41 and 60 pups were screened, respectively). Founder B_3 failed to produce any offspring, despite breeding for over 4 months with two different females.

A second round of microinjections was performed to generate additional founders. One out of six (17%) mice was positive for the transgene (Figure 5-12), and was identified as founder B_4. A third round of microinjections yielded a further potential founder, B_5. Founders B_4 and B_5 were bred with wild-type C57BL/6 mates, and both produced transgenic offspring.

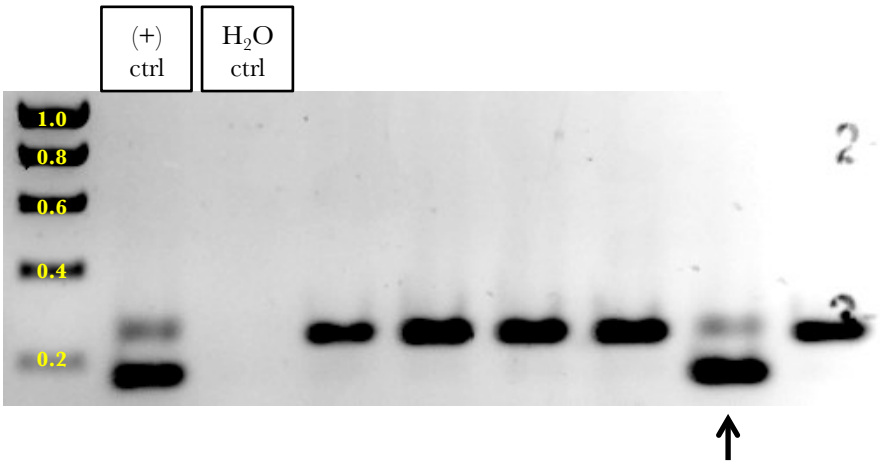


Figure 5-12: PCR genotyping of potential CK-B founders.

The transgene-specific band (163bp) was detected in a single mouse (arrow), subsequently named B_4. The control (wild-type *Ckb*) band was produced in all samples.

5.3.3.4. Determination of transgene copy number by qPCR

Since both CK-B and CK-M mice were generated by random integration of microinjected DNA, it was necessary to determine the number of transgene copies present in each individual founder line. The copy number qPCR protocol initially developed for allelic discrimination in CKmt mice was adapted for this purpose.

Unlike the CKmt mice, which were expected to carry either 0, 1, or 2 copies of the transgene due to targeted integration at ROSA26, there was no *a priori* indication of the number of copies in the CK-B and CK-M lines. As a result, a transgene-specific qPCR would only allow for determination of the relative copy number between transgenic lines, but not evaluation of the absolute number of transgene copies. Therefore, unlike the CKmt allelic discrimination qPCR, reactions were designed to amplify both the endogenous and transgenic allele, allowing wild-type mice to be used as a calibrator (n = 2 copies). Transgene-specific reactions were performed in parallel, to validate results.

5.3.3.4.1. *CK-M*

Transgene copy number qPCR was initially performed in CK-M mice, as in addition to the wild-type mice (n = 2 copies), our group maintains a line of CK-M knockout mice, which could be used as additional controls for calibration purposes. Briefly, the CK-M knockout was originally generated by recombinase-mediated exchange of a hygromycin resistance cassette into the genomic sequence, replacing a 212bp fragment including exon 2 of the coding sequence and portions of the adjacent introns[121,250]. This region was selected as a target for qPCR, as primers binding within the deleted fragment would not amplify the KO allele. Since it was necessary for the primers to amplify both wild-type gDNA and transgenic cDNA, the intronic fragments could not be used. Primers were therefore designed to bind in the 3' region of exon 2 (CKm_ex2_F and CKm_ex2_R), with a predicted amplicon size of 120bp.

qPCR was performed as described in section 4.3.3.1.1. Results were normalized to the copy number of *Apob*, and calibrated relative to a known wild-type (n = 2 copies). Control samples returned the expected results for knockout (n=2; no amplification), heterozygous (n=2; mean, 1.1; range, 0.9-1.2), and wild-type (n=5; mean, 2.0; range, 1.8-2.1) mice. Surprisingly, given that all CK-M mice were derived from the same founder, three distinct clusters of results were observed, and groups were named according to the number of transgene copies present. Group M-2 was the most common (n=20), with a mean of 3.8 copies and a range of 2.8-4.7. The remaining mice were allocated to group M-6 (n=5; mean, 7.8; range, 7.0-8.3) and group M-8 (n=3; mean, 10.0; range, 9.9-11.0). Results are summarized in Figure 5-13.

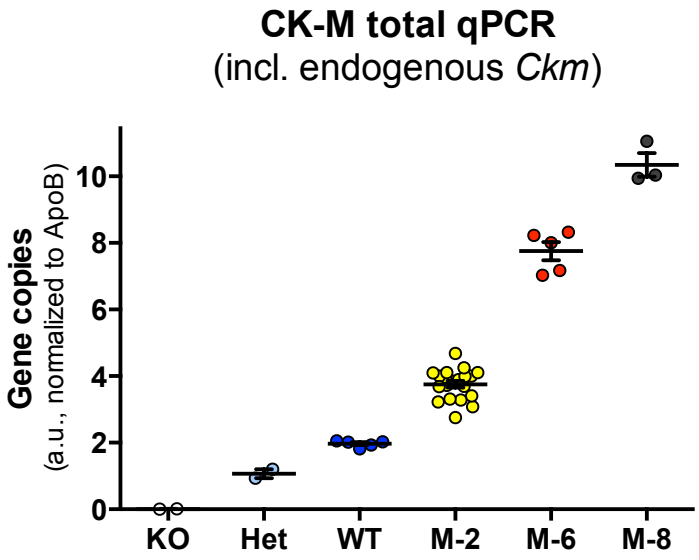


Figure 5-13: Results of total copy number qPCR in CK-M mice.

Transgenic mice have been grouped according to results, into groups with means of 3.8 (M-2, yellow), 7.8 (M-6, red) and 10.0 (M-8, brown), respectively. KO, knockout (0 copies of *Ckm*). Het, heterozygote (1 copy). WT, wild-type (2 copies). Bars represent mean ± SEM.

In order to validate these results, transgene-specific qPCR was performed using the CK-M genotyping primers (CKmb_ex7-8_F and HA_R). Transgenic DNA was not detected in knockout, heterozygote, or wild-type mice, as expected. In the absence of a calibrator of known transgene copy number, results were calibrated to a randomly selected sample from group M-2, which was assigned a value of 2 based on the results of total copy qPCR (4 total copies – 2 endogenous copies = 2 transgene copies). Transgenic mice were grouped according to the results of the total copy qPCR, and a similar distinction was noted between groups M-2 (mean, 1.9; range, 1.4-2.7), M-6 (mean, 6.0; range, 5.3-6.4), and M-8 (mean, 7.8; range, 7.3-8.3). A linear correlation was observed between results of total copy and transgene-specific qPCR (r^2=0.9697, Figure 5-14).

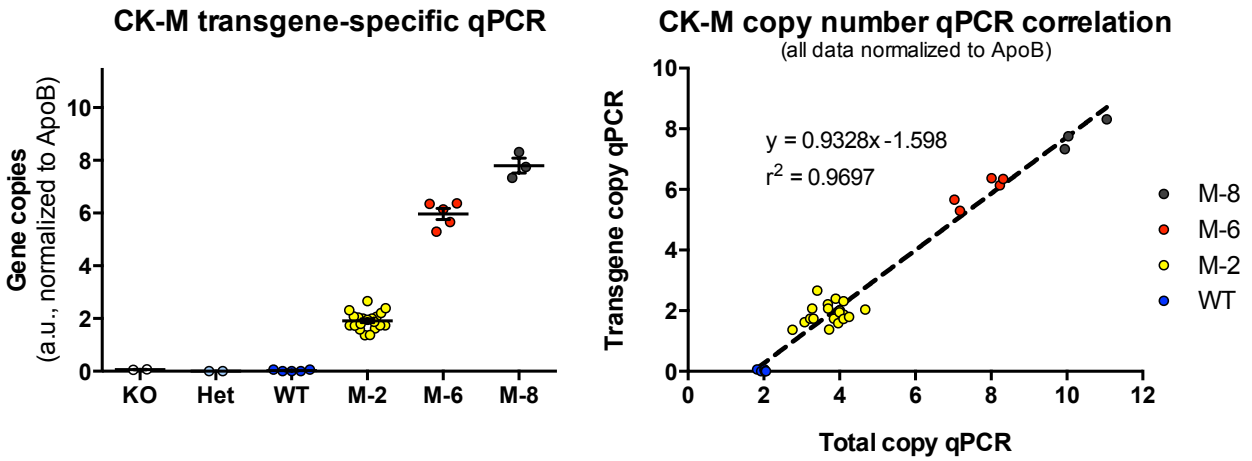


Figure 5-14: Results of transgene copy number qPCR in CK-M mice.

Left: Transgene copy number, by group. Bars represent mean ± SEM. **Right:** Comparison of results of total and transgenic copy number qPCR. A linear correlation is present, confirming that the results of both reactions can be directly compared. Knockout (KO) and heterozygous (Het) mice have been excluded from this graph, as they differ from all other groups with respect to endogenous *Ckm* copy number, and would therefore skew the results.

Overall, the results qPCR in CK-M mice suggest that there are three distinct groups, with respective transgene copy numbers of 2, 6, and 8 (Table 5-2). Since the mice are all derived from a single founder, this suggests that two distinct integration events have taken place, with different copy numbers. This hypothesis is addressed in detail in the section on FISH experiments (5.3.3.5) and discussion (5.4.3).

Group	n	Ckm copies			Estimated transgene copies
		Total	Total (adjusted)	Transgene	
KO	2	0.0	-	-	**-**
Het	2	1.1	-	-	**-**
WT	5	2.0	-	-	**-**
M-2	20	3.8	1.8	1.9	**2**
M-6	5	7.8	5.8	6.0	**6**
M-8	3	10.0	8.0	7.8	**8**

Table 5-2: Summary of CK-M copy number qPCR results.

The "Total (adjusted)" column represents the result of total copy qPCR, adjusted for the presence of two endogenous copies of *Ckm*. Transgenic groups were (retrospectively) named according to the number of transgene copies present.

5.3.3.4.2. *CK-B*

CK-B copy number qPCR was designed using an analogous protocol. Identification of specific primers was complicated by the presence of three pseudogenes in the mouse genome, with near-identical sequences[251]. Pseudogenes 2 and 3 span the entire length of the *Ckb* coding sequence, with homologies of 89% and 90%, respectively; however, pseudogene 2 is not thought to be present in C57BL/6[251]. Pseudogene 1 has a 3' deletion, and therefore the corresponding region was targeted to reduce the number of off-target binding sites. Despite extensive optimization, no primer pairs were found to be specific to the functional *Ckb* gene, without binding to pseudogene 3; therefore, primers were designed to intentionally amplify *Ckb* as well as pseudogene 3. Results were adjusted accordingly prior to analysis, by assigning wild-type calibrators a value of 4, rather than 2 (since a total of 4 loci were being amplified: two copies of each of *Ckb* and pseudogene 3), and subtracting 2 from the final result in all samples (to exclude the two copies of pseudogene 3).

Since our group does not have any CK-B knockout mice which could be used as controls, only wild-type mice could be used as a reference. For total copy qPCR, a single wild-type sample was arbitrarily selected as a calibrator. Mean copy number in wild-type mice was found to be 2.1 (range, 1.7-2.7).

The CK-B mice were derived from two different founders (B_4 and B_5), and were therefore considered as two distinct groups for analysis. Mice derived from founder B_4 had a mean of 5.4 copies of *Ckb* (range, 4.8-6.2), while offspring of founder B_5 had a mean of 4.0 copies (range, 2.8-5.1). A single mouse from founder B_4 (#4541) was found to have a significantly higher copy number (33.6 ± 2.9), and was therefore initially analyzed as its own group (Figure 5-15).

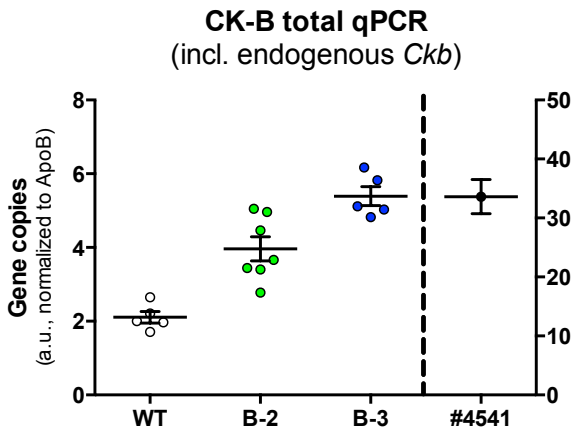


Figure 5-15: Results of total copy number qPCR in CK-B mice.

Bars represent mean ± SEM.

Transgene-specific qPCR was performed using the same primers as in the CK-M line (CKmb_ex7-8_F and HA_R). Based on the results of total copy qPCR, mice from founder B_5 were considered to have 2 copies of the transgene, and a single mouse was randomly selected as a calibrator. Mean transgene copy number was 1.5-fold higher in mice from founder B_4 (mean, 3.0; range, 2.8-3.4) than mice from B_5 (mean, 2.0; range, 1.9-2.3), and was undetectable in wild-type mice (Figure 5-16). Mouse #4541 remained a notable outlier, with 38.5 ± 3.1 copies of the transgene. There was a linear correlation between the results of total copy and transgene-specific qPCR (r^2=0.9921).

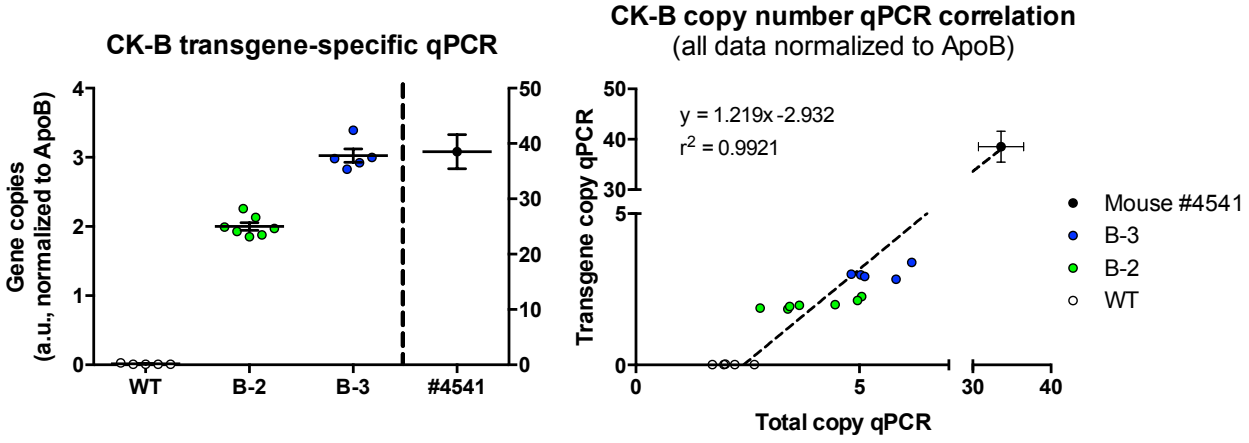


Figure 5-16: Results of transgene copy number qPCR in CK-B mice.

Left: Transgene copy number, by group. Bars represent mean ± SEM. **Right:** Comparison of results of total and transgenic copy number qPCR. Note that both axes are divided to allow for inclusion of mouse #4541 (error bars of #4541 represent SEM; error bars of other groups are omitted for clarity).

Overall, the results of qPCR in CK-B mice suggest that the lines derived from founders B_4 and B_5 have 3 and 2 copies of the transgene, respectively (Table 5-3). The single outlier from founder B_4, mouse #4541, was estimated to carry approximately 35 copies of the transgene, although there is a degree of uncertainty about the precise number, since total copy and transgene-specific reactions returned values of 31.6 and 38.5, respectively. Therefore, transgene copy number qPCR was repeated in offspring of mouse #4541 (using additional mice from group B-2 as calibrators), and their copy number was found to be ~30 (Figure 5-17).

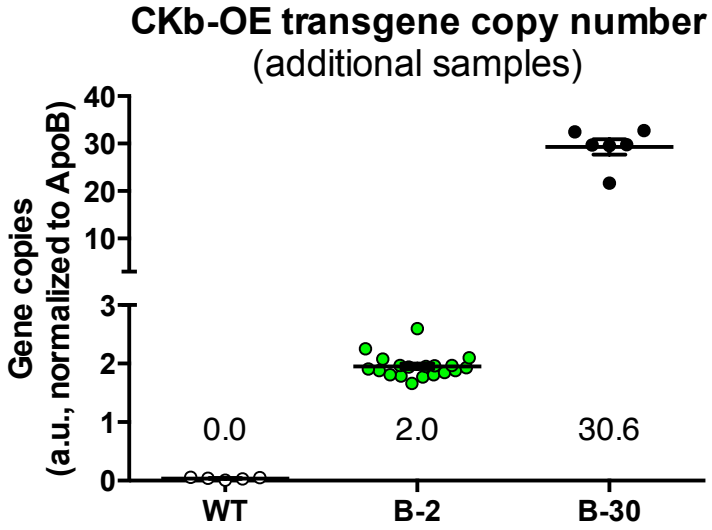


Figure 5-17: Results of total copy number qPCR in CK-B mice derived from mouse #4541.

Group	n	Ckb copies			Estimated transgene copies
		Total	Total (adjusted)	Transgene	
WT	5	2.1	-	-	**-**
B-2	7	4.0	2.0	2.0	**2**
B-3	5	5.4	3.4	3.0	**3**
Mouse #4541	1	33.6	31.6	38.5	**~35**
B-30	7	-	-	30.6	**~30**

Table 5-3: Summary of CK-B copy number qPCR results.

The "Total (adjusted)" column represents the result of total copy qPCR, adjusted for the presence of two endogenous copies of *Ckb*. Total copy number PCR was not performed in second-generation mice (B-30).

5.3.3.5. Visualization of transgene integration sites in CK-M mice by FISH

The results of copy number qPCR suggested that two separate transgene integration sites are present in CK-M mice derived from founder M_4. Fluorescence *in-situ* hybridization (FISH) assays were conducted to test this hypothesis. These experiments were conducted by Dr. Daniela Moralli, using fibroblasts cultured from ear biopsies from mice with 0, 2, 6, or 8 transgene copies, as determined by qPCR. The full alphaMHC_L-CKmHA vector was used as a probe in initial experiments, but was found to produce a strong signal on chromosome 14, most likely corresponding to the endogenous *MYH6* (αMHC) gene. An additional signal was observed in individual metaphases, and was thought to be located in chromosome 12. Therefore, samples were re-probed using digested transgenic vector backbone, without the αMHC promoter, and co-stained using bacterial artificial chromosome (BAC) probes against chromosomes 12 and 14. These experiments confirmed that two distinct chromosomal integration events had taken place in the original CK-M founder (Figure 5-18), and therefore two separate transgenic lines could be generated from these mice.

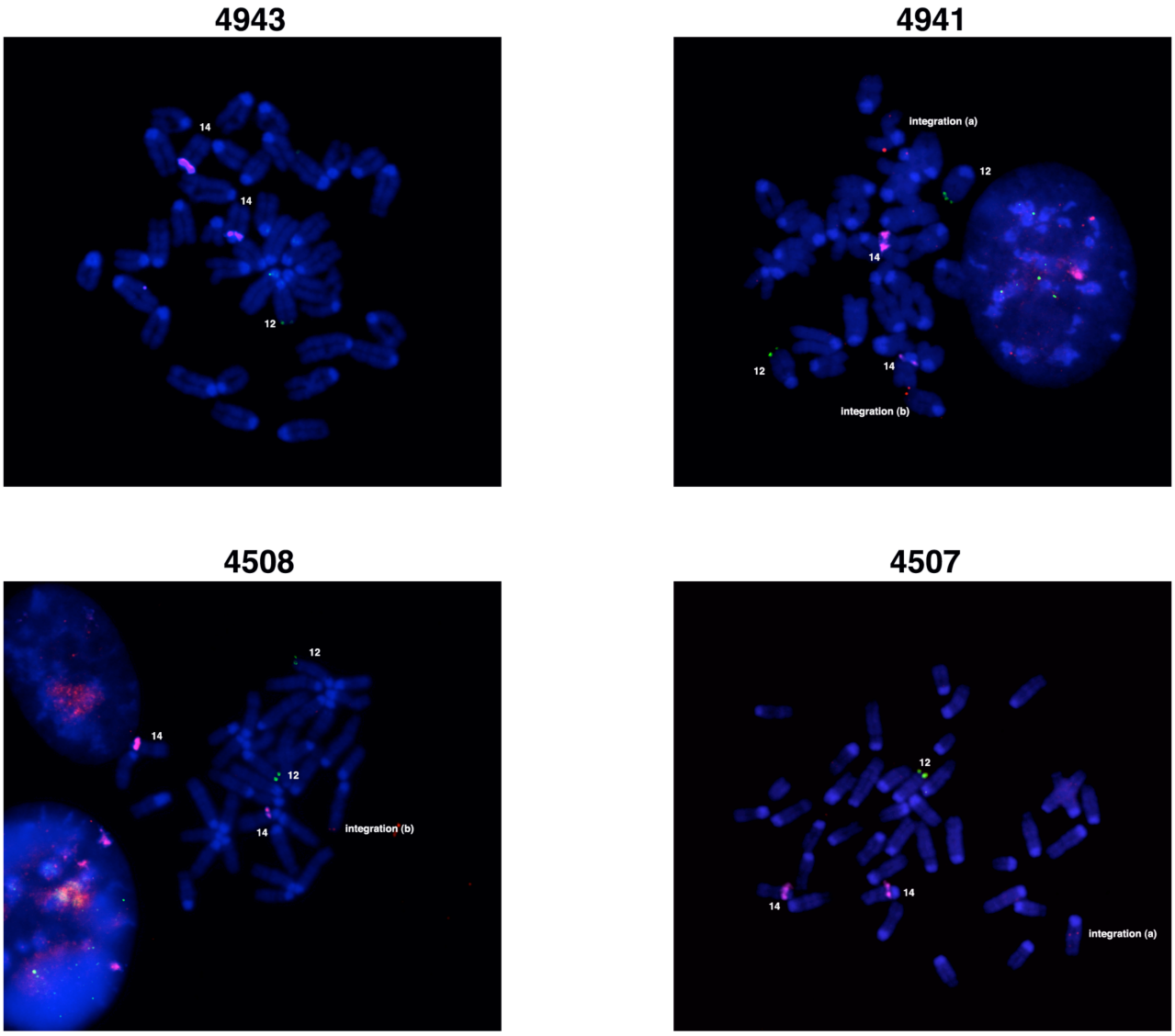


Figure 5-18: FISH assay in CKm-OE mice.

FISH experiments were performed in mice derived from the same founder, but with different transgene copy numbers as determined by qPCR: 0 (mouse #4943), 2 (#4508), 6 (#4507), or 8 (#4941). FISH probes were used to detect chromosome 14 (red), chromosome 12 (green), and the transgenic vector backbone (purple). These representative images demonstrate that two distinct integration events have taken place – a mid-arm site in mouse #4507 (A), and a subtelomeric site (B) in mouse #4508; significantly, both sites are present in mouse #4941, which has an estimated 8 transgene copies. While this does not pinpoint the precise genomic location of the insertion sites, the fact that two sites have been identified confirms that mice with 2 or 6 copies of the transgene can be bred as independent lines, if required.

5.3.3.6. Breeding strategy

5.3.3.6.1. *CK-M*

Based on the results of copy number qPCR, a hypothesis was made that CK-M mice carry two distinct integration sites, with 2 and 6 copies of the transgene; this was subsequently confirmed by FISH. Mice with 2 or 6 copies are currently being bred with wild-type mice, in an attempt to generate independent lines for each integration event. The current breeding statistics indicate that transgenic status does not seem to be affecting viability in either line, as an approximately Mendelian ratio of transgenic pups (59%) has been generated from the second generation onwards (Table 5-4).

	M-2	**M-6**	**Total**
Total pups	60	96	**156**
Transgenics	37	55	**92**
% Tg	62%	57%	**59%**

Table 5-4: Breeding statistics for CKm-OE mice.

5.3.3.6.2. *CK-B*

Transgenic mice are currently being bred for all three CK-B lines (2, 3, 30 copies). Breeding statistics indicate that transgenic status does not seem to be affecting viability in any line, as an approximately Mendelian ratio of transgenic pups (48%) has been generated from the second generation onwards (Table 5-5).

	B-2	**B-3**	**B-30**	**Total**
Total pups	59	50	57	**166**
Transgenics	31	22	27	**80**
% Tg	53%	44%	47%	**48%**

Table 5-5: Breeding statistics for CKb-OE mice.

5.3.4. Validation of the models

5.3.4.1. mRNA expression by qRT-PCR

5.3.4.1.1. *Methods and primer design*

Expression of *Ckm* and *Ckb* mRNA was assessed by qRT-PCR, using a similar protocol to that originally developed for CKmt-overexpressing mice. Specific primer pairs were designed to quantify transgenic, endogenous, and total mRNA expression for both lines. Due to the significant homology between the *Ckm* and *Ckb* coding sequences, the same sense primer was used for detection of transgenic and endogenous mRNA in both lines (CKmb_ex7-8_F). To specifically amplify transgenic mRNA, this primer was paired with the HA_R primer in both lines; for endogenous mRNA, antisense primers were designed to bind in the 3'-UTRs of each endogenous transcript (CKm_UTR_R and CKb_UTR_R, respectively). For total mRNA expression, pairs of primers spanning at least one exon-exon junction were designed for each line (CKm_ex5_F x CKm_ex6-5_R and CKb_ex6-7_F x CKb_ex8-7_R, respectively).

All results were normalized to expression of the reference gene *Polr2a*, as described in the chapter on CKmt-overexpressing mice.

5.3.4.1.2. *Quantification of transgenic, endogenous, and total mRNA transcripts in left ventricular tissue (CKm-OE)*

RNA was extracted from left ventricular tissue of wild-type mice (n=11) and CKm-OE mice from groups A (n=9), B (n=5), and C (n=3). Transgenic mRNA was absent in wild-types, but detectable in groups M-2 (mean ± SEM, 0.47 ± 0.25), M-6 (1.19 ± 0.53), and M-8 (1.46 ± 0.20). Transgenic mRNA expression increased with transgene copy number, and was significantly higher in transgenic groups M-6 and M-8, compared to group M-2 (Figure 5-19). The ratio of mRNA expression to transgene copy number was 0.24, 0.20, and 0.18, respectively, suggesting a linear relationship between copy number and mRNA expression.

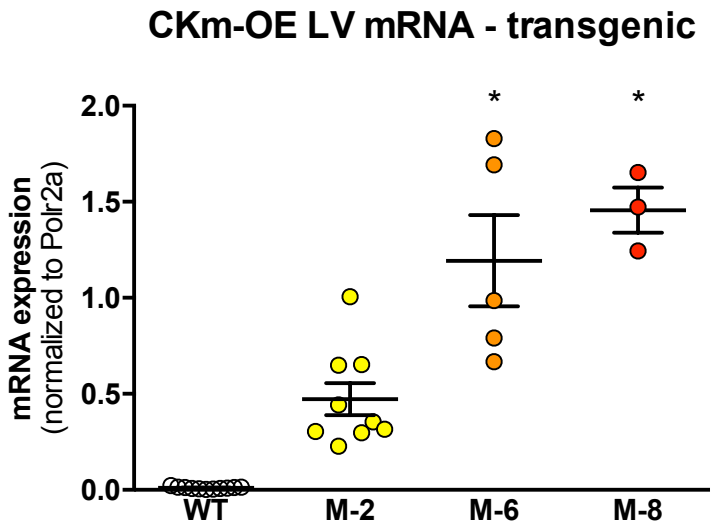


Figure 5-19: Transgenic mRNA expression in CKm-OE mice.

Results were analyzed by Kruskal-Wallis test with Dunn's multiple comparison test. Transgenic mRNA was not detected in wild-type samples. * denotes a significant difference compared to M-2.

Total *Ckm* mRNA expression was 0.36 ± 0.05 in wild-types, 0.50 ± 0.07 in group M-2, 1.40 ± 0.20 in group M-6, and 1.93 ± 0.40 in group M-8. As was the case for transgenic mRNA, expression was significantly higher in transgenic groups M-6 and M-8, compared to group M-2 (Figure 5-20).

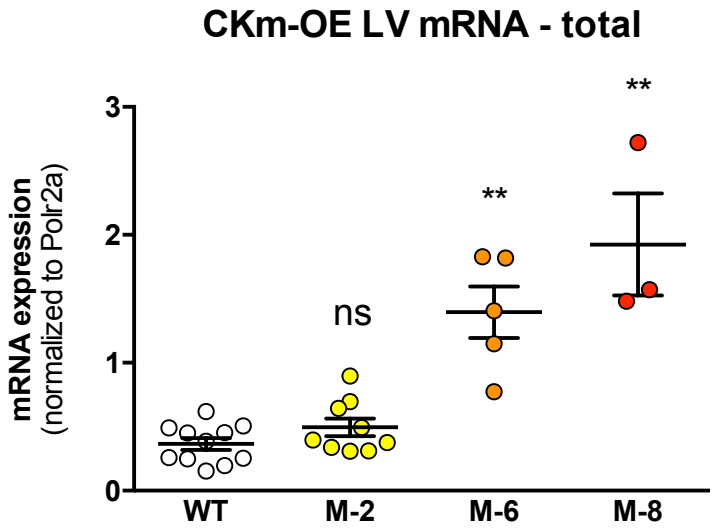


Figure 5-20: Total mRNA expression in CKm-OE mice.

Results were analyzed by Kruskal-Wallis test with Dunn's multiple comparison test. * denotes a significant difference compared to wild-type; ns, no significant difference compared to wild-type. There was no significant difference between transgenic groups.

Endogenous *Ckm* mRNA expression (Figure 5-21) was not significantly different in wild-types (0.82 ± 0.09) and transgenic groups M-2 (1.13 ± 0.10), M-6 (1.08 ± 0.18), and M-8 (1.29 ± 0.10).

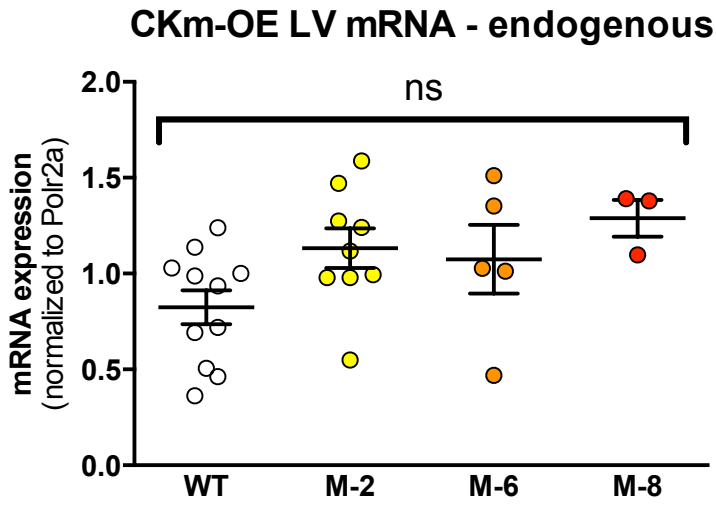


Figure 5-21: Endogenous mRNA expression in CKm-OE mice.

Results were analyzed by Kruskal-Wallis test with Dunn's multiple comparison test. There was no significant difference between groups.

5.3.4.1.3. *Quantification of transgenic, endogenous, and total mRNA transcripts in left ventricular tissue (CKb-OE)*

RNA was extracted from left ventricular tissue of wild-type mice (n=10) and CKb-OE mice from groups B-2 (n=5) and B-3 (n=4). Transgenic mRNA expression (Figure 5-22) was absent in wild-types, but detectable in groups B-2 (1.19 ± 0.11) and B-3 (1.24 ± 0.25).

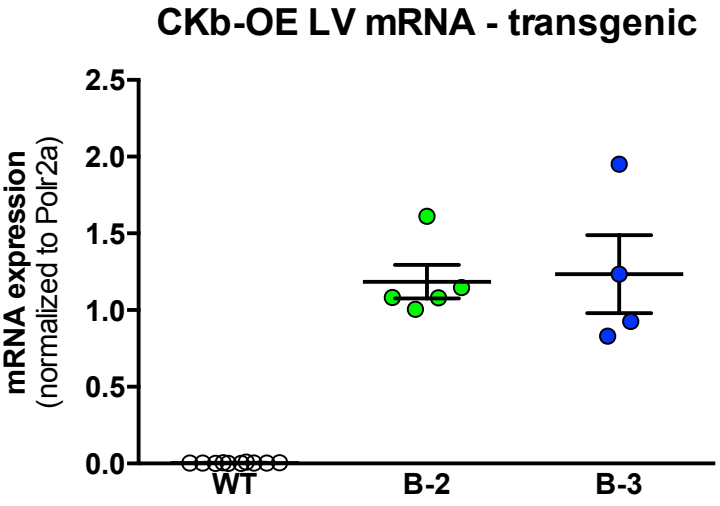


Figure 5-22: Transgenic mRNA expression in CKb-OE mice.

Results were analyzed by Kruskal-Wallis test with Dunn's multiple comparison test. There was no significant difference between transgenic groups.

Total *Ckb* mRNA expression was 0.02 ± 0.00 in wild-types, compared to 0.63 ± 0.15 in group B-2 and 0.83 ± 0.38 in group B-3 (Figure 5-23). There was no significant difference between transgenic groups.

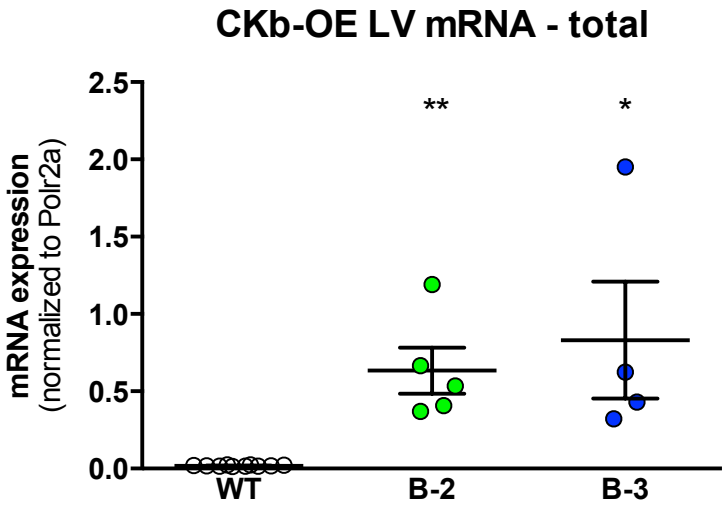


Figure 5-23: Total mRNA expression in CKb-OE mice.

Results were analyzed by Kruskal-Wallis test with Dunn's multiple comparison test. * denotes a significant difference compared to wild-type. There was no significant difference between transgenic groups.

There were no significant differences in endogenous *Ckb* mRNA expression (Figure 5-24) between wild-types (0.55 ± 0.05) and transgenic groups B-2 (0.76 ± 0.20) and B-3 (0.49 ± 0.04).

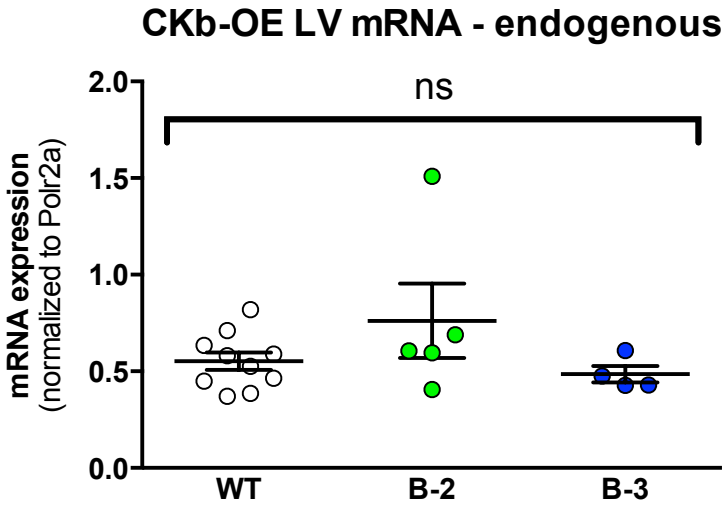


Figure 5-24: Endogenous mRNA expression in CKb-OE mice.

Results were analyzed by Kruskal-Wallis test with Dunn's multiple comparison test. There was no significant difference between groups.

5.3.4.1.4. *Tissue specificity of transgenic mRNA expression*

Tissue specificity of transgene expression was assessed by performing transgene-specific qRT-PCR in a panel of organs. In CK-M mice, the transgene was detected in all four cardiac chambers, but not in non-cardiac tissues (Figure 5-25).

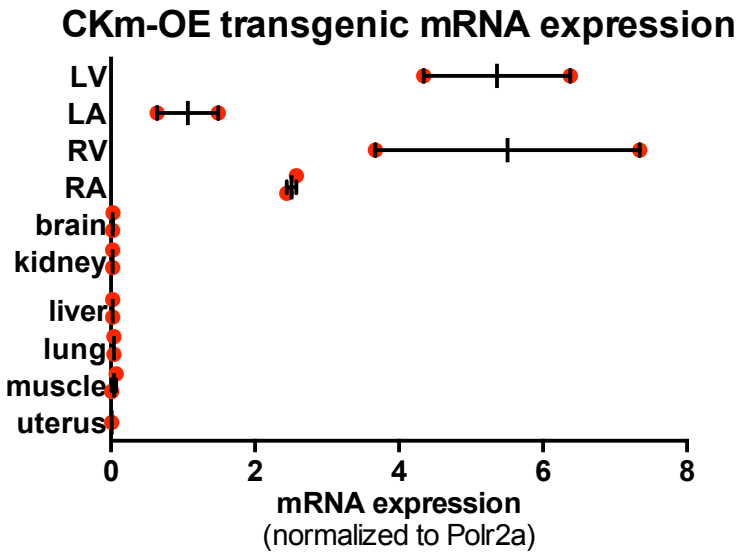


Figure 5-25: Tissue-specificity of transgenic mRNA expression in CK-M mice.

5.3.4.2. Protein expression by western blot

Protein was extracted from homogenized left ventricular tissue. Expression of transgenic protein was confirmed using an anti-HA antibody to specifically detect HA-tagged proteins. In CK-M mice, additional membranes were probed with an anti-CK-M antibody to quantify total protein expression. Similar experiments in CK-B mice were unsuccessful, despite optimization of antibody concentrations.

5.3.4.2.1. *Protein expression in CK-M mice*

Staining with an anti-HA antibody confirmed the presence of an HA-tagged protein of the expected size in CK-M mice with 2, 6, and 8 copies of the transgene (Figure 5-26). In agreement with the qPCR results described above, the transgenic protein band was noticeably more intense in lysates from mice with 6 or 8 copies, suggesting that transgene expression in these mice was higher than in mice with 2 copies.

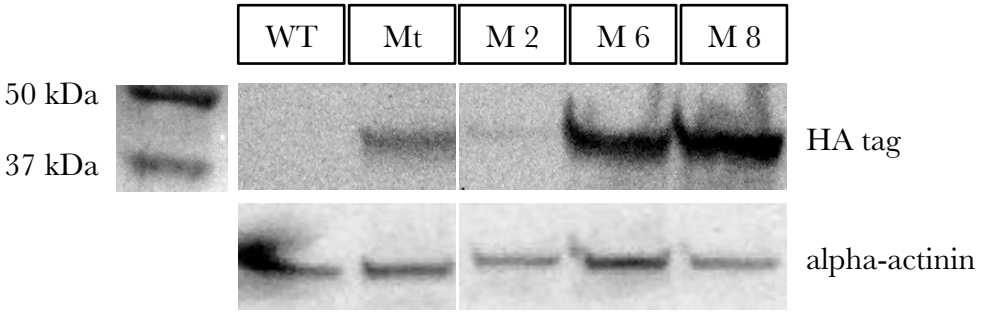


Figure 5-26: Representative western blot in CK-M mice.

Membranes were probed using an anti-HA antibody, and alpha-actinin was used as a protein loading control. WT, wild-type (negative control). Mt, CKmt-OE lysate (HA-positive control). M2-8, CKm-OE lysates with corresponding number of transgene copies.

In order to determine whether expression of transgenic protein was associated with a significant increase in total CK-M protein, additional membranes were probed using an anti-CK-M antibody (Figure 5-27). Mean CK-M expression, normalized to alpha-actinin, was >3-fold higher in lysates from mice with 6 or 8 transgene copies than in wild-type controls. These results are currently based on n=2 per transgenic group, and should therefore be confirmed in additional experiments.

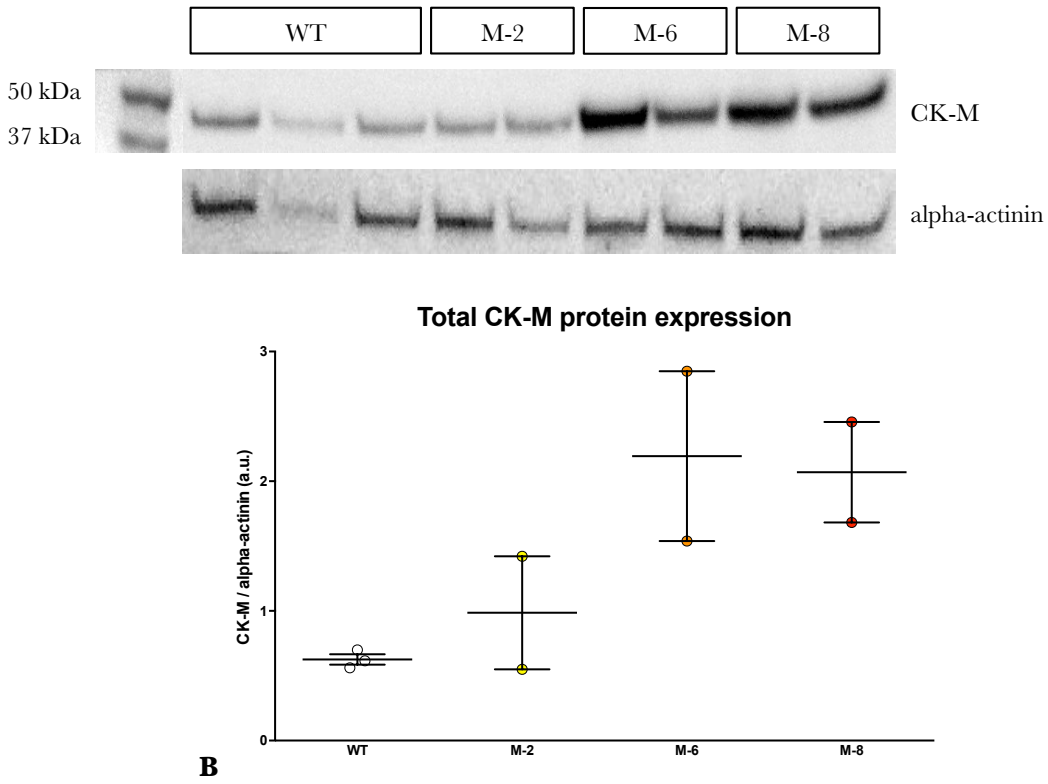


Figure 5-27: Total CK-M protein expression in CKm-OE mice.

(**A**) Western blot results. Numbers above the blot correspond to transgene copy number for each sample. (**B**) Quantification of CK-M protein expression, normalized to alpha-actinin. Results were analyzed by Kruskal-Wallis test with Dunn's multiple comparison test. There was no significant difference between groups.

5.3.4.2.2. *Protein expression in CK-B mice*

Staining with an anti-HA antibody confirmed the presence of an HA-tagged protein of the expected size in CK-B mice with 2 and 3 copies of the transgene (Figure 5-28).

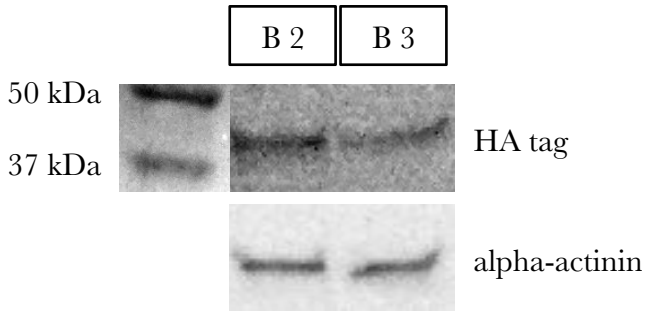


Figure 5-28: Representative western blot in CK-B mice.

Membranes were probed using an anti-HA antibody, and alpha-actinin was used as a protein loading control. B-2/3, CKb-OE lysates with corresponding number of transgene copies. This figure was adapted from the same membrane as the CK-M blot in Figure 5-27, and the controls (wild-type and CKmt-OE lysate) are not shown.

Despite attempts at optimization of antibody concentrations, staining for total CK-B was unsuccessful. This may be due to the relatively low level of CK-B expression in the myocardium; however, since the anti-HA antibody detects the expected band in transgenic samples, an equally sensitive anti-CK-B antibody would be expected to detect the same band. Therefore, further experiments will be conducted using alternative antibodies to establish a reliable protocol for quantification of total CK-B protein expression.

5.3.4.3. Enzymatic activity

5.3.4.3.1. *Total creatine kinase activity and relative activities of isoenzymes (CKm-OE)*

Creatine kinase activity was assayed in left ventricular tissue from wild-type (n=10) and CKm-OE mice (group M-2, n=9; group M-6, n=6; group M-8, n=3). Total CK activity was significantly higher in groups

M-6 and M-8 (WT, 3.93 ± 0.32 IU / mg protein; group M-2, 3.53 ± 0.24; group M-6, 9.10 ± 0.61; group M-8, 9.54 ± 0.81). Analysis of individual isoenzyme activities confirmed that the difference was driven by an increase in CK-MM activity (WT, 2.47 ± 0.15 IU / mg protein; group M-2, 2.47 ± 0.15; group M-6, 7.11 ± 0.40; group M-8, 7.64 ± 0.75). CK-MB activity was also significantly increased in group M-8 (WT, 0.16 ± 0.02 IU / mg protein; group M-2, 0.13 ± 0.01; group M-6, 0.23 ± 0.03; group M-8, 0.32 ± 0.09). There were no significant differences in activities of the CKmt and CK-BB isoenzymes (Figure 5-29).

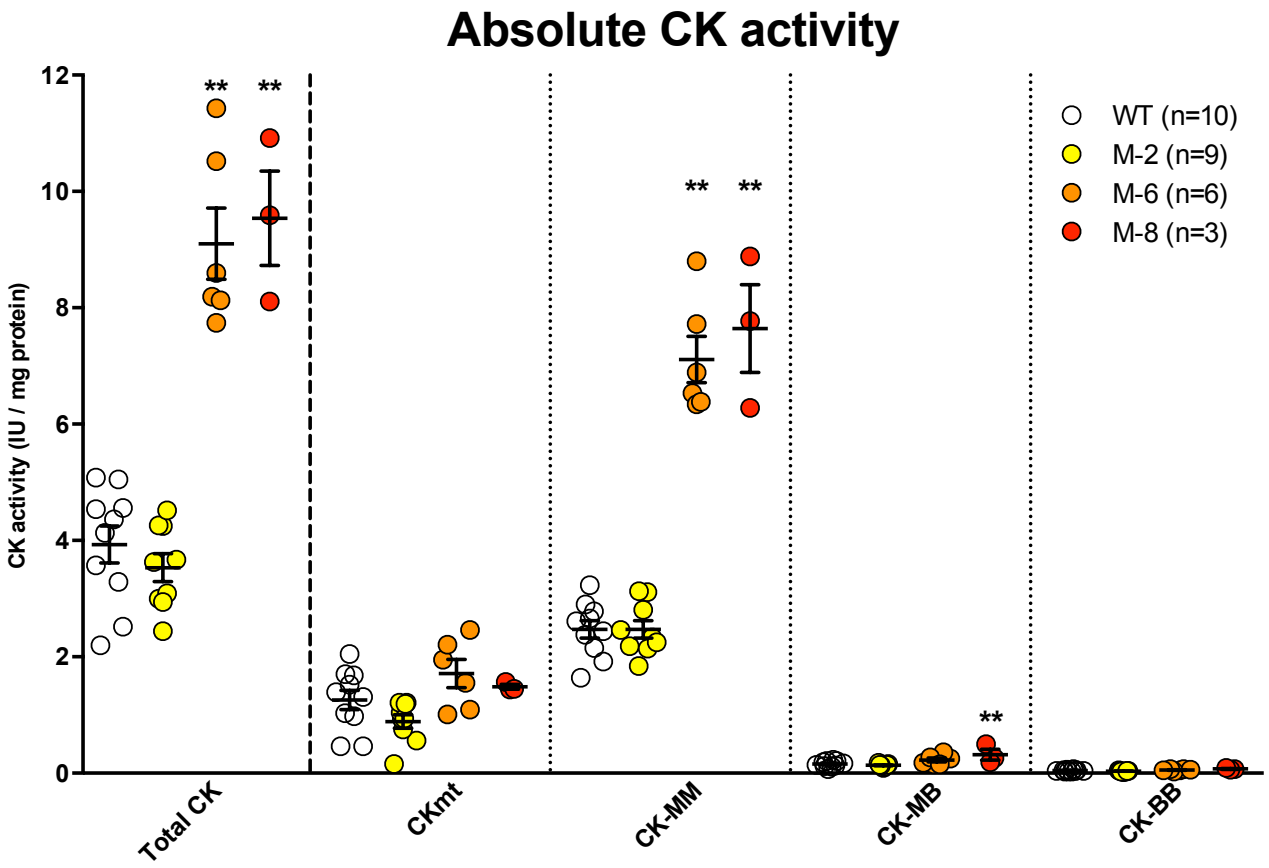


Figure 5-29: Creatine kinase activity in CKm-OE mice.

Results were analyzed by Kruskal-Wallis test with Dunn's multiple comparison test. ** denotes a significant difference compared to wild-type.

Neither total CK nor CK-MM activity were increased in group M-2, relative to wild-type mice. Since there was a degree of variability in absolute CK activity within groups, relative activities of CK-MM were compared (expressed as a percentage of total CK; Figure 5-30). CK-MM activity in group M-2 was not

significantly increased (WT, 64.3 ± 2.2%; group M-2, 70.7 ± 2.7%; group M-6, 77.4 ± 1.7%; group M-8, 80.0 ± 1.2%).

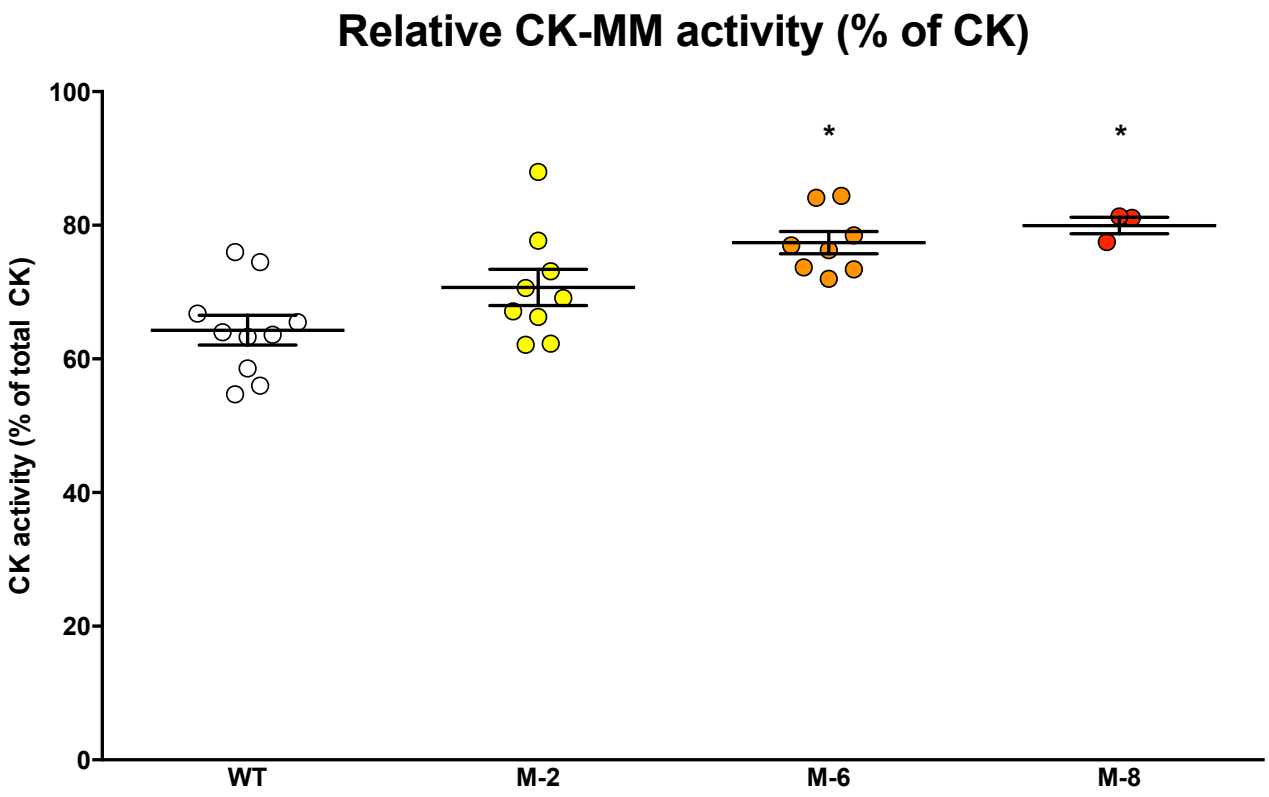


Figure 5-30: Relative activity of creatine kinase MM in CKm-OE mice.

Results were analyzed by Kruskal-Wallis test with Dunn's multiple comparison test. * denotes a significant difference compared to wild-type.

5.3.4.3.2. *Total creatine kinase activity and relative activities of isoenzymes (CKb-OE)*

Creatine kinase activity was assayed in left ventricular tissue from wild-type (n=7) and CKb-OE mice (group B-2, n=5; group B-3, n=4; group B-30, n=5; Figure 5-31). Total CK activity was not significantly higher in transgenic mice (WT, 3.39 ± 0.44 IU / mg protein; group B-2, 2.87 ± 0.52; group B-3, 3.29 ± 0.70; group B-30, 5.41 ± 0.57). Group B-30 had significantly higher activity of both CK-BB (WT, 0.04 ± 0.00 IU / mg protein; group B-2, 0.04 ± 0.01; group B-3, 0.04 ± 0.01; group B-30, 0.32 ± 0.03) and CK-MB (WT, 0.15 ± 0.02 IU / mg protein; group B-2, 0.25 ± 0.03; group B-3, 0.25 ± 0.05; group B-30, 1.51 ± 0.18).

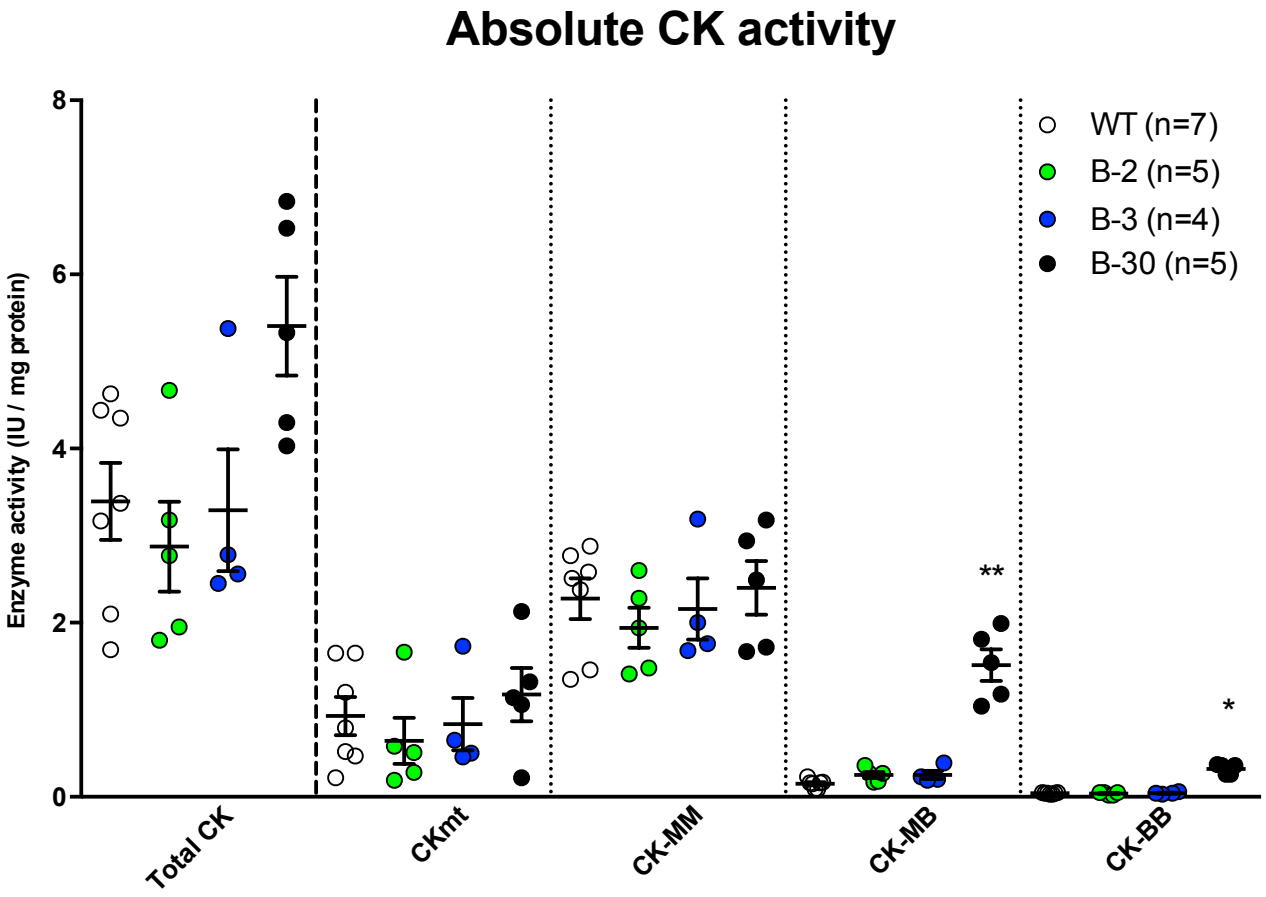


Figure 5-31: Creatine kinase activity in CKb-OE mice.

Results were analyzed by Kruskal-Wallis test with Dunn's multiple comparison test. * denotes a significant difference compared to wild-type.

When relative CK isoenzyme activities were analyzed (Figure 5-32), group B-30 had significantly higher activities of CK-BB (WT, 1.3 ± 0.2%; group B-2, 1.4 ± 0.2%; group B-3, 1.5 ± 0.3%; group B-30, 5.7 ± 0.4%) and CK-MB (WT, 4.6 ± 0.2%; group B-2, 9.0 ± 0.4%; group B-3, 7.8 ± 0.3% group B-30, 27.2 ± 1.6%). There were no significant increases in groups B-2 and B-3.

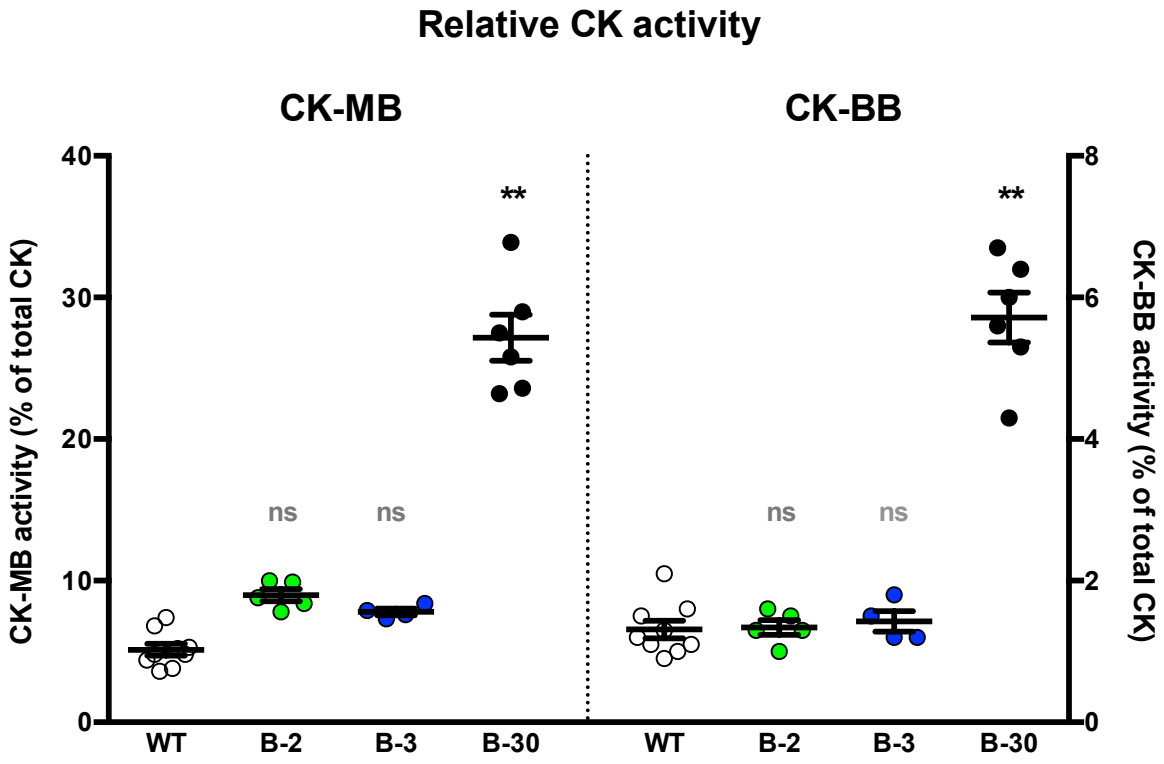


Figure 5-32: Creatine kinase MB and BB activity in CKb-OE mice, expressed as a percentage of total CK activity.

Results were analyzed by Kruskal-Wallis test with Dunn's multiple comparison test. ** denotes a significant difference compared to wild-type. ns, no significant difference compared to wild-type.

5.3.4.4. Citrate synthase activity as a marker of mitochondrial volume

Since previous studies in knockout models, as well as the CKmt-OE mice described in Chapter 4, have demonstrated that changes in CK activity can lead to compensatory adjustments in mitochondrial biogenesis, citrate synthase activity was measured in left ventricular tissue as a marker of mitochondrial volume (Figure 5-33). No significant differences were observed in CKm-OE mice (WT, 0.88 ± 0.06 IU / mg protein; group M-2, 0.89 ± 0.05; group M-6, 0.88 ± 0.00; group M-8, 0.98 ± 0.03) or CKb-OE mice from groups B-2 and B-3 (WT, 0.75 ± 0.07 IU / mg protein; group B-2, 0.68 ± 0.07; group B-3, 0.75 ± 0.09).

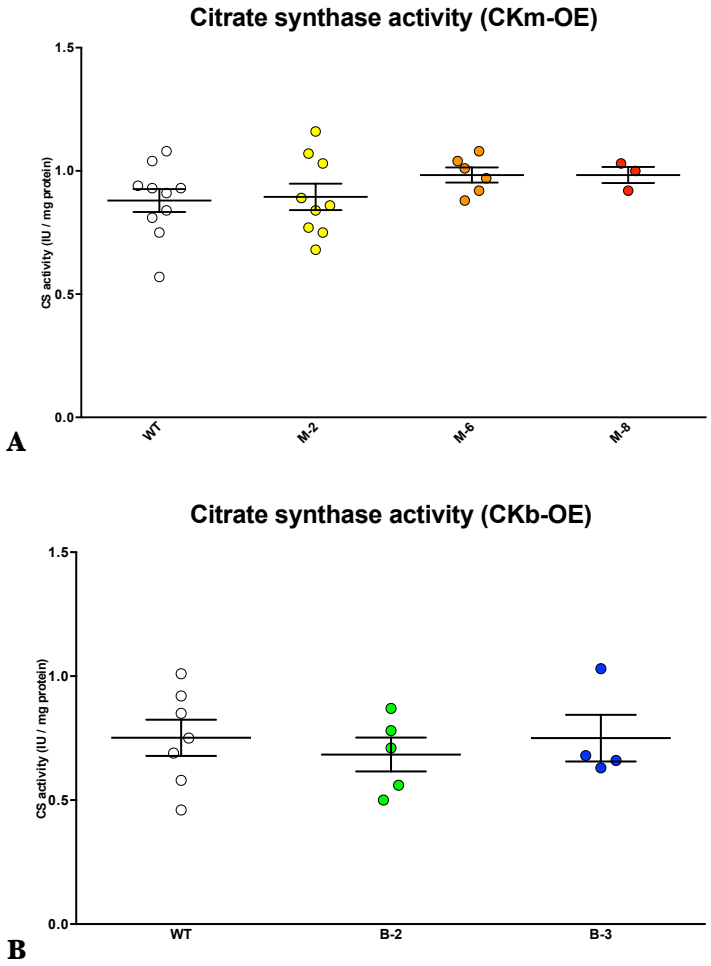


Figure 5-33: Citrate synthase activity in CKm-OE and CKb-OE mice.

(**A**) CKm-OE. (**B**) CKb-OE. Results were analyzed by one-way ANOVA with Bonferroni's multiple comparison test. No significant differences were observed between groups in either transgenic line.

5.4. Discussion

Transgenic mice overexpressing CK-M or CK-B were generated by random integration. Pronuclear injection of DNA into fertilized B6CBAF1 oocytes yielded one CK-M founder and two CK-B founders capable of producing transgenic offspring. Transgene copy number was determined by qPCR, and indicated the presence of two integration sites in the CK-M founder with 2 and 6 copies, respectively; this finding was confirmed by FISH. The CK-B founders had 2 and 3 transgene copies, respectively, while a single transgenic mouse was found to have a significantly higher copy number (~30). Transgene expression was confirmed in both lines at the mRNA level, and CK-MM activity was significantly higher in CK-M mice with 6 or 8

copies of the transgene. In CK-B mice, there was an increase in CK-MB activity, but no detectable change in CK-BB activity. Transgenic mice with varying copy numbers were mated with wild-type mice to generate multiple independent lines, which will be used for further experiments.

5.4.1. Generation of transgenic mice by pronuclear microinjection and random integration

CK-M and CK-B mice were generated by random integration, in contrast to the targeted integration technique used for CKmt mice in Chapter 4. The rationale behind changing strategies was that the expression levels observed in CKmt mice were relatively low. Reverting to a random integration approach could overcome this limitation in two ways. First, while PhiC31 integration was used to ensure integration of a single copy in the CKmt model, random integration frequently leads to insertion of multiple transgene copies, which can be associated with higher expression levels. Second, low expression in CKmt mice may have been due to regulatory elements at the ROSA26 locus. It is worth noting that random integration does not guarantee the absence of similar effects at different loci; therefore, multiple founder lines should ideally be generated for each transgenic project using this method. A significant disadvantage of using random integration is that it may lead to disruption of endogenous genes, which can have unpredictable phenotypic effects. If present, such effects are likely to be recessive in nature, and would therefore only have an immediately obvious effect on phenotype in homozygous mice. The frequency of integration mutagenesis has been reported as 7%, although this may be an underestimate since relatively mild phenotypes are likely to go undetected[252]. Therefore, this must be taken into account, and necessitates the generation of multiple lines for each construct, since any unintended effect of transgene integration would be unlikely to be observed in mice with different integration sites.

Two separate founder lines were generated in the CK-B model; in addition, a single F_1 mouse appeared to have a significantly higher number of transgene copies, and was therefore treated as having a separate integration event. This yielded a total of three distinct lines of CK-B mice.

In the CK-M model, only one founder capable of producing transgenic offspring was generated. Unexpectedly, qPCR revealed the presence of different copy numbers in CK-M mice, suggesting that two independent integration events had taken place. This hypothesis was confirmed by FISH. Therefore, while all CK-M mice were generated from the same founder, they carried two different transgene insertions which differed with respect to copy number and locus; therefore, they were bred separately, and considered as two distinct transgenic lines.

5.4.2. Transgene copy number

The number of transgene copies that are inserted into the genome by random integration is unpredictable, and often varies between lines. For example, in a single study on the β-MHC promoter, transgene copy numbers in mice generated by microinjection ranged from 1 to 265[253]. Significantly, a positive correlation was observed between copy number and transgene expression levels, suggesting that it is possible to study the effect of various levels of expression by using multiple transgenic lines. A similar relationship between copy number and transgene expression was subsequently described for the αMHC promoter[254]. This supports the observation that CK-M mice with greater copy numbers (6 or 8) have markedly higher levels of expression than mice with only 2 copies.

5.4.3. Multiple integration sites in individual founder mice

The results of copy number qPCR in CK-M mice suggested the presence of multiple integration sites. Specifically, mice derived from a single founder were found to have either 2, 6, or 8 copies of the transgene. Since these copy numbers are additive (2+6=8), it was hypothesized that this was due to the presence of two integration sites (with 2 and 6 copies, respectively), and that mice with 8 copies were carrying both of these

sites. While the presence of multiple integration sites in individual founder mouse was an unexpected finding, similar observations have been previously reported[255,256]. In fact, it has been suggested that multiple integration sites may be present in 10-20% of mice generated by random integration[210]. The fact that a single CK-B mouse from founder B_4 was found to have a significantly higher copy number (~30 copies vs 3 in littermates) can be interpreted in the same manner.

The relative number of first-generation CK-M mice with each copy number (20 mice with 2 copies, 5 with 6 copies, 3 with 8 copies) suggested that the 6-copy integration site was occurring less frequently. This could be due to mosaicism in the founder mouse, with a relatively smaller proportion of germ cells carrying the 6-copy insertion. Alternatively, the presence of the 6-copy integration site could be adversely affecting embryonic viability, due to a toxic effect of high transgene expression, or disruption of an endogenous gene. If this was the case, one would expect to see a relatively low ratio of transgenic pups in subsequent generations; however, the breeding statistics (59% transgenic pups) suggest that this is not the case.

5.4.4. Transgene expression and activity

5.4.4.1. CK-M

Total mRNA expression was moderately increased in group M-2 (39%), but substantially increased in group M-6 (289%) and group M-8 (436%). This was associated with a significant increase in CK-MM activity in both groups M-6 and M-8 (by 187% and 209%, respectively). CK-MB activity was also significantly increased in group M-8 (by 104%), suggesting that transgenic CK-M was forming heterodimers with endogenous CK-B. This conclusion is supported by the results of *in vitro* validation experiments, as HEK293 cells transfected with CK-M were found to have functional CK-MM and CK-MB dimers (see section 3.3.1.6).

The level of CK-M overexpression in groups M-6 and M-8 (*i.e.*, mice with 6 or 8 copies of the transgene, respectively) is significantly higher than that observed in CKmt or CK-B mice. Significantly, the degree of CK-M overexpression is of a similar magnitude to the recently published studies by Weiss's group, who reported a ~70% increase in CK-M protein expression and total CK activity in their tetracycline-inducible model[145]. Interestingly, a subsequent publication from the same group reported markedly higher levels of overexpression, with a ~200% increase in CK-M protein expression and CK flux, and a ~300% increase in total CK activity[146]. The most recent publication quotes only CK flux, which is increased by less than 50% in transgenic mice[257]. While there seems to be some variability between these studies, the CK-M model described in this thesis is associated with a comparable level of overexpression, and should therefore be a suitable model for further experiments. If higher expression levels are required, mice carrying the 6-copy insertion site can be bred to homozygosity, which should lead to a further increase in CK-M activity.

5.4.4.2. CK-B

Relative to wild-types, total mRNA expression was increased 31.5-fold in group B-2, and 41.5-fold in group B-3. This is a markedly greater relative increase than that observed in CKmt and CK-M mice, but this is most likely due to the fact that endogenous expression of CK-B is significantly lower than that of the other CK isoenzymes. Accordingly, total CK activity was not increased in these mice, suggesting that the absolute level of CK-B overexpression was relatively low. Nonetheless, there was a significant increase in CK-MB activity, suggesting that the transgenic protein was enzymatically active.

It may be surprising to note that overexpression of CK-B increased the total activity of CK-MB, rather than CK-BB. This observation can be explained by the relative abundance of the CK-M and CK-B isoforms, in the context of their ability to form both homodimers (CK-MM, CK-BB) and heterodimers (CK-MB). Expression of HA-tagged CK-B has been confirmed at the protein level; however, the total amount of CK-B protein is likely to remain significantly lower than the amount of CK-M. Since there is no evidence to suggest that CK-B favors formation of CK-BB homodimers over CK-MB heterodimers, the stoichiometry suggests that additional copies of CK-B would be more likely to bind to CK-M, which is more prevalent. This would

lead to an increase in CK-MB activity, as observed in this model. It remains possible that there is a slight elevation in CK-BB activity, but that this is below the limit of detection of the isoenzyme assay.

Analogous findings have been reported in transgenic mice expressing CK-B in skeletal muscle[258]. Since skeletal muscle does not normally express CK-B, CK-MM constitutes 100% of cytosolic CK activity (*i.e.,* excluding CKmt) in wild-type mice. Expression of CK-B was associated with detectable levels of CK-BB activity (8%), but this was significantly lower than the activity of CK-MB (32%).

Second-generation offspring of the mouse with a higher copy number (group B-30) were found to have significantly increased activities of both CK-MB (>10-fold) and CK-BB (8-fold), and these mice are therefore constitute a more promising model of CK-B overexpression than the first-generation groups (B-2 and B-3).

5.5. Conclusions and future work

The experiments described in this chapter have led to the generation and initial validation of two models of CK overexpression. Multiple transgenic lines are currently being expanded, and further work is being planned to determine the phenotypic effects of CK-M and CK-B overexpression in the heart.

Transgenic F_1 mice are currently being bred with wild-type mates to generate additional mice for further experiments. Separate lines are being established for each transgene integration event, *i.e.*, two lines of CK-M mice (2 or 6 copies), and three lines of CK-B mice (2, 3, or ~30 copies). Since each of these lines differs with respect to transgene copy number and insertion site, it would be prudent to confirm that copy number is uniform in their transgenic offspring. If this confirms that transgene copy number is stable for each line, subsequent litters can be genotyped by standard PCR alone, provided that the lines are not crossed. Finally, since both models were generated on a mixed (C57BL/6 x CBA) background, they require backcrossing onto a pure C57BL/6 background before further experiments can be performed.

Once molecular validation of the CK-M and CK-B models is complete, initial phenotyping will be performed using the methods described in Chapter 4. If CK-M and CK-B overexpression is not found to adversely affect viability, growth, or baseline cardiovascular phenotype, further studies will be conducted to determine whether this is beneficial in models of cardiovascular disease. Finally, since multiple lines are available for each construct, it should be possible to determine whether any potential effects correlate with the level of CK overexpression.

6. CREATINE AND THE MITOCHONDRIAL PERMEABILITY TRANSITION PORE

6.1. Introduction

This chapter discusses a series of experiments which sought to determine whether increasing intracellular creatine could protect against ischemia/reperfusion injury by inhibition of the mitochondrial permeability transition pore (mPTP). The functional characteristics and putative structure of the mPTP are introduced, and evidence for a role of the mPTP in ischemia/reperfusion injury, and a link between mPTP and the creatine kinase system, is reviewed. The experimental section describes the validation of an *in vitro* model of creatine augmentation, and development of a protocol for measuring mPTP opening, which is subsequently applied to this model.

6.1.1. The mitochondrial permeability pore (mPTP)

6.1.1.1. Calcium-induced mitochondrial permeabilization

The mitochondrial permeability transition is a rapid increase in inner mitochondrial membrane (IMM) permeability, classically induced by matrix calcium. While the precise structure responsible for this phenomenon is yet to be definitively established, Haworth and Hunter provided the first detailed description of a calcium-mediated mitochondrial permeability transition nearly 40 years ago[259]. Exposure of isolated bovine heart mitochondria to exogenous calcium led to a conformational change and non-specific permeabilization, as evidenced by influx of sucrose or other solutes into the matrix (the size limit was subsequently determined to be ~1.5kDa). This was accompanied by loss of ionic and proton gradients across the IMM, and uncoupling of respiration. Mitochondria incubated in a hypotonic solution underwent a

similar conformational change, but maintained respiratory coupling until calcium was added to induce the permeability transition, indicating that uncoupling was the result of a change in IMM permeability, rather than mitochondrial conformation. In addition to calcium, several anions were found to induce a similar transition, including phosphate, arsenate, and fatty acids – however, this effect was abolished in the presence of calcium chelators, and was therefore considered to be dependent on the availability of endogenous calcium. The divalent strontium ion, which is transported by the same mechanism as Ca^{2+}, did not induce a permeability transition, providing further evidence that this is a calcium-specific phenomenon. Several factors were found to inhibit mitochondrial permeabilization, including NADH, ADP, Mg^{2+}, mitochondrial energization, and acidic pH. Finally, more recent studies have demonstrated that the critical factor directly responsible for mPTP opening is intramitochondrial generation of reactive oxygen species (ROS)[260,261].

6.1.1.2. Function and structure of the mPTP

While most studies into the function of the mPTP in the heart have focused on its effects in pathological processes, particularly ischemia/reperfusion injury (see section 6.1.2), comparatively little is known about its physiological role. There is evidence to suggest that it may be involved in regulation of mitochondrial metabolism and calcium homeostasis, and/or a component of a programmed necrotic cell death pathway – however, no conclusive functions have been identified to date[262,263].

Since the mPTP was first described on a functional, rather than structural basis, extensive research has been conducted to identify the proteins involved in pore formation. Most studies have concentrated on the role of the adenine nucleotide translocase (ANT) and voltage-dependent anion channel (VDAC), particularly via putative contact sites between ANT on the inner mitochondrial membrane and VDAC on the outer membrane. In one study, complexes consisting of ANT, VDAC, and hexokinase were found to possess mPTP-like characteristics, which were attributed to the direct interaction between ANT and VDAC[264,265]. Further studies suggested a significant role for cyclophilin D (CypD), via direct interaction with VDAC and/or ANT[266,267]. A putative structure incorporating these components is presented in Figure 6-1.

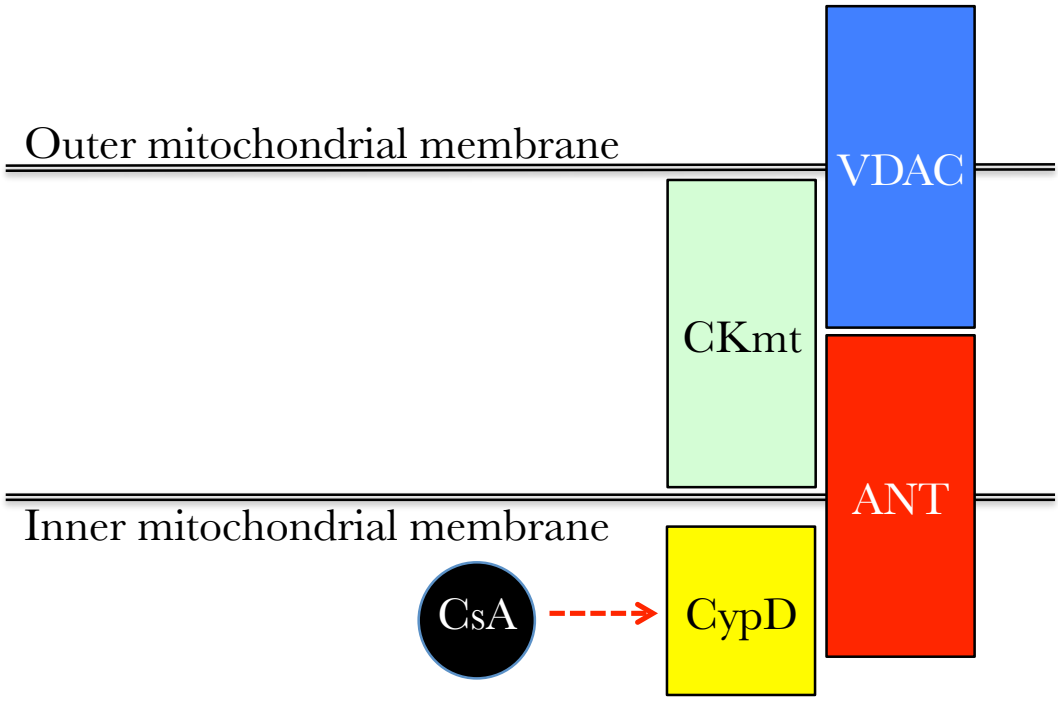


Figure 6-1: Putative structure of the mitochondrial permeability transition pore.

The mPTP is classically thought to be formed by the adenine nucleotide translocase (ANT) on the inner mitochondrial membrane, and the voltage-dependent anion channel (VDAC) on the outer mitochondrial membrane. The matrix protein cyclophilin D (CypD) plays a regulatory role, and constitutes the target for mPTP inhibition by cyclosporin A (CsA, see section 6.1.1.3). Mitochondrial creatine kinase (CKmt) is not thought to be directly involved in pore formation, but may regulate mPTP opening by interacting with VDAC and/or ANT. Figure adapted from Zamzami *et al.* [268]

Genetic knockout studies have been performed to determine whether ANT, VDAC, and/or CypD are required for mPTP formation. Mitochondria lacking ANT were still capable of undergoing permeability transition, indicating that ANT is not a necessary component of the mPTP[269]. However, in the absence of ANT, higher Ca^{2+} concentrations were required to initiate mPTP opening, suggesting that it may play a regulatory role. This is further supported by the observation that mPTP opening is affected by modulators of ANT, such as atractyloside (which inhibits ANT, and promotes mPTP opening) or ADP (which stimulates ANT, and inhibits the mPTP)[270]. Significantly, this regulation was absent in ANT-deficient mitochondria, indicating that the effects of these molecules on mPTP are mediated by ANT[269]. VDAC, on the other hand, does not seem to play a significant structural or regulatory role in mPTP opening, as genetic ablation of VDAC does not prevent mPTP formation or decrease its sensitivity to Ca^{2+}[271,272]. Finally, a series of studies demonstrated that mPTP opening can also occur in the absence of CypD, but requires significantly higher Ca^{2+} stimulation, suggesting that while CypD is not absolutely required for mPTP opening, it plays an important regulatory role.

6.1.1.3. Inhibition by cyclosporin A

Inhibition by the immunosuppressive drug cyclosporin A (CsA) is a characteristic feature of the mPTP. Initial studies into its effects on isolated mitochondria demonstrated that CsA blocks calcium efflux, allowing mitochondria to accumulate high amounts of calcium[273]. This observation was subsequently attributed to inhibition of the mPTP[274]. The mechanism of CsA-mediated inhibition was initially thought to involve blocking the interaction between the adenine nucleotide translocase (ANT) and a peptidyl-prolyl cis-trans isomerase[275,276], later identified as cyclophilin D (CypD)[277,278]. The crystal structure of CypD bound to CsA has been resolved, providing a structural basis for this interaction[279]. The CypD-ANT hypothesis was called into question by the finding that sanglifehrin A (SfA), which inhibits the enzymatic activity of CypD but not its binding to ANT, also inhibits mPTP opening[280]. This suggests that CsA and SfA inhibit the mPTP via a mechanism other than preventing the interaction between CypD and the ANT. In knockout studies, the inhibitory effect of CsA was preserved in the absence of the ANT[269], but absent in CypD-deficient mitochondria[281], confirming that inhibition of the mPTP by CsA is mediated by its interaction with CypD, independently of the ANT.

The recently proposed model of an mPTP formed by ATP synthase[282] provides a novel molecular mechanism for inhibition of the mPTP by CsA. CypD has been shown to bind to the lateral stalk of ATP synthase and affect its enzymatic activity[283], and this interaction was shown to be sensitive to CsA. Furthermore, the ATP synthase inhibitor benzodiazepine-423 (Bz-423), which binds at the same site, was found to promote mPTP opening in a concentration-dependent manner, but this effect was abolished by high P_i concentrations (which would promote binding of CypD, and displace Bz-423)[282]. Significantly, the effect of Bz-423 was preserved in the presence of high P_i when CypD binding was abolished (due to either absence of CypD or inhibition by CsA), indicating that this specific interaction is crucial for mPTP sensitization by CypD (and conversely, inhibition by CsA).

6.1.2. The mPTP in cardiac ischemia/reperfusion injury, and evidence for a protective effect of mPTP inhibition

There is ample experimental and clinical evidence implicating the mPTP in cardiac ischemia/reperfusion injury. Initial studies demonstrated a calcium-dependent permeability transition in isolated heart mitochondria[284,285], which could be inhibited by CsA[274]. CsA was subsequently shown to prevent cell death in intact ventricular cardiomyocytes exposed to *in vitro* anoxia/reoxygenation injury[286]. The protective effect of CsA was confirmed in animal models of ischemia/reperfusion, initially *ex vivo* in perfused hearts[287,288]. These models were also used to confirm that mPTP plays a causal role in cardiomyocyte death[289], and that pore opening occurs during cardiac reperfusion, rather than ischemia[290]. The mPTP is thought to be "primed" for opening during ischemia by the increase in Ca^{2+} and P_i and depletion of adenine nucleotides, but remains closed due to the low pH and de-energization of mitochondria; on reperfusion, these inhibitory conditions are reversed, leading to mPTP opening.

Subsequent *in vivo* studies demonstrated that inhibition of mPTP opening immediately before or at the onset of reperfusion significantly reduces infarct size[291,292]. Most recently, a clinical trial found that administration of CsA before coronary revascularization in patients with ST segment elevation myocardial infarction was associated with decreased infarct size in the acute setting[293], and this effect remained significant at 6 months post-infarction[294]. These results demonstrate that the mPTP plays a causal role in cardiac ischemia/reperfusion injury, and provide direct evidence that inhibition of mPTP opening can have a cardioprotective effect, in both experimental and clinical settings.

Finally, there is evidence that transient, low-conductance opening of the mPTP can have a protective effect, *e.g.* during ischemic preconditioning[295,296]. The most likely explanation is that transient mPTP opening acts as a release mechanism, allowing excess calcium to escape the mitochondria[297]. Whether this mechanism plays a significant role *in vivo* remains to be established.

6.1.3. The mPTP and the creatine kinase system

The mitochondrial isoenzyme of creatine kinase (CKmt) has been historically associated with regulation of mPTP opening due to its close association with two proteins implicated in mPTP formation, the adenine nucleotide translocase (ANT) and voltage-dependent anion channel (VDAC)[264]. While these proteins have been excluded as essential components of the pore itself, there is evidence that they can regulate its activity (particularly in the case of the ANT). Furthermore, CKmt, along with ANT and VDAC, was thought to be involved in formation of contact sites between the inner and outer mitochondrial membranes, which could play a role in energy transport and regulation of mPTP opening[298].

Reconstitution of the ANT-VDAC complex with hexokinase in artificial vesicles was found to induce a permeability-transition-like event in response to Ca^{2+}, which was prevented by substitution of CKmt for hexokinase[265]. This effect could simply be attributed to the lack of hexokinase, rather than the presence of CKmt; however, it was abolished by dimerization of CKmt, and it was therefore concluded that octameric CKmt can stabilize the ANT-VDAC complex and prevent pore activation. However, since ANT and VDAC are no longer considered sufficient to form the mPTP, the observed change in vesicle permeability is unlikely to have been a "true" mPTP event, and these results must therefore be interpreted with caution.

A more convincing link between the CK system and mPTP was demonstrated in transgenic mice, expressing human ubiquitous CKmt in the liver (a tissue which does not normally express detectable amounts of CKmt, or any other CK isoenzyme)[149]. In mitochondria isolated from these mice, creatine and cyclocreatine were found to inhibit mPTP opening[299]; the metabolically inactive creatine analog β-guanidinopropionic acid (β-GPA) did not[150]. This effect was not observed when CKmt was inactivated by incubating mitochondria without exogenous Mg^{2+}, a necessary co-factor for the enzyme (ATP synthase and other intramitochondrial enzymes remained active due to the presence of endogenous Mg_{2+} in the matrix). Finally, addition of exogenous CKmt or CK-BB to mitochondria isolated from wild-type mice did not affect mPTP opening. These findings suggest that the mPTP can be regulated by the CK system, in a process that requires (1) substrate availability in the form of creatine or cyclocreatine, (2) enzymatic activity of CKmt, and (3)

intramitochondrial localization of CKmt. Since cardiac mitochondria satisfy all of these conditions, it is feasible that mPTP opening can be inhibited by augmenting creatine availability, CKmt activity, or both.

Conversely, a study into the neuroprotective effect of creatine in Huntington's disease did not demonstrate inhibition of the mPTP by creatine[300]. Mitochondria isolated from the brains of rats on a creatine-supplemented diet were found to have the same calcium-induced swelling response to those from mice on a control diet. A possible explanation for this discrepancy in findings is that the predominant isoform of CK in brain is cytosolic CK-BB. The ubiquitous isoform of CKmt is also expressed, but at far lower levels. Since inhibition of mPTP by creatine in liver mitochondria was only observed in the presence of endogenous, mitochondrially-localized CKmt, it is possible that CKmt expression in wild-type rat brain mitochondria is insufficient for this effect to be observed.

6.1.4. The cardioprotective effect of creatine and creatine kinase

Transgenic mice overexpressing the creatine transporter in the heart (CrT-OE) are described in detail in section 1.5.1. Briefly, hearts isolated from mice with moderately elevated myocardial creatine concentrations (20%-100% above normal) were found to be less susceptible to ischemia/reperfusion injury, as evidenced by more rapid and sustained functional recovery[144]. *In vivo* studies demonstrated a 27% reduction in infarct size following coronary artery ligation and reperfusion. The most likely mechanism for this protective effect is preservation of energetic status due to increased phosphocreatine, which would replenish ATP and maintain a favorable ΔG_{ATP}. In addition, CrT-OE hearts had significantly greater glycogen stores, which could provide the cell with additional substrate for glycolysis during ischemia. Finally, since there is evidence to suggest that the creatine kinase system can affect mPTP opening, a key pathophysiological event in ischemia/reperfusion injury, it is possible that this may be one of the mechanisms by which creatine exerts its cardioprotective effects.

Conversely, creatine-deficient (GAMT$^{-/-}$) mice demonstrate an impaired functional and energetic response to ischemia/reperfusion [107]. This provides further evidence that the creatine kinase system plays an important role in protecting the heart against the effects of ischemic injury.

6.2. Aims and hypotheses

The goal of the experiments described in this chapter was to study the effect of moderately elevated intracellular creatine on mPTP opening as a possible cardioprotective mechanism – specifically, to (1) establish an *in vitro* model of creatine elevation analogous to that observed in the CrT-OE transgenic mice, (2) implement and validate an assay to assess susceptibility to mPTP opening, and (3) determine whether creatine supplementation can inhibit mPTP opening.

The hypothesis was that moderately increased intracellular creatine inhibits activation of the mPTP, which may contribute to the beneficial effect of creatine elevation in myocardial ischemia/reperfusion injury.

6.3. Methods and results

6.3.1. Experimental design

There are a variety of techniques which have been used for assessment of mPTP function. The most direct method is to isolate mitochondria and challenge them with increasing doses of calcium. This eventually leads to mPTP opening, which can be detected spectrophotometrically, either (1) using calcium-sensitive dyes, as a sudden, large, and sustained increase in intramitochondrial calcium concentration, or (2) without additional dyes, as a decrease in absorbance due to mitochondrial swelling (typically at a wavelength of 500-550nm).

Calcium-loading of isolated mitochondria is the most simple and direct method of measuring mPTP opening; however, for the purpose of this experiment, it would be more informative to measure mPTP opening in intact cells. The goal was to apply an *in vitro* model to determine whether mPTP opening during ischemia/reperfusion could be affected by elevating creatine in cardiomyocytes. If such an effect was present, this would only be detectable in isolated mitochondria if the effect was mediated by a structural or functional change within the mitochondria themselves. It would therefore be more appropriate to study mPTP opening in intact cardiac cells, to account for extramitochondrial factors and mimic the *in vivo* setting as closely as possible. Primary cardiomyocytes could be used for this purpose, but cell isolation is a traumatic process, and the quality of cells can be variable between experiments. Furthermore, in this specific model, individual CrT-OE hearts would have to be pre-selected for appropriate creatine levels. To overcome these limitations, cardiac-derived HL-1 cells were used. HL-1 cells maintain a cardiac phenotype, and can be cultured indefinitely *in vitro*. Previous work in our group has demonstrated that intracellular creatine in HL-1 cells can be increased by culturing cells in media with elevated creatine concentrations. Therefore, these cells could serve as a model to determine the effect of creatine elevation on mPTP opening.

6.3.2. Optimization of creatine incubation conditions

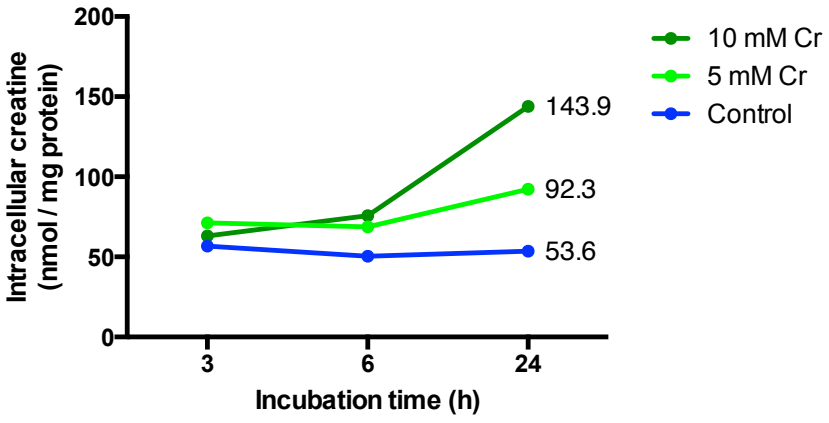
In order to establish an *in vitro* model to study the effect of creatine on mPTP opening, it was first necessary to determine conditions under which intracellular creatine concentrations were increased to the cardioprotective level observed in the hearts of CrT-OE mice.

Based on the results of studies on creatine uptake kinetics in cultured cells[301], a pilot experiment was conducted to determine the effect of creatine supplementation on intracellular concentration at 3, 6, and 24 hours. HL-1 cells were seeded in 6-well plates at a density of 1 x 10^5 cells per well, cultured for 24 hours, and incubated in standard Claycomb medium (control), or Claycomb medium supplemented with 5mM or 10mM creatine.

Individual wells were washed twice with PBS to remove residual creatine-containing media, and harvested by trypsinization and centrifugation. Pellets were snap-frozen in liquid nitrogen, homogenized using a stainless steel percussion homogenizer, and resuspended in 0.4M perchloric acid. An aliquot was removed for determination of protein concentration using the Lowry assay. The remaining homogenate was neutralized with 1M KOH, and centrifuged for 5min at 6000g, and supernatant was filtered using a 0.45μm filter. Metabolite concentrations were determined by high-performance liquid chromatography (HPLC), using a Supelco LC-18 reverse phase column (25cm x 4.6mm, 5 μM pore size), Jasco PU-2089 Plus pump, and Jasco UV-2075 Plus UV detector (detection at 205nm). Since the goal was to determine the total intracellular creatine pool, regardless of phosphorylation status, creatine concentration was calculated as the sum of the areas under the phosphocreatine and creatine peaks. Results were normalized to sample protein concentration, as described previously[302].

Results are summarized in Figure 6-2. Control cells had similar creatine concentrations to wild-type left ventricular tissue (historical data[144,303]), at all timepoints. Creatine concentrations did not increase above the normal range at 3 or 6 hours. Incubation for 24 hours in media supplemented with 5mM or 10mM creatine increased intracellular concentrations by a similar degree to that observed in CrT-OE mice (63% and 153% above controls, respectively). To maximize the probability of finding a suitable dose in HL-1 cells, 24-hour incubations in both creatine concentrations (5mM and 10mM) were used for all subsequent experiments.

Figure 6-2: Optimization of creatine pre-incubation conditions for mPTP assays.



HL-1 cells were incubated in standard Claycomb medium (blue), or medium supplemented with either 5mM or 10mM creatine (light/dark green), for 3, 6, or 24 hours. Intracellular creatine concentration was measured by HPLC, and normalized to protein concentration. Data labels are mean concentrations in samples incubated for 24 hours; the 24-hour incubation with 5mM or 10mM creatine was used for all subsequent assays.

6.3.3. Measurement of mPTP opening

6.3.3.1. Calcein release as an indicator of mPTP opening

6.3.3.1.1. *Background*

Calcein (3,6-dihydroxy-2,4-bis-[N,N'-di-(carboxymethy1)-aminomethyl] fluoran) is a fluorescein derivative, originally developed for measurements of calcium at low concentrations[304]. Due to its hydrophilic properties, it neither crosses nor binds to lipid membranes, and is therefore a useful tool for staining cells and their subcompartments. In order to facilitate delivery of calcein into cells, a membrane-permeant acetomethoxyl ester, calcein-AM, has been developed. Calcein-AM crosses the cell membrane (and, under certain conditions, internal membranes), where it is cleaved by cellular esterases to form free, membrane-impermeant calcein, effectively trapping the dye in the relevant compartment. Calcein-AM is therefore commonly applied as an indicator of cell viability (specifically, membrane integrity), or to detect intercellular junctions.

The mPTP non-specifically permeabilizes the mitochondrial membrane to solutes up to 1,500 Da. This creates a channel through which calcein (622 Da) can passively diffuse, and permeabilization of mitochondria to calcein can therefore be used as an indicator of mPTP opening. A method has been described allowing selective loading of mitochondria with calcein, based on the observation that divalent metal ions quench calcein fluorescence[305]. Cells are loaded with calcein-AM, which accumulates (and is de-esterified, *i.e.* trapped) in both the cytosol and mitochondria. Cobalt chloride is added to quench cytosolic fluorescence; since mitochondria are impermeable to Co^{2+}, mitochondrial calcein fluorescence is preserved[306]. mPTP opening allows calcein to exit the mitochondria, leading to a redistribution and quenching of fluorescence, which can be directly observed (Figure 6-3). Originally developed in hepatocytes, this method has been successfully applied to image mPTP opening in several cell types, including primary cardiomyocytes[261,307,308].

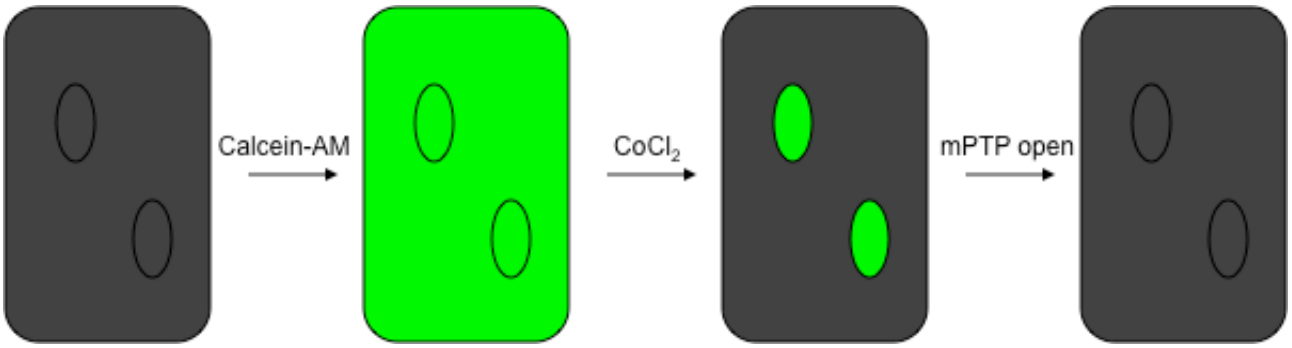


Figure 6-3: Calcein-AM mPTP protocol.

Cells are loaded with calcein-AM, which is de-esterified in both the cytosol and mitochondria. Addition of $CoCl_2$ quenches cytosolic, but not mitochondrial fluorescence. Induction of mPTP opening leads to permeabilization of the mitochondrial inner membrane and redistribution of calcein into the cytosol, where its fluorescence is quenched by Co^{2+}.

6.3.3.1.2. *Protocol and optimization*

Cells were loaded with 1μM calcein-AM and 1mM $CoCl_2$ in Hank's balanced salt solution (HBSS, Sigma H8264) for 15min at 37°C[306]. Addition of $CoCl_2$ resulted in quenching of cytosolic fluorescence, as visualized by epifluorescence microscopy (Figure 6-4).

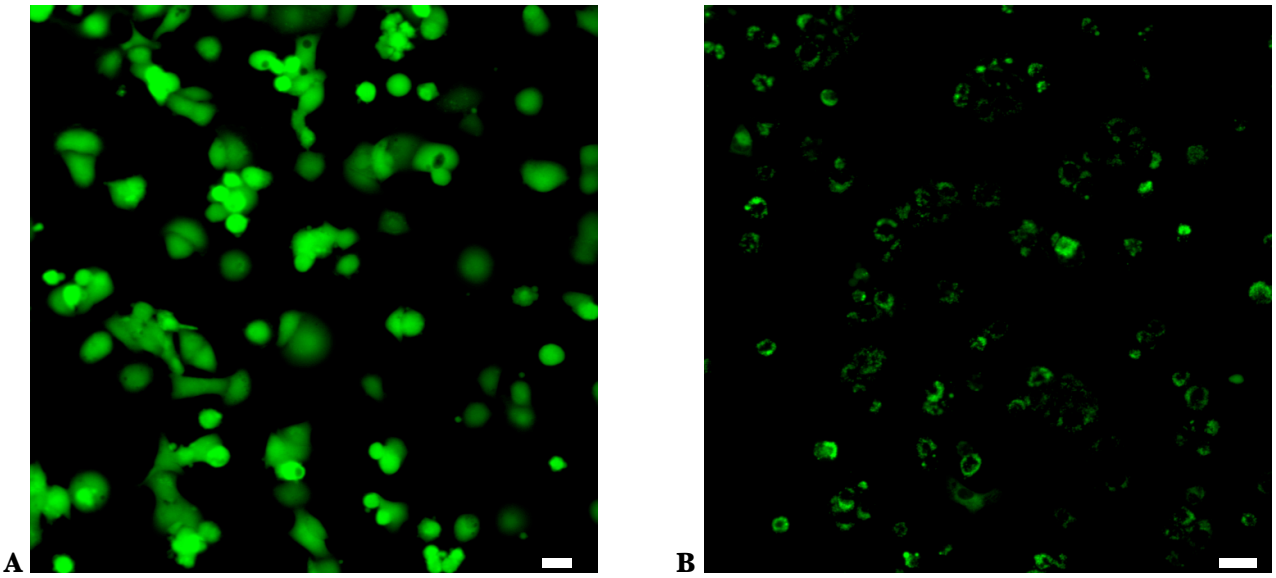


Figure 6-4: Calcein pilot experiment.

HL-1 cells loaded with 1μM calcein-AM (left), or 1μM calcein-AM + 1mM $CoCl_2$ (right), demonstrating quenching of cytosolic fluorescence by $CoCl_2$. Scale bars, 20μm.

Calcein fluorescence has been shown to be independent of sampling rate, indicating that laser photobleaching of the dye is unlikely[306]. To confirm that this is the case, individual cells were imaged every 5min for a period of 30min, and mean calcein fluorescence intensity was found to remain constant throughout (Figure 6-5).

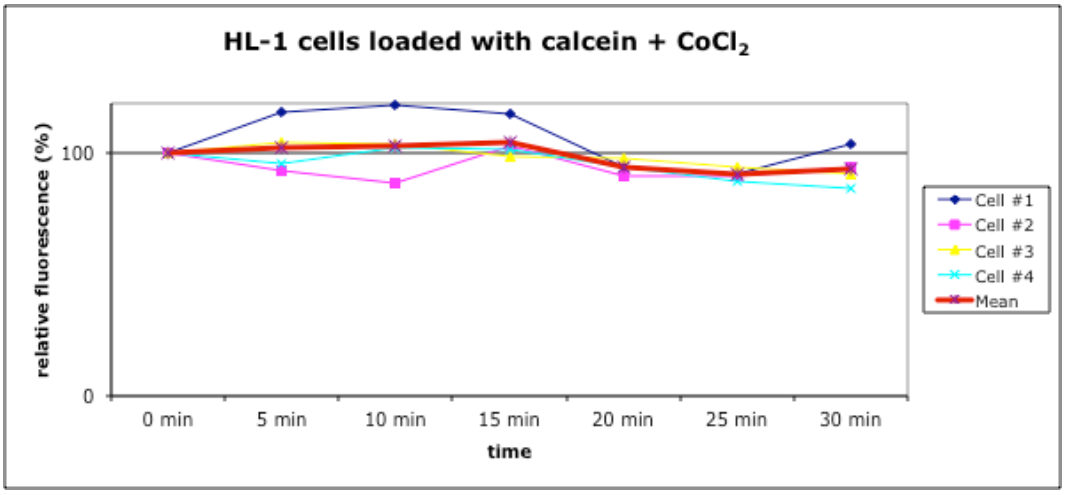


Figure 6-5: Calcein photostability.
Serial imaging of cells loaded with calcein and $CoCl_2$, demonstrating lack of laser photobleaching of calcein fluorescence.

Cells were treated with hydrogen peroxide (H_2O_2) to induce oxidative stress and mPTP opening. Since there were no published studies using an analogous protocol in HL-1 cells, initial experiments were performed using 100μM H_2O_2, a dose which has been shown to induce mPTP in neonatal rat ventricular cardiomyocytes[309,310]. This dose proved ineffective at inducing a time-dependent decrease in calcein fluorescence, and a wider range of H_2O_2 concentrations was therefore tested to empirically determine the appropriate dose. Cells were loaded with calcein-AM and $CoCl_2$, incubated for 30min with 10-fold dilutions of H_2O_2, from 8.8M (undiluted) to 880μM, and imaged by epifluorescence microscopy (Figure 6-6).

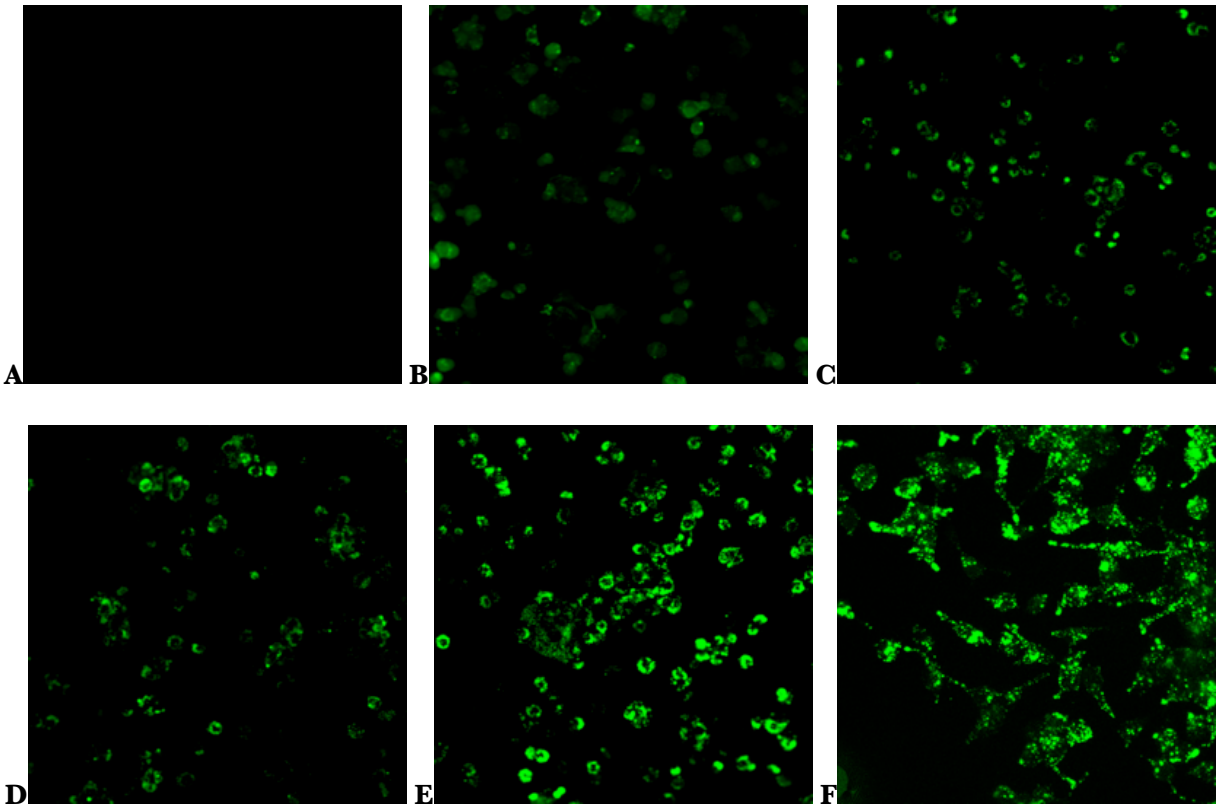


Figure 6-6: Dose-response experiment for H_2O_2 induction of mPTP opening in HL-1 cells.

Images are representative fields of view from wells incubated for 30min with 10-fold dilutions of H_2O_2 (**A**, 8.8M; **B**, 880mM; **C**, 88mM; **D**, 8.8mM; **E**, 880μM; **F**, control). Image acquisition settings are identical for all panels. Simultaneous phase-contrast imaging confirmed that cells were present at a similar density in all fields of view (not shown).

High concentrations of H_2O_2 (880mM and 8.8M) were found to rapidly induce loss of calcein fluorescence, and were excluded on the basis that the toxic effect would likely be too strong for a protective intervention to prevent. The experiment was repeated using the remaining concentrations; while mPTP opening was rapid in cells incubated in 88mM H_2O_2, the 8.8mM dose was found to produce a gradual reduction in calcein fluorescence, and was therefore used for subsequent optimization experiments. In individual cells, however, exposure to 8.8mM H_2O_2 was found to cause relatively early redistribution of calcein fluorescence, with signs of cell membrane blebbing noticeable in phase-contrast images (Figure 6-7).

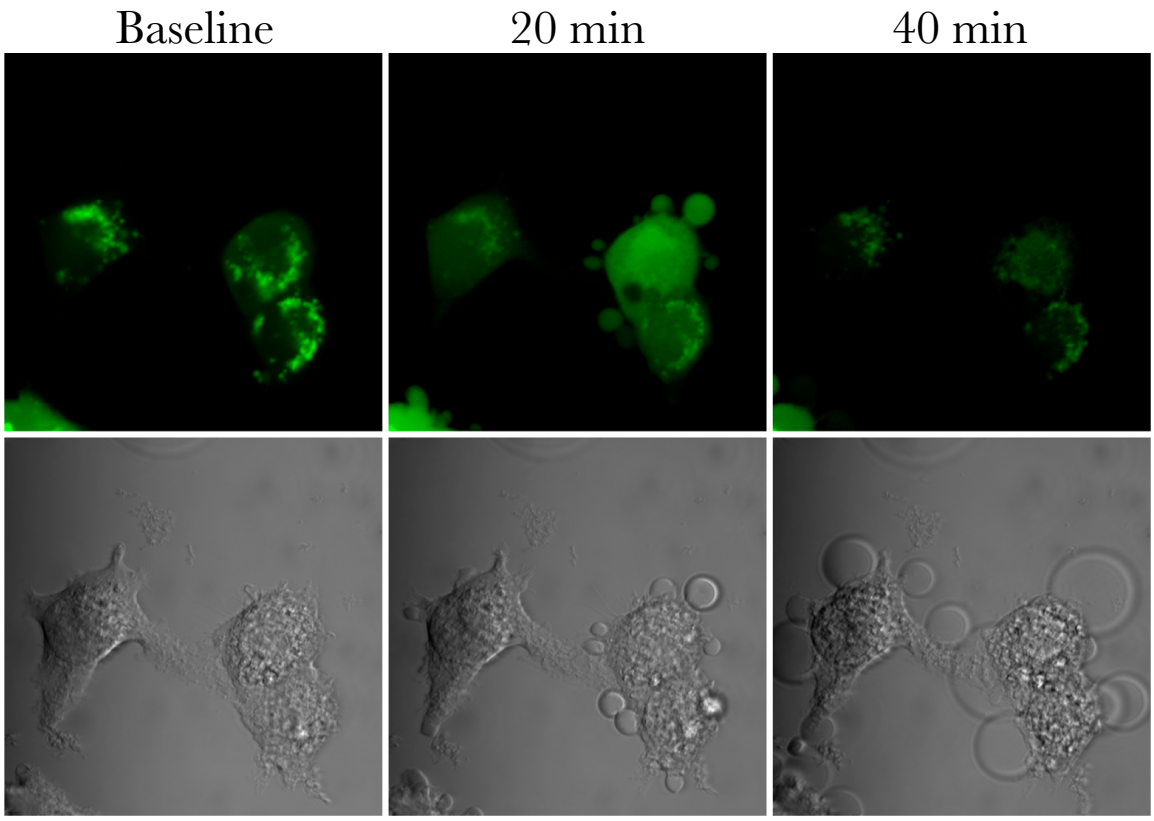


Figure 6-7: mPTP induction by H_2O_2.

Calcein fluorescence (top) and phase-contrast images (bottom) during incubation in 8.8mM H_2O_2, at baseline (left), 20min (center), and 40min (right). H_2O_2 caused marked redistribution of calcein fluorescence at 20min, with formation of calcein-containing blebs; by 40min, calcein fluorescence was decreased, and all cells showed clear signs of cell death.

Since this could indicate that the 8.8mM dose was too high, subsequent experiments were performed using a 5-fold lower H_2O_2 concentration of 1.6mM, and cytoplasmic blebbing was not apparent during incubations up to 60 min. In order to determine whether the mPTP inhibitor cyclosporin A (CsA) could prevent H_2O_2-induced calcein loss, 1μM CsA was added to individual wells (during both calcein loading and H_2O_2 incubation), as a positive control. Three consecutive experiments were performed, with 6-15 cells per treatment group in each experiment (Figure 6-8). Individual regions of interest (ROIs) were manually drawn around cells, and images were analyzed using ImageJ. Calcein data were quantified as both mean fluorescence and standard deviation of fluorescence within each cell, since inadequate cytosolic quenching of calcein could lead to a decrease in standard deviation without a reduction in mean (*i.e.*, redistribution of calcein out of mitochondria into the cytosol would lead to a decrease in calcein compartmentalization, and consequently a decrease in fluorescence standard deviation).

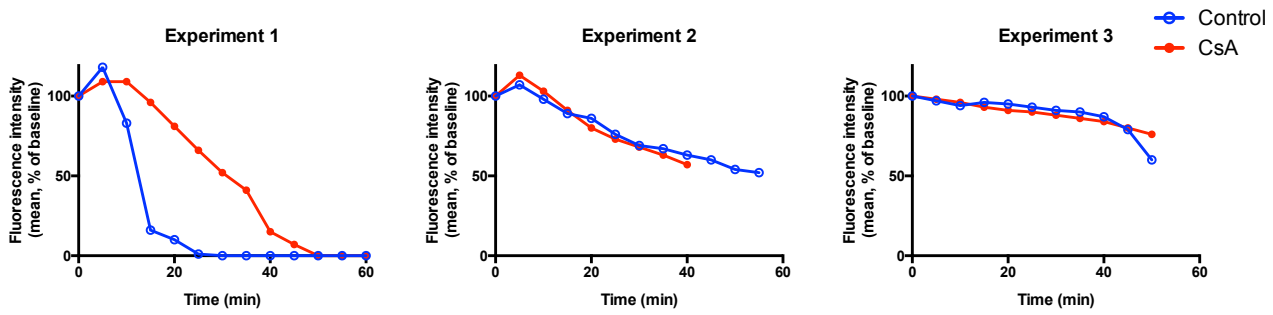


Figure 6-8: Quantification of calcein release in response to H_2O_2.

Results of three consecutive assays, measuring calcein fluorescence in HL-1 cells exposed to 1.6mM H_2O_2 (blue) or 1.6mM H_2O_2 + 1μM CsA (red). Values are expressed as mean of mean fluorescence, normalized to baseline for each sample.

The first assay yielded the expected result – both control and CsA-treated cells displayed a reduction in calcein signal over time, but this was delayed approximately two-fold by CsA. This effect was not observed in the second assay. In the third assay, there was a slight reduction in calcein loss in CsA-treated samples (CsA mean, 73% of F_0; control mean, 60% of F_0); however, it became apparent that a proportion of cells were undergoing severe morphological changes while maintaining calcein signal (Figure 6-9).

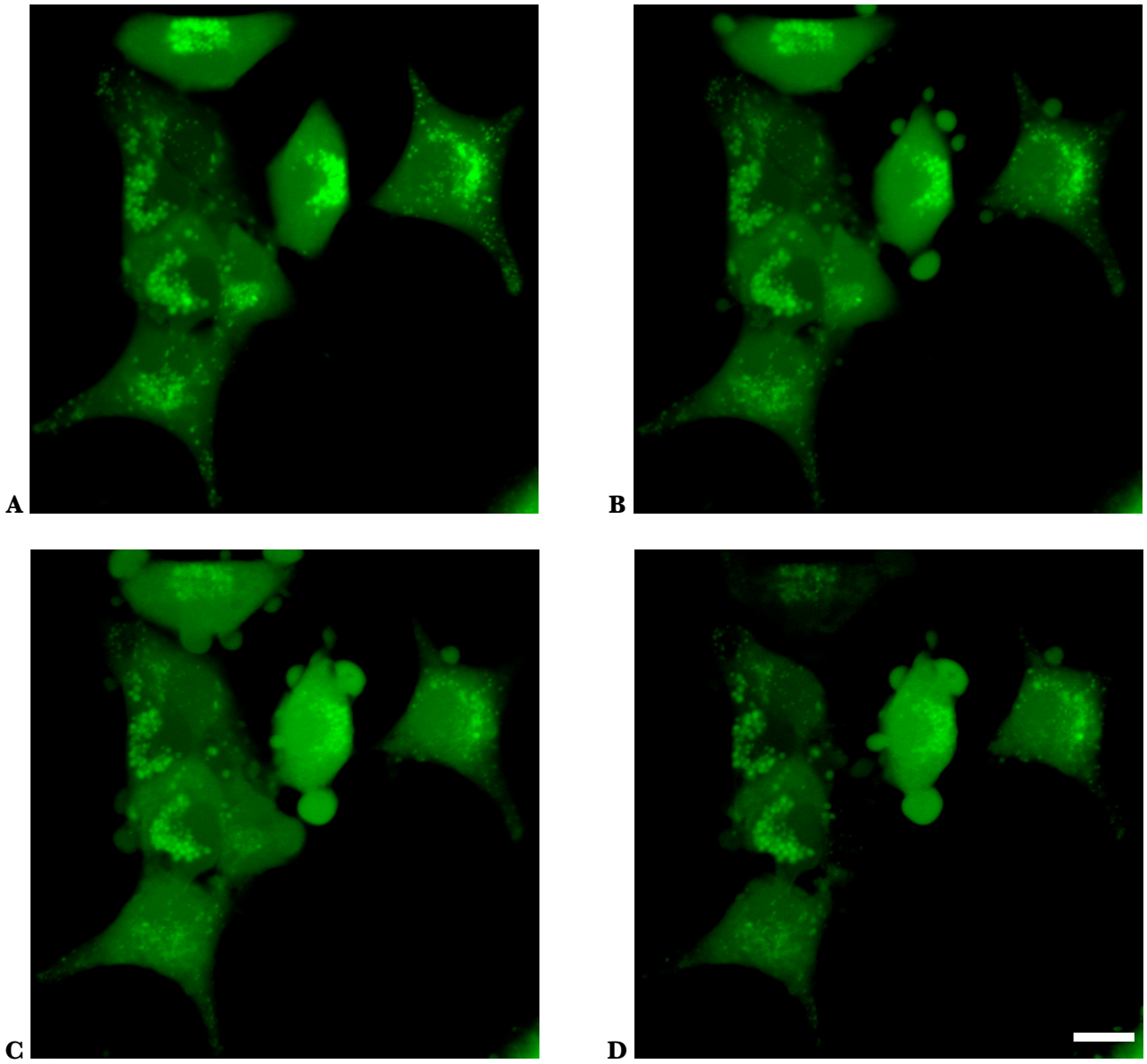


Figure 6-9: Time-lapse imaging of calcein release in response to H_2O_2.

Representative images of calcein fluorescence in control HL-1 cells incubated in 1.6mM H_2O_2, taken from Experiment C. After acquisition of a baseline image (A), cells were scanned every 5min. Cytoplasmic blebbing was evident at 20min post-H_2O_2 (B). Cell fluorescence remained relatively stable until 45min (C), but at 50min two cells seemed to abruptly and almost completely lose cytoplasmic calcein signal (D). One of these cells retained a degree of punctate fluorescence, possibly indicating cell membrane rupture with preserved intracellular compartmentalization. Scale bar, 20μm.

6.3.3.1.3. *Calcein subcellular localization experiments*

The sequence of events observed in cells exposed to H_2O_2, namely a sudden, late loss of compartmentalized calcein signal, quickly followed by cell lysis, is not characteristic of mPTP opening. This raises the possibility that the redistribution of calcein signal is not actually due to the mPTP, and the signal may actually be localized in a different type of organelle altogether. Significantly, a study into the effects of hypoxia in

hepatocytes used calcein-AM to image lysosomes, and observed a strikingly similar sequence of events – a late, discrete event leading to rapid loss of lysosomal calcein, followed almost immediately by cell death and rupture[311]. A more recent study also found that, under appropriate loading conditions, calcein is preferentially accumulated in the lysosomes of HeLa cells, and the distribution of calcein signal appears to follow a similar, punctate pattern to that observed in the HL-1 experiments described above[312]. Therefore, the unexpected response to H_2O_2 could be explained by the fact that calcein was loading not actually loading mitochondria, but another type of organelle, possibly lysosomes.

To determine whether calcein/$CoCl_2$ staining was labeling mitochondria and/or lysosomes, co-localization studies were performed using organelle-specific dyes. Sample images from stain optimization experiments are presented in Figure 6-10, demonstrating the loading pattern of MitoTracker Red and LysoTracker Red (Molecular Probes).

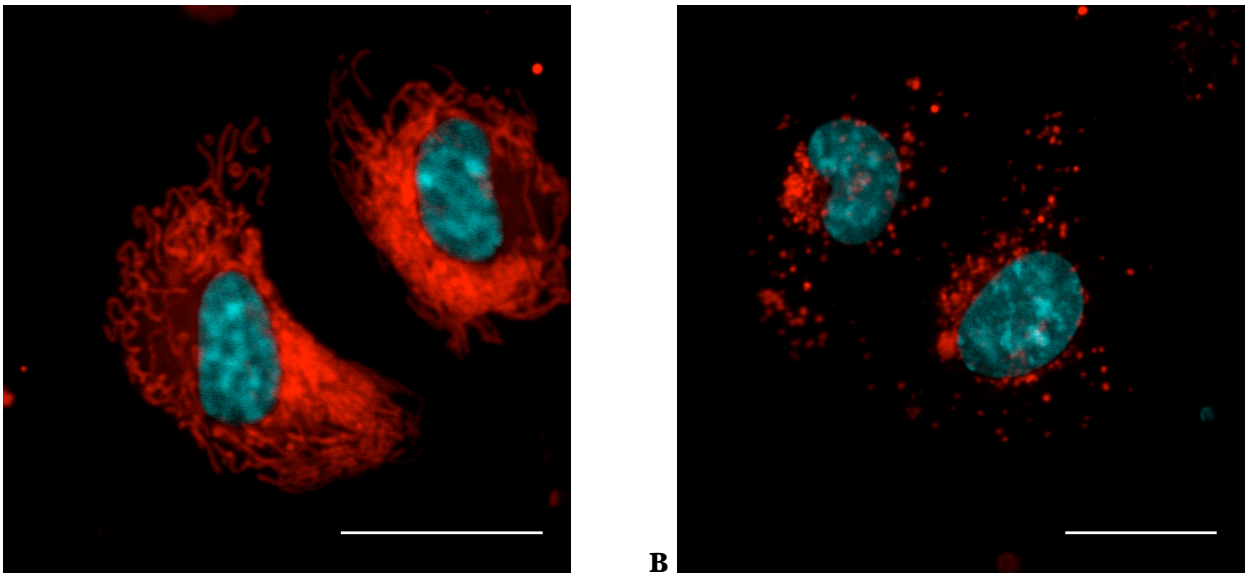


Figure 6-10: Mitochondrial and lysosomal staining in HL-1 cells.

HL-1 cells stained with MitoTracker Red (200nM, A) or LysoTracker Red (50nM, B). Nuclei were counter-stained with Hoechst 33258 (cyan). Scale bars, 20μm.

For co-localization experiments, cells were pre-loaded with MitoTracker Red or LysoTracker Red in PBS for 30min at 37°C, loaded with calcein-AM/$CoCl_2$ for 15min at 37°C, washed in PBS to remove residual dyes, and incubated in PBS supplemented with Hoechst 33258 for confocal imaging:

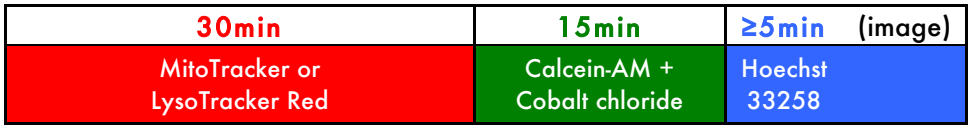


Figure 6-11: **General incubation protocol for calcein subcellular localization experiments.**

In mitochondrial co-localization experiments with MitoTracker Red, the punctate distribution of calcein fluorescence was not found to overlap with the mitochondrial network. This suggests that, in this setting, the calcein-AM/$CoCl_2$ staining protocol was not specifically loading mitochondria. Representative images are presented on the following pages (Figure 6-12, Figure 6-13; all scale bars are 20μm).

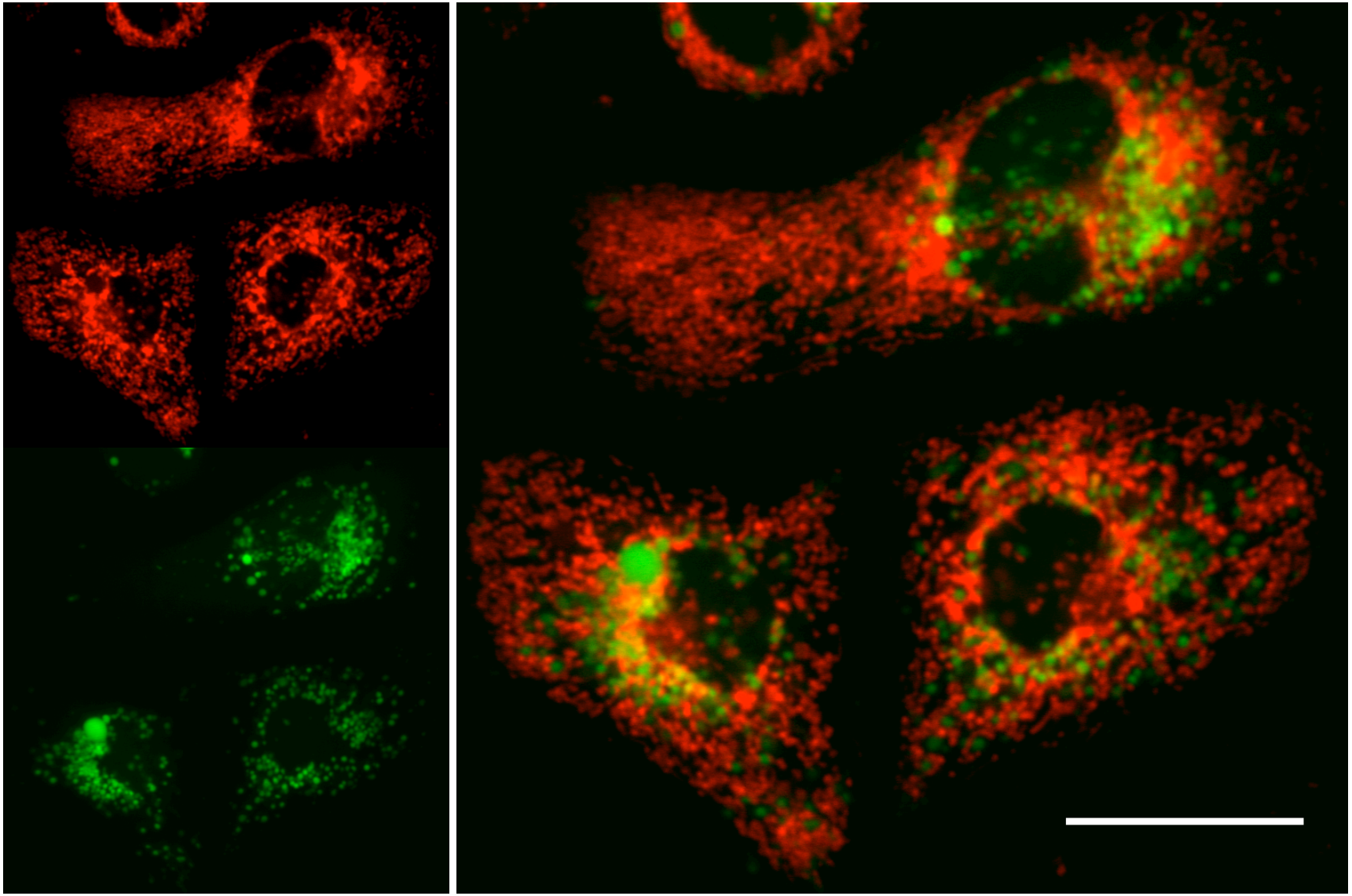


Figure 6-12: MitoTracker Red and calcein. HL-1 cells co-stained with MitoTracker Red (red) and calcein (green), demonstrating that calcein loading is not localized to mitochondria.

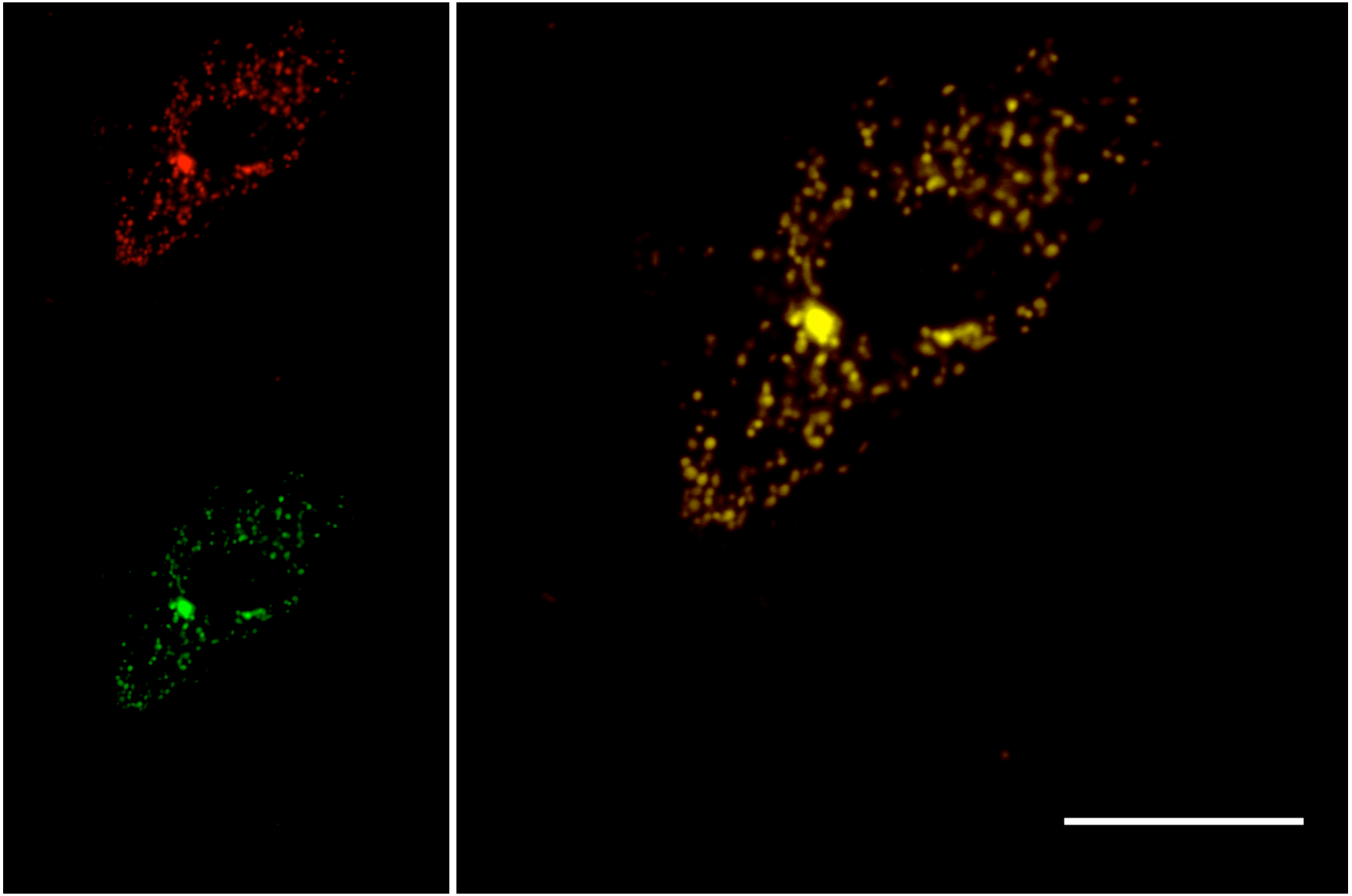


Figure 6-13: LysoTracker Red and calcein. HL-1 cell co-stained with LysoTracker Red (red) and calcein (green), demonstrating that calcein fluorescence corresponds to lysosomes.

6.3.3.1.4. *Summary of results and conclusions*

The results of co-localization experiments clearly demonstrate that, under the conditions used, calcein is being loaded into the lysosomes, rather than mitochondria. This problem could potentially be overcome by optimizing the loading conditions; however, an alternative method was sought to avoid any unexpected effects of ineffective mitochondrial loading.

6.3.3.2. Photoactivation of tetramethylrhodamine methyl ester (TMRM) and mPTP opening

6.3.3.2.1. *Background*

Tetramethylrhodamine methyl ester (TMRM) is a cationic dye, which is preferentially accumulated by mitochondria in proportion to the mitochondrial membrane potential[313]. TMRM can be used for two different types of experiments, depending on the concentration used. At low concentrations (in the nM range), loss of mitochondrial membrane potential leads to release of TMRM from mitochondria, and a decrease in fluorescence. When high (μM-range) concentrations of TMRM are used, accumulation of the dye inside mitochondria causes formation of aggregates between molecules, which leads to quenching of fluorescence[314,315]. In this setting, release of TMRM into the cytosol leads to "dequenching," observed as an *increase* in fluorescence.

Redistribution of TMRM fluorescence can therefore be used to detect mPTP activation; significantly, TMRM can also be used to induce pore opening (Figure 6-14). Laser illumination of TMRM leads to intramitochondrial generation of reactive oxygen species (ROS)[316,317], which directly induces mPTP opening, without the requirement for additional stimuli (*e.g.,* H_2O_2). Photoactivation of TMRM has been used to simultaneously induce and visualize mPTP opening in both primary cardiomyocytes and HL-1 cells[167,291]. It has also been demonstrated that TMRM dequenching is accompanied by redistribution of calcein out of the mitochondria, confirming that this corresponds to mPTP opening[167,316].

There are two significant advantages of using the TMRM-based method as an mPTP assay. First, the fact that laser illumination of TMRM can be used to induce mPTP opening simplifies the protocol, as no additional stimuli are required. Second, measurements can also be repeated in multiple, remote fields of view in a single dish, as mPTP opening is limited to cells that are illuminated. This is a significant improvement over the methods applied in calcein-based experiments, which simultaneously induce mPTP opening in the entire cell population.

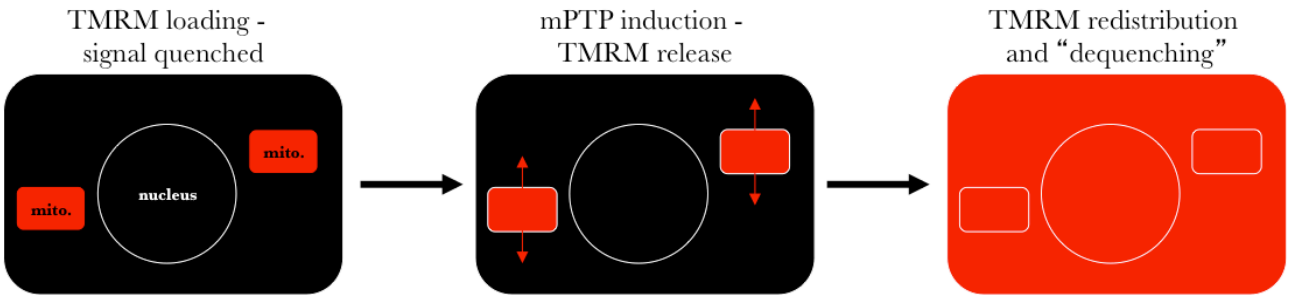


Figure 6-14: TMRM mPTP protocol.

Cells are loaded with TMRM, which is sequestered in the mitochondria, leading to quenching of fluorescence. Laser illumination of TMRM generates intramitochondrial reactive oxygen species, which induces mPTP opening. Permeabilization of the mitochondrial inner membrane leads to redistribution of TMRM into the cytosol, and "dequenching" of TMRM fluorescence.

In order to confirm mitochondrial loading of TMRM and compare the staining patterns of TMRM and calcein, co-localization experiments were performed using TMRM, calcein, and MitoTracker dyes. Representative images are presented on the following pages (Figure 6-15, Figure 6-16, Figure 6-17).

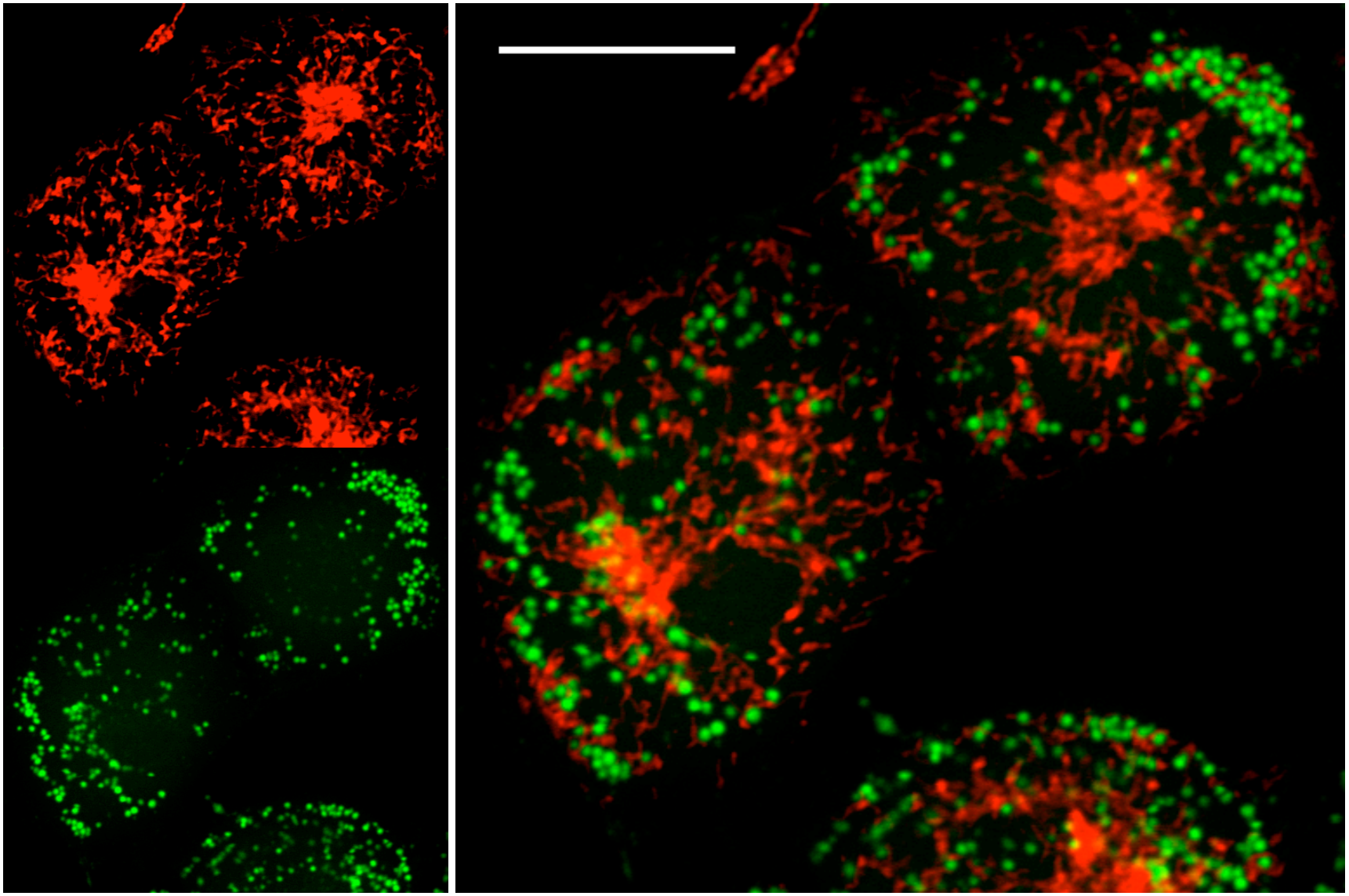


Figure 6-15: TMRM and calcein.
HL-1 cells co-stained with TMRM (red) and calcein (green), demonstrating that the dyes do not co-localize.

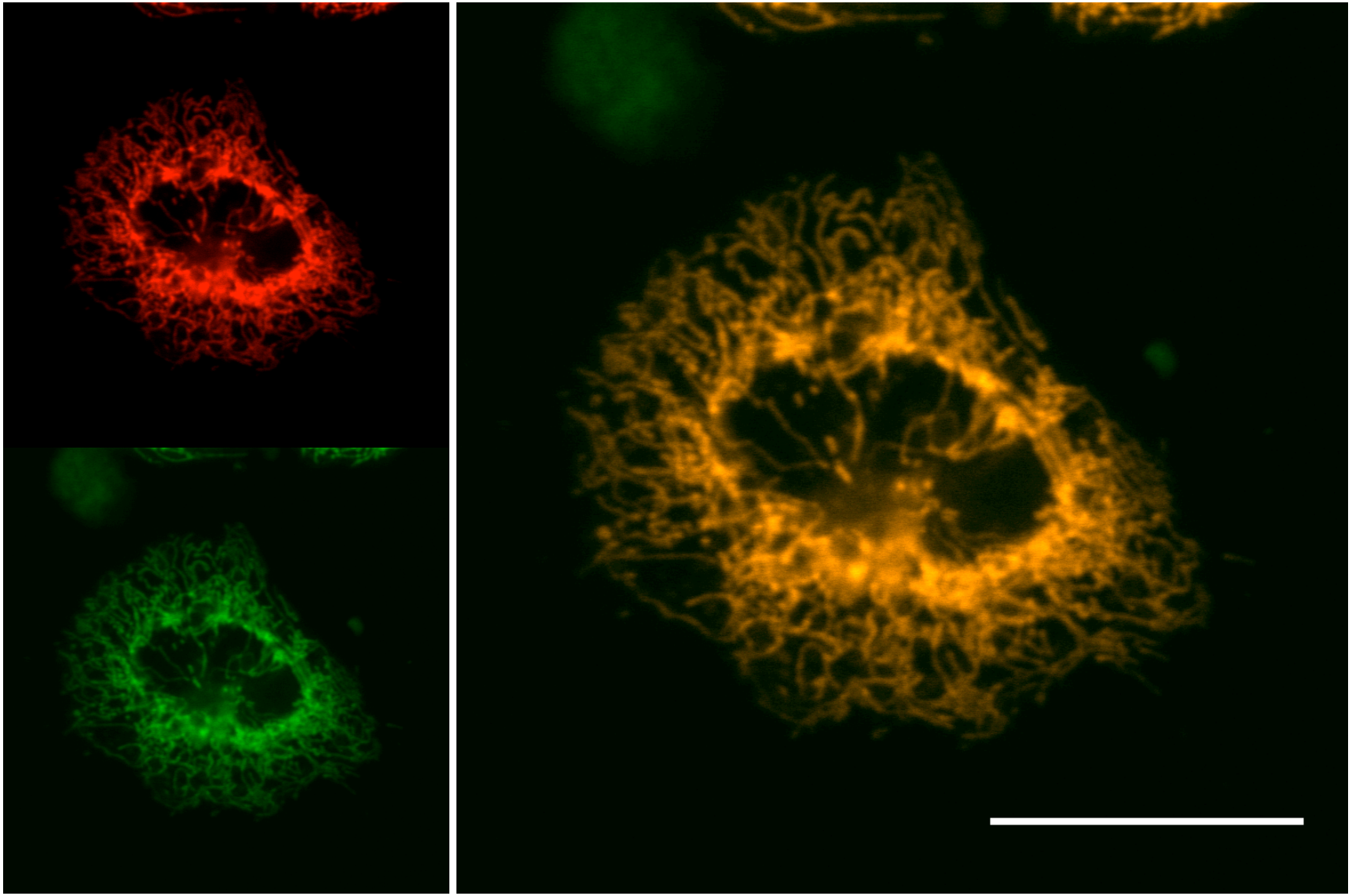


Figure 6-16: MitoTracker Red and Green. HL-1 cell co-stained with MitoTracker Red (red) and MitoTracker Green (green), demonstrating co-localization of both mitochondrial dyes (yellow).

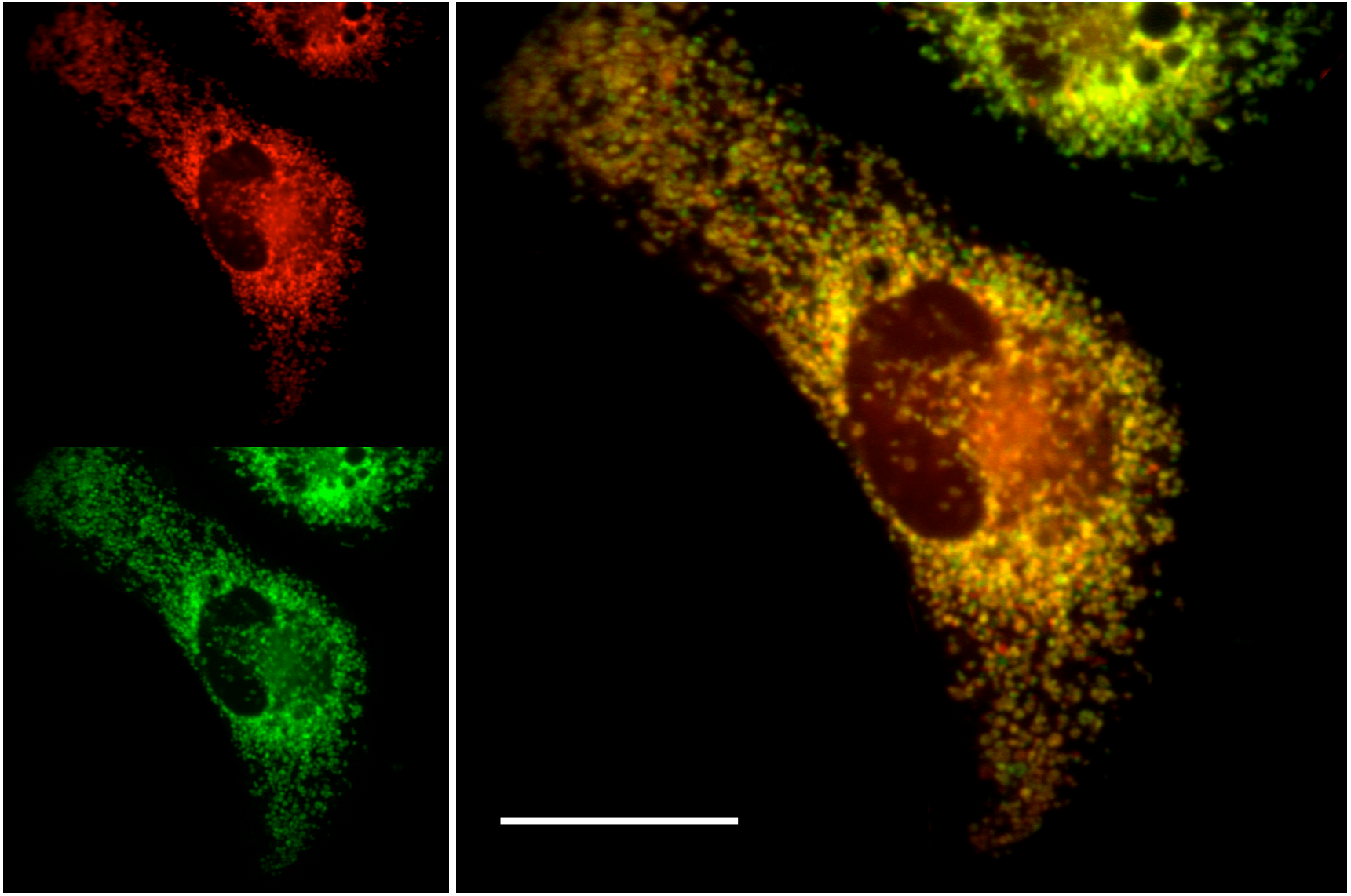


Figure 6-17: TMRM and MitoTracker Green. HL-1 cell co-stained with TMRM (red) and MitoTracker Green (green), demonstrating that TMRM fluorescence corresponds to mitochondria.

6.3.3.2.2. *Protocol and optimization*

HL-1 cells (1 x 10^5) were seeded in 35mm glass-bottom confocal dishes (PAA Labs), and incubated for 48 hours. Cells were loaded with 3μM TMRM (Sigma) in HBSS for 15min at 37°C. After loading, cells were washed with HBSS and transferred to the heated stage of a Zeiss LSM 510 MetaHead confocal microscope, enclosed in an incubator with temperature (37°C) and CO_2 (5%) regulation.

Following a 5min equilibration period without illumination, cells were continuously scanned with a 1.2mW 543nm He-Ne laser to induce mPTP opening (Figure 6-18). Images were acquired at a spatial resolution of 512x512 pixels, with a temporal resolution of 1.97s, for a period of ~8min (240 frames total). Laser power (5%), detector gain, and optical settings were optimized empirically, and remained constant for all experiments. Multiple independent fields of view (2-4) were routinely acquired in each dish.

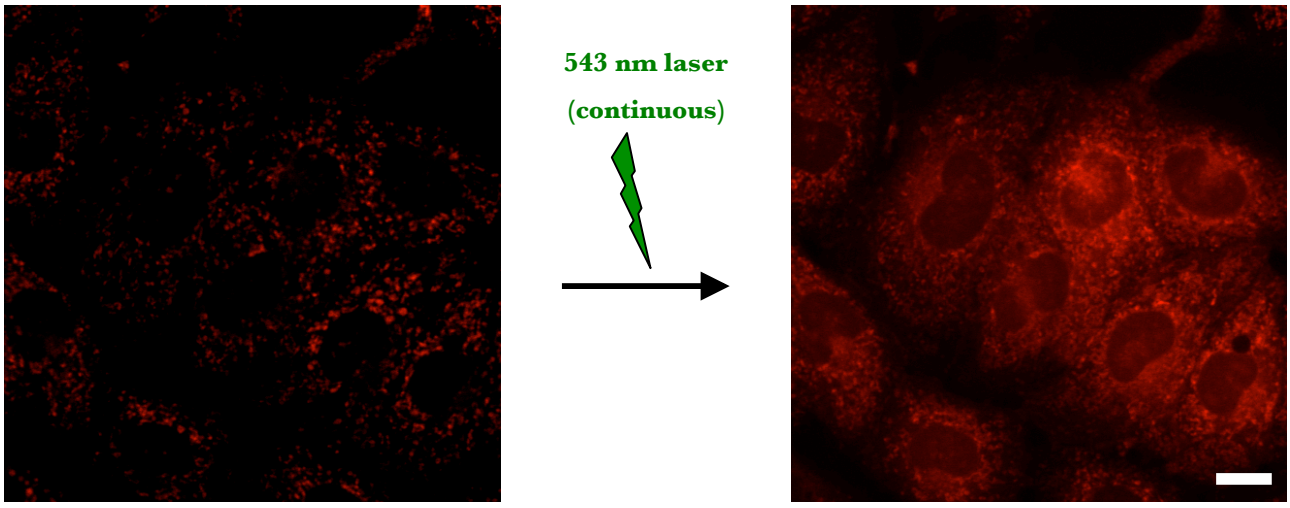


Figure 6-18: TMRM pilot assay.

Representative confocal images demonstrating the TMRM-based mPTP assay in HL-1 cells. At baseline (left), TMRM is sequestered inside the mitochondria, and fluorescence is quenched. Continuous laser illumination leads to induction of mPTP opening and redistribution of TMRM fluorescence (right). Scale bar, 20μm.

Images were processed using Zeiss LAS software and ImageJ (NIH). Polygonal regions of interest (ROIs) were manually drawn around individual cells, and mean fluorescence was calculated for each cell at each timepoint (Figure 6-19). Raw data were transferred to Microsoft Excel for further analysis. The baseline fluorescence (F_0) and maximum fluorescence across all timepoints (F_{max}) were identified for each ROI. The fluorescence intensity corresponding to a 50%-maximal increase was calculated ($F_{50} = F_0 + [F_{max} - F_0]/2$). Finally, the timepoint at which a given ROI exceeded its F_{50} was identified, and used as a measure of time to mPTP opening (t_{50}).

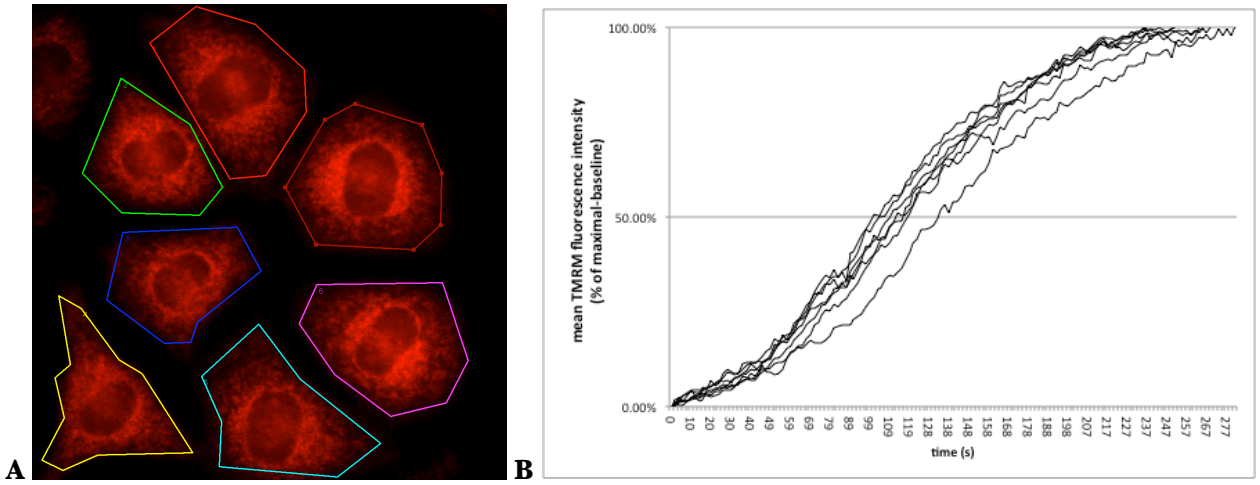


Figure 6-19: Quantification of TMRM fluorescence.

(**A**) Representative image of HL-1 cells at maximum fluorescence, demonstrating regions of interest for quantification of TMRM fluorescence. (**B**) Representative trace of TMRM fluorescence, normalized to baseline and maximal values for each individual cell. The horizontal line at 50% corresponds to F_{50}, and the time at which a given cell crosses this threshold is termed t_{50}.

To validate the model, cyclosporin A (CsA, 0.5μM, Sigma) was added as a positive control during both TMRM loading and imaging. As the reagents are known to be unstable, stock aliquots of both TMRM (3mM) and CsA (1mM) were stored at −20°C, and used for a single day's experiments. Cyclosporin A was found to significantly increase time to mPTP opening, as expected (Figure 6-20).

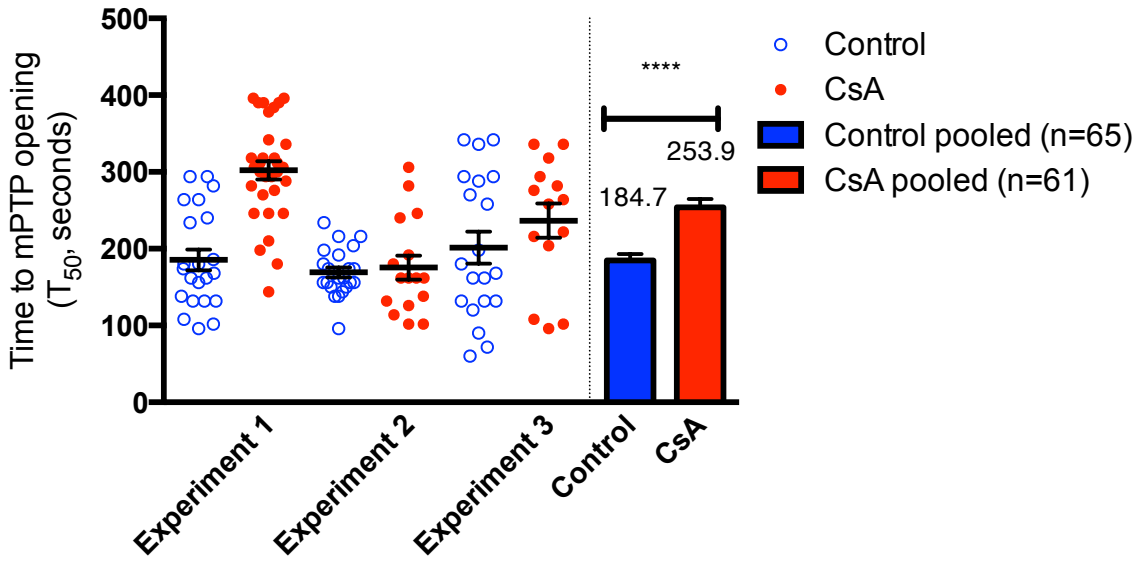


Figure 6-20: mPTP inhibition by cyclosporin A (CsA).

Cells were incubated with 0.5μM CsA, or vehicle control (0.05% v/v ethanol), and mPTP opening was induced by laser illumination of TMRM-loaded cells. Time to mPTP opening (t_{50}) varied within and between samples for both treatment types, but mean t_{50} was 37% higher in CsA-treated cells ($p<0.0001$).

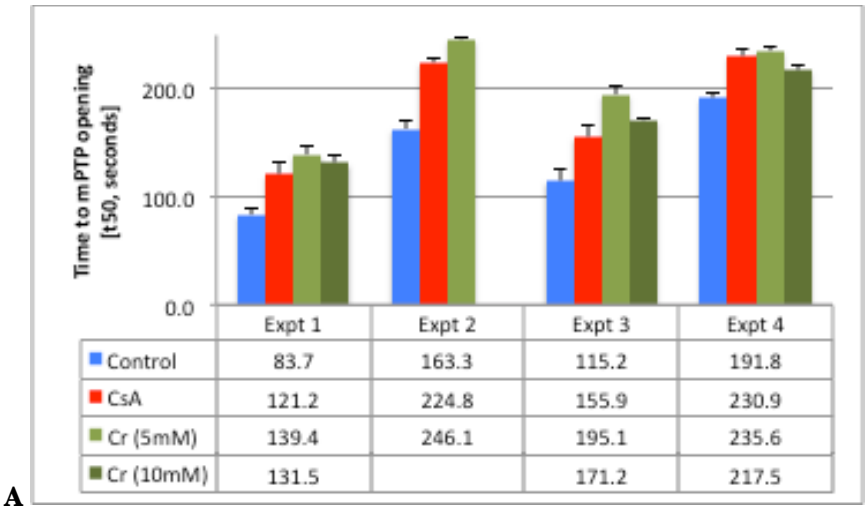
6.3.3.3. Results

The TMRM-based protocol for measurement of mPTP opening was established as described above. The method was validated using CsA as a positive control, demonstrating that inhibition of mPTP opening could be observed as an increase in t_{50}. The subsequent goal of the study was to apply this protocol to creatine-treated cells, in order to determine whether elevation of intracellular creatine would have an effect on mPTP opening.

Four independent, consecutive experiments were performed, comprising 9-16 samples per treatment (Figure 6-21). Absolute values of t_{50} in control samples varied between experiments (84-192s); however, the relative differences between groups were consistent, and results were therefore normalized to control samples for each experiment.

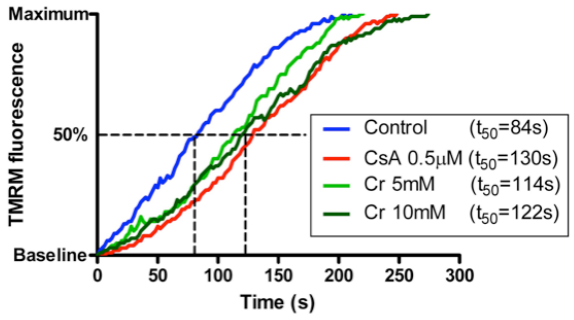
For the following set of experiments, cyclosporin A (0.5μM) was used as a positive control, and delayed mPTP opening to a similar degree as that observed in pilot experiments (mean t_{50}, 136% vs control; $p<0.05$).

Increasing intracellular creatine by 24-hour incubation in 5mM or10mM Cr was found to significantly delay mPTP opening (154% and 145% vs control, respectively; $p<0.01$).

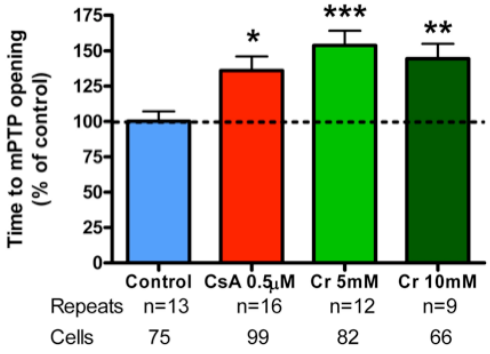


	Expt 1	Expt 2	Expt 3	Expt 4
Control	83.7	163.3	115.2	191.8
CsA	121.2	224.8	155.9	230.9
Cr (5mM)	139.4	246.1	195.1	235.6
Cr (10mM)	131.5		171.2	217.5

A



B



C

Figure 6-21: Elevation of intracellular creatine inhibits mPTP opening.

(**A**) Raw data, demonstrating variation in absolute values of t_{50} between experiments, but consistent relative effect of CsA and creatine treatments. Note that in experiment #2 data were not acquired for cells incubated in 10mM Cr – this was due to a microscope technical failure. (**B**) Representative traces of TMRM fluorescence in individual HL-1 cells from experiment #1, by treatment group. (**C**) Summarized results of 4 independent experiments. Pre-incubation with Cr significantly increased time to mPTP opening. Cyclosporin A, an established mPTP inhibitor, delayed mPTP opening by a similar amount.

6.4. Discussion

The goal of the experiments described in this chapter was to determine whether increasing intracellular creatine is associated with inhibition of the mitochondrial permeability transition pore (mPTP). Initial studies were conducted using calcein to directly visualize mPTP opening. These experiments were unsuccessful, and calcein was surprisingly found to accumulate in lysosomes, rather than mitochondria – this finding should be addressed, since previous studies have used redistribution of calcein as a marker of mPTP opening. Initial reports found that in cells loaded with calcein-AM (without quenching by $CoCl_2$), the signal was distributed uniformly throughout the cytoplasm, but was specifically *not* present in the mitochondria (which were identified by staining with the dye tetramethylrhodamine methyl ester [TMRM])[311,318]. Induction of mPTP opening caused an increase in mitochondrial calcein signal, which was interpreted as direct evidence of calcein influx via the mPTP. However, it was subsequently demonstrated that equimolar concentrations of TMRM quench calcein fluorescence, an effect confirmed in both isolated mitochondria and intact cells[306]. Therefore, it is possible that the perceived increase in calcein fluorescence after mPTP induction may have actually been due to "dequenching" of calcein which was already present in the mitochondria, rather than a genuine influx of calcein. Previous experiments in HL-1 cells co-loaded with calcein and TMRM found that induction of mPTP opening leads to a progressive reduction in calcein signal, in parallel with an increase in TMRM signal[167]. This was interpreted as an indication that the decrease in calcein and increase in TMRM are equivalent measures of mPTP opening in HL-1 cells; however, in light of the quenching properties of TMRM described above, it may be that the redistribution of TMRM fluorescence was simply quenching calcein signal, rather than leading to a genuine change in calcein distribution. This would reconcile the apparent contradiction between the fact that calcein has been used to test mPTP opening in HL-1 cells, while the experiments in this chapter found that, under the same conditions, calcein was loaded into the lysosomes instead.

Since co-localization experiments questioned the validity of calcein release as a marker of mPTP opening in this model, an alternative approach was adopted, using TMRM. The results ultimately demonstrated that moderately elevated creatine inhibits activation of the mitochondrial permeability transition pore, which

would indicate that the cardioprotective effect of creatine may extend beyond its classical role in cellular energetics. The specific mechanism by which this occurs remains to be established, but possible explanations include (1) stabilization of the pore via enzymatic activity of CKmt, (2) improved calcium homeostasis, and (3) substrate-level modulation of F_OF_1-ATP synthase, which has recently been found to play a key role in the permeability transition. These mechanisms are discussed in detail below.

It has been confirmed that mitochondrial creatine kinase (CKmt) does not directly form part of the mPTP complex; however, there is evidence that CKmt stabilizes the pore and prevents its activation. Furthermore, this effect is thought to be dependent on enzymatic activity, as it requires the presence of both CKmt and creatine. Therefore, it is possible that augmenting the cellular creatine pool could strengthen this effect. This effect could be less pronounced in HL-1 cells than *in vivo*, as they express CKmt at a significantly lower level than ventricular cardiomyocytes (0.2 vs ≥2.0 IU/mg protein, respectively). However, our group has demonstrated that incubating HL-1 cells under the loading conditions used in the mPTP assay (5mM creatine for 24h) increases not only total creatine, but also phosphocreatine content (16.5 ± 0.4 nmol/mg protein, vs 5.2 ± 0.2 in control cells)[144], indicating that CK activity in these cells is sufficient to phosphorylate an augmented creatine pool.

An alternative explanation is that inhibition of the mPTP by creatine may simply be a downstream effect of globally improved energetic status. One of the key factors leading to induction of mPTP opening during ischemia/reperfusion is calcium overload, which is primarily attributed to ATP depletion and the resulting inactivation of Ca^{2+}-ATPase pumps. In this context, the additional energy reserves provided by increased phosphocreatine stores, as well as the preservation of ΔG_{ATP} observed during ischemia/reperfusion in CrT-OE hearts, could delay the onset of calcium pump inactivation and preserve calcium homeostasis, which would in turn delay or prevent activation of the mPTP. However, in this context the TMRM-based model of mPTP opening differs from *in vivo* ischemia/reperfusion in two significant respects: (1) the trigger for mPTP opening is local, intramitochondrial ROS generation, which would not depend on extramitochondrial calcium, and (2) the laser-generated ROS burst is a discrete, immediate stimulus, as opposed to the gradual, cumulative effect of ischemia followed by reperfusion; as such, it is unlikely that cytosolic calcium homeostasis

would be disturbed prior to mPTP opening. Therefore, while improved calcium handling remains a possible mechanism for the cardioprotective effect observed *in vivo*, it is unlikely to explain the *in vitro* findings in HL-1 cells loaded with TMRM.

A recently published paper provides evidence that the mPTP is formed by dimers of F_OF_1-ATP synthase[282]. The study also analyzed whether the direction of the reaction catalyzed by ATP synthase had an effect on mPTP opening. Isolated mitochondria were incubated under conditions which favored either ATP synthesis (respiratory substrates, ADP, and hexokinase/glucose to remove ATP), or ATP hydrolysis (ATP, and CK/phosphocreatine to replenish ATP). Mitochondrial sensitivity to calcium-induced pore opening was decreased two-fold by stimulation of ATP hydrolysis. Since creatine elevation augments intracellular phosphocreatine stores, this finding could provide a novel mechanism for creatine-mediated inhibition of mPTP via substrate-level regulation of the ATP synthase. It is worth noting, however, that the hypothesis that F_OF_1-ATP synthase is the structural unit of the mPTP is a relatively novel concept, and as such requires validation in further studies. Furthermore, to unequivocally prove that the F_OF_1-ATP synthase is required for mPTP formation, it would be necessary to produce genetic knockout models similar to those used for ANT, VDAC, or CypD; given the central role of the complex in cellular energy production, this is a considerable challenge.

Finally, these results should be interpreted with a degree of caution, as there are differences between the *in vitro* model of mPTP activation and *in vivo* myocardial ischemia/reperfusion injury. HL-1 cells are a cardiac-derived line, but they are structurally and metabolically different from ventricular cardiomyocytes. Furthermore, myocardial ischemia/reperfusion injury comprises a variety of disturbances, including oxygen and nutrient deprivation, which is considerably more complex than TMRM-mediated generation of reactive oxygen species. While the results clearly demonstrate that elevated intracellular creatine can, in isolation, inhibit mPTP activation in cardiac-derived cells, they cannot conclusively determine whether this effect occurs *in vivo*, and if so, whether it is sufficient to contribute to the protective effect observed in CrT-OE mice. Further studies can be conducted to elucidate the *in vivo* mechanism, as described below.

6.5. Conclusions and future work

The finding that creatine inhibits activation of the mitochondrial permeability transition pore *in vitro* indicates that the beneficial effect of creatine may extend beyond its role in cellular energetics. This provides further support for the finding that, *in vivo,* moderately elevated creatine protects the heart against ischemia/reperfusion injury.

To definitively confirm whether mPTP inhibition plays a role in creatine-mediated cardioprotection in the intact heart, it would be necessary to conduct further experiments using more refined methods, such as the "Hot-DOG" assay, which allows direct measurement of mPTP opening in the *ex vivo* perfused heart by measuring mitochondrial uptake of H^3-tagged deoxyglucose[290]. If hearts from CrT-OE mice were found to be resistant to mPTP activation, and the degree of mPTP inhibition correlated inversely with the extent of ischemia/reperfusion injury, this would provide additional evidence that inhibition of the mPTP plays a significant role in creatine-mediated cardioprotection. If this was found to be the case, it would provide rationale for further experiments into the mechanism by which creatine inhibits the mPTP, and identification of potential therapeutic applications. Since mPTP inhibition has been shown to be beneficial in human myocardial infarction[293], it is tempting to speculate whether increasing intracellular creatine would have a similar effect in clinical practice. While this could potentially be accomplished using genetic techniques, it is unlikely that these would act rapidly enough to be effective in the acute setting – therefore, administration of creatine with (as-yet unidentified) small molecules specifically increasing creatine uptake could be a more promising target.

The findings discussed in this chapter were included in a publication describing the cardioprotective effect of moderately elevated creatine in ischemia/reperfusion injury[144].

7. SUMMARY AND FUTURE WORK

The ultimate goal of the work described in this thesis is to determine whether increasing enzymatic activity in the creatine kinase (CK) system is beneficial in models of heart disease. Initial experiments were performed *in vitro* in cultured cells. This served two purposes, namely to validate the CK expression constructs prior to generation of transgenic mice, and to test the effects of CK overexpression on cell viability in a model of simulated ischemia/reperfusion injury. Hemagglutinin-tagged CKmt, CK-M, and CK-B were expressed in both HL-1 cardiomyocytes and HEK293 cells, and enzymatic activity of each isoenzyme was confirmed. In addition, immunocytochemistry was performed to determine the subcellular localization of CKmt, which was found to be expressed in the mitochondria, as expected. Antibiotic selection was used to generate stably transfected HEK293 cell lines, which can be used for future experiments; however, attempts at generating stable lines in HL-1 cells, or lines expressing a CKmt-EGFP fusion protein, proved unsuccessful.

Once the expression constructs were validated *in vitro*, the next step was to determine the effect of CK overexpression in a model of simulated ischemia/reperfusion injury in cardiomyocyte-derived HL-1 cells. Extensive optimization was performed to empirically determine the appropriate experimental conditions, using epifluorescence microscopy and subsequently flow cytometry to quantify cell death. Once the protocol was established, it was validated using a positive control, the caspase inhibitor zVAD-FMK. Transfection with CKmt was found to significantly reduce cell death in this model, by approximately 32%. There was no evidence for a protective effect in cells transfected with the cytosolic CK isoenzymes; this is of particular interest with respect to CK-M, which has recently been shown to reduce myocardial necrosis in *ex vivo* ischemia/reperfusion[146]. This may indicate that the *in vitro* model is not an accurate representation of ischemia/reperfusion injury in the intact heart; alternatively, there are methodological differences which could specifically mask a protective effect of CK-M, as discussed in Chapter 3. Further work is being planned in this model, and assays will be repeated to verify the observed results.

Since CKmt was found to be the most promising target *in vitro*, it was the first CK isoenzyme selected for generation of transgenic mice. This was accomplished using a relatively novel strategy, using the enzyme PhiC31 integrase to insert a single transgene copy at the ROSA26 locus in embryonic stem cells, followed by blastocyst injection to generate chimeric founder mice. The main advantage of this approach is that it ensures integration of a single transgene copy at a known genomic locus. This reduces the risk of unpredictable effects of copy number and/or integration site, which in turn negates the need for multiple lines to be generated and screened in parallel, as is the case for traditional random integration approaches. The efficiency of blastocyst injections was relatively low, but chimeric founder mice capable of producing transgenic offspring were ultimately generated. The transgene was expressed at the mRNA and protein levels in a cardiac-specific manner, but did not drive a significant increase in total CKmt protein or activity. In an attempt to overcome this limitation, mice were bred to homozygosity. A further increase in transgene expression was observed, and the significant increase in CKmt activity (~30%) was deemed sufficient for further experiments. Initial phenotyping indicated that these mice grow and develop normally, and exhibit normal cardiac function at baseline and under increased workload. The only significant difference, relative to wild-type littermates, was a decrease in citrate synthase activity, which may indicate a lower mitochondrial volume in these mice. This is a plausible finding, as discussed in section 4.4.3.2, but requires validation by other methods to confirm whether there are genuine changes in mitochondrial number or structure in these mice. Finally, subcellular localization of transgenic CKmt was assessed by electron microscopy, which confirmed that the protein was being expressed in the mitochondria; however, further work is required to resolve the specific intramitochondrial location.

Further transgenic models were established to overexpress the cytosolic isoenzymes, CK-M and CK-B, in the myocardium. While the relatively modest level of overexpression observed in the CKmt model was deemed sufficient due to the specific localization of CKmt in the mitochondrial intermembrane space, higher expression levels would be desirable for the cytosolic isoenzymes. Therefore, a traditional pronuclear microinjection approach was used to allow for random integration of multiple transgene copies. Founder mice were generated for both CK-M and CK-B lines, and gave rise to multiple lines of transgenic offspring with different integration events (as evidenced by differences in transgene copy number, as well as M-FISH

experiments in the CK-M line). There was no clear increase in total CK-M mRNA, protein, or activity in mice with 2 copies of the transgene; however, in mice with 6 or 8 copies, a several-fold increase in expression was observed. In CK-B mice with 2 or 3 copies, there was a pronounced increase in total CK-B mRNA (due to relatively low expression of the endogenous CK-B transcript, compared to CKmt or CK-M), but this was not sufficient to drive a large increase in enzymatic activity, as CK-MB activity increased by <70%. In addition, a single mouse was found to have a distinct integration event, with an estimated copy number of ~30. This may be a more promising line for the CK-B model, as offspring of this mouse were found to have markedly higher myocardial activities of CK-MB and CK-BB.

The results of molecular validation in all lines (CKmt, CK-M, and CK-B) are summarized in Table 7-1.

			mRNA expression			Total protein	Enzymatic activity				
Line	Group	Transgene copy no.	Transgenic (relative)	Total	Endogenous		Total CK	CKmt	CK-MM	CK-MB	CK-BB
CKmt	Tg+/-	1	n/a	141%	102%	114%	106%	113%	101%	115%	108%
	Tg+/+	2	251%	186%	110%	135%	109%	127%	98%	125%	114%
CK-M	A	2	n/a	136%	137%	158%	90%	70%	100%	85%	77%
	B	6	253%	382%	130%	351%	232%	136%	287%	143%	125%
	C	8	308%	527%	156%	331%	243%	118%	309%	200%	166%
CK-B	A	2	n/a	3410%	138%		85%	69%	85%	167%	95%
	B	3	104%	4471%	88%		97%	90%	95%	168%	106%
	C	~30					159%	90%	95%	1008%	805%

Table 7-1: Summary of molecular validation of all CK-overexpressing transgenic lines.

Data are expressed as the percentage of mean in wild-type littermate controls, except for expression of transgenic mRNA, which is expressed relative to the transgenic line with the lowest copy number for each model. Parameters which were significantly increased are highlighted ($p \leq 0.05$). Note that, although protein expression is greatly increased in CK-M mice, this is based on a relatively small sample size (see Figure 5-27).

Based on the results of molecular validation, it seems unlikely that transgenic mice with low copy numbers (2-3) will be suitable models for studying the effects of CK-M and CK-B overexpression. Therefore, future work will primarily focus on expanding the CK-M line with 6 copies, and the CK-B line with ~30 copies. Since both of these lines, as well as the CKmt mice, were generated on a mixed genetic background, they will be backcrossed onto a pure C57BL/6 background prior to further experiments. In an effort to expedite this

process, microsatellite markers will be used to estimate the degree of congenicity with respect to C57BL/6 of individual mice in these lines, to select the most suitable candidates for backcrossing.

Once these lines are established on a pure genetic background, it will be possible to perform experiments to determine whether overexpression of CK isoenzymes is beneficial in models of heart disease. In the first instance, the response to acute ischemia/reperfusion injury will be evaluated; subsequent experiments will be performed to determine whether CK overexpression is beneficial in models of chronic heart failure. It is tempting to speculate that both CKmt and CK-M could be protective in acute ischemia/reperfusion, as CKmt emerged as the most promising target in the *in vitro* model described in this thesis, while CK-M overexpression has been recently shown to reduce ischemia/reperfusion injury by another group[146]. It is more difficult to predict the effect of CK-B overexpression, as comparatively little is known about the role of this isoenzyme in the myocardium. Nonetheless, it will be interesting to see whether CK-B has a similar effect to CK-M, as this would indicate whether increasing total CK activity in the cytosolic compartment is beneficial in itself, or whether any effect is dependent on association of CK to sarcomeric structures, which is a feature of CK-M but not CK-B. Finally, there is reason to suspect that increasing the activity of multiple components of the CK system, particularly combining increased CK activity with increased substrate availability, could have additive effects. Our group have previously developed and validated a model of mice overexpressing the creatine transporter[144], which could be crossed with the mice described in this thesis to generate double-transgenic models for further study.

In addition to the work on models of CK overexpression, a series of experiments was performed to determine whether increasing intracellular creatine can inhibit opening of the mitochondrial permeability transition pore (mPTP). Our group has shown that moderate elevation of myocardial creatine protects the heart against ischemia/reperfusion injury, and it is known that mPTP opening plays a significant role in this process. There is evidence that the CK system can regulate mPTP opening, summarized in section 6.1.3. Therefore, it is possible that the protective effect of creatine is partially mediated by inhibition of the mPTP. Experiments were performed in cardiac-derived HL-1 cells, and incubation in extracellular creatine was optimized to achieve a similar increase to the "therapeutic range" observed *in vivo*. Initial attempts at

measuring mPTP opening used a calcein-based method, but this was found to yield variable results, which may have been due to ineffective mitochondrial loading of the dye. An alternative strategy was adopted, using the rhodamine dye TMRM to both induce and visualize mPTP opening. This protocol was successfully optimized, and used to demonstrate that creatine inhibits mPTP opening in HL-1 cells. This series of experiments was reported in our group's publication on mice overexpressing the creatine transporter[144]. Further experiments should be performed using cells transfected with the constructs described in Chapter 3, to determine whether overexpression of CK isoenzymes can have a similar effect (with or without creatine elevation). This would provide convincing evidence for a mechanistic link between the CK system and mPTP opening, and reinforce the case for further research into augmentation of CK activity as a therapeutic target in cardiac disease.

In summary, the experiments described in this thesis have generated a wide range of *in vitro* and *in vivo* models of creatine kinase overexpression. While a considerable amount of research has been devoted to determining whether loss of function in the CK system plays a causal role in cardiac pathology, the ultimate goal should be to focus on the opposite effect – namely, whether targeted augmentation of the CK system can improve the prognosis of patients with heart disease. The transgenic mice overexpressing CKmt, CK-M, and CK-B are a particularly promising tool in this regard, as they can be used for experiments in models of human disease, such as coronary artery ligation. This should permit a comprehensive study into the effects of increasing the activity of individual components of the myocardial CK system, which could potentially identify novel treatment targets. If this is successful, a considerable amount of translational research would still need to be conducted before similar approaches could be adopted in a clinical setting – this would require significant advances in gene therapy and/or identification of small molecules which specifically increase the activity of individual CK isoenzymes or creatine uptake. Therefore, while it is unrealistic to expect this work to have any significant clinical impact in the near future, it will finally be possible to definitively assess the putative therapeutic potential of the myocardial creatine kinase system, and the findings of these experiments may guide future research in the field.

APPENDICES

A. SUPPLEMENTARY MATERIALS AND METHODS

A.1. PCR protocols

Cloning PCR

Reaction mixture

Component	Unit	Stock	Final	Volume (µl)
HF Buffer	-	10x	1x	5.00
F primer	µM	100	0.5	0.25
R primer	µM	100	0.5	0.25
dNTP	mM (ea.)	25	0.2	0.40
Phusion polymerase	U/µl	2	1	0.50
DNA				1.50
H_2O				42.10
Total				**50.00**

Cycling conditions

Step	Temperature	Time (mm:ss)	Cycles
Activation	95°	10:00	
Denaturation	95°	00:30	15
Annealing	67.5-60.5° (-0.5°/cycle)	00:30	
Extension	72°	00:45	
Denaturation	95°	00:30	13
Annealing	60°	00:30	
Extension	72°	00:45	
Final extension	72°	10:00	

Genotyping PCR

Reaction mixture

Component	Unit	Stock	Final	Volume (µl)
Immolase buffer	-	10x	1x	2.00
F primer	µM	10	0.5	1.00
R primer	µM	10	0.5	1.00
dNTP	mM (ea.)	25	0.2	0.16
Immolase polymerase	U/µl	5	1	0.20
$MgCl_2$	mM	50	3	1.20
DNA				5.00
H_2O				7.44
Total				**20.00**

Cycling conditions

Step	Temperature	Time (mm:ss)	Cycles
Activation	95°	10:00	
Denaturation	95°	00:30	30
Annealing	70-55.5° (-0.5°/cycle)	00:30	
Extension	72°	00:30	
Final extension	72°	10:00	

A.2. PCR primers

Genotyping and qPCR primers			
Name	**Notes**	**Sequence (5'-3')**	**Length**
Polr2a_F	qPCR ref (mRNA)	TGTGCAGGAAACATGACCGA	20
Polr2a_R	qPCR ref (mRNA)	GAAGCAGACACAGCGCAAAA	20
36B4_F	qPCR ref (mRNA)	AGATTCGGGATATGCTGTTGG	21
36B4_R	qPCR ref (mRNA)	TCGGGTCCTAGACCAGTGTTC	21
ApoB_F (oIMR1544)	qPCR ref (gDNA)	CACGTGGGCTCCAGCATT	18
ApoB_R (oIMR1545)	qPCR ref (gDNA)	TCACCAGTCATTTCTGCCTTTG	22
Rosa26_F	Control / WT allele for CKmt	ATACCTTTCTGGGAGTTCTCTGCTGC	27
Rosa26_R (oIMR0316)	Control / WT allele for CKmt	GGAGCGGGAGAAATGGATATG	22
HA_R	R primer for all Tg-specific PCRs	TGCGTAATCTGGAACATCGT	20
Ckmt2_ex9-10_F		TCGGCAGATCAGAGGTTGAG	20
Ckmt2_UTR_R		ACCCATAAACTTGGAGGGATAAA	23
Ckmt2_ex8-9_F		AGCAAGGATCCACGCTTTTCT	22
Ckmt2_ex9_R		TCTGCCGATCCGATCTATGTT	22
Ckmt2_ex4_F	amplifies Tg and WT sequence	TGTCATCAAACTAAGGCACAATGGC	25
Ckmt2_ex5_R	amplifies Tg and WT sequence	GCCAGTGCGTACCCGAGAGG	20
Ckm&b_ex7-8_F		GCACAGGTGGCGTGGACA	18
Ckm_UTR_R		GGCACCAGCGCACACT	16
Ckm_ex5_F		CTGAAGAGCATGACGGAGCA	20
Ckm_ex6-5_R		TTGTTGTCGTTGTGCCAGATG	21
Ckm_ex2_F		TCAGGAGGAGTACCCAGACC	20
Ckm_ex2_R		ACATCGTCCAGAGTGAAGCC	20
Ckb_UTR_R		TAGGAAGCGGCAGCCTGATG	20
Ckb_ex6-7_F		CGGCCTCACTCAGATCGAAACT	22
Ckb_ex8-7_R		TGTCCACGCCACCTGTGC	18
Ckb_ex8_F		CTCGGAGGTGGAACTGGTG	19
Ckb_ex8_R		CATCGATTGCCTGACCCTG	19
Ckb_ex3_F	amplifies Tg and WT sequence	TTATTGAGGAGCGGCACGGCGGCTA	25
Ckb_ex4_R	amplifies Tg and WT sequence	CAGTGCGGGGGGAGACAGAAGCC	23

Cloning primers		
Name	**Sequence (5'-3')**	**Length**
Ckmt2_F_HindIII/Kozak	GACCAAGCTTAAGAAGAAGGATGGCCAGTGCCTTCTCAAAGTTGCT	46
Ckmt2_R_KpnI	CTAGGGTACCGACTTCCTGCCAAACTGAGGCA	32
Ckmt2_R_HA/stop/XbaI	CTAGTCTAGATCAAAGAGCGTAATCTGGAACATCGTATGGGTACTTCCTGCCAAACTGAGGCA	63
Ckmt2_F_SalI/Kozak	GGGGGTCGACACCATGGCCAGTGCCTTCTC	30
Ckmt2_R_HA/stop/HindIII	GGGGAAGCTTCATGCGTAATCTGGAACATCGTATGGGTACTTCCTGCCAAACTGAGG	57
Ckm_F_NheI/SalI/Kozak_c12t	GGGGCTAGCGTCGACACCATGCCGTTCGGTAACACCCAC	39
Ckm_R_HA/stop/XhoI	GGCCTCGAGCTATGCGTAATCTGGAACATCGTATGGGTACTTCTGCGCGGGGATCATGT	59
Ckb_F_NheI/SalI/Kozak	CCCCGCTAGCGTCGACACCATGCCCTTCTCCAACAGCCAT	40
Ckb_R_HA/stop/KpnI/HindIII	CCGAAGCTTGGTACCTATGCGTAATCTGGAACATCGTATGGGTACTTCTGGGCCGGCATGAGGTC	65

Primer pairs - by transgenic line / reaction					
Mouse line	**Reaction**	**F primer**	**R primer**	**Product (bp)**	**Notes**
CKmt	**Genotyping**	Ckmt2_ex9-10_F	HA_R	158	(+) in Tg+/- & Tg+/+
		Rosa26_F	Rosa26_R	508	(+) in WT & Tg+/-
	qPCR - Tg	Ckmt2_ex9-10_F	HA_R	158	
	qPCR - End.	Ckmt2_ex9-10_F	Ckmt2_UTR_R	159	
	qPCR - Total	Ckmt2_ex8-9_F	Ckmt2_ex9_R	126	
	Tg copy # qPCR	Ckmt2_ex9-10_F	HA_R	158	(no total copy qPCR)
CK-M	**Genotyping**	Ckm&b_ex7-8_F	HA_R	209	(+) in all Tg
		Rosa26_F	Rosa26_R	508	ctrl: (+) in all samples
	qPCR - Tg	Ckm&b_ex7-8_F	HA_R	209	
	qPCR - End.	Ckm&b_ex7-8_F	Ckm_UTR_R	227	
	qPCR - Total	Ckm_ex5_F	Ckm_ex6-5_R	143	
	Total DNA copy # qPCR	Ckm_ex2_F	Ckm_ex2_R	120	
	Tg DNA copy # qPCR	Ckm&b_ex7-8_F	HA_R	209	
CK-B	**Genotyping**	Ckm&b_ex7-8_F	HA_R	209	(+) in all Tg
		Rosa26_F	Rosa26_R	508	ctrl: (+) in all samples
	qPCR - Tg	Ckm&b_ex7-8_F	HA_R	209	
	qPCR - End.	Ckm&b_ex7-8_F	CKb_UTR_R	222	
	qPCR - Total	Ckb_ex6-7_F	Ckb_ex8-7_R	215	
	Total DNA copy # qPCR	Ckb_ex8_F	Ckb_ex8_R	92	amplifies 2 pseudogenes!
	Tg DNA copy # qPCR	Ckm&b_ex7-8_F	HA_R	209	
qPCR ref (mRNA expression)		Polr2a_F	Polr2a_R	117	
qPCR ref (gDNA copy number)		ApoB_F	ApoB_R	74	

A.3. Quantitative real-time PCR protocols

Quantitative real-time PCR with reverse transcription (mRNA expression)								
Reaction mixture					**Cycling conditions**			
Component	**Unit**	**Stock**	**Final**	**Volume (µl)**	**Step**	**Temperature**	**Time (mm:ss)**	**Cycles**
SYBR RT Master Mix	-	2x	1x	5.00	Reverse transcription	50°	10:00	
Forward primer	µM	50	0.625	0.06	Activation	95°	5:00	
Reverse primer	µM	50	0.625	0.06	Denaturation	95°	00:10	40
iScript RT				0.20	Annealing/extension	58°	00:30	
H_2O				2.68	[Read SYBR Green]			
RNA (pre-diluted)	ng/µl	1	0.2	2.00	Denaturation	95°	00:10	
Total				**10.00**	Melt curve [Read SYBR Green]	65-90° (+0.5°/step)	00:05	

Quantitative real-time PCR without reverse transcription (DNA copy number)								
Reaction mixture					**Cycling conditions**			
Component	**Unit**	**Stock**	**Final**	**Volume (µl)**	**Step**	**Temperature**	**Time (mm:ss)**	**Cycles**
SYBR RT Master Mix	-	2x	1x	5.000	Activation	95°	10:00	
Forward primer	µM	50	0.625	0.125	Denaturation	95°	00:15	40
Reverse primer	µM	50	0.625	0.125	Annealing/extension	60°	01:00	
H_2O				2.750	[Read SYBR Green]			
DNA (pre-diluted)	ng/µl	2.5	0.5	2.000	Denaturation	95°	00:15	
Total				**10.000**	Melt curve [Read SYBR Green]	65-95° (+0.5°/step)	00:05	

A.4. Antibodies

	Western blotting					
	Target	**Host species**	**Detection**	**Manufacturer**	**Product number**	**Dilution**
Primary antibodies	Hemagglutinin tag	Rat	-	Roche	11867431001	1:200,000
	beta-tubulin	Rabbit	-	Abcam	ab6046	1:5,000
	alpha-actinin	Mouse	-	Sigma	A7811	1:10,000
	CKmt	Rabbit	-	Abgent	AP7072b	1:10,000
	CK-M	Goat	-	Santa Cruz	sc-15161	1:1,000
Secondary antibodies	Rat IgG	Rabbit	HRP	Dako	P044901	1:10,000
	Rabbit IgG	Goat	HRP	Santa Cruz	sc-2030	1:10,000
	Mouse IgG	Goat	HRP	Promega	W4021	1:10,000
	Goat IgG	Rabbit	HRP	Abcam	ab6741	1:10,000

	Immunocytochemistry					
	Target	**Host species**	**Fluorophore**	**Manufacturer**	**Product number**	**Dilution**
Primary antibodies	Hemagglutinin tag	Rat	-	Roche	11867431001	1:1500
	Complex IV	Mouse	-	Abcam	ab14744	1:100
	alpha-MHC	Mouse	-	Abcam	ab50967	1:200
Secondary antibodies	Rat IgG	Goat	Alexa546	Molecular Probes	A-11081	1:200
	Mouse IgG	Goat	Alexa488	Molecular Probes	A-11001	1:400

A.5. Solutions and media

A.5.1. Media and antibiotics for bacterial culture

Culture media (acquired from AGTC Bioproducts) were prepared in distilled water and autoclaved before use. Agar was poured into bacteriological plates in a sterile fume hood. If required, antibiotics were added after cooling media to <60°C.

LB Agar (Lennox, AG-1083) – 35g per 1000ml dH_2O

1.0% w/v	Tryptone
0.5% w/v	NaCl
0.5% w/v	Yeast extract
1.5% w/v	Bacteriological agar

pH 7.0 ± 0.2 at 25°C

Luria broth (Miller's LB broth, AG-1551) – 25g per 1000ml dH_2O

1.0% w/v	Tryptone
1.0% w/v	NaCl
0.5% w/v	Yeast extract

pH 7.0 ± 0.2 at 25°C

Antibiotics

The following concentrations were used, unless otherwise specified:

Ampicillin	100µg/ml
Kanamycin	50µg/ml
Geneticin	200µg/ml
Penicillin	100U/ml
Streptomycin	100µg/ml

A.5.2. Solutions for nucleic acid work

Ear-notch lysis buffer

100mM	EDTA
50mM	Tris-HCl, pH 8
1%	SDS
200mM	NaCl

HotSHOT extraction buffer

25mM	NaOH
0.2mM	EDTA
pH 12	

HotSHOT neutralization buffer

40mM	Tris-HCl
pH 5	

TE

10mM	Tris-HCl
1mM	EDTA
pH 8	

T0.1E

10mM	Tris-HCl
0.1mM	EDTA
pH 8	

TBE

89mM	Tris borate, pH 8.3
2mM	EDTA

A.5.3. Solutions for protein work

RIPA extraction buffer

5ml	RIPA lysis buffer (Sigma R0278), consisting of:	
	150mM	NaCl
	1.0% v/v	IGEPAL® CA-630
	0.5% w/v	Sodium deoxycholate
	0.1% w/v	SDS
	50mM	Tris
	pH 8	
1mM	DTT	
1x	Protease inhibitor cocktail (Roche, Germany)	

Laemmli western blot loading buffer (4 x)

0.25M	Tris-HCl, pH 6.8
6% w/v	SDS
40% v/v	Glycerol
20% v/v	β-mercaptoethanol
0.04% v/v	Bromophenol blue

Tris-HEPES running buffer (Pierce 28368)

0.1M	Tris
0.1M	HEPES
0.87% w/v	SDS
pH 8	

Transfer buffer

39mM	Glycine
48mM	Tris-base
0.0375% w/v	SDS
20% v/v	Methanol

B. GENERATION OF TRANSGENIC MODELS

B.1. Transgenics report: CKmt-OE

THE WELLCOME TRUST CENTRE FOR HUMAN GENETICS

The Henry Wellcome Building, Roosevelt Drive, Oxford, OX3 7BN
Tel: +44 (0)1865 287 836 Fax: +44 (0)1865 287 501
transgenics@well.ox.ac.uk www.well.ox.ac.uk

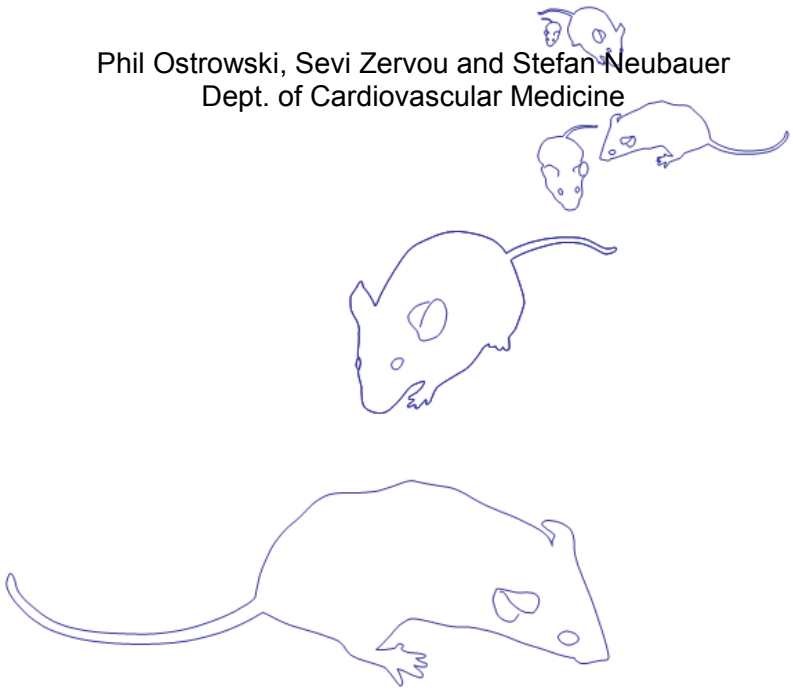
UNIVERSITY OF OXFORD

Documentation

A C G G G C T G A A A T G T T T T C A G T A A C A C A G T C T A A T G G C G G T C A G T A C A

Generation of a transgenic model harbouring a construct expressing *Ckmt2* under the control of the alpha-MHC promoter targeted to the *Rosa26* locus

Phil Ostrowski, Sevi Zervou and Stefan Neubauer
Dept. of Cardiovascular Medicine



Date: 14-07-2011

Summary

A transgenic construct consisting of the mouse Ckmt2 gene under the control of the alpha-MHC promoter was cloned into the integrase mediated cassette exchange vector, CB92. This vector was then transfected into ES cells together with PhiC31 integrase and recombinant clones were obtained which harboured the transgenes within the *Rosa26* locus. Recombinant clones were then injected into blastocysts and chimeras were generated.

Methodology

The PhiC31 integrase can be used to catalyse the unidirectional recombination between specific attB and attP sequences and can thus be used for the high efficiency insertion of transgenic constructs into defined locations within the genome. In contrast to conventional transgenic technology which relies on random insertion, models generated with this integrase are more defined, reliable and more meaningful comparative studies can be carried out for the functional analysis of mutation and polymorphism.

An ES cell line has been targeted at the *Rosa26* locus with a hygromycin selection cassette, within which PhiC31 attP sites flank the open reading frame of the hygromycin cassette. This ES cell line can be co-transfected with an incoming transgene, harbouring an attB site and a promoter-less neomycin selection cassette at the 5' end and a further attB site at the 3' end, together with a vector delivering the PhiC31 integrase. Recombination between the attP and attB sites leads to the exchange of the hygromycin open reading frame for neomycin and the integration of the transgene DNA (see figure 1).

A generic vector, CB92, has been constructed into which transgenic vectors can be cloned via a polylinker, making them suitable for integrase mediated insertion into the *Rosa26* locus. This shuttle vector contains an H19 insulator which helps maintain the expression characteristics of transgenic cassettes.

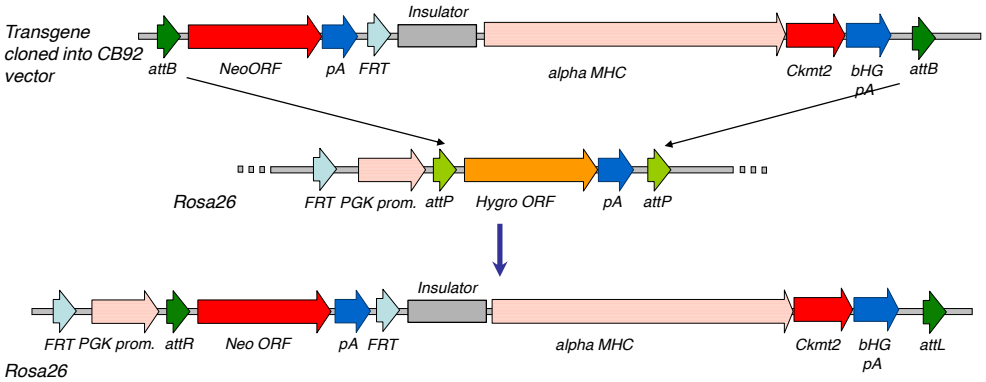


Figure 1 – principal of PhiC31 integrase mediated cassette exchange.

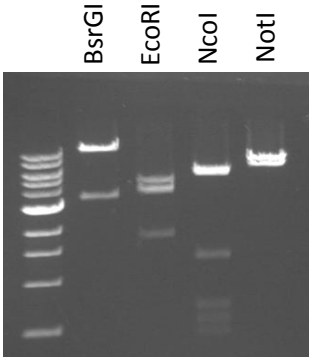
Cloning

The construct was received as a plasmid and the trangene was excised via NotI digestion. This fragment was cloned in the sense orientation, relative to the *Rosa26* gene, into the exchange vector CB92 via the NotI site within the polylinker.

The final vector was named CB92-aMHC-Ckmt2 and consists of the *Ckmt2* transgene together with the necessary machinery for achieving PhiC31 integrase mediated cassette exchange at the *Rosa26* locus.

This exchange plasmids was prepared as a Qiagen Maxiprep and diagnostic digests using NotI, BsrGI, NcoI and EcoRI were performed to verify the integrity of the vector (figure 2).

A



B

Enzyme	Fragment sizes (kb)
NotI	7.5, 6.4
NcoI	5.7, 5.2, 1.3, 0.6, 0.54, 0.4
EcoRI	4.5, 3.8, 3.6, 1.8, 0.14
BsrGI	10.5, 3.4

C

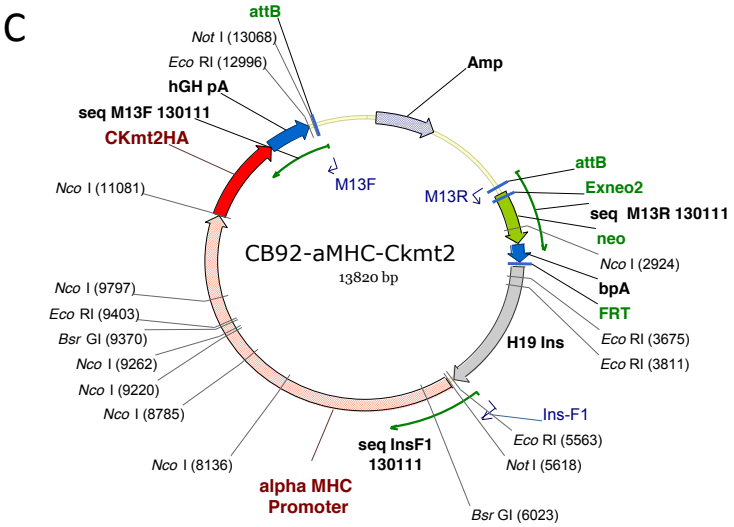


Figure 2 – A) and B) Upper panel shows the restriction digest profile of CB92-aMHC-Ckmt2, with the table on the upper right showing the predicted fragments. C) The lower panels show the plasmid maps of the exchange vector, including the sequenced regions and the locations of the restriction sites used for the restriction analysis.

The exchange plasmid, CB92-aMHC-Ckmt2 was sequenced to verify the cloning junctions and the integrity of the functional components of the PhiC31 integrase

system. Three sequence primers were used for sequence generation, M13R and M13F binding in the plasmid backbone and Ins-F1, binding within the insulator, just 5' of the position into which the transgenic construct was cloned. The position of these three sequenced regions is shown in figure 2 and the actual sequences obtained are shown below. Please note, these sequences cover only the junction fragments and full sequence information for the transgenic construct was not generated.

Seq Ins-F1

```
Query  1     TCGATCGGTTC-CTCTCCNCGCTGTGCAGATTTGGCTATAGCTAAATGGACAGACGATGC  59
             |||||||||||  ||||||  ||||||||||||||||||||||||||||||||||||||
Sbjct  5414  TCGATCGGTTCACTCTCCACGCTGTGCAGATTTGGCTATAGCTAAATGGACAGACGATGC  5473

Query  60    CGCGTGGTGGCAGTACAATACTACATATTGCTCGGCAGACGCGGCATAGGTTGGGGTCCG  119
             ||||||||||||||||||||||||||||||||||||||||||||||||||||||||||||
Sbjct  5474  CGCGTGGTGGCAGTACAATACTACATATTGCTCGGCAGACGCGGCATAGGTTGGGGTCCG  5533

Query  120   CTGTGACAAAGCTGTTAATTAAATCGATGAATTCGATATCAAGCTTACGCGTCTCGAGAG  179
             ||||||||||||||||||||||||||||||||||||||||||||||||||||||||||||
Sbjct  5534  CTGTGACAAAGCTGTTAATTAAATCGATGAATTCGATATCAAGCTTACGCGTCTCGAGAG  5593

Query  180   ATCTGCTAGCAGGCCTGGATCCGCGGCCGCTCTAGAACTAGTGGATCCTGCAAGGTCACA  239
             ||||||||||||||||||||||||||||||||||||||||||||||||||||||||||||
Sbjct  5594  ATCTGCTAGCAGGCCTGGATCCGCGGCCGCTCTAGAACTAGTGGATCCTGCAAGGTCACA  5653

Query  240   CAAGGGTCTCCACCCACCAGGTGCCCTAGTCTCAATTTCAGTTTCCATGCCTTGTTCTCA  299
             ||||||||||||||||||||||||||||||||||||||||||||||||||||||||||||
Sbjct  5654  CAAGGGTCTCCACCCACCAGGTGCCCTAGTCTCAATTTCAGTTTCCATGCCTTGTTCTCA  5713

Query  300   CAATGCTGGCCTCCCCAGAGCTAATTTGGACTTTGTTTTTATTTCAAAAGGGCCTGAATG  359
             ||||||||||||||||||||||||||||||||||||||||||||||||||||||||||||
Sbjct  5714  CAATGCTGGCCTCCCCAGAGCTAATTTGGACTTTGTTTTTATTTCAAAAGGGCCTGAATG  5773

Query  360   AGGAGTAGATCTTGTGCTACCCAGCTCTAAGGGTGCCCGTGAAGCCCTCAGACCTGGAGC  419
             ||||||||||||||||||||||||||||||||||||||||||||||||||||||||||||
Sbjct  5774  AGGAGTAGATCTTGTGCTACCCAGCTCTAAGGGTGCCCGTGAAGCCCTCAGACCTGGAGC  5833

Query  420   CTTTGCAACAGCCCTTTAGGTGGAAGCAGAATAAAGCAATTTTCCTTAAAGCCAAAATCC  479
             ||||||||||||||||||||||||||||||||||||||||||||||||||||||||||||
Sbjct  5834  CTTTGCAACAGCCCTTTAGGTGGAAGCAGAATAAAGCAATTTTCCTTAAAGCCAAAATCC  5893

Query  480   TGCCTCTAGACTCTTCTTCTCTGACCTCGGTCCCTGGGCTCTAGGGTGGGGAGGTGGGGC  539
             ||||||||||||||||||||||||||||||||||||||||||||||||||||||||||||
Sbjct  5894  TGCCTCTAGACTCTTCTTCTCTGACCTCGGTCCCTGGGCTCTAGGGTGGGGAGGTGGGGC  5953

Query  540   TTGGAAGAAGAAGGTGGGGAAGTGGCAAAAGCCGATCCCTAGGGCCCTGTGAAGTTCGGA  599
             ||||||||||||||||||||||||||||||||||||||||||||||||||||||||||||
Sbjct  5954  TTGGAAGAAGAAGGTGGGGAAGTGGCAAAAGCCGATCCCTAGGGCCCTGTGAAGTTCGGA  6013

Query  600   GCCTTCCCTGTACAGCACTGGCTCATAGATCCTCCTCCAGCCAAACATAGCAAGAAGTGA  659
             ||||||||||||||||||||||||||||||||||||||||||||||||||||||||||||
Sbjct  6014  GCCTTCCCTGTACAGCACTGGCTCATAGATCCTCCTCCAGCCAAACATAGCAAGAAGTGA  6073

Query  660   TACCTCCTTTGTGACTTCCCCAGGCCCAGTACCTGTCAGGTTGAAACAGGATTTAGAGAA  719
             ||||||||||||||||||||||||||||||||||||||||||||||||||||||||||||
Sbjct  6074  TACCTCCTTTGTGACTTCCCCAGGCCCAGTACCTGTCAGGTTGAAACAGGATTTAGAGAA  6133

Query  720   GCCTCTGAACTCACCTGAACTCTGAAGCTCATCCACCAAGCAAGCACCTAGGTGCCACTG  779
             ||||||||||||||||||||||||||||||||||||||||||||||||||||||||||||
Sbjct  6134  GCCTCTGAACTCACCTGAACTCTGAAGCTCATCCACCAAGCAAGCACCTAGGTGCCACTG  6193

Query  780   CTAGTTAGTATCCTACGCTGATAATATGCAGAGCTGGGCCACAGAAGTCCTGGGGTGTAG  839
             ||||||||||||||||||||||||||||||||||||||||||||||||||||||||||||
Sbjct  6194  CTAGTTAGTATCCTACGCTGATAATATGCAGAGCTGGGCCACAGAAGTCCTGGGGTGTAG  6253
```

```
Query  840   GAACTGACCAGTGACTTTTCAGTCGGCAAAGGTATGACCCCCTCAGCAGATGTAGTAATG  899
             ||||||||||||||||||||||||||||||||||||||||||||||||||||||||||||
Sbjct  6254  GAACTGACCAGTGACTTTTCAGTCGGCAAAGGTATGACCCCCTCAGCAGATGTAGTAATG  6313

Query  900   TCCCCTTAGATCCCATCCCAGGCAGGTCTCTAAGAGGACATGGGATGAGAGATGTAGTCA  959
             ||||||||||||||||||||||||||||||||||||||||||||||||||||||||||||
Sbjct  6314  TCCCCTTAGATCCCATCCCAGGCAGGTCTCTAAGAGGACATGGGATGAGAGATGTAGTCA  6373

Query  960   TGTGGCATTCCAAACACAGCTATCCACAGTGTCCCTTGCCCCTTCCACTTAGCCAGGAGG  1019
             ||||||||||||||||||||||||||||||||||||||||||||||||||||||||||||
Sbjct  6374  TGTGGCATTCCAAACACAGCTATCCACAGTGTCCCTTGCCCCTTCCACTTAGCCAGGAGG  6433

Query  1020  ACAGTAACCTTAGCCTATCTTTCTTCCTCCCCATCCTCCCAGGACACACCCCCTGGTCTG  1079
             ||||||||||||||||||||||||||||||||||||||||||||||||||||||||||||
Sbjct  6434  ACAGTAACCTTAGCCTATCTTTCTTCCTCCCCATCCTCCCAGGACACACCCCCTGGTCTG  6493

Query  1080  CAGTA  1084
             |||||
Sbjct  6494  CAGTA  6498
```

Insulator alpha-MHC promoter

M13F

```
Query  1      GGCGAATTGGAGCTCCNCCGCGGTGGCGATCCGTGGAGTACGCGCCCGGGGAGCCCAAGG  60
             ||||||||||||||| ||||||||||||||||||||||||||||||||||||||||||||
Sbjct  13177  GGCGAATTGGAGCTCCACCGCGGTGGCGATCCGTGGAGTACGCGCCCGGGGAGCCCAAGG  13118

Query  61     GCACGCCCTGGCACCCGCACCGCGGGGATCGCTCTAGAACTAGTGCGGCCGCCCGGGCGC  120
             ||||||||||||||||||||||||||||||||||||||||||||||||||||||||||||
Sbjct  13117  GCACGCCCTGGCACCCGCACCGCGGGGATCGCTCTAGAACTAGTGCGGCCGCCCGGGCGC  13058

Query  121    CACGTGTATACTAGTTTAAACGGCCGCTCTAGAACTAGTGGATCCCCCGGGCTGCAGGAA  180
             ||||||||||||||||||||||||||||||||||||||||||||||||||||||||||||
Sbjct  13057  CACGTGTATACTAGTTTAAACGGCCGCTCTAGAACTAGTGGATCCCCCGGGCTGCAGGAA  12998

Query  181    TTCAACAGGCATCTACTGAGTGGACCCAACGCATGAGAGGACAGTGCCAAGCAAGCAACT  240
             ||||||||||||||||||||||||||||||||||||||||||||||||||||||||||||
Sbjct  12997  TTCAACAGGCATCTACTGAGTGGACCCAACGCATGAGAGGACAGTGCCAAGCAAGCAACT  12938

Query  241    CAAATGTCCCACCGGTTGGGCATGGCCAGGTAGCCTATGCTGTGTCTGGACGTCCTCCTG  300
             ||||||||||||||||||||||||||||||||||||||||||||||||||||||||||||
Sbjct  12937  CAAATGTCCCACCGGTTGGGCATGGCCAGGTAGCCTATGCTGTGTCTGGACGTCCTCCTG  12878

Query  301    CTGGTATAGTTATTTTAAAATCAGAAGGACAGGGAAGGGAGCAGTGGTTCACGCCTGTAA  360
             ||||||||||||||||||||||||||||||||||||||||||||||||||||||||||||
Sbjct  12877  CTGGTATAGTTATTTTAAAATCAGAAGGACAGGGAAGGGAGCAGTGGTTCACGCCTGTAA  12818

Query  361    TCCCAGCAATTTGGGAGGCCAAGGTGGGTAGATCACCTGAGATTAGGAGTTGGAGACCAG  420
             ||||||||||||||||||||||||||||||||||||||||||||||||||||||||||||
Sbjct  12817  TCCCAGCAATTTGGGAGGCCAAGGTGGGTAGATCACCTGAGATTAGGAGTTGGAGACCAG  12758

Query  421    CCTGGCCAATATGGTGAAACCCCGTCTCTACCaaaaaaacaaaaaTTAGCTGAGCCTGGT  480
             ||||||||||||||||||||||||||||||||||||||||||||||||||||||||||||
Sbjct  12757  CCTGGCCAATATGGTGAAACCCCGTCTCTACCAAAAAAACAAAAATTAGCTGAGCCTGGT  12698

Query  481    CATGCATGCCTGGAATCCCAACAACTCGGGAGGCTGAGGCAGGAGAATCGCTTGAACCCA  540
             ||||||||||||||||||||||||||||||||||||||||||||||||||||||||||||
Sbjct  12697  CATGCATGCCTGGAATCCCAACAACTCGGGAGGCTGAGGCAGGAGAATCGCTTGAACCCA  12638

Query  541    GGAGGCGGAGATTGCAGTGAGCCAAGATTGTGCCACTGCACTCCAGCTTGGTTCCCAATA  600
             ||||||||||||||||||||||||||||||||||||||||||||||||||||||||||||
Sbjct  12637  GGAGGCGGAGATTGCAGTGAGCCAAGATTGTGCCACTGCACTCCAGCTTGGTTCCCAATA  12578

Query  601    GACCCCGCAGGCCCTACAGGTTGTCTTCCCAACTTGCCCCTTGCTCCATACCACCCCCCT  660
             ||||||||||||||||||||||||||||||||||||||||||||||||||||||||||||
Sbjct  12577  GACCCCGCAGGCCCTACAGGTTGTCTTCCCAACTTGCCCCTTGCTCCATACCACCCCCCT  12518
```

4

```
Query  661    CCACCCCATAATATTATAGAAGGACACCTAGTCAGACAAAATGATGCAACTTAATTTTAT  720
              ||||||||||||||||||||||||||||||||||||||||||||||||||||||||||||
Sbjct  12517  CCACCCCATAATATTATAGAAGGACACCTAGTCAGACAAAATGATGCAACTTAATTTTAT  12458

Query  721    TAGGACAAGGCTGGTGGGCACTGGAGTGGCAACTTCCAGGGCCAGGAGAGGCACTGGGGA  780
              ||||||||||||||||||||||||||||||||||||||||||||||||||||||||||||
Sbjct  12457  TAGGACAAGGCTGGTGGGCACTGGAGTGGCAACTTCCAGGGCCAGGAGAGGCACTGGGGA  12398

Query  781    GGGGTCACAGGGATGCCACCCATCAAGCTTCATGCGTAATCTGGAACATCGTATGGGTAC  840
              ||||||||||||||||||||||||||||||||||||||||||||||||||||||||||||
Sbjct  12397  GGGGTCACAGGGATGCCACCCATCAAGCTTCATGCGTAATCTGGAACATCGTATGGGTAC  12338

Query  841    TTCCTGCCAAACTGAGGCAGAGGAGGGGGCACCTTGATGTCTTGGCCTCTCTCCAGCTTC  900
              ||||||||||||||||||||||||||||||||||||||||||||||||||||||||||||
Sbjct  12337  TTCCTGCCAAACTGAGGCAGAGGAGGGGGCACCTTGATGTCTTGGCCTCTCTCCAGCTTC  12278

Query  901    TTTTCACAATCCACCAGGTAGTTGACTCCGTCAATAACAATCTGAACAAGCTCAACCTCT  960
              ||||||||||||||||||||||||||||||||||||||||||||||||||||||||||||
Sbjct  12277  TTTTCACAATCCACCAGGTAGTTGACTCCGTCAATAACAATCTGAACAAGCTCAACCTCT  12218

Query  961    GATCTGCCGATCCGATCTATGTTGGAAATATCGTACACATCTGCCACTGCAGCAGTGTCC  1020
              ||||||||||||||||||||||||||||||||||||||||||||||||||||||||||||
Sbjct  12217  GATCTGCCGATCCGATCTATGTTGGAAATATCGTACACATCTGCCACTGCAGCAGTGTCC  12158

Query  1021   ACACC  1025
              |||||
Sbjct  12157  ACACC  12153
```

attB hGH pA Ckmt2 cDNA

M13R

```
Query  1      AGCTGGGTACCGGGcccccccTCGACGCGCCGTCGACGTTTGATCCCCGCGGTGCGGGTG  60
              ||||||||||||||||||||||||||||||||||||||||||||||||||||||||||||
Sbjct  2197   AGCTGGGTACCGGGCCCCCCCTCGACGCGCCGTCGACGTTTGATCCCCGCGGTGCGGGTG  2256

Query  61     CCAGGGCGTGCCCTTGGGCTCCCCGGGCGCGTACTCCACGGATCAAACGCGCTGTTCTCC  120
              ||||||||||||||||||||||||||||||||||||||||||||||||||||||||||||
Sbjct  2257   CCAGGGCGTGCCCTTGGGCTCCCCGGGCGCGTACTCCACGGATCAAACGCGCTGTTCTCC  2316

Query  121    TCTTCCTCATCTCCGGGCCTTTCGACCTGCAGCCAATATGGGATCGGCCATTGAACAAGA  180
              ||||||||||||||||||||||||||||||||||||||||||||||||||||||||||||
Sbjct  2317   TCTTCCTCATCTCCGGGCCTTTCGACCTGCAGCCAATATGGGATCGGCCATTGAACAAGA  2376

Query  181    TGGATTGCACGCAGGTTCTCCGGCCGCTTGGGTGGAGAGGCTATTCGGCTATGACTGGGC  240
              ||||||||||||||||||||||||||||||||||||||||||||||||||||||||||||
Sbjct  2377   TGGATTGCACGCAGGTTCTCCGGCCGCTTGGGTGGAGAGGCTATTCGGCTATGACTGGGC  2436

Query  241    ACAACAGACAATCGGCTGCTCTGATGCCGCCGTGTTCCGGCTGTCAGCGCAGGGGCGCCC  300
              ||||||||||||||||||||||||||||||||||||||||||||||||||||||||||||
Sbjct  2437   ACAACAGACAATCGGCTGCTCTGATGCCGCCGTGTTCCGGCTGTCAGCGCAGGGGCGCCC  2496

Query  301    GGTTCTTTTTGTCAAGACCGACCTGTCCGGTGCCCTGAATGAACTGCAGGACGAGGCAGC  360
              ||||||||||||||||||||||||||||||||||||||||||||||||||||||||||||
Sbjct  2497   GGTTCTTTTTGTCAAGACCGACCTGTCCGGTGCCCTGAATGAACTGCAGGACGAGGCAGC  2556

Query  361    GCGGCTATCGTGGCTGGCCACGACGGGCGTTCCTTGCGCAGCTGTGCTCGACGTTGTCAC  420
              ||||||||||||||||||||||||||||||||||||||||||||||||||||||||||||
Sbjct  2557   GCGGCTATCGTGGCTGGCCACGACGGGCGTTCCTTGCGCAGCTGTGCTCGACGTTGTCAC  2616

Query  421    TGAAGCGGGAAGGGACTGGCTGCTATTGGGCGAAGTGCCGGGGCAGGATCTCCTGTCATC  480
              ||||||||||||||||||||||||||||||||||||||||||||||||||||||||||||
Sbjct  2617   TGAAGCGGGAAGGGACTGGCTGCTATTGGGCGAAGTGCCGGGGCAGGATCTCCTGTCATC  2676

Query  481    TCACCTTGCTCCTGCCGAGAAAGTATCCATCATGGCTGATGCAATGCGGCGGCTGCATAC  540
              ||||||||||||||||||||||||||||||||||||||||||||||||||||||||||||
Sbjct  2677   TCACCTTGCTCCTGCCGAGAAAGTATCCATCATGGCTGATGCAATGCGGCGGCTGCATAC  2736
```

```
Query  541   GCTTGATCCGGCTACCTGCCCATTCGACCACCAAGCGAAACATCGCATCGAGCGAGCACG  600
              ||||||||||||||||||||||||||||||||||||||||||||||||||||||||||||
Sbjct  2737  GCTTGATCCGGCTACCTGCCCATTCGACCACCAAGCGAAACATCGCATCGAGCGAGCACG  2796

Query  601   TACTCGGATGGAAGCCGGTCTTGTCGATCAGGATGATCTGGACGAAGAGCATCAGGGGCT  660
              ||||||||||||||||||||||||||||||||||||||||||||||||||||||||||||
Sbjct  2797  TACTCGGATGGAAGCCGGTCTTGTCGATCAGGATGATCTGGACGAAGAGCATCAGGGGCT  2856

Query  661   CGCGCCAGCCGAACTGTTCGCCAGGCTCAAGGCGCGCATGCCCGACGGCGATGATCTCGT  720
              ||||||||||||||||||||||||||||||||||||||||||||||||||||||||||||
Sbjct  2857  CGCGCCAGCCGAACTGTTCGCCAGGCTCAAGGCGCGCATGCCCGACGGCGATGATCTCGT  2916

Query  721   CGTGACCCATGGCGATGCCTGCTTGCCGAATATCATGGTGGAAAATGGCCGCTTTTCTGG  780
              ||||||||||||||||||||||||||||||||||||||||||||||||||||||||||||
Sbjct  2917  CGTGACCCATGGCGATGCCTGCTTGCCGAATATCATGGTGGAAAATGGCCGCTTTTCTGG  2976

Query  781   ATTCATCGACTGTGGCCGGCTGGGTGTGGCGGACCGCTATCANGACATAGCGTTGGCTAC  840
              |||||||||||||||||||||||||||||||||||||||| ||||||||||||||||||
Sbjct  2977  ATTCATCGACTGTGGCCGGCTGGGTGTGGCGGACCGCTATCAGGACATAGCGTTGGCTAC  3036

Query  841   CCGTGATATTGCTGAAGAGCTTGGCGGCGAATGGGCTGACCGCTTCCTCGTGCTTTACGG  900
              ||||||||||||||||||||||||||||||||||||||||||||||||||||||||||||
Sbjct  3037  CCGTGATATTGCTGAAGAGCTTGGCGGCGAATGGGCTGACCGCTTCCTCGTGCTTTACGG  3096

Query  901   TATCGCCGCTCCCGATTCGCAGCGCATCGCCTTCTATCGCCTTCTTGACGAGTTCTTCTG  960
              ||||||||||||||||||||||||||||||||||||||||||||||||||||||||||||
Sbjct  3097  TATCGCCGCTCCCGATTCGCAGCGCATCGCCTTCTATCGCCTTCTTGACGAGTTCTTCTG  3156

Query  961   AGGGGATCAATTCTCTAGAGCTCGCTGATCAGCCTCGACTGTGCCTT  1007
              |||||||||||||||||||||||||||||||||||||||||||||
Sbjct  3157  AGGGGATCAATTCTCTAGAGCTCGCTGATCAGCCTCGACTGTGCCTT  3203

attB          Neomycin resistance cassette                bGH pA
```

Integrase Mediated Cassette Exchange

The completed exchange vector harbouring the alpha-MHC-Ckmt2 construct was co-electroporated with an expression cassette for PhiC31 integrase into Acceptor ES cells. PhiC31 integrase catalyses the exchange between the attB sites within the exchange vectors and the attP sites lying within the *Rosa26* locus, preintegrated into the Acceptor ES cells (see figure 1). Cells were selected in 350 µg/ml G418 and resistant colonies were isolated, frozen and DNA was extracted for PCR analysis.

PCR screening of recombinant clones

The resulting clones were screened by PCR for the correct integration of transgenic construct at the 5' and 3' ends. For the 3' screen, a forward primer, AttL-PolyF1, which binds within the polylinker sequence directly 3' of the cloned transgene cassette present on the exchange vector was used together with a reverse primer, Rosa3HR-R, which binds within the *Rosa26* locus downstream of the attP site, to amplify a 518 bp product from correctly exchanged clones. A product can only be obtained if PhiC31 mediated integration occurs at the 3' attP site. Correct integration at the 5' end results in the reconstitution of a functional PGK-neomycin resistance cassette. To verify this event by PCR, a forward primer, ExPGK3, binds within the PGK promoter present in the ES cells at the *Rosa26* locus and a reverse primer, Ex-Neo2, binds within the Neomycin resistance cassette were used to amplify a 280 bp product.

The two PCRs were multiplexed and run in the same reaction. Figure 3 illustrates the PCR screening strategy and shows some typical results from this primary screen.

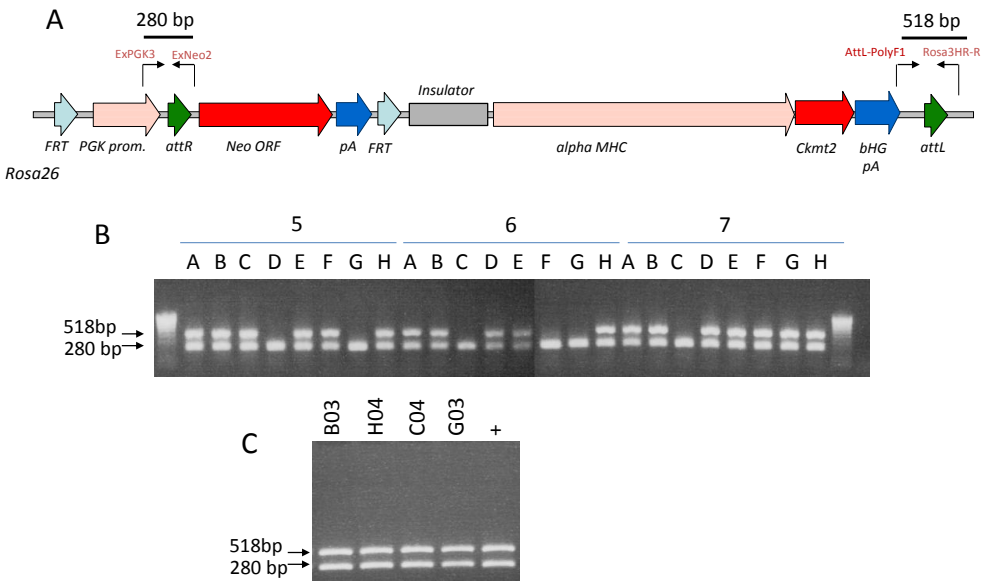


Figure 3 – (A) The exchanged *Rosa26* loci are shown with the positions of the genotyping primers. (B) PCR genotyping of the primary clones for exchange at the 5' and 3' end using the two primer combination AttL-PolyF1 and Rosa3HR-R; ExPGK3 and ExNeo2. The presence of a double band (products at 518 bp and 280 bp) signifies a correct PhiC31 integrase mediated cassette exchange. (C) Genotyping results of a new set of clones after having repeated the cell culture phase of the experiment (see text).

As can be seen in Figure 3, two types of clones are obtained following the transfections:

1) clones in which a recombination event has occurred only at the 5' end of the vector, thus reconstituting the neomycin cassette and giving the correct 280bp amplification product with the 5' PCR screening primers but showing no correct recombination at the 3' end of the vector. These clones are expected to have integrated the complete backbone of the exchange plasmid and are not suitable for further use.
2) Clones in which a recombination event has occurred both at the 5' and 3' ends of the vectors which has led to an exchange of the intervening sequence with the transgenic vector. These clones yield an amplification product with both the 5' and the 3' screening combinations.

Two clones harbouring the alpha-MHC-Ckmt2 construct were selected for thawing and expansion – E05 and H06.

Blastocyst injection of recombinant clones

ES cells clones harbouring the inserted variant transgenic constructs were injected into C57BL/6 blastocysts* and the resulting chimeric embryos were transferred to recipient pseudopregnant females. Pups were born and were assessed for their degree of chimerism using coat colour markers. The ES cells are derived from a F1 (129 x C57BL/6J) and are therefore of genotype Aa at the agouti locus and have an agouti coat colour. The host blastocysts are C57BL/6 and are therefore of genotype aa at the agouti locus and have a black coat colour. The degree to which the injected ES cells have contributed to the resulting chimera is thus easily assessed by the percentage of agouti coat colouring seen in the resulting chimeras.

Table 1 summarizes the results of the injection sessions

ES cell line	No. of blastocysts transferred	Pups born	Date of birth	Male Chimeras
E05	20*	9	15/04/2011	1 (30%)
E05	19*	9	15/04/2011	-
E05	10*	0	-	-

* Blastocysts used for this injection session were from albino C57Bl/6J mice, hence the resulting chimera is a mixture of albino cells and F1 cells (i.e. white-agouti chimera). Since the albino mutation is a recessive one and the host cells are genotypically aa (i.e. black), there is no difference in the strategy to identify germline transmission by coat colour genetics.

ES cell line	No. of blastocysts transferred	Pups born	Date of birth	Male Chimeras
H06	20	6	29/05/2011	1 (40%)

Although chimeras have been born from the injection sessions, the number of chimeras and in particular the % chimerism (i.e. the % contribution to the mouse that the recombinant ES cells have made) is quite low. It was subsequently decided to generate new clones from a further round of ES cell transfection.

The cell culture phase of the experiment was thus repeated and multiple new targeted clones were indentified which had correctly integrated the alpha-MHC-Ckmt2 transgenic construct correctly at the *Rosa26* locus. Four independent clones were identified and expanded ready for microinjection into blastocysts. The genotype of

these four clones, B03, H04, C04, G03, was also verified by PCR during the cell expansion phase (see Figure 3C).

Breeding recommendations

The existing chimeras should be bred at 7-8 weeks of age with C57Bl/6J females. The ES cells used are from an F1 background (C57BL/6J x 129) and are subsequently heterozygous at the agouti locus (Aa).

If germline transmission occurs when breeding with C57BL/6J females (genotype aa), the offspring will be a mixture of mice with genotype Aa and aa – these mice will be phenotypically agouti and black, respectively.

If germline transmission does not occur, i.e. the host C57BL/6J cells from the blastocyst contribute to the germ cells of the chimera, the resulting mice will be of genotype aa – these mice will be phenotypically black.

Subsequently, the presence of agouti pups in the F1 generation confirms that germline transmission has occurred, yet the absence of agouti pups in the F1 generation does not necessarily indicate that germline transmission has not occurred. We therefore recommend the genotyping of all the F1 pups. Since only one copy of the *Rosa26* locus harbours the transgene, 50% of the transmitted mice will be wild-type and 50% transgenic.

Appendix A – Transferred mice

ES cell line	Male Chimeras
E05	1(30%*)
H06	1(40%)

Appendix B – Genotyping protocols

1. PCR genotyping at the 5’ and 3’ end of the construct

Name	Amplification Product	Sequence
ExPGK3	280 bp	5’- CACGCTTCAAAAGCGCACGTCTG -3’
ExNeo2		5’ - GTTGTGCCCAGTCATAGCCGAATA G -3’
AttL PolyF1	518 bp	5’- GCACTAGTTCTAGAGCGATCCCC- 3’
Rosa3HR-R		5’- CGGGAGAAATGGATATGAAGTACTGGGC- 3’

Reaction Mix			Reaction conditions			
genomic Mouse DNA	100.0	ng	**Step**	**Temp.**	**Time**	**Cycles**
Primers	10	pmol	Denaturing	94°C	300s	1x
dNTPs	0.16	mM	Denaturing	94°C	30s	
Reaction Buffer	0.1	Vol	Annealing	57°C	60s	30x
MgCl2	3	mM	Extension	72°C	30s	
Taq Polymerase (Immolase)	1.0	U	Completion	72°C	420s	1x
Reaction Volume	20.0	µl		4°C	-	

B.2. Transgenics report: CKm-OE and CKb-OE

THE WELLCOME TRUST CENTRE FOR HUMAN GENETICS

The Henry Wellcome Building, Roosevelt Drive, Oxford, OX3 7BN
Tel: +44 (0)1865 287 836 Fax: +44 (0)1865 287 501
transgenics@well.ox.ac.uk www.well.ox.ac.uk

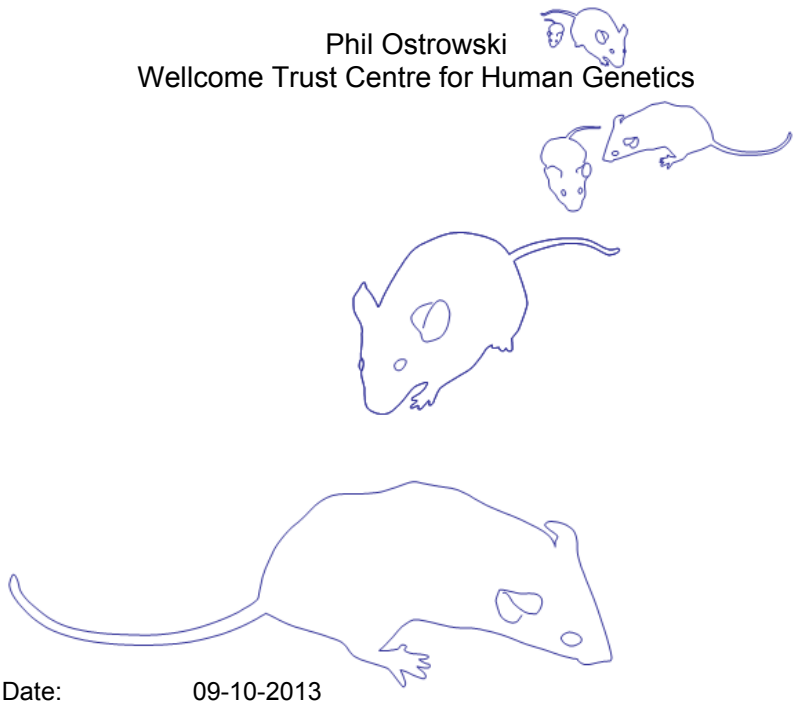
UNIVERSITY OF OXFORD

Documentation

A C G G G C T G A A A T G T T T T C A G T A A C A C A G T C T A A T G G C G G T C A G T A C A

Generation of a transgenic mouse
model overexpressing two isoforms of
creatine kinase (*Ckb* and *Ckm*) in mouse cardiomyocytes.

Phil Ostrowski
Wellcome Trust Centre for Human Genetics



Date: 09-10-2013

Summary

The transgenic constructs alpha-MHC-CKM and alpha-MHC-CKB, containing the mouse Myh6 (alpha-MHC) promoter driving the expression of either the murine *Ckm* or *Ckb* cDNA cassettes, were injected into the pronucleus of fertilized oocytes. Following overnight cultivation, the surviving two-cell embryos were transplanted into pseudo-pregnant foster mothers. The resulting pups were genotyped and two independent transgenic founder mice per construct were identified by PCR.

Purification of the transgenic construct

The transgenic constructs were isolated from the plasmids CB92-aMHC-CKM and CB92-aMHC-CKB by NotI digestion (figure 1A). The resulting ~7.4 kb fragment was isolated, purified, filtered using a micro-filtration unit (millipore) and diluted to a concentration of 5 ng/ µl in microinjection buffer (10 mM Tris-HCl pH 7.4, 0.1 mM EDTA). The construct purity and the concentration were verified by agarose gel electrophoresis.

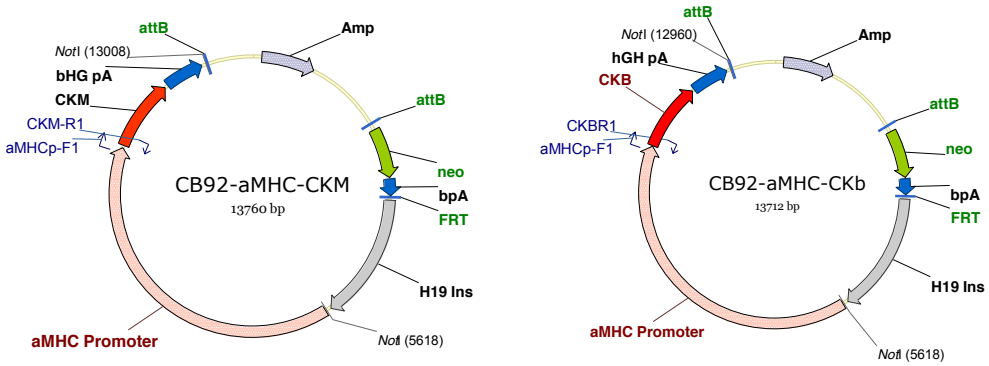


Fig. 1: Plasmid maps of the transgenic constructs showing the presence of aMHC (Myh6) promoter and the CKM or CKB cDNA cassettes. The positions of the primers used for genotyping are shown, together with the restriction enzyme sites used for the purification of the transgenic construct from the plasmid backbone.

Pronucleus microinjection

3 week old female B6CBAF1 mice were superovulated and mated with male B6CBAF1 mice. The resulting fertilized oocytes were collected from the oviduct of plugged female mice and cultured until two clear pronuclei were visible. The purified transgenic construct was microinjected into one of the pronuclei (figure 2) and injected embryos were cultivated overnight to the two-cell stage.

Two-cell embryos were then reimplanted into the oviduct of pseudopregnant CD1 foster mothers at 0.5 days post-coitum.

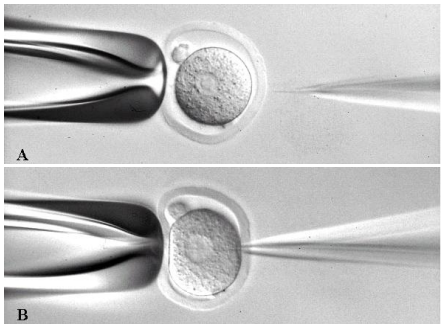


Figure 2: (A) Oocyte before injection. The male pronucleus is clearly visible. (B) Oocyte after injection. The male pronucleus is clearly enlarged, demonstrating the successful injection.

Between 18 and 19 days later, pups were born from the foster mothers. Table 1a and 1b summarizes the DNA microinjections performed which were performed.

Table 1a: alpha-MHC-Ckb: Summary of the microinjections and transfers

Transfer date	No. transferred	Date of Birth	No. of pups	Female	Male	Biospies	Founders
25/10/2012	32	14/11/2012	3	3	3	641-646	1 Female (#645)
25/10/2012	32	14/11/2012	3				
13/11/2012	30	02/12/2012	4	0	8	761-770	1 Male (#769)
13/11/2012	30	02/12/2012	4				
10/01/2013	30	29/01/2013	6	5	6	928-938	-
10/01/2013	30	29/01/2013	5				

Table 1b: alpha-MHC-Ckm: Summary of the microinjections and transfers

Transfer date	No. transferred	DOB	No. of pups	Female	Male	Biospies	Founders
18/10/2012	22	07/11/2012	5	3	8	630-640	1 Male (#635) 1 Female (#630)
18/10/2012	24	NP	0				
18/10/2012	24	07/11/2012	1				
18/10/2012	25	07/11/2012	5				
08/11/2012	30	27/11/2012	5	6	6	750-761	-
08/11/2012	31	27/11/2012	4				
08/11/2012	31	27/11/2012	3				
18/01/2013	24	07/02/2013	4	3	1	978-981	-
26/03/2013	23	NP	0	-	-	-	-
26/03/2013	23	NP	0	-	-	-	-

Screening for transgenic founders

A total of 25 mice were born form the injection of the alpha-MHC-Ckm construct and .a total of 27 mice were born from the injection of the alpha-MHC-Ckb construct. Genomic DNA was prepared, initially from tail biopsies and was genotyped by PCR using the primer combinations shown in table 2. The screening protocol is based on a

forward primer, aMHCp-F1, binding at the 3' of the promoter sequence and specific reverse primers, CKB-R1 or CKM-R1, binding in either the *Ckb* or *Ckm* cDNA sequences respectively amplifying a junction fragment between the promoter and the cDNA. Using genomic DNA from experiments in which the two constructs were positioned at the *ROSA26* locus at single copy, via PhiC31 integrase mediated cassette exchange, we were able to test the specificity of this PCR and also demonstrate its ability to detect the presence of the transgene at single copy.

Table 2: Genotyping primers

Primer	Sequence
CKM-R1	ATGATGAAGGGGTGACCTGGGTTGT
CKB-R1	ACAGTCATGATGTACGGGTG
aMHCp-F1	GTAGGAAAGTCAGGACTTCA

After genotyping of the tail biopsy, any putative positive pups were genotyped again using a secondary tissue sample obtained from the identifying ear biopsy.

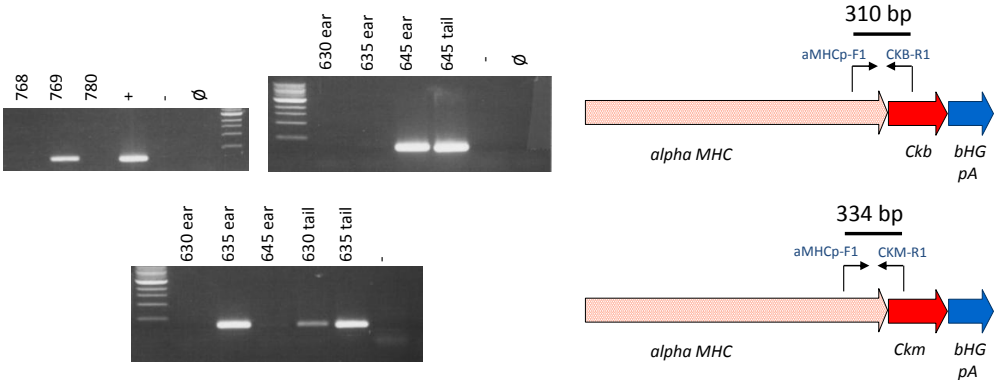


Figure 3: Screening for founders. PCR with the primers aMHC-F1 and CKB-R1 (top panels) or CKM-R1 (bottom panels) reveal the presence of a transgene specific 310 bp (for CKB) or 334 bp (for CKM) product (bottom panel).

As can be seen in figure 3, two independent founders (F0-769, F0-645) for alpha-MHC-Ckb and two independent founders (F0-635, F0-630) for alpha-MHC-Ckm could be identified using the transgene specific PCR. Interestingly, the screening results for founder F0-630 suggest that this founder is a mosaic as the ear biopsy was negative for the screening PCR, but the tail biopsy was positive for the PCR. This result is consistent the integration of the transgene occurring after the first cellular cleavage event, resulting in a mosaic or chimera of wild-type and transgenic cells. The overall transgenic efficiency following the injection of the two constructs was 7.7% (4/52 pups).

The founders have been passed onto the Neubauer racks within the Functional Genetics Facility at the Wellcome Trust Centre for Human Genetics.

Appendix

Table 3: Summary table of the transgenic founders

Tg (Myh6-Ckm)				
ID No.	**Generation**	**Date of Birth**	**Sex**	**Genotype**
F0-630	F0, Founder	07/11/2012	♀	TG/+
F0-635	F0, Founder	07/11/2012	♂	TG/+

Tg (Myh6-Ckb)				
ID No.	**Generation**	**Date of Birth**	**Sex**	**Genotype**
F0-645	F0, Founder	14/11/2012	♀	TG/+
F0-769	F0, Founder	02/12/2012	♂	TG/+

C. REFERENCES

1. Finegold, J. A., Asaria, P. & Francis, D. P. International Journal of Cardiology. *International Journal of Cardiology* 168, 934–945 (2013).
2. McMurray, J. J. V. *et al.* ESC Guidelines for the diagnosis and treatment of acute and chronic heart failure 2012: The Task Force for the Diagnosis and Treatment of Acute and Chronic Heart Failure 2012 of the European Society of Cardiology. Developed in collaboration with the Heart Failure Association (HFA) of the ESC. *Eur Heart J* 33, 1787–1847 (2012).
3. Yancy, C. W. *et al.* 2013 ACCF/AHA Guideline for the Management of Heart Failure: A Report of the American College of Cardiology Foundation/American Heart Association Task Force on Practice Guidelines. *Circulation* (2013). doi:10.1161/CIR.0b013e31829e8776
4. Go, A. S. *et al.* Heart Disease and Stroke Statistics--2013 Update: A Report From the American Heart Association. *Circulation* 127, e6–e245 (2013).
5. Lloyd-Jones, D. M. Lifetime Risk for Developing Congestive Heart Failure: The Framingham Heart Study. *Circulation* 106, 3068–3072 (2002).
6. Heidenreich, P. A. *et al.* Forecasting the future of cardiovascular disease in the United States: a policy statement from the American Heart Association. in *Circulation* 123, 933–944 (2011).
7. Barker, W. H., Mullooly, J. P. & Getchell, W. Changing incidence and survival for heart failure in a well-defined older population, 1970-1974 and 1990-1994. *Circulation* 113, 799–805 (2006).
8. Curtis, L. H. *et al.* Incidence and prevalence of heart failure in elderly persons, 1994-2003. *Arch Intern Med* 168, 418–424 (2008).
9. Effects of enalapril on mortality in severe congestive heart failure. Results of the Cooperative North Scandinavian Enalapril Survival Study (CONSENSUS). The CONSENSUS Trial Study Group. *N Engl J Med* 316, 1429–1435 (1987).
10. Pfeffer, M. A. *et al.* Effect of captopril on mortality and morbidity in patients with left ventricular dysfunction after myocardial infarction. Results of the survival and ventricular enlargement trial. The SAVE Investigators. *N Engl J Med* 327, 669–677 (1992).
11. Cohn, J. N., Tognoni, G.Valsartan Heart Failure Trial Investigators. A randomized trial of the angiotensin-receptor blocker valsartan in chronic heart failure. *N Engl J Med* 345, 1667–1675 (2001).
12. Maggioni, A. P. *et al.* Effects of valsartan on morbidity and mortality in patients with heart failure not receiving angiotensin-converting enzyme inhibitors. *J Am Coll Cardiol* 40, 1414–1421 (2002).
13. Pfeffer, M. A. *et al.* Effects of candesartan on mortality and morbidity in patients with chronic heart failure: the CHARM-Overall programme. *Lancet* 362, 759–766 (2003).
14. A randomized trial of beta-blockade in heart failure. The Cardiac Insufficiency Bisoprolol Study (CIBIS). CIBIS Investigators and Committees. *Circulation* 90, 1765–1773 (1994).
15. Packer, M. *et al.* The effect of carvedilol on morbidity and mortality in patients with chronic heart failure. U.S. Carvedilol Heart Failure Study Group. *N Engl J Med* 334, 1349–1355 (1996).
16. Effect of metoprolol CR/XL in chronic heart failure: Metoprolol CR/XL Randomised Intervention Trial in Congestive Heart Failure (MERIT-HF). *The Lancet* 353, 2001–2007 (1999).
17. Pitt, B. *et al.* The effect of spironolactone on morbidity and mortality in patients with severe heart failure. Randomized Aldactone Evaluation Study Investigators. *N Engl J Med* 341, 709–717 (1999).
18. Bristow, M. R. *et al.* Cardiac-resynchronization therapy with or without an implantable defibrillator in advanced chronic heart failure. *N Engl J Med* 350, 2140–2150 (2004).
19. Cleland, J. G. F. *et al.* The effect of cardiac resynchronization on morbidity and mortality in heart failure. *N Engl J Med* 352, 1539–1549 (2005).
20. Swedberg, K. *et al.* Ivabradine and outcomes in chronic heart failure (SHIFT): a randomised placebo-controlled study. *Lancet* 376, 875–885 (2010).
21. Velazquez, E. J. *et al.* Coronary-artery bypass surgery in patients with left ventricular dysfunction. *N Engl J Med* 364, 1607–1616 (2011).
22. Levy, D. *et al.* Long-term trends in the incidence of and survival with heart failure. *N Engl J Med* 347, 1397–1402 (2002).
23. Roger, V. L. *et al.* Trends in heart failure incidence and survival in a community-based population. *JAMA* 292, 344–350 (2004).
24. Curtis, L. H. *et al.* Early and long-term outcomes of heart failure in elderly persons, 2001-2005. *Arch Intern Med* 168, 2481–2488 (2008).
25. Neubauer, S. The failing heart--an engine out of fuel. *N Engl J Med* 356, 1140–1151 (2007).
26. Stanley, W. C., Recchia, F. A. & Lopaschuk, G. D. Myocardial substrate metabolism in the normal and failing heart. *Physiol Rev* 85, 1093–1129 (2005).
27. Kammermeier, H., Schmidt, P. & Jüngling, E. Free energy change of ATP-hydrolysis: a causal factor of early hypoxic failure of the myocardium? *Journal of Molecular and Cellular Cardiology* 14, 267–277 (1982).
28. Fiske, C. H. & Subbarow, Y. THE NATURE OF THE 'INORGANIC PHOSPHATE' IN VOLUNTARY MUSCLE. *Science* 65, 401–403 (1927).
29. Eggleton, P. & Eggleton, G. P. Further observations on phosphagen. *J Physiol (Lond)* 65, 15–24 (1928).
30. Lohmann, K. Über die enzymatische Aufspaltung der Kreatinphosphorsäure: zugleich ein Beitrag zum Chemismus der

Muskelkontraktion. *Biochem Z* 271, 264–277 (1934).
31. Wallimann, T., Wyss, M., Brdiczka, D., Nicolay, K. & Eppenberger, H. M. Intracellular compartmentation, structure and function of creatine kinase isoenzymes in tissues with high and fluctuating energy demands: the 'phosphocreatine circuit' for cellular energy homeostasis. *Biochem J* 281 (Pt 1), 21–40 (1992).
32. Yoshizaki, K., Watari, H. & Radda, G. K. Role of phosphocreatine in energy transport in skeletal muscle of bullfrog studied by 31P-NMR. *Biochim Biophys Acta* 1051, 144–150 (1990).
33. Bessman, S. P. & Geiger, P. J. Transport of energy in muscle: the phosphorylcreatine shuttle. *Science* 211, 448–452 (1981).
34. Wallimann, T. & Eppenberger, H. M. Localization and function of M-line-bound creatine kinase. M-band model and creatine phosphate shuttle. *Cell Muscle Motil.* 6, 239–285 (1985).
35. Saks, V. A., Kuznetsov, A. V., Kupriyanov, V. V., Miceli, M. V. & Jacobus, W. E. Creatine kinase of rat heart mitochondria. The demonstration of functional coupling to oxidative phosphorylation in an inner membrane-matrix preparation. *J Biol Chem* 260, 7757–7764 (1985).
36. Jacobus, W. E. Respiratory control and the integration of heart high-energy phosphate metabolism by mitochondrial creatine kinase. *Annu Rev Physiol* 47, 707–725 (1985).
37. Wallimann, T., Tokarska-Schlattner, M. & Schlattner, U. The creatine kinase system and pleiotropic effects of creatine. *Amino Acids* 40, 1271–1296 (2011).
38. Brosnan, J. T., da Silva, R. P. & Brosnan, M. E. The metabolic burden of creatine synthesis. *Amino Acids* 40, 1325–1331 (2011).
39. Guimbal, C. & Kilimann, M. W. A Na(+)-dependent creatine transporter in rabbit brain, muscle, heart, and kidney. cDNA cloning and functional expression. *J Biol Chem* 268, 8418–8421 (1993).
40. Loike, J. D., Zalutsky, D. L., Kaback, E., Miranda, A. F. & Silverstein, S. C. Extracellular creatine regulates creatine transport in rat and human muscle cells. *Proc Natl Acad Sci USA* 85, 807–811 (1988).
41. Bloch, K. & Schoenheimer, R. Studies in Protein Metabolism: Xi. the Metabolic Relation of Creatine and Creatinine Studied with Isotopic Nitrogen. *J Biol Chem* 131, 111–119 (1939).
42. Wyss, M. & Kaddurah-Daouk, R. Creatine and creatinine metabolism. *Physiol Rev* 80, 1107–1213 (2000).
43. BURGER, A., RICHTERICH, R. & AEBI, H. The Heterogenicity of Creatine Kinase. *Biochem Z* 339, 305–314 (1964).
44. Jacobs, H., Heldt, H. W. & Klingenberg, M. High activity of creatine kinase in mitochondria from muscle and brain and evidence for a separate mitochondrial isoenzyme of creatine kinase. *Biochem Biophys Res Commun* 16, 516–521 (1964).
45. Mühlebach, S. M. *et al.* Sequence homology and structure predictions of the creatine kinase isoenzymes. *Mol Cell Biochem* 133-134, 245–262 (1994).
46. Qin, W. *et al.* Molecular characterization of the creatine kinases and some historical perspectives. *Mol Cell Biochem* 184, 153–167 (1998).
47. Wallimann, T. & Hemmer, W. Creatine kinase in non-muscle tissues and cells. *Mol Cell Biochem* 133-134, 193–220 (1994).
48. Payne, R. M., Haas, R. C. & Strauss, A. W. Structural characterization and tissue-specific expression of the mRNAs encoding isoenzymes from two rat mitochondrial creatine kinase genes. *Biochim Biophys Acta* 1089, 352–361 (1991).
49. Bittl, J. A., DeLayre, J. & Ingwall, J. S. Rate equation for creatine kinase predicts the in vivo reaction velocity: 31P NMR surface coil studies in brain, heart, and skeletal muscle of the living rat. *Biochemistry* 26, 6083–6090 (1987).
50. Veksler, V. I. *et al.* Muscle creatine kinase-deficient mice. II. Cardiac and skeletal muscles exhibit tissue-specific adaptation of the mitochondrial function. *J Biol Chem* 270, 19921–19929 (1995).
51. Schmitt, T. & Pette, D. Increased mitochondrial creatine kinase in chronically stimulated fast-twitch rabbit muscle. *FEBS Lett* 188, 341–344 (1985).
52. Apple, F. S. & Rogers, M. A. Mitochondrial creatine kinase activity alterations in skeletal muscle during long-distance running. *J Appl Physiol* 61, 482–485 (1986).
53. Lyons, G. E. *et al.* Developmental regulation of creatine kinase gene expression by myogenic factors in embryonic mouse and chick skeletal muscle. *Development* 113, 1017–1029 (1991).
54. Fischer, A. *et al.* Changes in creatine transporter function during cardiac maturation in the rat. *BMC developmental biology* 10, 70 (2010).
55. Trask, R. V. & Billadello, J. J. Tissue-specific distribution and developmental regulation of M and B creatine kinase mRNAs. *Biochim Biophys Acta* 1049, 182–188 (1990).
56. Payne, R. M. & Strauss, A. W. Developmental expression of sarcomeric and ubiquitous mitochondrial creatine kinase is tissue-specific. *Biochim Biophys Acta* 1219, 33–38 (1994).
57. Fritz-Wolf, K., Schnyder, T., Wallimann, T. & Kabsch, W. Structure of mitochondrial creatine kinase. *Nature* 381, 341–345 (1996).
58. Rojo, M., Hovius, R., Demel, R. A., Nicolay, K. & Wallimann, T. Mitochondrial creatine kinase mediates contact formation between mitochondrial membranes. *J Biol Chem* 266, 20290–20295 (1991).
59. Stachowiak, O., Dolder, M. & Wallimann, T. Membrane-binding and lipid vesicle cross-linking kinetics of the mitochondrial creatine kinase octamer. *Biochemistry* 35, 15522–15528 (1996).
60. Rao, J. K., Bujacz, G. & Wlodawer, A. Crystal structure of rabbit muscle creatine kinase. *FEBS Lett* 439, 133–137 (1998).
61. Eder, M. *et al.* Crystal structure of brain-type creatine kinase at 1.41 A resolution. *Protein Sci.* 8, 2258–2269 (1999).
62. Eder, M., Fritz-Wolf, K., Kabsch, W., Wallimann, T. & Schlattner, U. Crystal structure of human ubiquitous mitochondrial creatine kinase. *Proteins* 39, 216–225 (2000).
63. Shen, Y. Q., Tang, L., Zhou, H. M. & Lin, Z. J. Structure of human muscle creatine kinase. *Acta Crystallogr. D Biol. Crystallogr.* 57, 1196–1200 (2001).
64. Bong, S. M. *et al.* Structural studies of human brain-type creatine kinase complexed with the ADP-Mg2+-NO3- -creatine transition-state analogue complex. *FEBS Lett* 582, 3959–3965 (2008).
65. Kottke, M., Wallimann, T. & Brdiczka, D. Dual electron microscopic localization of mitochondrial creatine kinase in brain mitochondria. *Biochem. Med. Metab. Biol.* 51, 105–117 (1994).
66. Kottke, M., Adams, V., Wallimann, T., Nalam, V. K. & Brdiczka, D. Location and regulation of octameric mitochondrial

creatine kinase in the contact sites. *Biochim Biophys Acta* 1061, 215–225 (1991).
67. Speer, O. *et al.* Octameric mitochondrial creatine kinase induces and stabilizes contact sites between the inner and outer membrane. *Biochem J* 385, 445–450 (2005).
68. Wegmann, G., Zanolla, E., Eppenberger, H. M. & Wallimann, T. In situ compartmentation of creatine kinase in intact sarcomeric muscle: the acto-myosin overlap zone as a molecular sieve. *J. Muscle Res. Cell. Motil.* 13, 420–435 (1992).
69. Ventura-Clapier, R., Kuznetsov, A., Veksler, V., Boehm, E. & Anflous, K. Functional coupling of creatine kinases in muscles: species and tissue specificity. *Mol Cell Biochem* 184, 231–247 (1998).
70. Trask, R. V., Strauss, A. W. & Billadello, J. J. Developmental regulation and tissue-specific expression of the human muscle creatine kinase gene. *J Biol Chem* 263, 17142–17149 (1988).
71. Sternberg, E. A. *et al.* Identification of upstream and intragenic regulatory elements that confer cell-type-restricted and differentiation-specific expression on the muscle creatine kinase gene. *Mol Cell Biol* 8, 2896–2909 (1988).
72. Buskin, J. N. & Hauschka, S. D. Identification of a myocyte nuclear factor that binds to the muscle-specific enhancer of the mouse muscle creatine kinase gene. *Mol Cell Biol* 9, 2627–2640 (1989).
73. Qin, W., Khuchua, Z., Klein, S. C. & Strauss, A. W. Elements regulating cardiomyocyte expression of the human sarcomeric mitochondrial creatine kinase gene in transgenic mice. *J Biol Chem* 272, 25210–25216 (1997).
74. Horlick, R. A., Hobson, G. M., Patterson, J. H., Mitchell, M. T. & Benfield, P. A. Brain and muscle creatine kinase genes contain common TA-rich recognition protein-binding regulatory elements. *Mol Cell Biol* 10, 4826–4836 (1990).
75. Ritchie, M. E. Human B creatine kinase gene expression in C2C12 cells is regulated by protein interactions involving the first exon. *Biochem Biophys Res Commun* 223, 762–769 (1996).
76. Papenbrock, T. & Wille, W. The 3' non-coding region of the mouse brain B creatine kinase mRNA: a sequence with exceptional homology among species. *Nucleic Acids Res* 14, 8690 (1986).
77. Reiss, N. A. & Kaye, A. M. Identification of the major component of the estrogen-induced protein of rat uterus as the BB isozyme of creatine kinase. *J Biol Chem* 256, 5741–5749 (1981).
78. Sömjen, D., Weisman, Y., Binderman, I. & Kaye, A. M. Stimulation of creatine kinase BB activity by 1 alpha,25-dihydroxycholecalciferol and 24R,25-dihydroxycholecalciferol in rat tissues. *Biochem J* 219, 1037–1041 (1984).
79. Ponticos, M. *et al.* Dual regulation of the AMP-activated protein kinase provides a novel mechanism for the control of creatine kinase in skeletal muscle. *EMBO J* 17, 1688–1699 (1998).
80. Ingwall, J. Is Creatine Kinase a Target for AMP-activated Protein Kinase in the Heart? *Journal of Molecular and Cellular Cardiology* 34, 1111–1120 (2002).
81. Dieni, C. A. & Storey, K. B. Comparative Biochemistry and Physiology, Part B. *Comparative Biochemistry and Physiology, Part B* 152, 405–412 (2009).
82. Lin, G., Liu, Y. & MacLeod, K. M. Regulation of muscle creatine kinase by phosphorylation in normal and diabetic hearts. *Cell. Mol. Life Sci.* 66, 135–144 (2008).
83. Boja, E. S., Phillips, D., French, S. A., Harris, R. A. & Balaban, R. S. Quantitative mitochondrial phosphoproteomics using iTRAQ on an LTQ-Orbitrap with high energy collision dissociation. *J. Proteome Res.* 8, 4665–4675 (2009).
84. Zhao, T. J., Yan, Y. B., Liu, Y. & Zhou, H. M. The Generation of the Oxidized Form of Creatine Kinase Is a Negative Regulation on Muscle Creatine Kinase. *Journal of Biological Chemistry* 282, 12022–12029 (2006).
85. Koyama, S. *et al.* Muscle RING-Finger Protein-1 (MuRF1) as a Connector of Muscle Energy Metabolism and Protein Synthesis. *Journal of Molecular Biology* 376, 1224–1236 (2008).
86. Willis, M. S. *et al.* Cardiac muscle ring finger-1 increases susceptibility to heart failure in vivo. *Circulation Research* 105, 80–88 (2009).
87. Nuss, J. E. *et al.* Oxidative modification and aggregation of creatine kinase from aged mouse skeletal muscle. *Aging (Albany NY)* 1, 557–572 (2009).
88. Shen, W. *et al.* Progressive loss of myocardial ATP due to a loss of total purines during the development of heart failure in dogs: a compensatory role for the parallel loss of creatine. *Circulation* 100, 2113–2118 (1999).
89. Beer, M. *et al.* Absolute concentrations of high-energy phosphate metabolites in normal, hypertrophied, and failing human myocardium measured noninvasively with (31)P-SLOOP magnetic resonance spectroscopy. *J Am Coll Cardiol* 40, 1267–1274 (2002).
90. Nascimben, L. *et al.* Creatine kinase system in failing and nonfailing human myocardium. *Circulation* 94, 1894–1901 (1996).
91. Hove, ten, M. *et al.* Mechanisms of creatine depletion in chronically failing rat heart. *Journal of Molecular and Cellular Cardiology* 38, 309–313 (2005).
92. Neubauer, S. *et al.* Downregulation of the Na(+)-creatine cotransporter in failing human myocardium and in experimental heart failure. *Circulation* 100, 1847–1850 (1999).
93. Ingwall, J. S. *et al.* The creatine kinase system in normal and diseased human myocardium. *N Engl J Med* 313, 1050–1054 (1985).
94. Khuchua, Z. A., Ventura-Clapier, R., Kuznetsov, A. V., Grishin, M. N. & Saks, V. A. Alterations in the creatine kinase system in the myocardium of cardiomyopathic hamsters. *Biochem Biophys Res Commun* 165, 748–757 (1989).
95. Laser, A. *et al.* Regional biochemical remodeling in non-infarcted tissue of rat heart post-myocardial infarction. *Journal of Molecular and Cellular Cardiology* 28, 1531–1538 (1996).
96. De Sousa, E. *et al.* Subcellular creatine kinase alterations. Implications in heart failure. *Circulation Research* 85, 68–76 (1999).
97. Lygate, C. A. *et al.* The creatine kinase energy transport system in the failing mouse heart. *Journal of Molecular and Cellular Cardiology* 42, 1129–1136 (2007).
98. Smith, C. S., Bottomley, P. A., Schulman, S. P., Gerstenblith, G. & Weiss, R. G. Altered creatine kinase adenosine triphosphate kinetics in failing hypertrophied human myocardium. *Circulation* 114, 1151–1158 (2006).
99. Neubauer, S. *et al.* Myocardial phosphocreatine-to-ATP ratio is a predictor of mortality in patients with dilated cardiomyopathy. *Circulation* 96, 2190–2196 (1997).
100. Weiss, R. G., Bottomley, P. A., Hardy, C. J. & Gerstenblith, G. Regional myocardial metabolism of high-energy phosphates during isometric exercise in patients with coronary artery disease. *N Engl J Med* 323, 1593–1600 (1990).

101. Neubauer, S. *et al.* 31P magnetic resonance spectroscopy in dilated cardiomyopathy and coronary artery disease. Altered cardiac high-energy phosphate metabolism in heart failure. *Circulation* 86, 1810–1818 (1992).
102. Fitch, C. D., Shields, R. P., Payne, W. F. & Dacus, J. M. Creatine metabolism in skeletal muscle. 3. Specificity of the creatine entry process. *J Biol Chem* 243, 2024–2027 (1968).
103. Wyss, M. & Wallimann, T. Creatine metabolism and the consequences of creatine depletion in muscle. *Mol Cell Biochem* 133-134, 51–66 (1994).
104. Horn, M., Remkes, H., Strömer, H., Dienesch, C. & Neubauer, S. Chronic phosphocreatine depletion by the creatine analogue beta-guanidinopropionate is associated with increased mortality and loss of ATP in rats after myocardial infarction. *Circulation* 104, 1844–1849 (2001).
105. Lorentzon, M. *et al.* In vivo effects of myocardial creatine depletion on left ventricular function, morphology, and energy metabolism--consequences in acute myocardial infarction. *J. Card. Fail.* 13, 230–237 (2007).
106. Schmidt, A. *et al.* Severely altered guanidino compound levels, disturbed body weight homeostasis and impaired fertility in a mouse model of guanidinoacetate N-methyltransferase (GAMT) deficiency. *Human Molecular Genetics* 13, 905–921 (2004).
107. Hove, ten, M. *et al.* Reduced inotropic reserve and increased susceptibility to cardiac ischemia/reperfusion injury in phosphocreatine-deficient guanidinoacetate-N-methyltransferase-knockout mice. *Circulation* 111, 2477–2485 (2005).
108. Schneider, J. E. *et al.* Cardiac structure and function during ageing in energetically compromised Guanidinoacetate N-methyltransferase (GAMT)-knockout mice - a one year longitudinal MRI study. *J Cardiovasc Magn Reson* 10, 9 (2008).
109. Boehm, E. A., Radda, G. K., Tomlin, H. & Clark, J. F. The utilisation of creatine and its analogues by cytosolic and mitochondrial creatine kinase. *Biochim Biophys Acta* 1274, 119–128 (1996).
110. Lygate, C. A. *et al.* Living without creatine: unchanged exercise capacity and response to chronic myocardial infarction in creatine-deficient mice. *Circulation Research* 112, 945–955 (2013).
111. Branovets, J. *et al.* Unchanged mitochondrial organization and compartmentation of high-energy phosphates in creatine-deficient GAMT-/- mouse hearts. *AJP: Heart and Circulatory Physiology* 305, H506–20 (2013).
112. Nabuurs, C. I. *et al.* Disturbed energy metabolism and muscular dystrophy caused by pure creatine deficiency are reversible by creatine intake. *J Physiol (Lond)* 591, 571–592 (2013).
113. Choe, C.-U. *et al.* L-arginine:glycine amidinotransferase deficiency protects from metabolic syndrome. *Human Molecular Genetics* 22, 110–123 (2013).
114. Lygate, C. A. *et al.* Chronic creatine deficiency is not the underlying cause of cardiac dysfunction in mice lacking the creatine biosynthetic enzyme arginine:glycine amidinotransferase. in *American Heart Association Scientific Sessions* (2013).
115. Choe, C. U. *et al.* Homoarginine Levels Are Regulated by L-Arginine:Glycine Amidinotransferase and Affect Stroke Outcome: Results From Human and Murine Studies. *Circulation* 128, 1451–1461 (2013).
116. Skelton, M. R. *et al.* Creatine Transporter (CrT; Slc6a8) Knockout Mice as a Model of Human CrT Deficiency. *PLoS ONE* 6, e16187 (2011).
117. Hurne, A. M., Chai, C. L. & Waring, P. Inactivation of rabbit muscle creatine kinase by reversible formation of an internal disulfide bond induced by the fungal toxin gliotoxin. *J Biol Chem* 275, 25202–25206 (2000).
118. Fossel, E. T. & Hoefeler, H. Complete inhibition of creatine kinase in isolated perfused rat hearts. *Am J Physiol* 252, E124–9 (1987).
119. Hamman, B. L. *et al.* Inhibition of the creatine kinase reaction decreases the contractile reserve of isolated rat hearts. *Am J Physiol* 269, H1030–6 (1995).
120. Tian, R., Nascimben, L., Kaddurah-Daouk, R. & Ingwall, J. S. Depletion of energy reserve via the creatine kinase reaction during the evolution of heart failure in cardiomyopathic hamsters. *Journal of Molecular and Cellular Cardiology* 28, 755–765 (1996).
121. van Deursen, J. *et al.* Skeletal muscles of mice deficient in muscle creatine kinase lack burst activity. *Cell* 74, 621–631 (1993).
122. Steeghs, K. *et al.* Use of gene targeting for compromising energy homeostasis in neuro-muscular tissues: the role of sarcomeric mitochondrial creatine kinase. *J. Neurosci. Methods* 71, 29–41 (1997).
123. Steeghs, K. *et al.* Altered Ca2+ responses in muscles with combined mitochondrial and cytosolic creatine kinase deficiencies. *Cell* 89, 93–103 (1997).
124. Ventura-Clapier, R. *et al.* Muscle creatine kinase-deficient mice. I. Alterations in myofibrillar function. *J Biol Chem* 270, 19914–19920 (1995).
125. Saupe, K. W., Spindler, M., Tian, R. & Ingwall, J. S. Impaired cardiac energetics in mice lacking muscle-specific isoenzymes of creatine kinase. *Circulation Research* 82, 898–907 (1998).
126. Spindler, M. *et al.* Mitochondrial creatine kinase is critically necessary for normal myocardial high-energy phosphate metabolism. *Am J Physiol Heart Circ Physiol* 283, H680–7 (2002).
127. Spindler, M. *et al.* Creatine kinase-deficient hearts exhibit increased susceptibility to ischemia-reperfusion injury and impaired calcium homeostasis. *Am J Physiol Heart Circ Physiol* 287, H1039–45 (2004).
128. Nahrendorf, M. *et al.* Creatine kinase knockout mice show left ventricular hypertrophy and dilatation, but unaltered remodeling post-myocardial infarction. *Cardiovascular Research* 65, 419–427 (2005).
129. Nahrendorf, M. *et al.* Multimodal functional cardiac MRI in creatine kinase-deficient mice reveals subtle abnormalities in myocardial perfusion and mechanics. *Am J Physiol Heart Circ Physiol* 290, H2516–21 (2006).
130. Lygate, C. A. *et al.* Cardiac phenotype of mitochondrial creatine kinase knockout mice is modified on a pure C57BL/6 genetic background. *Journal of Molecular and Cellular Cardiology* 46, 93–99 (2009).
131. Lygate, C. A. *et al.* Chronic creatine kinase deficiency eventually leads to congestive heart failure, but severity is dependent on genetic background, gender and age. *Basic Res Cardiol* 107, 276 (2012).
132. Boehm, E. *et al.* Maintained coupling of oxidative phosphorylation to creatine kinase activity in sarcomeric mitochondrial creatine kinase-deficient mice. *Journal of Molecular and Cellular Cardiology* 30, 901–912 (1998).
133. Boehm, E., Ventura-Clapier, R., Mateo, P., Lechène, P. & Veksler, V. Glycolysis supports calcium uptake by the sarcoplasmic reticulum in skinned ventricular fibres of mice deficient in mitochondrial and cytosolic creatine kinase.

Journal of Molecular and Cellular Cardiology 32, 891–902 (2000).
134. Dzeja, P. P. *et al.* Rearrangement of energetic and substrate utilization networks compensate for chronic myocardial creatine kinase deficiency. *J Physiol (Lond)* 589, 5193–5211 (2011).
135. Kaasik, A. *et al.* Energetic crosstalk between organelles: architectural integration of energy production and utilization. *Circulation Research* 89, 153–159 (2001).
136. Steeghs, K., Oerlemans, F. & Wieringa, B. Mice deficient in ubiquitous mitochondrial creatine kinase are viable and fertile. *Biochim Biophys Acta* 1230, 130–138 (1995).
137. Streijger, F. *et al.* Mice lacking the UbCKmit isoform of creatine kinase reveal slower spatial learning acquisition, diminished exploration and habituation, and reduced acoustic startle reflex responses. *Mol Cell Biochem* 256-257, 305–318 (2004).
138. Jost, C. R. *et al.* Creatine kinase B-driven energy transfer in the brain is important for habituation and spatial learning behaviour, mossy fibre field size and determination of seizure susceptibility. *The European journal of neuroscience* 15, 1692–1706 (2002).
139. Streijger, F. *et al.* Structural and behavioural consequences of double deficiency for creatine kinases BCK and UbCKmit. *Behav. Brain Res.* 157, 219–234 (2005).
140. Horn, M. *et al.* Chronic high-dose creatine feeding does not attenuate left ventricular remodeling in rat hearts post-myocardial infarction. *Cardiovascular Research* 43, 117–124 (1999).
141. Boehm, E. *et al.* Creatine transporter activity and content in the rat heart supplemented by and depleted of creatine. *Am J Physiol Endocrinol Metab* 284, E399–406 (2003).
142. Wallis, J. *et al.* Supranormal myocardial creatine and phosphocreatine concentrations lead to cardiac hypertrophy and heart failure: insights from creatine transporter-overexpressing transgenic mice. *Circulation* 112, 3131–3139 (2005).
143. Phillips, D. *et al.* Mice over-expressing the myocardial creatine transporter develop progressive heart failure and show decreased glycolytic capacity. *Journal of Molecular and Cellular Cardiology* 48, 582–590 (2010).
144. Lygate, C. A. *et al.* Moderate elevation of intracellular creatine by targeting the creatine transporter protects mice from acute myocardial infarction. *Cardiovascular Research* 96, 466–475 (2012).
145. Gupta, A. *et al.* Creatine kinase-mediated improvement of function in failing mouse hearts provides causal evidence the failing heart is energy starved. *J Clin Invest* 122, 291–302 (2012).
146. Akki, A. *et al.* Creatine kinase overexpression improves ATP kinetics and contractile function in postischemic myocardium. *AJP: Heart and Circulatory Physiology* 303, H844–H852 (2012).
147. Koretsky, A. P., Brosnan, M. J., Chen, L. H., Chen, J. D. & Van Dyke, T. NMR detection of creatine kinase expressed in liver of transgenic mice: determination of free ADP levels. *Proc Natl Acad Sci USA* 87, 3112–3116 (1990).
148. Miller, K., Halow, J. & Koretsky, A. P. Phosphocreatine protects transgenic mouse liver expressing creatine kinase from hypoxia and ischemia. *Am J Physiol* 265, C1544–51 (1993).
149. Miller, K., Sharer, K., Suhan, J. & Koretsky, A. P. Expression of functional mitochondrial creatine kinase in liver of transgenic mice. *Am J Physiol* 272, C1193–202 (1997).
150. Dolder, M., Walzel, B., Speer, O., Schlattner, U. & Wallimann, T. Inhibition of the mitochondrial permeability transition by creatine kinase substrates. Requirement for microcompartmentation. *J Biol Chem* 278, 17760–17766 (2003).
151. Graham, F. L., Smiley, J., Russell, W. C. & Nairn, R. Characteristics of a human cell line transformed by DNA from human adenovirus type 5. *J Gen Virol* 36, 59–74 (1977).
152. Claycomb, W. C. *et al.* HL-1 cells: a cardiac muscle cell line that contracts and retains phenotypic characteristics of the adult cardiomyocyte. *Proc Natl Acad Sci USA* 95, 2979–2984 (1998).
153. Delcarpio, J. B., Lanson, N. A., Field, L. J. & Claycomb, W. C. Morphological characterization of cardiomyocytes isolated from a transplantable cardiac tumor derived from transgenic mouse atria (AT-1 cells). *Circulation Research* 69, 1591–1600 (1991).
154. Truett, G. E. *et al.* Preparation of PCR-quality mouse genomic DNA with hot sodium hydroxide and tris (HotSHOT). *BioTechniques* 29, 52, 54 (2000).
155. Livak, K. J. & Schmittgen, T. D. Analysis of relative gene expression data using real-time quantitative PCR and the 2(-Delta Delta C(T)) Method. *Methods* 25, 402–408 (2001).
156. Radonić, A. *et al.* Guideline to reference gene selection for quantitative real-time PCR. *Biochem Biophys Res Commun* 313, 856–862 (2004).
157. Brattelid, T. *et al.* Reference gene alternatives to Gapdh in rodent and human heart failure gene expression studies. *BMC Mol Biol* 11, 22 (2010).
158. OLIVER, I. T. A spectrophotometric method for the determination of creatine phosphokinase and myokinase. *Biochem J* 61, 116–122 (1955).
159. Szasz, G., Waldenström, J. & Gruber, W. Creatine kinase in serum: 6. Inhibition by endogenous polyvalent cations, and effect of chelators on the activity and stability of some assay components. *Clinical Chemistry* 25, 446–452 (1979).
160. Quinlan, P. T., Thomas, A. P., Armston, A. E. & Halestrap, A. P. Measurement of the intramitochondrial volume in hepatocytes without cell disruption and its elevation by hormones and valinomycin. *Biochem J* 214, 395–404 (1983).
161. Srere, P., Brazil, H. & Gonen, L. The citrate condensing enzyme of pigeon breast muscle and moth flight muscle. *Acta Chem Scand* 17, s129–s134 (1963).
162. LOWRY, O. H., ROSEBROUGH, N. J., FARR, A. L. & RANDALL, R. J. Protein measurement with the Folin phenol reagent. *J Biol Chem* 193, 265–275 (1951).
163. Kozak, M. An analysis of 5'-noncoding sequences from 699 vertebrate messenger RNAs. *Nucleic Acids Res* 15, 8125–8148 (1987).
164. Yenofsky, R. L., Fine, M. & Pellow, J. W. A mutant neomycin phosphotransferase II gene reduces the resistance of transformants to antibiotic selection pressure. *Proc Natl Acad Sci USA* 87, 3435–3439 (1990).
165. Teixeira, G. *et al.* Synergistic protective effect of cyclosporin A and rotenone against hypoxia-reoxygenation in cardiomyocytes. *Journal of Molecular and Cellular Cardiology* 56, 55–62 (2013).

166. Brady, N. R., Hamacher-Brady, A. & Gottlieb, R. A. Proapoptotic BCL-2 family members and mitochondrial dysfunction during ischemia/reperfusion injury, a study employing cardiac HL-1 cells and GFP biosensors. *Biochim Biophys Acta* 1757, 667–678 (2006).
167. Ong, S.-B. *et al.* Inhibiting mitochondrial fission protects the heart against ischemia/reperfusion injury. *Circulation* 121, 2012–2022 (2010).
168. Aström-Olsson, K. *et al.* Impact of hypoxia, simulated ischemia and reperfusion in HL-1 cells on the expression of FKBP12/FKBP12.6 and intracellular calcium dynamics. *Biochem Biophys Res Commun* 422, 732–738 (2012).
169. Allen, C. B., Schneider, B. K. & White, C. W. Limitations to oxygen diffusion and equilibration in in vitro cell exposure systems in hyperoxia and hypoxia. *Am J Physiol Lung Cell Mol Physiol* 281, L1021–7 (2001).
170. Thornberry, N. A. *et al.* A novel heterodimeric cysteine protease is required for interleukin-1 beta processing in monocytes. *Nature* 356, 768–774 (1992).
171. Yuan, J., Shaham, S., Ledoux, S., Ellis, H. M. & Horvitz, H. R. The C. elegans cell death gene ced-3 encodes a protein similar to mammalian interleukin-1 beta-converting enzyme. *Cell* 75, 641–652 (1993).
172. Fearnhead, H. O., Dinsdale, D. & Cohen, G. M. An interleukin-1 beta-converting enzyme-like protease is a common mediator of apoptosis in thymocytes. *FEBS Lett* 375, 283–288 (1995).
173. Gottlieb, R. A., Gruol, D. L., Zhu, J. Y. & Engler, R. L. Preconditioning rabbit cardiomyocytes: role of pH, vacuolar proton ATPase, and apoptosis. *J Clin Invest* 97, 2391–2398 (1996).
174. Yaoita, H., Ogawa, K., Maehara, K. & Maruyama, Y. Attenuation of ischemia/reperfusion injury in rats by a caspase inhibitor. *Circulation* 97, 276–281 (1998).
175. Hamacher-Brady, A. *et al.* Response to myocardial ischemia/reperfusion injury involves Bnip3 and autophagy. *Cell Death Differ* 14, 146–157 (2007).
176. Ai, H.-W., Shaner, N. C., Cheng, Z., Tsien, R. Y. & Campbell, R. E. Exploration of New Chromophore Structures Leads to the Identification of Improved Blue Fluorescent Proteins †. *Biochemistry* 46, 5904–5910 (2007).
177. Garcia-Gras, E. *et al.* Suppression of canonical Wnt/beta-catenin signaling by nuclear plakoglobin recapitulates phenotype of arrhythmogenic right ventricular cardiomyopathy. *J Clin Invest* 116, 2012–2021 (2006).
178. Ljubkovic, M., Marinovic, J., Fuchs, A., Bosnjak, Z. J. & Bienengraeber, M. Targeted expression of Kir6.2 in mitochondria confers protection against hypoxic stress. *J Physiol (Lond)* 577, 17–29 (2006).
179. Haghikia, A. *et al.* Signal transducer and activator of transcription 3-mediated regulation of miR-199a-5p links cardiomyocyte and endothelial cell function in the heart: a key role for ubiquitin-conjugating enzymes. *Eur Heart J* 32, 1287–1297 (2011).
180. Boltzen, U. *et al.* Alternatively spliced tissue factor and full-length tissue factor protect cardiomyocytes against TNF-α-induced apoptosis. *Journal of Molecular and Cellular Cardiology* 52, 1056–1065 (2012).
181. Min, C. K. *et al.* Coupling of ryanodine receptor 2 and voltage-dependent anion channel 2 is essential for Ca 2+transfer from the sarcoplasmic reticulum to the mitochondria in the heart. *Biochem J* 447, 371–379 (2012).
182. Khuchua, Z. A. *et al.* Octamer formation and coupling of cardiac sarcomeric mitochondrial creatine kinase are mediated by charged N-terminal residues. *J Biol Chem* 273, 22990–22996 (1998).
183. Schlattner, U. *et al.* C-terminal lysines determine phospholipid interaction of sarcomeric mitochondrial creatine kinase. *J Biol Chem* 279, 24334–24342 (2004).
184. Eimre, M. *et al.* Distinct organization of energy metabolism in HL-1 cardiac cell line and cardiomyocytes. *Biochimica et Biophysica Acta - Bioenergetics* 1777, 514–524 (2008).
185. Guyton, A. C. & Hall, J. E. *Textbook of Medical Physiology, 11th ed.* (2006).
186. Coburn, R. F., Ploegmakers, F., Gondrie, P. & Abboud, R. Myocardial myoglobin oxygen tension. *Am J Physiol* 224, 870–876 (1973).
187. Friedrich, G. & Soriano, P. Promoter traps in embryonic stem cells: a genetic screen to identify and mutate developmental genes in mice. *Genes Dev* 5, 1513–1523 (1991).
188. Soriano, P. Generalized lacZ expression with the ROSA26 Cre reporter strain. *Nat Genet* 21, 70–71 (1999).
189. Sohal, D. S. *et al.* Temporally regulated and tissue-specific gene manipulations in the adult and embryonic heart using a tamoxifen-inducible Cre protein. *Circulation Research* 89, 20–25 (2001).
190. Mao, J., Barrow, J., McMahon, J., Vaughan, J. & McMahon, A. P. An ES cell system for rapid, spatial and temporal analysis of gene function in vitro and in vivo. *Nucleic Acids Res* 33, e155 (2005).
191. Hohenstein, P. *et al.* High-efficiency Rosa26 knock-in vector construction for Cre-regulated overexpression and RNAi. *Pathogenetics* 1, 3 (2008).
192. Nyabi, O. *et al.* Efficient mouse transgenesis using Gateway-compatible ROSA26 locus targeting vectors and F1 hybrid ES cells. *Nucleic Acids Res* 37, e55 (2009).
193. Zambrowicz, B. P. *et al.* Disruption of overlapping transcripts in the ROSA beta geo 26 gene trap strain leads to widespread expression of beta-galactosidase in mouse embryos and hematopoietic cells. *Proc Natl Acad Sci USA* 94, 3789–3794 (1997).
194. Strathdee, D., Ibbotson, H. & Grant, S. G. N. Expression of transgenes targeted to the Gt(ROSA)26Sor locus is orientation dependent. *PLoS ONE* 1, e4 (2006).
195. Hasegawa, K. & Nakatsuji, N. Insulators prevent transcriptional interference between two promoters in a double gene construct for transgenesis. *FEBS Lett* 520, 47–52 (2002).
196. Belteki, G., Gertsenstein, M., Ow, D. W. & Nagy, A. Site-specific cassette exchange and germline transmission with mouse ES cells expressing phiC31 integrase. *Nat Biotechnol* 21, 321–324 (2003).
197. Lakso, M. *et al.* Targeted oncogene activation by site-specific recombination in transgenic mice. *Proc Natl Acad Sci USA* 89, 6232–6236 (1992).
198. Dymecki, S. M. Flp recombinase promotes site-specific DNA recombination in embryonic stem cells and transgenic mice. *Proc Natl Acad Sci USA* 93, 6191–6196 (1996).
199. Chen, C.-M., Krohn, J., Bhattacharya, S. & Davies, B. A comparison of exogenous promoter activity at the ROSA26

locus using a ΦiC31 integrase mediated cassette exchange approach in mouse ES cells. *PLoS ONE* 6, e23376 (2011).
200. Buerger, A. *et al.* Dilated cardiomyopathy resulting from high-level myocardial expression of Cre-recombinase. *J. Card. Fail.* 12, 392–398 (2006).
201. Molkentin, J. D. & Robbins, J. With great power comes great responsibility: using mouse genetics to study cardiac hypertrophy and failure. *Journal of Molecular and Cellular Cardiology* 46, 130–136 (2009).
202. Bersell, K. *et al.* Moderate and high amounts of tamoxifen in α-MHC-MerCreMer mice induce a DNA damage response, leading to heart failure and death. *Dis Model Mech* (2013). doi:10.1242/dmm.010447
203. Tiivel, T. *et al.* Developmental changes in regulation of mitochondrial respiration by ADP and creatine in rat heart in vivo. *Mol Cell Biochem* 208, 119–128 (2000).
204. Ng, W. A., Grupp, I. L., Subramaniam, A. & Robbins, J. Cardiac myosin heavy chain mRNA expression and myocardial function in the mouse heart. *Circulation Research* 68, 1742–1750 (1991).
205. Lyons, G. E. In situ analysis of the cardiac muscle gene program during embryogenesis. *Trends Cardiovasc Med* 4, 70–77 (1994).
206. Izumo, S. *et al.* Myosin heavy chain messenger RNA and protein isoform transitions during cardiac hypertrophy. Interaction between hemodynamic and thyroid hormone-induced signals. *J Clin Invest* 79, 970–977 (1987).
207. Deschepper, C. F., Olson, J. L., Otis, M. & Gallo-Payet, N. Characterization of blood pressure and morphological traits in cardiovascular-related organs in 13 different inbred mouse strains. *J Appl Physiol* 97, 369–376 (2004).
208. Barrick, C. J., Rojas, M., Schoonhoven, R., Smyth, S. S. & Threadgill, D. W. Cardiac response to pressure overload in 129S1/SvImJ and C57BL/6J mice: temporal- and background-dependent development of concentric left ventricular hypertrophy. *ajpheart.physiology.org*
209. Waterston, R. H. *et al.* Initial sequencing and comparative analysis of the mouse genome. *Nature* 420, 520–562 (2002).
210. Brinster, R. L., Chen, H. Y., Trumbauer, M. E., Yagle, M. K. & Palmiter, R. D. Factors affecting the efficiency of introducing foreign DNA into mice by microinjecting eggs. *Proc Natl Acad Sci USA* 82, 4438–4442 (1985).
211. Auerbach, A. B. *et al.* Strain-dependent differences in the efficiency of transgenic mouse production. *Transgenic Res* 12, 59–69 (2003).
212. Eggan, K. *et al.* Hybrid vigor, fetal overgrowth, and viability of mice derived by nuclear cloning and tetraploid embryo complementation. *Proc Natl Acad Sci USA* 98, 6209–6214 (2001).
213. George, S. H. L. *et al.* Developmental and adult phenotyping directly from mutant embryonic stem cells. *Proc Natl Acad Sci USA* 104, 4455–4460 (2007).
214. Hitz, C., Wurst, W. & Kuhn, R. Conditional brain-specific knockdown of MAPK using Cre/loxP regulated RNA interference. *Nucleic Acids Res* 35, e90–e90 (2007).
215. Maltsev, V. A., Wobus, A. M., Rohwedel, J., Bader, M. & Hescheler, J. Cardiomyocytes differentiated in vitro from embryonic stem cells developmentally express cardiac-specific genes and ionic currents. *Circulation Research* 75, 233–244 (1994).
216. Sánchez, A., Jones, W. K., Gulick, J., Doetschman, T. & Robbins, J. Myosin heavy chain gene expression in mouse embryoid bodies. An in vitro developmental study. *J Biol Chem* 266, 22419–22426 (1991).
217. Laird, C. D. Chromatid structure: relationship between DNA content and nucleotide sequence diversity. *Chromosoma* 32, 378–406 (1971).
218. Tesson, L., Heslan, J.-M., Ménoret, S. & Anegon, I. Rapid and accurate determination of zygosity in transgenic animals by real-time quantitative PCR. *Transgenic Res* 11, 43–48 (2002).
219. Sakurai, T., Kamiyoshi, A., Watanabe, S., Sato, M. & Shindo, T. Rapid zygosity determination in mice by SYBR Green real-time genomic PCR of a crude DNA solution. *Transgenic Res* 17, 149–155 (2008).
220. Chen, M. *et al.* Prodeath signaling of G protein-coupled receptor kinase 2 in cardiac myocytes after ischemic stress occurs via extracellular signal-regulated kinase-dependent heat shock protein 90-mediated mitochondrial targeting. *Circulation Research* 112, 1121–1134 (2013).
221. Glyn, M. C. & Ward, B. J. Contraction in cardiac endothelial cells contributes to changes in capillary dimensions following ischaemia and reperfusion. *Cardiovascular Research* 48, 346–356 (2000).
222. Young, A. A., Barnes, H., Davison, D., Neubauer, S. & Schneider, J. E. Fast left ventricular mass and volume assessment in mice with three-dimensional guide-point modeling. *J. Magn. Reson. Imaging* 30, 514–520 (2009).
223. Gardner, R. L. Mouse chimeras obtained by the injection of cells into the blastocyst. *Nature* 220, 596–597 (1968).
224. Gossler, A., Doetschman, T., Korn, R., Serfling, E. & Kemler, R. Transgenesis by means of blastocyst-derived embryonic stem cell lines. *Proc Natl Acad Sci USA* 83, 9065–9069 (1986).
225. Schwartzberg, P. L., Goff, S. P. & Robertson, E. J. Germ-line transmission of a c-abl mutation produced by targeted gene disruption in ES cells. *Science* 246, 799–803 (1989).
226. Subramaniam, A. *et al.* Tissue-specific regulation of the alpha-myosin heavy chain gene promoter in transgenic mice. *J Biol Chem* 266, 24613–24620 (1991).
227. Maier, T., Güell, M. & Serrano, L. Correlation of mRNA and protein in complex biological samples. *FEBS Lett* 583, 3966–3973 (2009).
228. Vogel, C. & Marcotte, E. M. Insights into the regulation of protein abundance from proteomic and transcriptomic analyses. *Nat. Rev. Genet.* 13, 227–232 (2012).
229. Tian, Q. *et al.* Integrated genomic and proteomic analyses of gene expression in Mammalian cells. *Mol. Cell Proteomics* 3, 960–969 (2004).
230. Gulick, J., Subramaniam, A., Neumann, J. & Robbins, J. Isolation and characterization of the mouse cardiac myosin heavy chain genes. *J Biol Chem* 266, 9180–9185 (1991).
231. Subramaniam, A., Gulick, J., Neumann, J., Knotts, S. & Robbins, J. Transgenic analysis of the thyroid-responsive elements in the alpha-cardiac myosin heavy chain gene promoter. *J Biol Chem* 268, 4331–4336 (1993).
232. Adolph, E. A., Subramaniam, A., Cserjesi, P., Olson, E. N. & Robbins, J. Role of myocyte-specific enhancer-binding factor (MEF-2) in transcriptional regulation of the alpha-cardiac myosin heavy chain gene. *J Biol Chem* 268, 5349–5352

(1993).
233. Molkentin, J. D., Jobe, S. M. & Markham, B. E. Alpha-myosin heavy chain gene regulation: delineation and characterization of the cardiac muscle-specific enhancer and muscle-specific promoter. *Journal of Molecular and Cellular Cardiology* 28, 1211–1225 (1996).
234. Molkentin, J. D., Kalvakolanu, D. V. & Markham, B. E. Transcription factor GATA-4 regulates cardiac muscle-specific expression of the alpha-myosin heavy-chain gene. *Mol Cell Biol* 14, 4947–4957 (1994).
235. Wegmann, G., Huber, R., Zanolla, E., Eppenberger, H. M. & Wallimann, T. Differential expression and localization of brain-type and mitochondrial creatine kinase isoenzymes during development of the chicken retina: Mi-CK as a marker for differentiation of photoreceptor cells. *Differentiation* 46, 77–87 (1991).
236. Xiao, B. *et al.* Structure of mammalian AMPK and its regulation by ADP. *Nature* 472, 230–233 (2011).
237. Saupe, K. W., Spindler, M., Hopkins, J. C., Shen, W. & Ingwall, J. S. Kinetic, thermodynamic, and developmental consequences of deleting creatine kinase isoenzymes from the heart. Reaction kinetics of the creatine kinase isoenzymes in the intact heart. *J Biol Chem* 275, 19742–19746 (2000).
238. Spindler, M. *et al.* Alterations in the myocardial creatine kinase system precede the development of contractile dysfunction in beta(1)-adrenergic receptor transgenic mice. *Journal of Molecular and Cellular Cardiology* 35, 389–397 (2003).
239. Askenasy, N. & Koretsky, A. P. Transgenic livers expressing mitochondrial and cytosolic CK: mitochondrial CK modulates free ADP levels. *Am J Physiol, Cell Physiol* 282, C338–46 (2002).
240. Brosnan, M. J., Chen, L., Van Dyke, T. A. & Koretsky, A. P. Free ADP levels in transgenic mouse liver expressing creatine kinase. Effects of enzyme activity, phosphagen type, and substrate concentration. *J Biol Chem* 265, 20849–20855 (1990).
241. Hardie, D. G. AMP-activated protein kinase: an energy sensor that regulates all aspects of cell function. *Genes Dev* 25, 1895–1908 (2011).
242. Scarpulla, R. C. Nuclear activators and coactivators in mammalian mitochondrial biogenesis. *Biochim Biophys Acta* 1576, 1–14 (2002).
243. Wu, Z. *et al.* Mechanisms controlling mitochondrial biogenesis and respiration through the thermogenic coactivator PGC-1. *Cell* 98, 115–124 (1999).
244. Zong, H. *et al.* AMP kinase is required for mitochondrial biogenesis in skeletal muscle in response to chronic energy deprivation. *Proc Natl Acad Sci USA* 99, 15983–15987 (2002).
245. Gordon, J. W., Scangos, G. A., Plotkin, D. J., Barbosa, J. A. & Ruddle, F. H. Genetic transformation of mouse embryos by microinjection of purified DNA. *Proc Natl Acad Sci USA* 77, 7380–7384 (1980).
246. Costantini, F. & Lacy, E. Introduction of a rabbit beta-globin gene into the mouse germ line. *Nature* 294, 92–94 (1981).
247. Harbers, K., Jähner, D. & Jaenisch, R. Microinjection of cloned retroviral genomes into mouse zygotes: integration and expression in the animal. *Nature* 293, 540–542 (1981).
248. Wagner, E. F., Stewart, T. A. & Mintz, B. The human beta-globin gene and a functional viral thymidine kinase gene in developing mice. *Proc Natl Acad Sci USA* 78, 5016–5020 (1981).
249. Roman, B. B., Wieringa, B. & Koretsky, A. P. Functional equivalence of creatine kinase isoforms in mouse skeletal muscle. *J Biol Chem* 272, 17790–17794 (1997).
250. van Deursen, J. & Wieringa, B. Targeting of the creatine kinase M gene in embryonic stem cells using isogenic and nonisogenic vectors. *Nucleic Acids Res* 20, 3815–3820 (1992).
251. van Deursen, J. *et al.* Genetic variability of the murine creatine kinase B gene locus and related pseudogenes in different inbred strains of mice. *Genomics* 12, 340–349 (1992).
252. Palmiter, R. D. & Brinster, R. L. Germ-line transformation of mice. *Annu. Rev. Genet.* 20, 465–499 (1986).
253. Knotts, S., Rindt, H. & Robbins, J. Position independent expression and developmental regulation is directed by the beta myosin heavy chain gene's 5' upstream region in transgenic mice. *Nucleic Acids Res* 23, 3301–3309 (1995).
254. Gulick, J. *et al.* Transgenic remodeling of the regulatory myosin light chains in the mammalian heart. *Circulation Research* 80, 655–664 (1997).
255. Wagner, E. F., Covarrubias, L., Stewart, T. A. & Mintz, B. Prenatal lethalities in mice homozygous for human growth hormone gene sequences integrated in the germ line. *Cell* 35, 647–655 (1983).
256. Kucera, G. T., Bortner, D. M. & Rosenberg, M. P. Overexpression of an Agouti cDNA in the skin of transgenic mice recapitulates dominant coat color phenotypes of spontaneous mutants. *Dev Biol* 173, 162–173 (1996).
257. Gupta, A. *et al.* Creatine kinase-overexpression improves myocardial energetics, contractile dysfunction and survival in murine Doxorubicin cardiotoxicity. *PLoS ONE* 8, e74675 (2013).
258. Brosnan, M. J., Raman, S. P., Chen, L. & Koretsky, A. P. Altering creatine kinase isoenzymes in transgenic mouse muscle by overexpression of the B subunit. *Am J Physiol* 264, C151–60 (1993).
259. Hunter, D. R., Haworth, R. A. & Southard, J. H. Relationship between configuration, function, and permeability in calcium-treated mitochondria. *J Biol Chem* 251, 5069–5077 (1976).
260. Kowaltowski, A. J., Castilho, R. F. & Vercesi, A. E. Opening of the mitochondrial permeability transition pore by uncoupling or inorganic phosphate in the presence of Ca2+ is dependent on mitochondrial-generated reactive oxygen species. *FEBS Lett* 378, 150–152 (1996).
261. Kim, J.-S., Jin, Y. & Lemasters, J. J. Reactive oxygen species, but not Ca2+ overloading, trigger pH- and mitochondrial permeability transition-dependent death of adult rat myocytes after ischemia-reperfusion. *Am J Physiol Heart Circ Physiol* 290, H2024–34 (2006).
262. Brenner, C. & Moulin, M. Physiological Roles of the Permeability Transition Pore. *Circulation Research* 111, 1237–1247 (2012).
263. Elrod, J. W. & Molkentin, J. D. Physiologic Functions of Cyclophilin D and the Mitochondrial Permeability Transition Pore. *Circ J* 77, 1111–1122 (2013).
264. Beutner, G., Ruck, A., Riede, B., Welte, W. & Brdiczka, D. Complexes between kinases, mitochondrial porin and adenylate translocator in rat brain resemble the permeability transition pore. *FEBS Lett* 396, 189–195 (1996).

265. Beutner, G., Rück, A., Riede, B. & Brdiczka, D. Complexes between porin, hexokinase, mitochondrial creatine kinase and adenylate translocator display properties of the permeability transition pore. Implication for regulation of permeability transition by the kinases. *Biochim Biophys Acta* 1368, 7–18 (1998).
266. Crompton, M., Virji, S. & Ward, J. M. Cyclophilin-D binds strongly to complexes of the voltage-dependent anion channel and the adenine nucleotide translocase to form the permeability transition pore. *Eur J Biochem* 258, 729–735 (1998).
267. Woodfield, K., Rück, A., Brdiczka, D. & Halestrap, A. P. Direct demonstration of a specific interaction between cyclophilin-D and the adenine nucleotide translocase confirms their role in the mitochondrial permeability transition. *Biochem J* 336 (Pt 2), 287–290 (1998).
268. Zamzami, N. & Kroemer, G. The mitochondrion in apoptosis: how Pandora's box opens. *Nat. Rev. Mol. Cell Biol.* 2, 67–71 (2001).
269. Kokoszka, J. E. *et al.* The ADP/ATP translocator is not essential for the mitochondrial permeability transition pore. *Nature* 427, 461–465 (2004).
270. Hunter, D. R. & Haworth, R. A. The Ca2+-induced membrane transition in mitochondria. I. The protective mechanisms. *Arch Biochem Biophys* 195, 453–459 (1979).
271. Krauskopf, A., Eriksson, O., Craigen, W. J., Forte, M. A. & Bernardi, P. Properties of the permeability transition in VDAC1(-/-) mitochondria. *Biochim Biophys Acta* 1757, 590–595 (2006).
272. Baines, C. P., Kaiser, R. A., Sheiko, T., Craigen, W. J. & Molkentin, J. D. Voltage-dependent anion channels are dispensable for mitochondrial-dependent cell death. *Nat Cell Biol* 9, 550–555 (2007).
273. Fournier, N., Ducet, G. & Crevat, A. Action of cyclosporine on mitochondrial calcium fluxes. *J Bioenerg Biomembr* 19, 297–303 (1987).
274. Crompton, M., Ellinger, H. & Costi, A. Inhibition by cyclosporin A of a Ca2+-dependent pore in heart mitochondria activated by inorganic phosphate and oxidative stress. *Biochem J* 255, 357–360 (1988).
275. Halestrap, A. P. & Davidson, A. M. Inhibition of Ca2(+)-induced large-amplitude swelling of liver and heart mitochondria by cyclosporin is probably caused by the inhibitor binding to mitochondrial-matrix peptidyl-prolyl cis-trans isomerase and preventing it interacting with the adenine nucleotide translocase. *Biochem J* 268, 153–160 (1990).
276. Griffiths, E. J. & Halestrap, A. P. Further evidence that cyclosporin A protects mitochondria from calcium overload by inhibiting a matrix peptidyl-prolyl cis-trans isomerase. Implications for the immunosuppressive and toxic effects of cyclosporin. *Biochem J* 274 (Pt 2), 611–614 (1991).
277. Connern, C. P. & Halestrap, A. P. Purification and N-terminal sequencing of peptidyl-prolyl cis-trans-isomerase from rat liver mitochondrial matrix reveals the existence of a distinct mitochondrial cyclophilin. *Biochem J* 284 (Pt 2), 381–385 (1992).
278. Tanveer, A. *et al.* Involvement of cyclophilin D in the activation of a mitochondrial pore by Ca2+ and oxidant stress. *Eur J Biochem* 238, 166–172 (1996).
279. Kajitani, K. *et al.* Crystal structure of human cyclophilin D in complex with its inhibitor, cyclosporin A at 0.96-A resolution. *Proteins* 70, 1635–1639 (2008).
280. Clarke, S. J., McStay, G. P. & Halestrap, A. P. Sanglifehrin A acts as a potent inhibitor of the mitochondrial permeability transition and reperfusion injury of the heart by binding to cyclophilin-D at a different site from cyclosporin A. *J Biol Chem* 277, 34793–34799 (2002).
281. Basso, E. *et al.* Properties of the permeability transition pore in mitochondria devoid of Cyclophilin D. *Journal of Biological Chemistry* 280, 18558–18561 (2005).
282. Giorgio, V. *et al.* Dimers of mitochondrial ATP synthase form the permeability transition pore. *Proc Natl Acad Sci USA* (2013). doi:10.1073/pnas.1217823110
283. Giorgio, V. *et al.* Cyclophilin D modulates mitochondrial F0F1-ATP synthase by interacting with the lateral stalk of the complex. *J Biol Chem* 284, 33982–33988 (2009).
284. Crompton, M., Costi, A. & Hayat, L. Evidence for the presence of a reversible Ca2+-dependent pore activated by oxidative stress in heart mitochondria. *Biochem J* 245, 915–918 (1987).
285. Crompton, M. Kinetic evidence for a heart mitochondrial pore activated by Ca2+, inorganic phosphate and oxidative stress. *European Journal of Biochemistry* (1988).
286. Nazareth, W., Yafei, N. & Crompton, M. Inhibition of anoxia-induced injury in heart myocytes by cyclosporin A. *Journal of Molecular and Cellular Cardiology* 23, 1351–1354 (1991).
287. Griffiths, E. J. & Halestrap, A. P. Protection by Cyclosporin A of ischemia/reperfusion-induced damage in isolated rat hearts. *Journal of Molecular and Cellular Cardiology* 25, 1461–1469 (1993).
288. Halestrap, A. P., Connern, C. P., Griffiths, E. J. & Kerr, P. M. Cyclosporin A binding to mitochondrial cyclophilin inhibits the permeability transition pore and protects hearts from ischaemia/reperfusion injury. *Mol Cell Biochem* 174, 167–172 (1997).
289. Di Lisa, F., Menabò, R., Canton, M., Barile, M. & Bernardi, P. Opening of the mitochondrial permeability transition pore causes depletion of mitochondrial and cytosolic NAD+ and is a causative event in the death of myocytes in postischemic reperfusion of the heart. *J Biol Chem* 276, 2571–2575 (2001).
290. Griffiths, E. J. & Halestrap, A. P. Mitochondrial non-specific pores remain closed during cardiac ischaemia, but open upon reperfusion. *Biochem J* 307 (Pt 1), 93–98 (1995).
291. Hausenloy, D. J., Duchen, M. R. & Yellon, D. M. Inhibiting mitochondrial permeability transition pore opening at reperfusion protects against ischaemia-reperfusion injury. *Cardiovascular Research* 60, 617–625 (2003).
292. Argaud, L. *et al.* Specific inhibition of the mitochondrial permeability transition prevents lethal reperfusion injury. *Journal of Molecular and Cellular Cardiology* 38, 367–374 (2005).
293. Piot, C. *et al.* Effect of cyclosporine on reperfusion injury in acute myocardial infarction. *N Engl J Med* 359, 473–481 (2008).
294. Mewton, N. *et al.* Effect of cyclosporine on left ventricular remodeling after reperfused myocardial infarction. *J Am Coll Cardiol* 55, 1200–1205 (2010).

295. Hausenloy, D. J., Yellon, D. M., Mani-Babu, S. & Duchen, M. R. Preconditioning protects by inhibiting the mitochondrial permeability transition. *Am J Physiol Heart Circ Physiol* 287, H841–9 (2004).
296. Saotome, M. *et al.* Transient opening of mitochondrial permeability transition pore by reactive oxygen species protects myocardium from ischemia-reperfusion injury. *Am J Physiol Heart Circ Physiol* 296, H1125–32 (2009).
297. Korge, P. *et al.* Protective Role of Transient Pore Openings in Calcium Handling by Cardiac Mitochondria. *Journal of Biological Chemistry* 286, 34851–34857 (2011).
298. Dolder, M., Wendt, S. & Wallimann, T. Mitochondrial creatine kinase in contact sites: interaction with porin and adenine nucleotide translocase, role in permeability transition and sensitivity to oxidative damage. *Biological signals and receptors* 10, 93–111 (2001).
299. O'Gorman, E. *et al.* The role of creatine kinase in inhibition of mitochondrial permeability transition. *FEBS Lett* 414, 253–257 (1997).
300. Brustovetsky, N., Brustovetsky, T. & Dubinsky, J. M. On the mechanisms of neuroprotection by creatine and phosphocreatine. *J Neurochem* 76, 425–434 (2001).
301. Zervou, S. *et al.* A role for Thioredoxin interacting protein (Txnip) in cellular creatine homeostasis. *AJP: Endocrinology and Metabolism* (2013). doi:10.1152/ajpendo.00637.2012
302. Neubauer, S. *et al.* Impairment of energy metabolism in intact residual myocardium of rat hearts with chronic myocardial infarction. *J Clin Invest* 95, 1092–1100 (1995).
303. Hove, M. T. *et al.* Creatine uptake in mouse hearts with genetically altered creatine levels. *Journal of Molecular and Cellular Cardiology* 45, 453–459 (2008).
304. Wallach, D. F. H., Surgenor, D. M., Soderberg, J. & Delano, E. Preparation and Properties of 3,6-Dihydroxy-2,4-bis-[N-N´-di-(carboxymethyl)-aminomethyl] fluoran. *Anal. Chem.* 31, 456–460 (1959).
305. Wallach, D. F. H. & Steck, T. L. Fluorescence Techniques in Microdetermination of Metals in Biological Materials. II. an Improved Method for Direct Complexometric Titration of Calcium in Small Serum Samples. *Anal Biochem* 6, 176–180 (1963).
306. Petronilli, V. *et al.* Transient and long-lasting openings of the mitochondrial permeability transition pore can be monitored directly in intact cells by changes in mitochondrial calcein fluorescence. *Biophys J* 76, 725–734 (1999).
307. Katoh, H., Nishigaki, N. & Hayashi, H. Diazoxide opens the mitochondrial permeability transition pore and alters Ca2+ transients in rat ventricular myocytes. *Circulation* 105, 2666–2671 (2002).
308. Hausenloy, D., Wynne, A., Duchen, M. & Yellon, D. Transient mitochondrial permeability transition pore opening mediates preconditioning-induced protection. *Circulation* 109, 1714–1717 (2004).
309. Akao, M., O'rourke, B., Teshima, Y., Seharaseyon, J. & Marbán, E. Mechanistically distinct steps in the mitochondrial death pathway triggered by oxidative stress in cardiac myocytes. *Circulation Research* 92, 186–194 (2002).
310. Schaller, S. *et al.* TRO40303, a new cardioprotective compound, inhibits mitochondrial permeability transition. *J Pharmacol Exp Ther* 333, 696–706 (2010).
311. Zahrebelski, G. *et al.* Progression of subcellular changes during chemical hypoxia to cultured rat hepatocytes: a laser scanning confocal microscopic study. *Hepatology* 21, 1361–1372 (1995).
312. Tenopoulou, M., Kurz, T., Doulias, P.-T., Galaris, D. & Brunk, U. T. Does the calcein-AM method assay the total cellular 'labile iron pool' or only a fraction of it? *Biochem J* 403, 261–266 (2007).
313. Ehrenberg, B., Montana, V., Wei, M. D., Wuskell, J. P. & Loew, L. M. Membrane potential can be determined in individual cells from the nernstian distribution of cationic dyes. *Biophys J* 53, 785–794 (1988).
314. Emaus, R. K., Grunwald, R. & Lemasters, J. J. Rhodamine 123 as a probe of transmembrane potential in isolated rat-liver mitochondria: spectral and metabolic properties. *Biochim Biophys Acta* 850, 436–448 (1986).
315. Scaduto, R. C., Jr & Grotyohann, L. W. Measurement of Mitochondrial Membrane Potential Using Fluorescent Rhodamine Derivatives. *Biophys J* 76, 469–477 (1999).
316. Zorov, D. B., Filburn, C. R., Klotz, L. O., Zweier, J. L. & Sollott, S. J. Reactive oxygen species (ROS)-induced ROS release: a new phenomenon accompanying induction of the mitochondrial permeability transition in cardiac myocytes. *J Exp Med* 192, 1001–1014 (2000).
317. Zorov, D. B., Juhaszova, M. & Sollott, S. J. Mitochondrial ROS-induced ROS release: an update and review. *Biochim Biophys Acta* 1757, 509–517 (2006).
318. Nieminen, A. L., Saylor, A. K., Tesfai, S. A., Herman, B. & Lemasters, J. J. Contribution of the mitochondrial permeability transition to lethal injury after exposure of hepatocytes to t-butylhydroperoxide. *Biochem J* 307 (Pt 1), 99–106 (1995).